An-Najah National University

Faculty of Graduates Study

Improving Ductility Behavior of Sway-Special Exterior Beam-Column Joints Using Ultra-High Performance Concrete.

By

Fayez Raed Abusafaqa

Supervisor

Dr. Mohammed Samaaneh

Co-Supervisor

Dr. Monther Dwaikat

This Thesis is Submitted in Partial Fulfillment of the Requirements for the Degree of Master of Structural Engineering, Faculty of Gratuities Studies, An-Najah National University, Nablus, Palestine 2020.

2020

Improving Ductility Behaviour of Sway-Special Exterior Beam-Column Joints Using Ultra-High Performance Concrete.

By

Fayez Raed Fayez Abusafaqa

This thesis was defended successfully on 21/1/2020 and approved by:

Defense Committee Members	Signature
- Dr. Mohammed Samaaneh / Supervisor	....
- Dr. Monther Dwaikat / Co - Supervisor	....
- Dr. Alfarabi Sharif// External Examiner	....
- Dr. Mahmoud Dwaikat// Internal Examiner	....

Dedication

Praise be to Allah, the Master Creator and Knowing Everything.

To the Prophet Mohammed

Blessings and Peace be upon him

To my Father and Mother

To my supervisors

To my teachers

To my family

To that Angel enlightening my life

To my friends who always supported me

To every one wishes me the best and waits my success

I dedicate this work

Acknowledgment

First of all, praise to Allah who inspired me the patient to complete this work. I would like to extend my thanks to my supervisors Dr. Mohammed Samaaneh and Dr. Monther Dwaikat for their insightful ideas, wise views and precious time and support.

Special gratitude for the Dr. Mahmoud Dwaikat from the civil engineering department for his support in the beginning of research.

Special Mention for my father and mother for their unlimited social and financial support. Words cannot describe your favors.

I also would thanks the stuff of civil engineering department especially Dr. Abdul Razzaq Touqan for helping me improving my engineering sense.

Profound gratitude for my brother, friend and colleague Ali Ghneimat for his support and help on performing the simulations with his own laptops.

I am thankful for my second family my friends in Tulkarem for their supporting and helping on performing the simulations.

الإقرار

انا الموقع أدناه مقدم الرسالة التي تحمل عنوان:

Improving Ductility Behavior of Sway-Special Exterior Beam-Column Joints Using Ultra-High Performance Concrete.

أقر بأن ما اشتملت عليه هذه الرسالة إنما هي نتاج جهدي الخاص، باستثناء ما تم الإشارة اليه حيثما ورد، وأن هذه الرسالة ككل، أو أي جزء منها لم يقدم لنيل أي درجة أو لقب علمي أو بحثي لدى أي مؤسسة تعليمية أو بحثية أخرى.

Declaration

The work provided in this thesis, unless otherwise referenced, is the researcher's own work, and has not been submitted elsewhere for and other degree or qualification

Student's Name:	اسم الطالب: فايز رائد أبو سفاقة
Signature:	التوقيع:
Date:	التاريخ:

Table of Content

.Table of Figures

sList of Table

Symbols and Abbreviations

ALR: Axial load ratio.

AVG: Average.

BCJ: Beam-column joint.

CBM: column to beam moment capacity.

DI: Displacement Ductility index.

ECC: Engineering cementitious composite.

F.E: Finite element.

FRP: Fiber reinforce polymer.

HPFRC: High performance fiber reinforced concrete.

HSC: High strength concrete.

HSFRC: High strength fiber reinforced concrete.

SCC: Self consolidation concrete.

SFRC: Steel fiber reinforced concrete.

S-FRP: Steel fiber reinforced polymers.

STD: Standard Deviation.

UHPC: Ultra-high performance concrete.

UHPFRC: Ultra- high performance fiber reinforced concrete.

A_{ch}: Area of the core.

A_g: Area of the section.

A_g: Area of the Section.

A_{gc}: Cross-sectional area of the column.

A_{sh}: Area of transverse reinforcement through the section.

A_{sb}: Area of tensile reinforcement.

A_{st}: Area of compression reinforcement.

A_v: Area of hoops cross section.

A_{vx}: Area of hoops cross section in the x direction.

A_{vy}: Area of hoops cross section in the y direction.

A: Fit Parameter in Graybeal (2007) UHPC model.

a: Depth of the equivalent block from the top fibers of the compression zone.

$b_{b,max}$: Maximum effective width of the beam.

b_b: Width of the Beam.

b_{cc}: Center to center width of the concrete core.

b_c: Factor in Birtel and Mark (2006) model for evaluating compression damage.

b_{cc}: Core dimension perpendicular to the stirrups legs.

b_{co}: Width of the column.

b_{cx}: Center to center core width for rectangular sections in x direction.

b_{cy}: Center to center core width for rectangular sections in y direction.

b_j: Width of the joint.

b_t: Factor in Birtel and Mark (2006) model for evaluating tension damage.

B: Fit Parameter in Graybeal (2007) UHPC model.

d_B: Effective depth of the beam.

d_{CC}: Center to center depth of the concrete core.

d_S: Centre to centre diameter of the spiral

d_{bar}: Bar diameter.

d_c: Compressive damage.

d_{co}: Effective depth of the column.

d_f: Fiber diameter.

d_j: Effective depth of the Joint.

d_s: Spiral diameter.

d_{sc}: Depth of the compression reinforcement from the top compression zone.

d_{st}: Depth of the tensile reinforcement from the top compression zone.

d_t: Tensile damage.

E_0: Initial Modulus of Elasticity.

E_c: Concrete Modulus of Elasticity.

E_{sec}: Secant Modulus of Elasticity.

F_u: Ultimate strength of steel.

f_c: Actual stress in concrete.

f_c': Concrete compressive strength.

f_c': Concrete compressive strength.

f_{c0}': Unconfined concrete compressive strength.

f_{cc}': Confined concrete compressive strength.

f_l: Lateral confinement pressure in the concrete core.

f_{le}: Effective lateral confinement pressure in the concrete core.

f_{lex}: Effective confinement pressure in the x direction for rectangular sections.

f_{lex}: Effective confinement pressure in the y direction for rectangular sections.

f_{st}: Actual stress in compression reinforcement (MPa).

f_t: Concrete tension strength.

f_y: The steel yield strength.

f_{yt}: Yield Strength of the Transverse Reinforcements.

G: The Potential Flow.

h_b: The sectional depth of the beam.

h_{co}: The sectional depth of the column.

h_{co}: The sectional depth of the column.

h_j: The depth of the joint.

h_x: Distance between the crossties.

j: Distance between the tension and compression force couple in the joint.

K_c: A parameter to define the shape of the plane of failure in the three parameters **Willam** and **Warnke (1975)** yield surface

k_1,k_2,k_3: Stress block parameters for rectangular section.

k_{1sr}: Effective confinement ratio of the effectiveness pressure restored in the concrete.

k_{2sr}: Effective confinement pressure in the hoops

k_e: Confinement effectiveness coefficient in Mander et al. (1988) confined concrete model.

K: Relation ration in Saatcioglu and Razvi (1992) confined concrete model.

L_C: Length of the column.

L_b: Length of the beam.

L_f: Fiber diameter.

L_s: Shear span length (mm).

l_0: Critical length in columns and beams.

l_d: Development length for straight bars.

l_{dh}: Development length for bars with standard 90°hook.

M_j: Moment in the joint.

M_{yb}: Flexural moment yield capacity of the beam.

$\sum M_b$: Summations of flexural strength of beams.

$\sum M_c$: Summations of flexural strength of columns.

N:The normal force in the column.

P_{cr}: The cracking load capacity.

P_p: The peak load capacity.

P_u: The ultimate load capacity.

P_y: The yielding load capacity.

$\bar{p}$: The hydrostatics pressure stresses.

$\bar{q}$: The mises equivalent.

R_E: Modular ratio in Saenz (1964) model.

R_ε: Strain ratio in Saenz (1964) model.

R_σ: stress ratio in Saenz (1964) model.

R: Relation ratio in Saenz (1964) model.

r: Modular ratio in Mander et al. (1988) confined concrete model.

s': Clear spacing between stirrups.

s_1: Spacing between longitudinal reinforcement in rectangular section.

s_{max}: Maximum spacing between the transverse reinforcements.

SF: Strength factor.

s: Center to center distance between stirrups.

T_S: Tension force provided by the reinforcement.

V_{CJ}: Joint shear strength provided by concrete.

V_{Cb}: Shear strength resisted by concrete.

V_{Co}: Shear force in the column.

V_{Jh}: Joint shear strength.

V_S: Shear strength provided by transverse reinforcement.

V_{SJ}: Joint shear strength provided by transverse reinforcement.

V_{UHPCJ}: Joint shear strength provided By UHPC.

V_b: Shear capacity of the beam.

V_{fib}: Shear stresses provided by the fibers.

V_{sb}: Shear strength resisted by transverse reinforcement.

v_f: Volumetric facture of fiber.

f: Factor to consider the Size effect.

w_i: The ith clear Distance between adjacent longitudinal bars.

x_{ub}: Depth of the neutral axis from the top fiber of the compression zone.

x_{yb}: Depth of the neutral axis at yield stage from the compression Zone.

$\hat{\bar{\sigma}}_{max}$: The maximum principle stresses.

$\tilde{\varepsilon}_c^{in}$: Inelastic compression strain.

$\tilde{\varepsilon}_c^{pl}$: Compression plastic strain.

$\tilde{\varepsilon}_t^{ck}$: Tensile cracking strain.

$\tilde{\varepsilon}_t^{pl}$: Tensile plastic strain.

$(\sigma_{b0}/\sigma_{c0})$: The ratio of the biaxial stresses to the uniaxial stresses.

Δ_{cr}: Deflection crossponding to the cracking load capacity.

Δ_u: Deflection crossponding to the ultimate load capacity.

Δ_u: The ultimate deflection.

Δ_y: Deflection crossponding to the yielding load capacity.

α_0: Linearity deviation parameter.in Graybeal (2007) UHPC model.

α_{sc}, β_{sc} and y_{sc}: Are shear co-efficient in Alosta and Khan (2018) expression for calculating shear strength provided by concrete.

ε_0: Strain Crossponding to the Peak Stress.

ε_{0c}^{el}: Elastic undamaged compressive strain

ε_{0t}^{el}: Elastic undamaged tensile strain

ε_c: Traced unconfined concrete strain.

ε_{c0}: Strain at peak unconfined compressive strength.

ε_{cc}: Strain at peak confined compressive strength.

ε_c^{el}: Effective elastic compression strain

ε_{cr}: Cracking strain for concrete.

ε_f: Ultimate Strain.

ε_n: Normalized strain.

ε_t^{el}: Effective elastic tensile strain

ρ_b: Longitudinal reinforcement ratio in the beam.

ρ_c: Longitudinal reinforcement ratio in the column.

ρ_{cc}: Ratio of longitudinal reinforcement area to the area of concrete core.

σ_1: Principle stresses in the first direction.

σ_2: Principle stresses in the second direction.

σ_N: Axial stresses in the column.

σ_c: Traced unconfined concrete Stress.

σ_{cc}: Traced confined concrete stress.

σ_{cc}: Traced confined concrete stress.

σ_f: Stress at maximum strain.

σ_{t0}: Maximum tensile stresses in concrete.

σ_x: Stresses in x axis.

σ_y: Stresses in y axis.

τ_{xy}: Shear Stress in the element.

ω_c: Recovery parameters in compression.

ω_t: Recovery parameters in tension.

γ: Factor to consider the type of the joints. Its equal 10 for exterior BCJ according to ACI 318 code.

εs: Strain in steel.

φ: The dilation angle.

ϵ: Eccentricity parameter.

Improving Ductility Behavior of Sway-Special Exterior Beam-Column Joints Using Ultra-High Performance Concrete.

By

Fayez Abu-Saffaqa

Supervisor

Dr. Mohammad Samaaneh

Co-Supervisor

Dr. Monther Dwaikat

Abstract

The joints are the most critical parts in the frame system. Thus, the design codes include the ACI code provide sticky requirements for designing the joints of sway-special moment resisting frame (SMRF) to avoid joints failure with reasonable level of ductility under seismic load. However, the assemblage of many types of reinforcements (transverse and longitudinal) causes implementations difficulties. This research is aimed to improve ductility behaviour of exterior sway-special exterior beam-column joint (BCJ) using ultra-high performance concrete (UHPC) with dispensing the transverse reinforcements in the joint to overcome the implementations difficulties.

The UHPC class B with 2% volumetric fracture of fibers, as recognized by the federal high-way administrations (FHWA), is used. The study is conducted numerically using the finite element (FE) program ABAQUS. By using this program (ABAQUS), a 3-D non-linear model is build and validated using published experimental data. After that, a matrix of the

main parameters affected the joints behaviour is conducted. These parameters include the beam to column depth ratio (0.6 to 1.6 with 0.1 increments), the axial load ratio (0.25 and 0.5) and the longitudinal reinforcements ratio in column (1% and 2%). The simulation results of the matrix models are used to compare the behaviour of sway-special detailings joints and the joints strengthened with UHPC in terms of strength, ductility and the obtained mode of failure. The results assure the ability of using UHPC in strengthening the joints of SMRF with no reduction on strength and ductility.

Further, the joints strengthened with UHPC show preferences on strength and ductility behaviours at the low column to beam moment capacity ratio with some violations. In ordered to check out these violations, the confined moment capacity of the column is evaluated using Saatcioglu and Razvi model (1992) for the confined reinforced concrete. After that, the confined to unconfined (according to ACI code) ratio is calculated and validated numerically. The ratio is found to range between 1.12 and 1.34 depending on the axial load ratio and the longitudinal reinforcements ratio in column. This range is related to the dimensions and the reinforcement details of the column used in this study with reduction equal 11% for considering the stress hardening in the steel reinforcements. Finally, the analytical model proposed by Alosta and Khan (2017) for evaluating the shear capacity of the exterior BCJs without stirrups is used to evaluate the shear capacity of the UHPC joints and optimize the volumetric fracture of fibers.

In short, this research states that UHPC as defined by the FHWA can be used in strengthening the exterior SMRF BCJ at the low confined CBM ratio with optimizing the required volumetric fracture of fiber depending on the demand shear capacity.

CHAPTER ONE

1. INTRODUCTION

1.1 Overview

Reinforced Concrete (RC) column-beam joint (BCJ) is critical region that needs special attention since it joins the frame members to develop and sustain their ultimate capacity and ensure its continuity as shown by **Sarkar et al. (2007).** Sudden change in geometry and the complexity of stresses affect the joints are the reasons for their complex behaviour. The BCJ's behaviour depends on many factors related to the geometry, reinforcing amount and details, material strength and loading pattern as summarized by **Park and Paulay (1975).** Therefore, the joint should have the adequate stiffness and strength to resist the internal forces induced by the frame member **Kaliluthin et al. (2014).** Many concepts were adopted by the codes (including ACI code) to enhance the behaviour of the joints especially under cyclic loading and load reversal including weak beam-strong column to prevent the soft story mechanisms, provide sufficient development length for the reinforcement to avoid bonds problem and avoiding brittle failure in any case. These concepts require considerable structural properties conjunction on three levels, which are stiffness, strength and ductility. However, the ability of the structure to deform and absorb the energy is one of the most significant features under cyclic and dynamic loadings. Therefore, researchers have been interested in studying joint behavior and its ductility. However, concrete is a brittle material that on other word means non-ductile material. Hence, researchers tried to enhance its ductility using many techniques including the use of transverse reinforcements. Therefore, researchers establish three categories of reinforcement detailing depend on sway level, region seismicity and construction importance, which are ordinary sway, intermediate, and special. However, under cyclic loading the sway special detailing is used.

1.2 Problem Statement

Traditionally, sway special detailings is used for highly seismic region. However, the required closely spaced transvers reinforcements cause difficulties in implementation due to the lack of qualified workmanship. Hence, it is generally not laidout as in drawings details as mentioned by Gencoglu and Eren (2002). Thus, there is a need to relax or remove the transverse reinforcements without affecting the capacity and the ductility of the joints. In addition, the high complex stresses affecting the joints cause severe damage to the joints in way that they need costly rehabilitations. Thus, a strong, stiff and ductile material is needed.

In the last decades, the fiber reinforced materials raised as one of the most attractive materials to strengthen the joints. Many researches studied the use of steel fiber reinforced concrete (SFRC) and high strength concrete. These studies yielded on relaxing the amount of transverse reinforcements in the joints. A new fiber reinforced material with superior properties called ultra-high performance concrete (UHPC) is developed. This material with strain hardening behavior in tension take the researchers attentions. However, a limited studies are conducted on using this material for strengthening the joints.

1.3 Scope of Research

My research is aimed to improve ductile behavior of sway-special exterior BCJ using UHPC. The joints are designed according to ACI-318 and then the transverse reinforcements detailings is replaced with UHPC. The displacement ductility is used to quantify the ductility of the joint. The definition proposed by Cohn and Bartlett (1982) which define the displacement ductility as the ratio of the displacement crossponding to the load of 85% of the maximum load in the post peak descending portion to the displacement crossponding to the first yield in the tensile steel.

The study is performed numerically using finite element (F.E) approach. The commercial F.E program ABAQUS is used to build a non-linear 3D models for the joints. The implicit static analysis is used to traced the behavior of the joints under monotonic and cyclic loads. The concrete damage plasticity model (CDP) provided in ABAQUS is used to simulate the quasi-brittle behavior of the concrete and UHPC. The constitutive stress-strain curves required to define the CDP for concrete are gathered from the literature, while the UHPC class B with 2% volumetric fracture of fiber as recognized by the FHWA is used. Finally, an elastic-perfectly plastic model is assumed for the steel reinforcements.

The model is used to conduct a comparison between the behavior of UHPC strengthened joints without stirrups with the sway special detailing joints in terms of strength, ductility and the obtained mode of failure. The ability of dispensing the transverse detailings of the sway special requirements is checked. The range of the parameters is covering the lower limit of column to beam moment capacity (CBM) ratio. Based on the results, the UHPC shows preference behavior even at the lower CBM ratio. Thus, the research is extended to study the behavior of the UHPC strengthened joints at CBM ratio violating the ratio specified by the ACI code. The moment capacity of the columns is evaluated using the actual confined stress-strain model of concrete. Finally, an analytical model proposed by Alosta and Khan (2018) is used to relate the required compression and tension capacities of the UHPC with the demanded capacities.

1.5 Objectives and Methodology

The following sub-objectives are achieved in order to study the effect of UHPC on the ductility and the validity of its use in the sway-special joints.

1- Extended literature review on the behavior of the BCJ and the main parameters affecting the ductility of the joints. In addition, the requirements for the sway-special moment resisting frame design is gathered from the ACI-318 code. In addition, the behavior of UHPC and other steel fiber reinforced materials are presented. Finally, a numerical study on the behavior of UHPC using CDP and ABAQUS are presented.

2- Build 3-D non linear finite element models using ABAQUS. The modeling includes both geometry and material non-linearity’s. The issues related to the modeling procedure are studied and discussed, while the input data are gathered and reported from the literature.
3- Validate the model using available test data, the model input data include mesh sensitivity study and dilation angle are calibrated using the experimental data.
4- Establish a matrix of the main parameters affecting the joints as gathered from the literature review.
5- Perform the simulations and gather the needed data for comparisons from ABAQUS.
6- Check the failure mechanisms for all models. After that, conduct comparisons between the UHPC and sway-special joints in terms of load capacity, ductility and modes of failure.
7- Tracing the stages of failures for a set of models in ABAQUS to explain the behaviors of the model.
8- Improve the research output through calibrating the parameters.
9- Present the results in a proper way, write the conclusions of the study and provide recommendations for engineers on using UHPC joints. Also, future works are presented to enhance the model and further studies needed to generalize the results.

CHAPTER TWO

2. LITERATURE REVIEW.

2.1 Overview.

The joints behavior affect the overall behavior of the structure. Once a brittle failure occurs in joints, a discontinuity of frame member is produced leading to structure failures at low levels of ductility as mentioned by Ghobarah and Said (2002). Avoiding brittle failure of joints can improve the behavior of the system, and confirm its capacity until failure occurs in the weakest member that is preferred to be in a horizontal members as recommended in the design codes. In the last decades, the term of ductility become one of the most importance design criteria. In this chapter, the definitions of ductility and its levels are presented. In addition, various methods to quantify the ductility are showed. After that, the design requirements for sway-special moment resisting frame (SMRF) according to ACI-318 code are gathered. Also, different methods for strengthening the RC BCJ and enhancing their ductility are summarized. Finally, the mechanical and structural behavior of UHPC are presented further to different studies on using numerical approach to investigate the behaviors of structures and sub-structures.

2.2 Joints Ductility.

After San Francisco earthquake (1906), the wide destruction and deficit in the RC structures sparked discussion on the importance of incorporating requirements designed to improve the constructions to withstand horizontal forces. Hence, the first explicit policy and legal code in seismic safety of construction was established in California in 1925.

With the recurrence of earthquakes, support for seismic research has increased and the codes grown more complicated with respect to seismic design. In 1971, the seismic codes adopted in broad scales. The recommendations of **Blume (1961)**, also called father of earthquake engineering, in considering not only the horizontal forces but also the ductility of structure that must undergo in earthquake. **Stanford University website.**

The ductility in its pure definition means the ability of material to go large deformation in the plastic range before fracture (**Hughes 2009)**. However, there are four levels of ductility namely: material ductility, sectional ductility, membered ductility and structural ductility.

The material ductility, can be obtained from the stress strain diagram for both tension and compression. The material ductility can be used to improve the overall ductility. Hence, researchers try to use ductile materials like steel or used hybrid materials.

Sectional ductility can be determined from basic principles of mechanics. Clearly, the shape of the section and its dimension have a large effect on the section ductility. However, the sectional ductility is less than the material ductility, since it is difficult to have the same behavior and stress on all points in the section.

The next level of ductility is the member ductility, which can be reached just for the weakest member of the frame.

Finally, the structural ductility, can be significantly affected if brittle failure in joints occurs; due to discontinuity on the discharging load path. In other word, the ductility of the joint can control the overall ductility of the system.

Clearly, the need of strong and ductile joints that can deform and absorb energy under bi-directional stress is important; since it is governing the overall ductility of the system, and saving it until reaching the required load through keeping the system continuity (**Sarkar et al. 2007 and Kaliluthin et al. 2014**).

Briefly, there are many types of ductility include the rotational ductility, drift ductility and displacement ductility. In this research, the displacement ductility is used. The displacement ductility can be defined as the ratio of the ultimate deflection to the deflection crossponding to yielding of steel reinforcement **(Park and Paulay 1975, Cohn and Bartlett 1982 and azizinamini et al. 1999)**.

However, there are many approaches to define the ultimate deflection. the design codes include the ACI code define the ultimate displacement using stress-strain failure limits. These failure limits include: the compressive stress in concrete reaches 85% of the maximum compressive strength in the post peak descending portion ($0.85\grave{f_c}$), strain of the concrete reaches 0.003, maximum tensile strain in steel reaches 0.12 (ε_s=0.12) and the ultimate stress in the steel (F_u).

Another approach to define the ultimate displacement is proposed by **Cohn and Bartlett (1982).** The displacement ductility index can be estimated by the ratio of the displacement crossponding to the load of 85% of the maximum load in the post peak descending portion to the displacement crossponding to the first yield in the tensile steel. This definition is used in calculating the displacement ductility for the joints in this research unless reaching the ultimate strain of the steel bars. **Figure 2.1** shows the test results for steel grade 60 (414 MPa) which widely used in Palestine with ultimate strain of 0.24. However, the ultimate tensile strain for steel used in Palestine is ranged between 0.17 and 0.24 depending on manufacturing provenance. A value of 0.18 is used for defining the ultimate tensile strain of the steel.

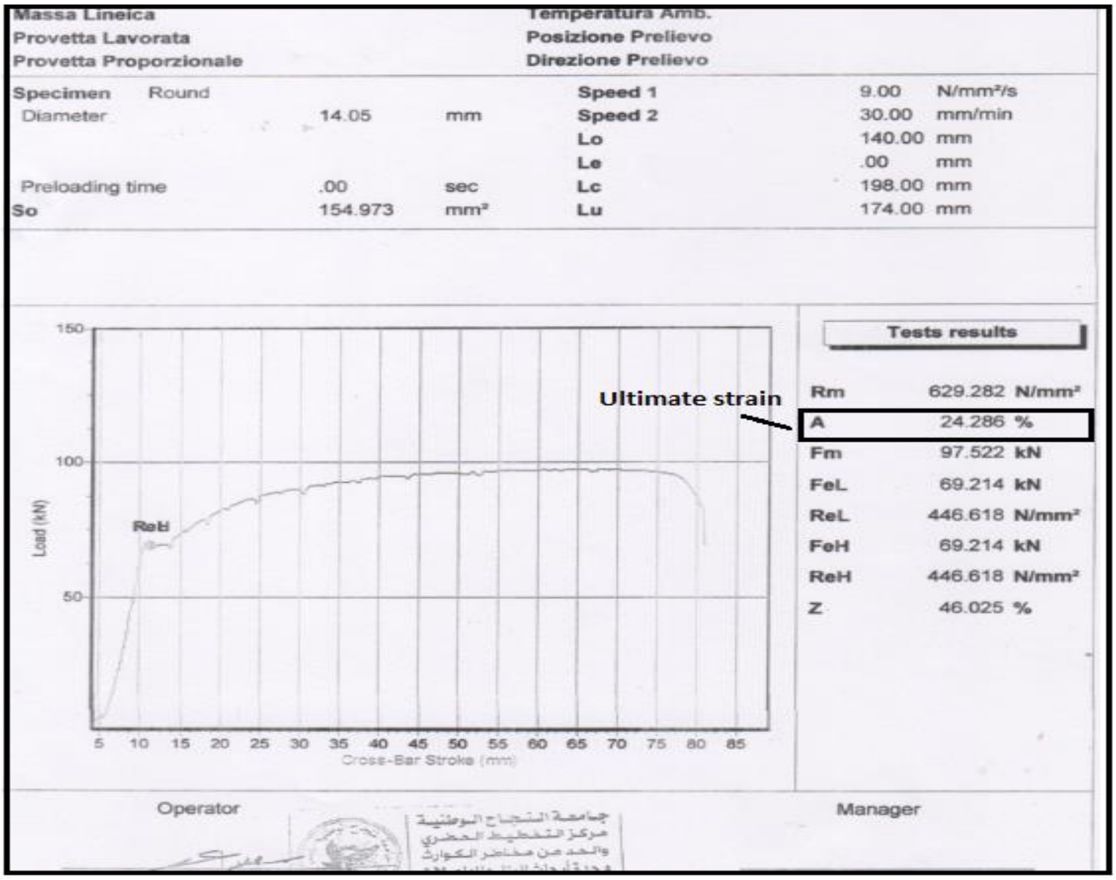

Figure 2. 1: Stress-Strain Test Results for Steel Grade 60. (An-Najah University Laboratory).

The behavior of the materials controls the overall behavior of the section. Concrete suffers brittleness. Hence, it is often used with other hybrid materials to enhance its ductility. The ductility of steel makes it proper material to confine the concrete and enhance its behavior. Concrete confinement using steel can be achieved by many techniques including the use of stirrups or spirals, steel jacketing, circular concrete filed steel tube and steel fiber reinforced polymer S-FRP. Moreover, researchers improved many generations of concrete with superior properties in terms of strength, permeability and chemical resistance including high strength concrete (HSC) and ultra-high performance concrete (UHPC). Similar to conventional concrete, HSC and UHPC suffering brittleness. Hence, they are often used with steel fiber to enhance its ductility.

Finally, there are many techniques to enhance joints strength and ductility. The next section presents the **ACI-318** requirements for designing high ductile frames.

2.3 Special Moment Resisting Frame Joints.

The ACI-ASCE 352 (1985) classified the joints into two type depending on loading conditions:

TYPE 1: In this type, the frame members are designed to satisfy the strength requirements only. In this type, connections are designed according to ACI code excluding Chapter 21. The moment resistance is achieved by strength. However, this type is used for the members with insignificant inelastic deformation.

TYPE 2: in this type the connection are designed to dissipate energy under reversal of deformation in the inelastic range. The frame members are designed to satisfy ductility requirements according to Chapter 21 in the ACI code. This types of joint are designed to sustain strength under some oscillations and lateral load.

The ACI code classify the design requirements for the moment resisting joints (TYPE2) into three categories which are ordinary, intermediate and special. This classification is related to the seismic design category and type of the structural framing, which represents a level of toughness. Clearly, as the level of ductility increase from ordinary to special, the energy that the system can dissipate, and the detailing requirements increase. However, the sway-special requirements in design for seismic load or vibration is the most recommended.

The ACI 318 (2011) provides designing requirements for special moment resisting frames. These requirements mainly aimed to allow the system to dissipate energy under seismic load, and to assure that flexure mode of failure in beams will occur in case of catastrophic scenario. These instructions represent the minimum requirements of reinforcing details and dimensions for beams, columns and joints.

In this study, the joints are firstly designed as part of sway-special moments resisting frame. Hence, it is importance for conceptual design purposes to presents these requirements.

In this section, the instructions for designing the sway special resisting frame members are extracted from the **ACI** code. These instructions represent the minimum requirements that must be satisfied. However, the frame system can be divided to three parts as follow:

a- Flexure Members of Special Moment Frames.

For beams and or any members subjected to factored axial force less than $0.1A_g f_c'$, the following conditions shall be satisfied:

- Clear span length to depth ratio for the member shall not be less than four; standing on experimental evidence that the behavior of the beams under reversal displacement in the nonlinear are significantly different from the behaviors of relatively slenderness members. Hence, the shear deformations cannot be neglected.
- The width of the member shall not be less than:

  - 250mm, this restriction is derived from practice.
  - 30% of its depth, this restriction is added to avoid lateral buckling.

- The effective width of the beam shall not exceed **Equation 2.1**. These restrictions are illustrated in **Figure 2.2**.

$$b_{b,max}(b_w) = b_{co} + min\begin{cases} 0.75\ c_1 = 0.75\ h_{co} \\ c_2 = b_{co} \end{cases} \quad [2.1]$$

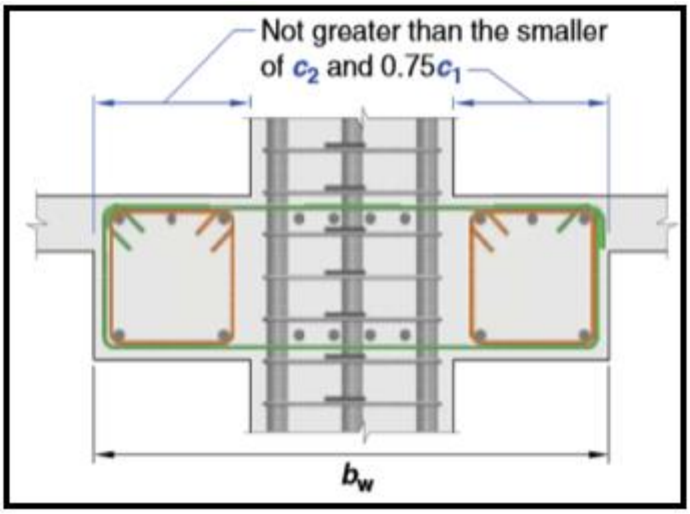

Figure 2. 2: Maximum Effective Width of the Wide Beam (ACI Code-318).

- The negative moment strength at the face of the joint shall not exceed twice the positive moment strength. In addition, the strength at any section through the members shall not be less than one fourth of the maximum strength at the face of the joints.
- Referring to constructional requirements, at least two bars at the top and the bottom of the beam shall be provided.
- Transverse reinforcement for concrete confinement shall be provided over length l_0 equal twice the member depth at distance not more than **Equation 2.2.**

$$s_{max} = min\begin{cases} d_b/4 \\ six\ times\ the\ minmum\ bar\ diameter \\ 150\ mm \end{cases} \quad [2.2]$$

- The first hoops shall be provided at distance not more than 50 mm from the face of the support.
- Behind the critical length l_0 or where the stirrups are not required, stirrups shall be provided at distance not more than $d/2$ mm. Different hoops types are shown in **Figure 2.3**.

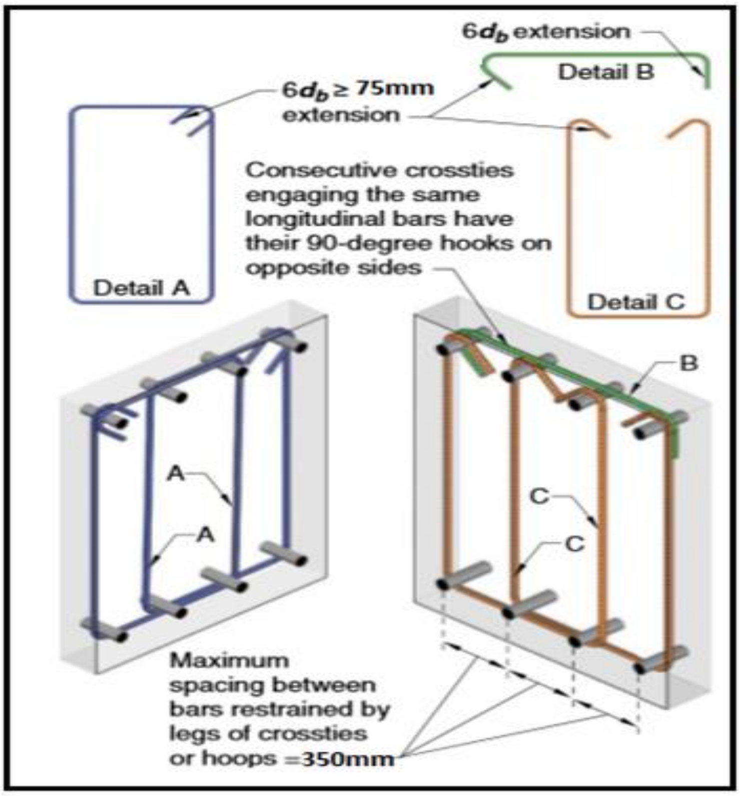

Figure 2.3: Example of Overlapping Hoops (ACI Code-318).

b- Member Subjected to Axial and Bending Loads.

For columns or members subjected to axial load more than $0.1A_g f_c'$, the following requirements shall be satisfied:

- The width of the column shall not be less than 300mm, also the depth to width ratio shall not exceed 2.5.
- In order to avoid flexure yielding of the columns which may be lead to complete collapse, the flexure strength of column shall be at least 20% greater than the flexure of the beams as

$$\sum M_c \geq (6/5) \sum M_b \qquad [2.3]$$

Where:

$\sum M_c$: The flexural strength of the column calculate considering the factorial axial load consistent with the lateral load, resulting of the lowest flexure strength.

$\sum M_b$: The flexure strength of the beams evaluated at the face of the supports. In case of T-beam construction, the contribution of the slab reinforcement within the effective slab width shall be considered.

- Transverse reinforcement at length l_0 from the two ends shall be provide at distance not exceed **Equation 2.2.**
- The minimum amounts of transverse reinforcement through a section at length l_0 shall not be less than **Equation 2.4** at distance not more than **Equation 2.5**. Beyond the critical length l_0, the spacing between stirrups (s) shall not exceed half the member depth. **Figure 2.4** shows an example of transverse reinforcement in the column.

$$A_{sh}min = max \begin{cases} 0.3\frac{sb_{cc}f_c'}{f_{yt}}[\left(\frac{A_g}{A_{ch}}\right) - 1] \\ 0.09\frac{sb_{cc}f_c'}{f_{yt}} \\ 0.2\frac{sb_{cc}f_c'}{f_{yt}}k_f k_n \frac{P_u}{A_{ch}} \end{cases} \qquad [2.4]$$

$$s_{max} = 100 + \frac{350-h_x}{3} \qquad [2.5]$$

Where:

A_g: Area of the section.

A_{ch}: Area of the core.

b_{cc}: Core dimension perpendicular to the stirrups legs.

h_x: Distance between the crossties ≤ 250mm.

k_f: Concrete strength factor $= \frac{6894 f_c'}{25000} + 0.6 \geq 1$.

k_n: Confinement effectiveness factor $= \frac{n_l}{n_l - 2}$.

n_l: is the number of longitudinal bars or bar bundles around the perimeter of a column core with rectilinear hoops that are laterally supported by the corner of hoops or by seismic hooks.

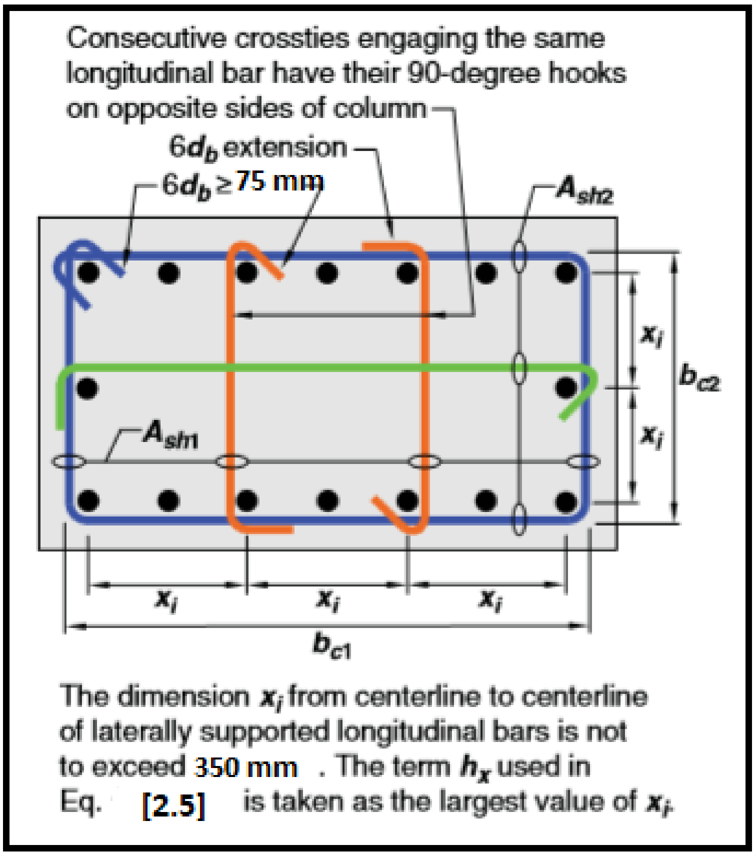

Figure 2. 4: Example of Transverse Reinforcement in Columns (ACI Code-318).

c- **Joints of Special Moments Frame.**

The following requirements shall be satisfied in the joint of special moments frames:

- Joints shear stress shall be calculated for a stresses of $1.25f_y$ in the beam longitudinal tensile reinforcement.
- The depth of the beam on direction of extending beam longitudinal bars shall not be less 20 times the greater bar diameter.
- Transverse reinforcement provided in the joints shall not be less than **Equation 2.4** at distance not more than 150mm. However, this amount can be reduced by half where a frame members from four direction confined the joint
- The minimum development length in tension for the deformed bars is depends on existing hook. However, for bars with standard 90° hook, the development length l_{dh} shall satisfied **Equation 2.6**. while the development length l_d for the straight bar shall Satisfied **Equation 2.7.**

$$l_{dh} = \max\ (8d_{bar}, 150mm) \qquad [2.6]$$

$$l_d = \begin{cases} 2.5l_{dh}, & d < 300mm \\ 3.25l_{dh}, & d \geq 300mm \end{cases} \qquad [2.7]$$

Finally, this section presents the ACI code approach to enhance the ductility and confine joints core. However, researchers used many techniques and materials to confine the joints and enhance their strength and ductility as mentioned in **ACI-ASCE Committee 352**.

These techniques include using another detailing (**Roberto and Leon 1998)**, steel jacketing (**Ghobarah et al. 1996)** and FRB sheets (**Ghobarah and said 2001).** However, the new proposed detailings do not solve the related problems of implementations difficulties, while the steel and CFRP jacketing can used in the post construction stage.

In the last decades, researchers developed many generation of hybrid cement based materials reinforced with fibers. These materials show preferences in terms of tension and compression behavior than the normal concrete. They are more suitable for ductile moment resistance frame design (DMRF). These materials include steel fiber reinforced concrete (SFRC), high strength fiber reinforced concrete (HSFRC) and ultra-high performance fiber reinforced concrete (UHPFRC). However, many types of fibers materials were used with many shapes. In the following section, the mechanical behavior of these materials is presented.

2.4 Mechanical Behavior and Mix Proportions of Fiber Reinforced Materials.

This section presents the mix proportions and the tensile and compressive behavior of some of fiber reinforced materials. These materials include: steel fiber reinforced concrete (SFRC), high strength fiber reinforced concrete (HSFRC) and ultra-high performance fiber reinforced concrete (UHPFRC).

For the SFRC, the mix proportions for the material is tabulated in Table 2.1 as tested by Lee et al. (2013).

Table 2. 1: Typical Mix Proportions for SFRC (Lee et al. 2013)

Material	Weigh (kg / cube)
Cement	384
(Water/Cement)	0.5 (192)
Coarse Aggregate	1073
Fine Aggregate	697
v_f	0.5

Bencardino et al. (2014) experimentally investigated the effect of fiber on the compression behavior of the normal concrete. The results show that the fibers insignificantly increased the compressive strength of the concrete while the strain at failure exhibits higher value than 0.0035 which usually adopted in the guidelines. Figure 2.5 shows the effect of steel fibers in the compression behavior of the normal concrete.

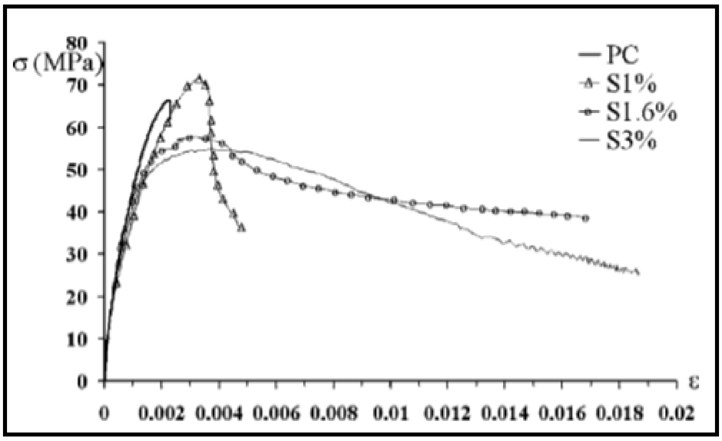

Figure 2. 5: Effect of Steel Fibers on the Behavior of Normal Concrete under Compression.

Nataraja et al. (1999) improved a constitutive model for SFRC up to 50 MPa under compression. The model considered the reinforcing index (RI) as an important parameter that can control the behavior of the SFRC.

Li et al. (2018) experimentally investigated the effect of fibers on the stress-strain behavior of SFRC under monotonic and cyclic tension with different volumetric fracture of fibers (M05-M20 mean v_f equals 0.5-2%). The results show that the tensile capacity, the peak strain and the toughness were improved with the inclusion of steel fibers. **Figure 2.6** shows the effect of steel fibers on the tensile behavior of concrete.

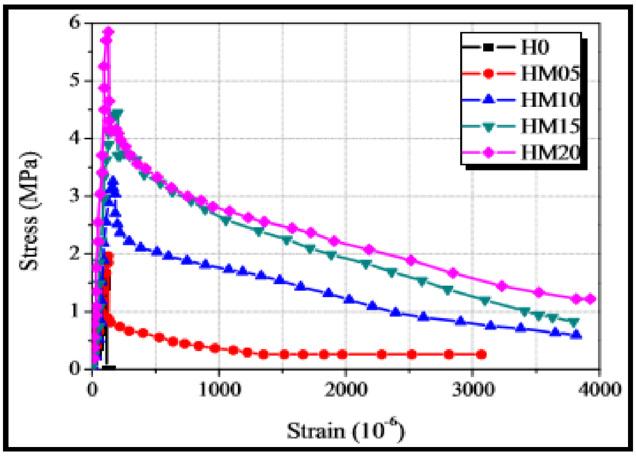

Figure 2. 6: Effect of Steel Fibers on the Behavior of Normal Concrete under Tension.

Sujivorakul (2012) developed a model for predicting the tensile behavior of hooked fiber reinforced concrete. **Figures 2.7** and **2.8** shows the behavior of HF-FRC under tension and the proposed model, respectively. It is clear that the use of hooked fibers improve the tensile behavior of concrete.

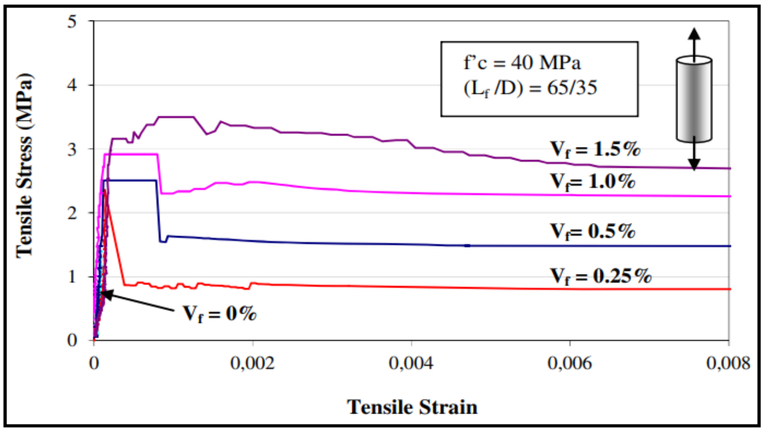

Figure 2. 7: Effect of Hooked Steel Fibers on the Tensile Behavior of Concrete (Sujivorakul 2012).

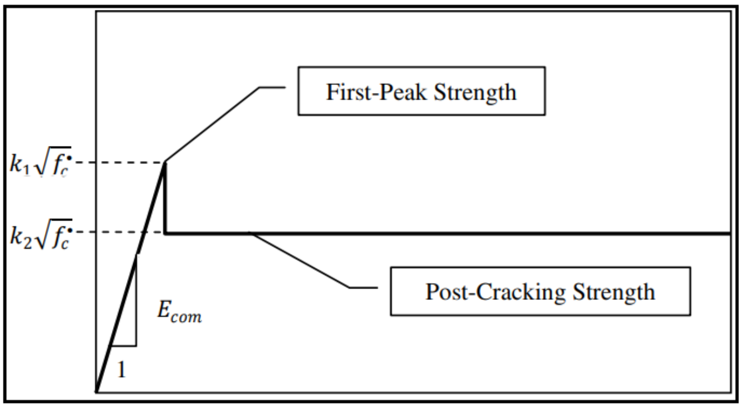

Figure 2. 8: Constitutive Stress-Strain Curve for Hooked Steel Fiber Reinforce Concrete under Tension (Sujivorakul 2012).

For HSFRC, the typical mix proportions for the material are tabulated in Table 2.2 as tested by Wadekar and Pandit (2014).

Table 2. 2: Typical Mix Proportions for SFRC (Wadekar and Pandit 2014)

Material	**Weight (kg/Cube)**
Ordinary Cement	472
Water/Cement	0.32 (150)
Silica fume	27.8
Fly ash	55.7
Fine aggregate	702
Coarse aggregate	1045
Superplasticizer	18 ml / kg of cement
Water Binder Ratio	0.25

Bhargava et al. (2006) experimentally investigated the compressive behavior of HSFRC. Two types of fibers were used (a and b), with (b) have higher aspect ratio of fibers. In addition, two volumetric fracture of fibers were used (L1 refer to 1.5% and L2 refer to 2%). The results show that the volumetric fracture of fiber and the aspect ratio have a significant effect on the compressive behavior of HSC. **Figure 2.9** shows the effect of steel fibers on the behavior of HSC.

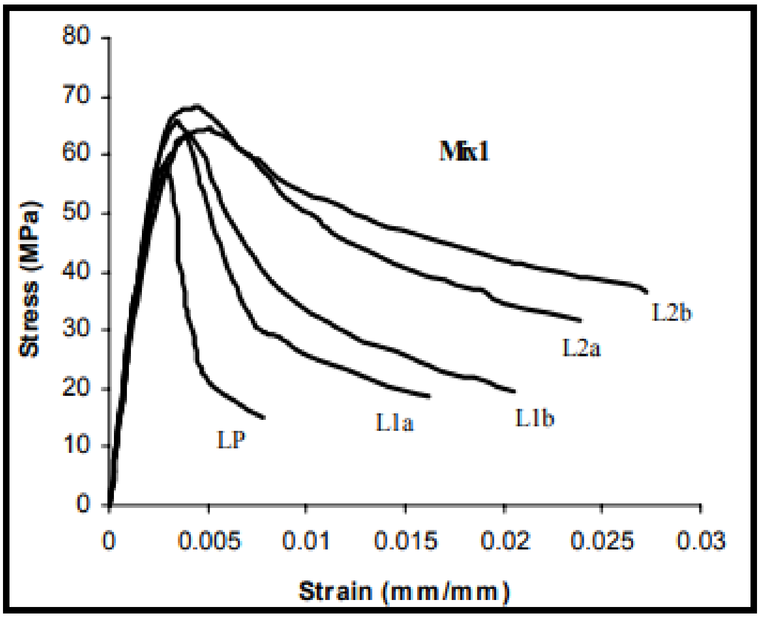

Figure 2. 9: Effect of Steel Fibers on the Compressive Behavior of HSC (Bhargava et al. 2006)

Sivakumar and Santhanam (2007) experimentally studied the tensile behavior of HSC reinforced with many types of fibers include hooked steel. The results show that fiber addition enhanced the pre-peak as well the post-peak behavior of the material. **Figure 2.10** shows the effect of different fiber mixes on the tensile test for HSC.

For design and test purposes, **Figure 2.11** shows the constitutive stress-strain model for HSFRC as provided by The International Union of Laboratories and Experts in Construction Materials (RILEM).

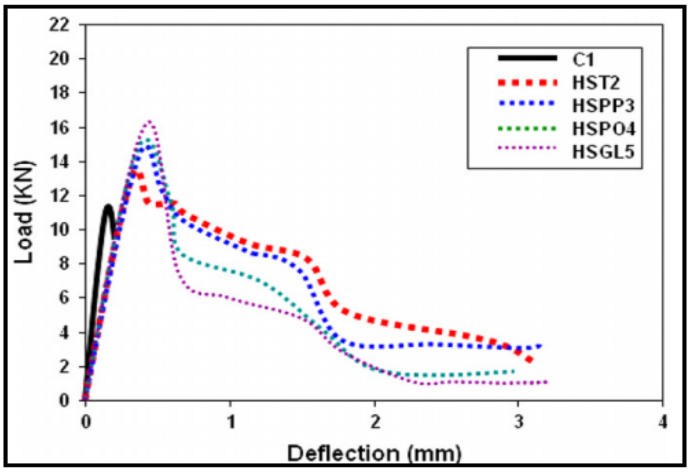

Figure 2. 10: Effect of Inclusion Steel Fibers on the Tensile Behavior of HSC (Sivakumar and Santhanam 2007).

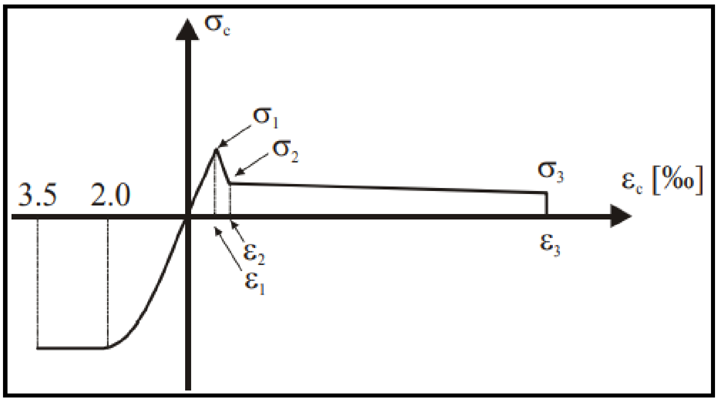

Figure 2. 11: Constitutive Stress-Strain Model for HSFRC. (Vandewalle et al. 2003).

High performance concrete (HPC) is another class of cement based material. The main properties that characterized the HPC is the high durability comparing with normal concrete rather than the high strength appears as mentioned by Mehta and Aitcin (1990).

The silica fume is used to achieve lower porosity as shown in **Figure 2.12**. In another words, the high performance concrete can be a high strength concrete but not vice versa.

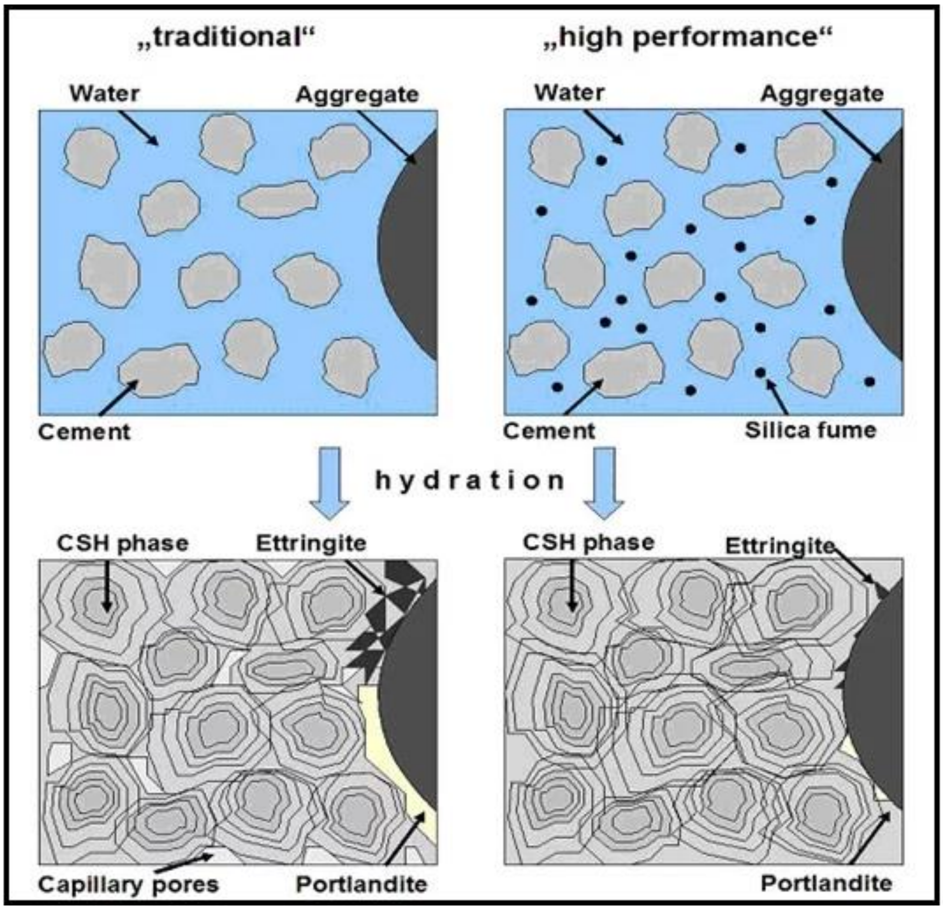

Figure 2. 12: Effect of Using Silica Fume on the Hydration Process (The Constructor Website)

Ultra-high performance concrete is a new generation of high performance concrete that shows superior properties in tension and compression behavior, durability and other mechanical properties. Thus, it is one of the most attractive fiber reinforced materials that can be used to enhance the joints behavior; This cement based material is often used with fibers; to enhance its tension behavior as indicate by **Française de Génie (2002)**.

Although there are many UHPC products with different mixing proportion and different behaviors, they share many characteristic. UHPC material tend to have compressive strength more than 150 MPa, low water cement ratio with high binder percentage and high-range water reducing admixture to enhance its rheological properties as **Graybeal (2006)** explained.

Similar to normal concrete and high strength concrete, UHPC without the use of fibers is brittle, many types of fibers were used to enhance its tension behaviour, these fibers can be sorted depending on material type: steel, carbon…etc., shape of fibers: hooked, straight, twisted...etc., and aspect ratio, (the length of fibers dividing by its diameter).

As mentioned earlier, there are many types of UHPC products in the market with different mix components and mechanical behaviour. The federal highway administration **FHWA (2018**), define the major properties of UHPC material and its mechanical behaviour, the FHWA approved six UHPC products, remarked as U-A throw U-F, from different manufacturing provenance and study there characteristics. Although there are many differences on mix proportions and reinforcement indexes between them as shown in **Table 2.3**, there are many similarities. The FHWA remark the UHPC must have a multi crack zone that allow the material to go into stiffening and provide ductile tensile behaviour.

Table 2. 3: Mix Proportions and Fibers Reinforcement Index for UHPC Classes. (FHWA-HRT-18-036).

ID		U-A	U-B	U-C	U-D	U-E	U-F
MIX DESIGN		kg/m^3	kg/m^3	kg/m^3	kg/m^3	kg/m^3	kg/m^3
Pre-blended dry powders		2078	2085	2136	2195	1920	2210
Water		165	210	159	130	225	143
Chemical admixture	Liquid	13.7	28.7	N.A	53	44	39
	Solid	N.A	N.A	Pre-blended	N.A	N.A	0.89
Steel fiber content (Percent)			Short/long				
	2	126	52/106	123.6	156	156	168
	3	247	78/159	242	234	234	-
	3.25	-	-	-	-	-	253
	4	329	104/202	323	312	312	337
	4.5	370	117/239	363	351	351	379
Steel fiber			Short/long				
Tensile strength (MPa)		1100	2100	2400	3750	3750	3750
Length (mm)		30	13/20	13	13	13	13
Diameter (mm)		0.55	0.3	0.3	0.2	0.2	0.2

N.A: Not available.

Extensive researches in FHWA were conducted to investigate the behavior of UHPC products. However, two areas of the research are presented in this thesis, which are compressive and tensile behavior.

Compressive test for a series of cylinders (75*150mm), at least three cylinders for each class, were conducted. The tests shown that all products have a linear elastic behavior until 50% of the peak compressive strength.

Thereafter, the compressive behavior begins to exhibit softening and thus a non-linear response. Moreover, the main factors describing the compression stress strain behavior prior reaching the peak were investigated. These factors include the peak compressive strength, strain at peak, modulus of elasticity and damaged parameter in addition to poissons ratio.

Figure 2.13 presents the peak compressive strength and the modulus of elasticity related for UHPC classes. Also, the figure shows a best fit for the data yields in an expression for the modulus of elasticity as a function of its compressive strength, which is compatible with the expression proposed by **Graybeal (2007)** as shown in **Equation 2.8.**

$$Ec = 3750\sqrt{fc}\ \text{(MPa)} \qquad [2.8]$$

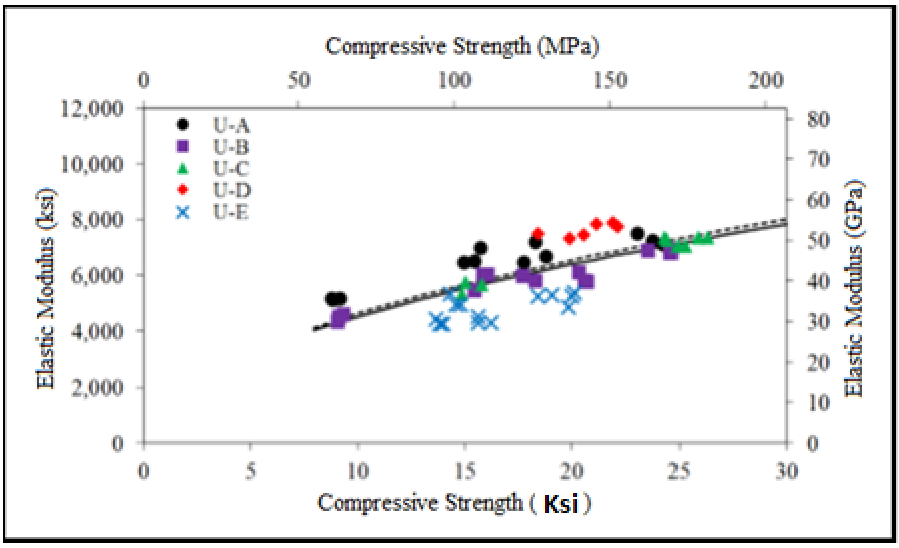

Figure 2. 13: Compressive Strength versus Modulus of Elasticity for UHPC Classes. (FHWA-HRT-18-036).

Figures 2.14 and **2.15** show the average axial strain at peak compressive strength and Poisson's ratio for each class, respectively.

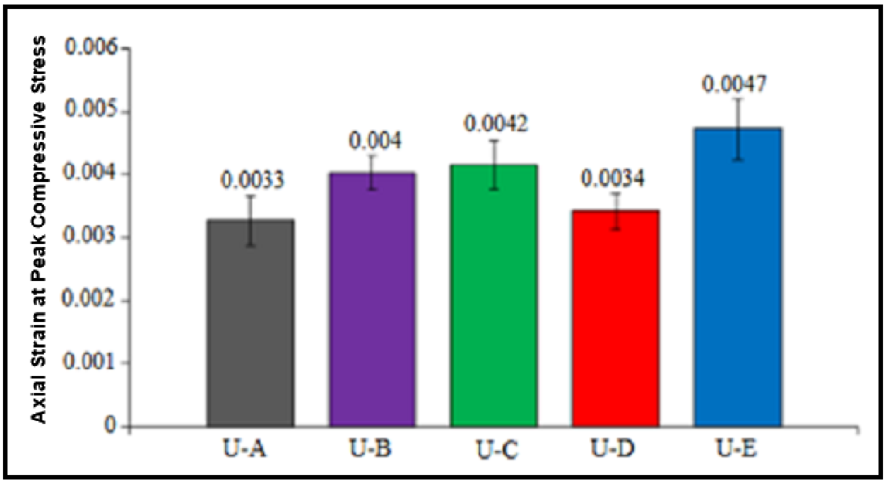

Figure 2. 14: Average Axial Strain at Peak Compressive Stress. (FHWA-HRT-18-036).

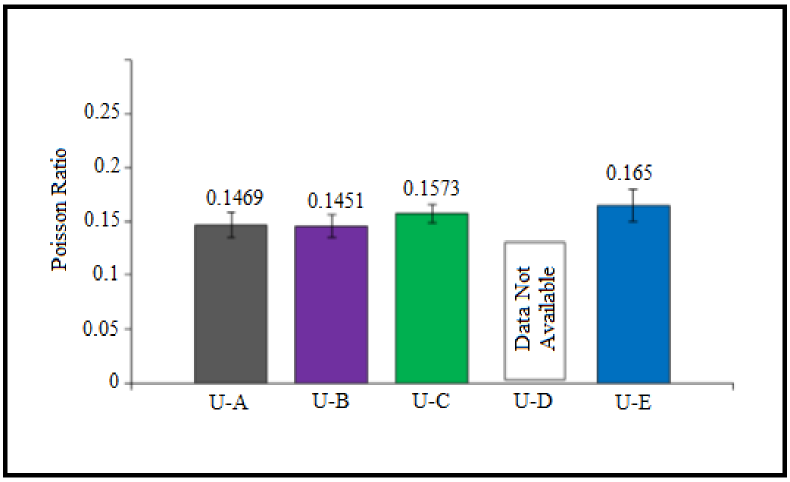

Figure 2. 15: Average Poissons Ratio for UHPC Classes. (FHWA-HRT-18-036).

In engineering design and for simulation purpose, constitutive stress strain model are used, **Graybeal (2007)** proposed an equation to describe the compressive stress strain behavior for UHPC prior to peak, the expression, as shown in **Equation 2.9** describes the compressive stress for UHPC as a function of deviation linear elastic response.

$$\sigma_c = \varepsilon c \; Ec \; (1 - \alpha_0) \quad [2.9]$$

Where:

σ_c: Compressive strength of UHPC attached to traced compression strain ε_c.

E_c: UHPC elastic modulus.

α_0: Linearity deviation parameter (also called damage parameter).

As shown in **Equation 2.10,** the linear deviation parameter α_0 is a function of the normalized strain, which defined in expression in **Equation 2.11**, and other fit parameters A and B, which can be extracted from **Table 2.4**. Once the damage parameter α_0 is obtained, the crossponding stress can calculated.

$$\alpha = A \; x^B \quad [2.10]$$

$$\varepsilon_n = \frac{\varepsilon_c \; E_c}{f_c'} \quad [2.11]$$

Where:

ε_n: Normalized Strain.

ε_c: Traced Compressive strain.

f_c': Peak compressive stress.

Table 2. 4: A and B Fit Parameters. (FHWA-HRT-18-036).

Material	Fit Parameter		
	A	*B*	R^2
U-A	0.16	2.683	0.875
U-B	0106	2.606	0.864
U-C	0.095	2.792	0.849
U-D	0.108	3.168	0.939
U-E	0.115	2.764	0.871
Average	0.106	2.754	0.841

Figure 2.16 shows a comparisons between the measured and the calculated stress-strain curves.

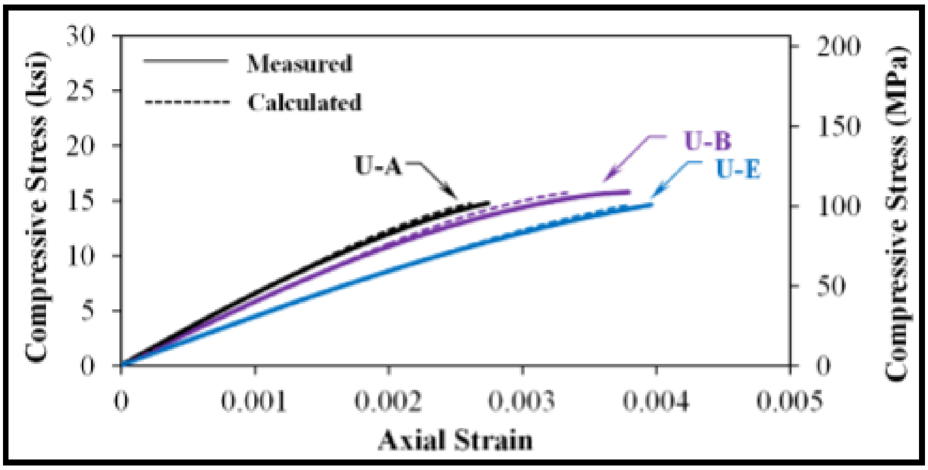

Figure 2. 16: Comparisons between the Measured and the Calculated Stress-Strain Curves.

UHPC Tension Behaviour According to FHWA .

In NSC, the tension capacity can be neglected. However, it is not the same for UHPC with fiber content; because UHPC demonstrates to have a strain hardening behaviour as reported by **Graybeal (2007).** In addition, its shows that first cracking strain is about 0.0002 as mentioned by **Graybeal**

(2007). Therefore, the tension capacity is often characterized by value of first cracking strength as well as a peak post-cracking strength.

FHWA studied the behaviour of the UHPC classes using direct tension test method. However, since matrix formulation, type of fibers, percent content and fibers orientation are not unique, several characteristic can be observed. **Figure 2.17** presents an idealized tension behaviour, which is divided into three phases:

Phase one: represents the elastic behaviour of the material until first crack occurs, this value affected by fibers. Once the cracking value is almost reached, more fibers got engaged yielding a higher cracking strength than the material matrix without fibers. This phase represents the formation of first discrete cracks which can be remarked by clear stress discontinuity.

Phase two: multi crack zone are formulated between the matrix and the fibers bridge without widening in the cracks opening while strain accumulation, these cracks continue until the fibers pull out from the matrix leading to discrete cracks. This phenomena represents the strain hardening in UHPC. Depending on multi factors: fibers orientation, type of fibers and reinforcing index, many characterization of this phase can observed. However, the FHWA considers any material without multi crack zone as a non-UHPC material.

Phase three: in this phase the cracks begin localization into discrete cracks, the cracks openings become wider and increase with fibers bridging the cracks de-bonded and pull out from the matrix, during this load the remainder of the materials unload elastically.

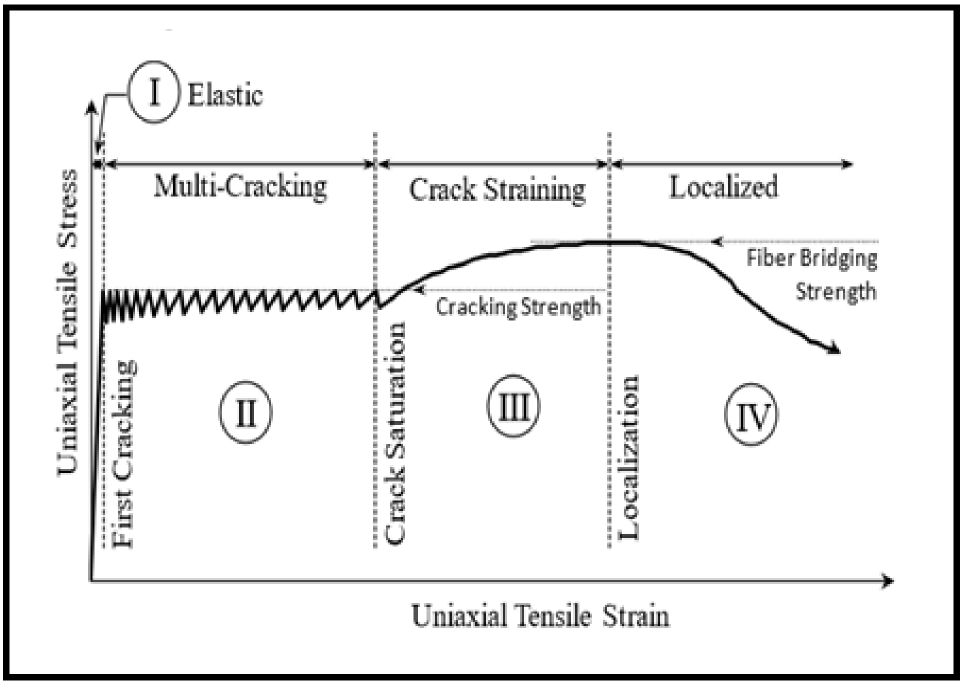

Figure 2. 17: Idealized Tension Behavior for UHPC. (FHWA-HRT-18-036).

The direct tension test results for UHPC classes with different fiber contents are summarized in T**ables 2.5** and **2.6**. Moreover, **Figure 2.18** shows a comparison between the different tensile behaviour for UHPC classes with 2% fibers content.

Table 2. 5: First Cracking Results from Direct Tension Test. (FHWA-HRT-18-036).

ID	V_f	Age in days	AVG $\grave{f_c}$ MPa	Virtual Pick method				0.02 percent offset method			
				Cracking Stress		Cracking Strain		Cracking Stress		Cracking Strain	
				AVG MPa	STD MPa	AVG 10^{-5}	STD 10^{-5}	AVG MPa	STD MPa	AVG 10^{-5}	STD 10^{-5}
U-A	2	6	112	5.5	0.58	52	23	4.83	0.59	33	2
U-A	3	5	95.8	7.63	0.15	37	6	7.49	0.16	36	1
U-A	3	5	105	7.12	0.47	34	5	6.87	0.58	34	1
U-A	3	27	128	8.03	0.72	44	9	7.31	0.72	34	1
U-A	3	29	148	7.25	0.51	20	8	7.75	0.43	35	1
U-B	2	6	112	7.22	1.25	44	18	6.98	1.51	38	4
U-B	2	28	153	7.32	*	18	*	7.56	*	38	*
U-B	3.25	5	101	8.38	01	40	12	8.35	1.44	41	2
U-C	2	1	64.8	5.79	0	20	4	5.91	0.04	34	0
U-C	2	4	93.8	5.79	1.25	48	31	5.22	1.83	32	3
U-C	4.5	1	73.8	5.72	0.59	31	12	5.51	0.65	33	2
U-C	4.5	15	132	4.98	1.7	27	18	5.27	0.95	32	3
U-D	1	1	94.5	3.37	*	18	*	3.07	*	28	*
U-D	1	7	137	2.94	0.25	21	21	2.49	0.23	25	0
U-D	2	1	93.8	7.03	0.29	32	10	6.92	0.42	34	1
U-D	2	7	128	7.45	0.83	26	11	7.44	0.45	33	2
U-D	2.5	1	96.5	8.83	0.83	33	21	8.61	0.23	38	2
U-D	3	1	91	7.70	0.33	27	12	7.61	0.33	36	1
U-D	3	1	84.8	8.68	1.46	36	15	8.58	1.42	38	3
U-D	3	7	126	9.01	0.25	42	12	8.5	0.54	37	1
U-D	3	7	122	9.64	0.9	29	1	9.7	1.72	39	1
U-D	4	1	100	10.2	1.29	42	7	10.1	1.51	41	3
U-D	4	7	124	11.5	0.71	42	2	11.5	0.79	43	1
U-E	2	4	91.7	6.51	0.88	30	10	6.15	1.2	38	3
U-E	2	14	112	7.08	0.83	26	10	6.98	1.05	39	3
U-E	3.25	5	95.8	9.75	0.43	48	7	9.53	0.64	44	1
U-E	3.25	13	105	8.54	0.97	48	14	8.09	0.75	40	1

Table 2. 6: Summary of Localization Point and Ultimate Strength from Direct Tensile Test. (FHWA-HRT-18-036).

ID	V_f	Age (days)	AVG $\grave{f_c}$	Localization Point (Visual Method)				Ultimate Point			
				Localization Stress		Localization Strain		Ultimate Stress		Strain at Ultimate	
				AVG	STD	AVG	STD	AVG	STD	AVG	STD
			MPa	MPa	MPa	10^{-5}	10^{-5}	MPa	MPa	10^{-5}	10^{-5}
U-A	2	6	112	6.42	0.77	347	93	6.47	0.78	287	96
U-A	3	5	95.8	9.76	1.3	279	3	9.76	1.3	280	35
U-A	3	5	105	9.22	0.80	321	45	9.25	0.81	311	41
U-A	3	29	128	9.48	0.94	291	74	9.51	0.94	280	76
U-B	2	28	148	8.32	*	356	*	8.36	*	328	*
U-B	3.25	5	112	10.1	0.57	392	42	10.1	0.58	388	30
U-C	2	1	153	6.07	0.11	600	19	6.10	0.07	38	12
U-C	2	4	101	5.73	1.15	102	58	5.87	1.27	51	27
U-C	4.5	1	64.8	5.95	0.83	360	77	6	0.78	96	80
U-C	4.5	15	93.8	6.42	0.89	410	65	6.44	0.88	125	73
U-D	1	7	73.8	3.58	*	85	*	3.59	*	82	*
U-D	2	1	132	7.76	0.5	392	159	8.09	0.21	247	149
U-D	2	7	94.5	7.9	0.51	385	175	8.31	0.37	262	211
U-D	2.5	1	137	9.12	*	446	*	9.43	*	251	*
U-D	3	1	93.8	8.16	0.46	297	70	8.32	0.45	201	68
U-D	3	1	128	9.45	0.91	271	48	9.5	1.87	214	81
U-D	3	7	96.5	9.36	0.33	457	72	9.81	0.26	198	76
U-D	3	7	91	11.7	1.3	432	80	11.7	1.25	402	52
U-D	4	1	84.8	12.5	0.88	288	71	12.5	0.89	274	76
U-D	4	7	126	12.5	0.13	328	24	12.5	0.13	326	24
U-E	2	4	122	6.96	1.1	404	107	7.06	1	321	172
U-E	2	14	100	8.76	1.27	506	13	8.78	1.28	498	186
U-E	3.25	5	124	11.8	0.95	392	206	11.8	0.93	375	181
U-E	3.25	13	91.7	10.4	0.77	376	8	10.4	0.77	377	8

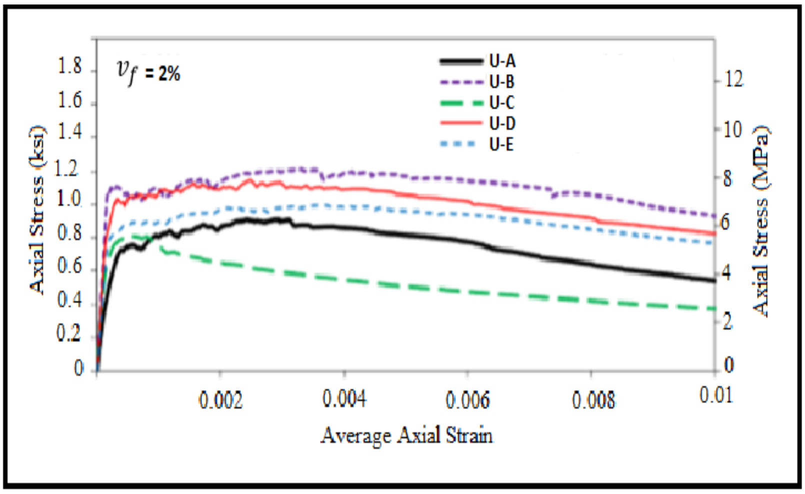

Figure 2. 18: Comparison between the Tensile Behaviors for UHPC Classes with 2% Volumetric Fracture of Fiber (FHWA-HRT-18-036).

In short, FHWA adopted six out of many UHPC products. The behavior of these products (classes) have well defined characteristics. Based on **Figure 2.18,** UHPC class B (U-B) show preferences in terms of tensile capacity and strain hardening. Hence, the study are conducted using U-B. However, there are many studies conducted on non-recognized UHPC products. Although, some of these products have high volumetric fracture of fibers, the tensile behavior of the material do not shows multi-cracking zone. Therefore, it is not easy to define UHPC properties without its component. This is investigated based on the different behaviour of UHPC products when varying the mix components as presented in the literature. **Table 2.7** shows the components of a commercial UHPC products called "DUCTAL".

Table 2. 7: Typical UHPC Components. (DUCTAL).

Material	Amount (kg/m^3)	Percent by weight
Portland Cement	712	28.5
Fine Sand	1020	40.8
Silica Fume	231	9.3
Ground Quartz	211	8.4
Superplasticizer	30.7	1.2
Accelerator	30	1.2
Steel Fibers	156	6.2
Water	109	4.4

In the last few years, the researchers effort concentrated on studying UHPC behaviour because of its grate characteristics. However, many factors affect the mechanical behaviour of UHPC including type of fibers, reinforcing index, defined as the aspect ratio times the volumetric ratio of fibers, orientation of fibers and volumetric fracture of macro and micro fibers.

Hakeem (2011) in his MSc thesis studied the physical and mechanical properties for “DUCTAL” concrete. The result showed that the compressive strength was 163 MPa with elastic modulus of 75 GPa, while the tensile flexure strength was 21 MPa, and the compressive strength was increased by using heat-cool

Graybeal (2007) conducted tests on UHPC considering the effect of fiber orientations on compressive and flexure tensile strength. The study showed that the fibers have no effect on the compressive strength. On the other hand, the flexure strength can be reduced more than 67% when the fibers are perpendicularly aligned to the principal flexural tensile forces.

Wuest et al. (2008) studied the effect of fibers orientation and indicates it has a direct effect on strain hardening. The study shows that a coefficient of orientation of less than 0.64 does not allow strain hardening response. The coefficient can be calculated using digital three dimensional photography, **Krenchel (1964)** presented the coefficient as a function of the fibers volume v_f in each alignment direction angle θ. The value of one represent the fibers in parallel direction and zero represent perpendicular fibers with respect to the principle tensile direction.

Yoo & Yoon (2015) tested large reinforced UHPC beams as shown in **Figure 2.19**. The studied parameters were the reinforcement steel ratio (ρ_b = 0.95% and ρ_b = 1.5%), fibers length and fibers type.

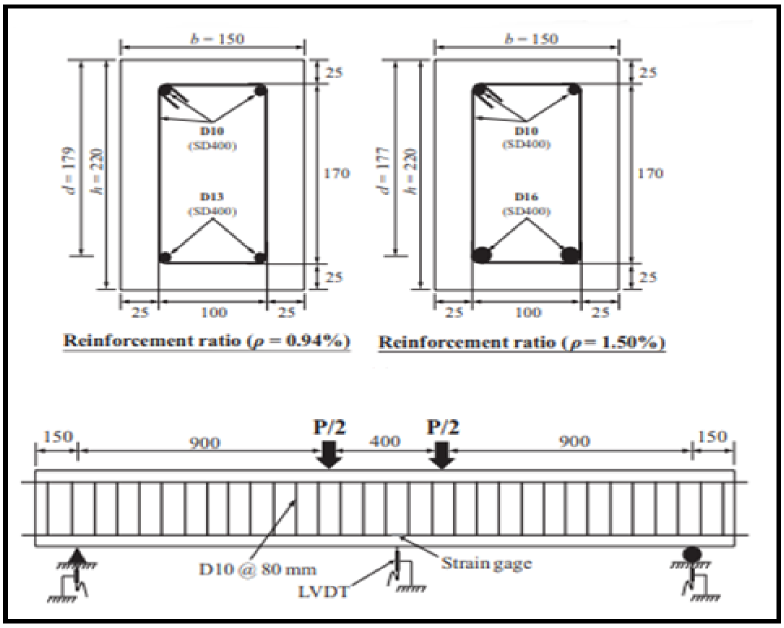

Figure 2. 19: Test Setup and Section Details. (Yoo and Yoon 2015).

Table 2.8 shows the properties of fibers. The results showed that fibers content and shape have insignificant effect in compressive strength and modulus of elasticity of UHPC.

Table 2. 8: Properties of Steel Fibers. (Yoo and Yoon 2015).

Type of Fibers	d_f (mm)	L_f (mm)	Aspect Ratio (L_f/d_f)	Density (g/cm^3)	Tensile strength (MPa)	Elastic Modulus (GPa)
Smooth Steel Fiber	0.2	13	65	7.9	2788	200
	0.2	19.5	97.5	7.9	2500	200
	0.3	30	100	7.9	280	200
Twisted Steel Fiber	0.3	30	100	7.9	2428	200

Table 2.9 shows results for the compression tests. Another major finding of the research was the decrease in ductility with increasing fiber content. The tension capacity is not neglected which in turn contribute to delaying the yield in the tensile steel reinforcement as shown in **Table 2.10.** However, the ductility was improved when using twisted and long fibers. In addition, the fiber content has significant positive effect on the load capacity.

Table 2. 9: Summary of Mechanical Tests Results for UHPC (Yoo and Yoon 2015).

Name	Compression Test ASTM C 39			Flexure Test JCI-S002-2003	
	f_c' (MPa)	ε_{c0} (mm/mm)	E_c (MPa)	f_{MOR} (MPa)	δ_{MOR} (MM)
NF	200.9	Not Available	45265	8.18	0.0034
S13	211.8	0.00453	46732.5	19.26	0.54
S19.5	209.7	0.00484	46880.5	30.69	0.75
S30	209.7	0.00458	46772.9	31.91	1.57
T30	232.1	0.00528	46797.6	32.24	1.06

Table 2. 10: Summary of Flexure Test Results for UHPC Beam. (Yoo and Yoon 2015).

Name	ρ_b (%)	First Cracking		Yielding State		Peak State		Ultimate State	Ductility Index		Failure Mode
		P_{cr} (kN)	Δ_{cr} (mm)	P_y (kN)	Δ_y (mm)	P_p (kN)	Δ_p (mm)	Δ_u (mm)	$\frac{\Delta_p}{\Delta_y}$	$\frac{\Delta_u}{\Delta_y}$	
NF	0.94	36.6	1.12	46	9.15	62.6	94.53	94.63	10.33	10.34	CC
	1.5	30.6	1.09	77.9	12.06	97.9	70.03	73.13	6.06	6.06	CC
S13	0.94	26.6	0.75	80.6	11.96	87.3	28.41	52.61	2.38	4.40	RR
	1.5	23.3	0.67	109.9	1.73	124.1	20.3	51.43	1.59	4.04	RR
S19.5	0.94	18	0.82	78	11.54	93.3	30.51	50.68	2.64	4.39	RR
	1.5	16.7	0.63	103.3	12.29	125.2	43.35	65.63	3.53	5.34	RR
S30	0.94	21.3	1.12	79.9	11.33	95.9	30.46	79.81	2.69	7.04	RR
	1.5	18.7	0.61	105.3	13.01	124.6	45.28	72.90	3.48	5.6	RR
T30	T30	0.94	18	0.78	77.9	11.03	96.6	36.22	65.74	3.28	5.86
		1.5	1.7	0.51	111.9	13.22	133.9	43.64	81.88	3.30	6.20

Note: CC: Ultimate failure occur with concrete crushing. RR: Ultimate failure occur with rebar rupture.

Prem et al. (2012) conducted tests on cubes and cylinder for five UHPC mixes with different index ratio, the stress strain characteristic shows that the pre-peak region has linear ascending portion. In addition, the post peak curve is strongly dependent on the fiber type and fiber content, and it is almost as steep as ascending curve for lower fiber contents and may be more ductile for the higher fiber contents. In addition, the flexural and split tensile strength showed a linear relationship between values at the age of 28 days and reinforcement index.

Shehab Eldin et al. (2017) performed test on cylinder and cube specimens with different mixes contain different fibers aspect ratios, the result were compatible with those from **Prem et al. (2012), Yoo and Yoon (2015).**

Moreover, the results show that strain at peak compression load increase with increase the fiber content and aspect ratio as shown in **Figure 2.20.**

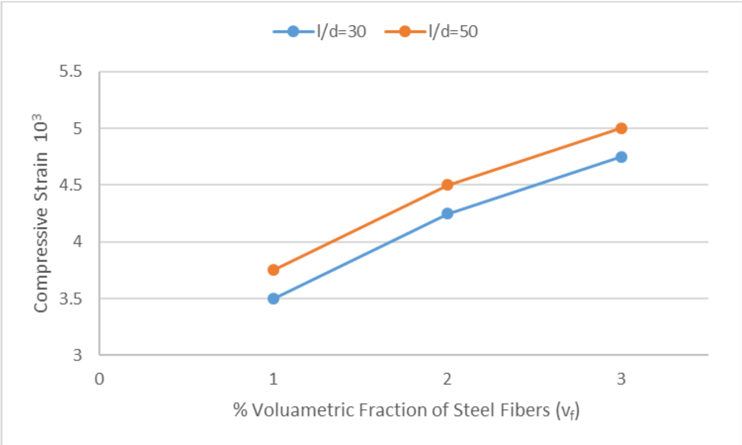

Figure 2. 20: Compressive Strain at Different Steel Fiber Ratios and Aspect Ratios. (Shehab Eldin et al. 2017).

The mix components of the material control its behavior. Thus, with using proper amount of fibers UHPC is an attractive material to use in enhancing the joints of sway-special behavior. Many UHPC products are available in the market. However, the definition of the FHWA recognize a six products which characterized with multi-cracking zone in their tensile behavior. This prosperity make these products more attractive to use in this research. The UHPC class U-B (as recognized by FHWA) shows preferences among the other products. Thus, it is used in this research.

The next section presents the structural behavior of a joints strengthened with steel fiber reinforced materials.

2.5 Behaviour of Joints Strengthened with Fiber Reinforced Material.

In the last decades, the use of hybrid fiber reinforced materials attracted more attention for strengthening the reinforced concrete constructions. **Gencoglu and Eren (2002**) used SFRC to enhance the ductility of exterior beam column joints, the results show that the amount of stirrups needs in the joints can be reduced. **Shannag et al. (2005)** experimentally investigated the behaviors of high performance steel fiber reinforced concrete (HPFRC) beam-column joints, the results showed that the load carrying capacity, the energy dissipation and the stiffness degradation rate were enhanced. **Ganesan et al. (2014)** used high strength concrete (HSC) of M60 grade with crimped steel fibers and polypropylene fibers to experimentally investigate the behavior of beam-column joints under cyclic loads, the results showed that the use of fibers gave betters performance in terms of energy dissipation capacity and stiffness degradation. In addition, the results assure the ability to reduce congestion of reinforcement in beam-column joints.

Recently, the use of ultra-high performance concrete (UHPC) in construction attracted more researchers. Many techniques were used to strengthened the joints using UHPC. These techniques include the use of UHPC in joint intersection, UHPC jacketing and using UHPC in the joint and the plastic hinge zones in beam and columns.

Alkhatib in his MSc thesis (2015) conducted a comparisons between behaviors of exterior BCJs with different fiber reinforced materials and reinforcements detailings in the joint intersection as in **Table 2.11**. The dimensions and the reinforcement details are shown in **Figures 2.21** and **2.22**, respectively.

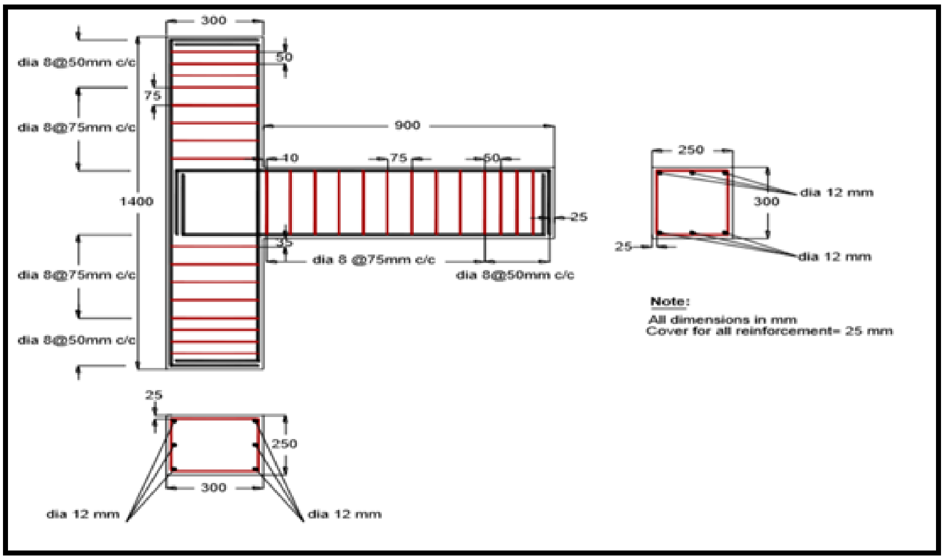

Figure 2. 21: Reinforcement Detailings and Dimensions for BCJ-12MM. (Alkhatib 2015).

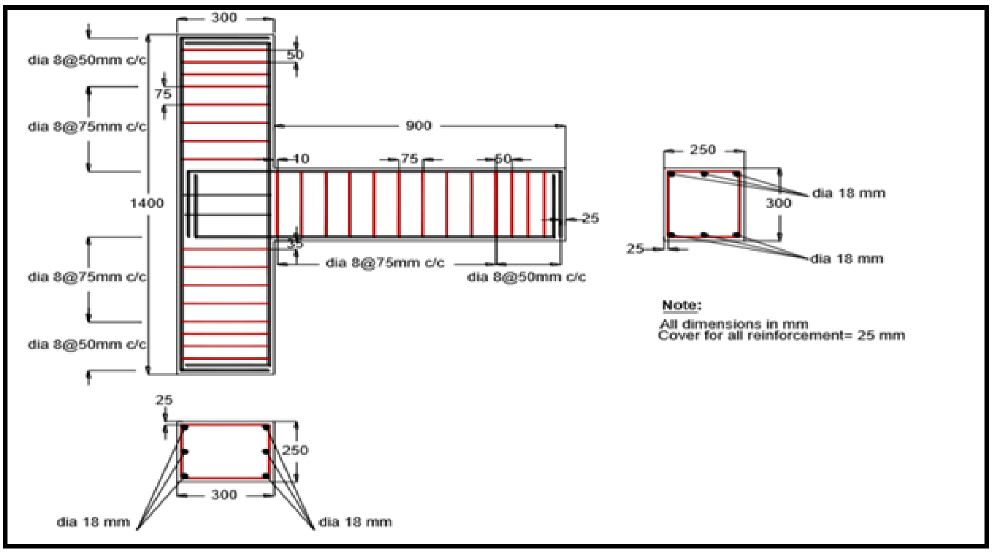

Figure 2. 22: Reinforcement Detailings and Dimensions for BCJ-S-18MM. (Alkhatib 2015).

Table 2. 11: Specimens Details. (Alkhatib 2015).

S. No	No. of Specimens	Specimens	Details	Test Method
1	1	NC-BCJ-12MM	Control sample reinforced with normal steel Ø12 and no stirrups in the joint region.	Monotonic and cyclic
2	1	NC-BCJ-18MM	Control sample reinforced with normal steel Ø18 and no stirrups in the joint region.	Monotonic and cyclic
3	1	NC-BCJ-S-18MM	Control sample reinforced with normal steel Ø18 and stirrups in the joint region.	Monotonic and cyclic
4	1	SFRC-BCJ-12MM	Sample reinforced with normal steel Ø12, SFRC joint and no stirrups in the joint region.	Monotonic and cyclic
5	1	SFRC-BCJ-S-12MM	Sample reinforced with normal steel Ø12, SFRC joint and stirrups in the joint region.	Monotonic and cyclic
6	1	SFRC-BCJ-18MM	Sample reinforced with normal steel Ø18, SFRC joint and no stirrups in the joint region	Monotonic and cyclic
7	1	SFRC-BCJ-S-18MM	Sample reinforced with normal steel Ø18, SFRC joint and stirrups in the joint region.	Monotonic and cyclic
8	1	UHPC-BCJ-12MM	Sample reinforced with normal steel Ø18, UHPC joint and no stirrups in the joint region	Monotonic and cyclic

The main goal of the study was to investigate the behavior of the exterior BCJs using steel fiber reinforced material. The specimens were poured and cured then placed in the testing machine, four rods were used at each columns ends to avoid rotations and provide fixed end. After that, a uniform stress of 2 MPa was applied at the free end of the column to represent the axial load in reality. **Figure 2.23** shows the machine and test conditions.

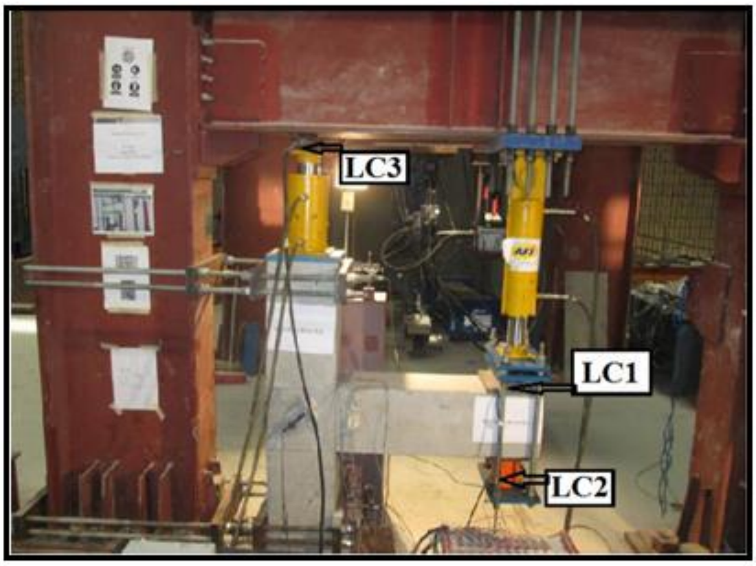

Figure 2. 23: Machine Test and Testing Conditions. (Alkhatib 2015).

Finally, the deflection of the tip beam was monitored until failure occurs. **Figure 2.24** shows a comparison on behavior of BCJ-18mm specimens under monotonic load. Moreover, **Tables 2.12** and **2.13** summarize the results and show the mode of failure for each specimens for monotonic and cyclic load, respectively. The results show that flexure failures at the beam were get when using UHPC and SFRC without transverse reinforcements. However, the columns to beam moment capacity (CBM) ratio used is more than two without considering the confinement effect in case of use higher axial load ratio (ALR). Behind this ratio, the behavior of the joints and the ability of replacement can not be guaranteed.

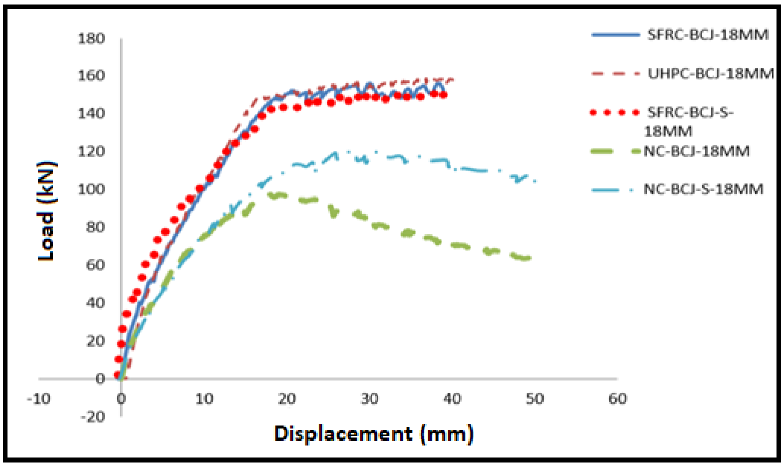

Figure 2. 24: Load–Deflection Results for Monotonic Tests. (Alkhatib 2015).

Table 2. 12: Ultimate Load and Mode of Failure for BCG-18MM Monotonic Tests. (Alkhatib 2015).

Specimens	Ultimate Load (KN)	Enhancement (%)	Test Type	Mode of Failure
NC-BCJ-18MM	97.2	control	Monotonic	Joint shear failure
NC-BCJ-S-18MM	119.5	22.94	Monotonic	Joint shear failure
SFRC-BCJ-18MM	156	60.49	Monotonic	Flexural failure
SFRC-BCJ-S-18MM	151	55.35	Monotonic	Flexural failure
UHPC-BCJ-18MM	160	64.61	Monotonic	Flexural failure

Table 2. 13: Ultimate Load and Mode of Failure for BCG-18MM Cyclic Tests. (Alkhatib 2015).

Specimens	Ultimate Load (KN)	Enhancement (%)	Test Type
NC-BCJ-18MM	99	Control	Cyclic
NC-BCJ-S-18MM	123.4	24.65	Cyclic
SFRC-BCJ-18MM	150	51.52	Cyclic
SFRC-BCJ-S-18MM	155	56.57	Cyclic
UHPC-BCJ-18MM	157	58.59	Cyclic

Khan et al. (2018) Experimentally investigated the performance of exterior beam column joints strengthened with thin UHPC plates. Four identical specimens were tested with high beam reinforcement ratio were used to promote the joints failure without yielding of the beam bars. The specimens details and the scheme of the UHPC jacket are shown in **Figures 2.25** and **2.26**, respectively.

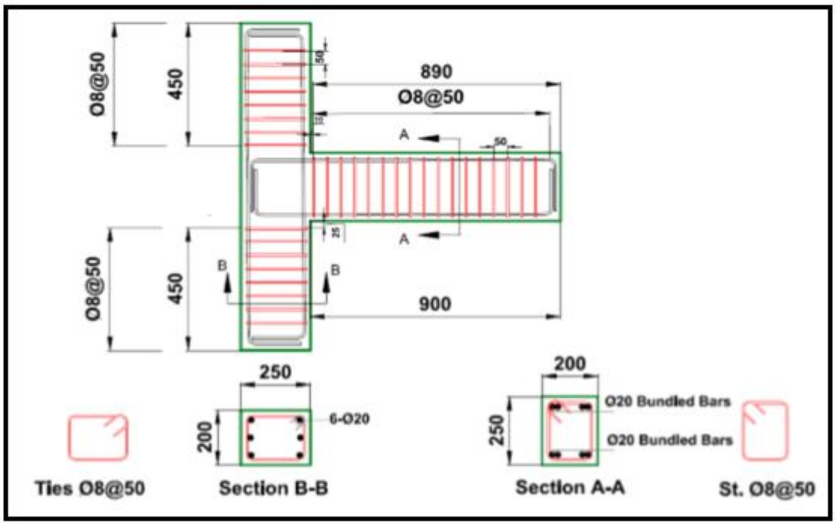

Figure 2. 25: Reinforcement Detailing and Dimensions. (Khan et al. 2018).

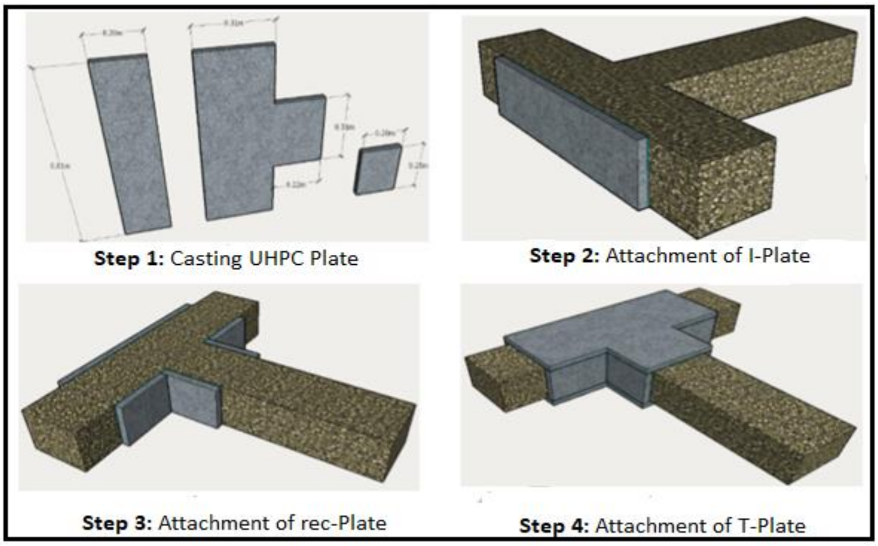

Figure 2. 26: Strengthening Process and Scheme Jacketing for Specimens TE. (Khan et al. 2018).

The studied parameters were the existing of UHPC jackets and the method of attaching the plates to the substrate surface as shown in **Table 2.14**.

Table 2. 14: Summary of Test Loading Scheme. (Khan et al. 2018).

Specimens ID	Description	Strengthening Method	Loading Type
TC	Control	-	Reversed Cyclic
TS1	Strengthened	Sandblasting and in Situ Casting of UHPFRC	Reversed Cyclic
TS2	Strengthened		
TE	Strengthened	Prefabricated UHPFRC-PLATES	Reversed Cyclic

Two methods of strengthening were performed: using sandblast technique with cast in situ UHPC plates, and using moulds and prefabricated UHPC plates with epoxy adhesive material. The specimens were designated by TC, TS1, TS2 and TE. TC was an ordinary concrete joints without transverse reinforcement and it represents the control joints. TS1 and TS2 were replicated specimens with UHPC jacketing using sandblasting techniques, while in TE an epoxy material called Sikadur was used to attach a prefabricated UHPC plates as shown in **Figure 2.26**.

The specimens were placed in the test machine as shown in **Figure 2.27**, then a 150 kN axial load was applied to the top of the column. Finally, a cyclic load was applied to the tip of the beam until failure.

The results showed the effectiveness of using UHPC jackets with sandblasting techniques in transferring the failure from joint shear failure to preferred vertical flexure failure on the beam. On the other hand, the specimens TE show brittle failure due to detachment of UHPC plates with the concrete cover from the reinforced concrete core. However, all the strengthening specimens show improvement on behavior on term of strength and energy dissipated. **Figures 2.28** and **2.29** show the envelop curves for the test for the specimens and the energy dissipate respectively. Moreover, **Table 2.15** shows the improvement of the joints behavior in terms of strength and stiffness.

Finally, a comparison between the results of many strengthening method are shown in **Table 2.16**, the comparison shows advantages for using cast in situ UHPC jacketing in terms of strength, stiffness and energy dissipation.

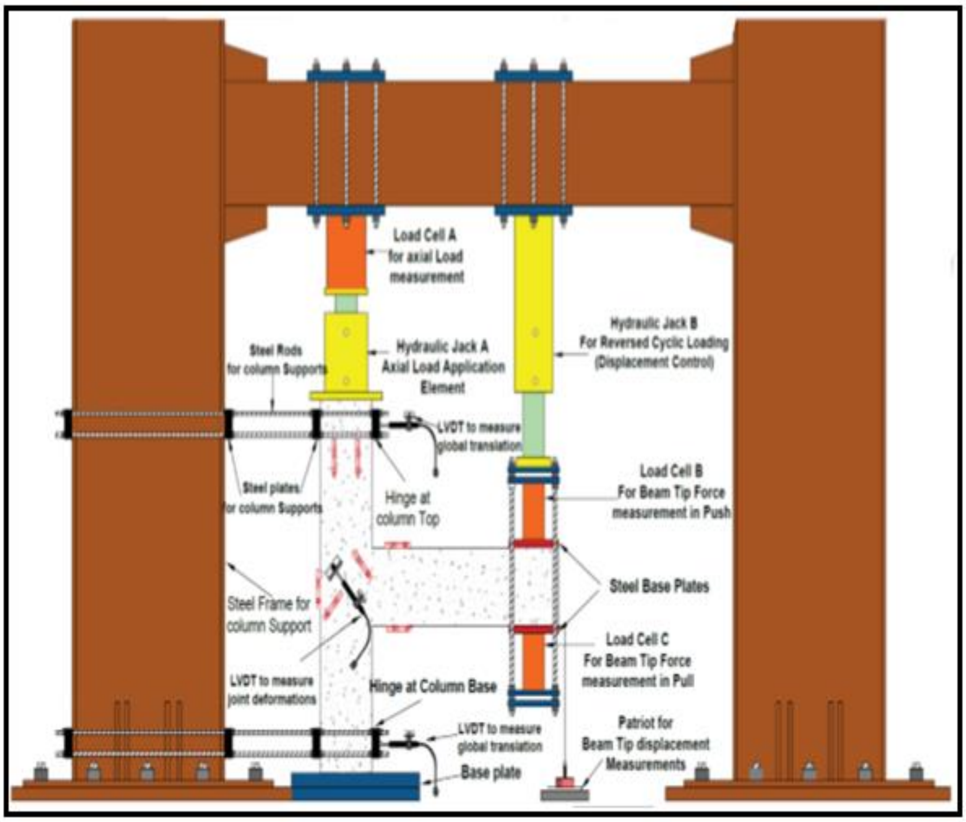

Figure 2. 27: Test Setup. (Khan et al. 2018).

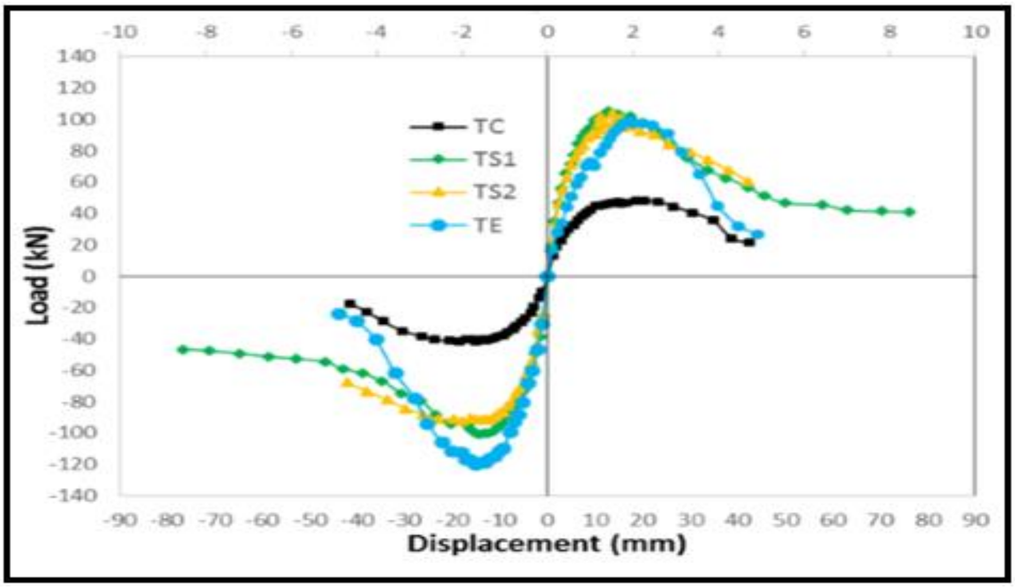

Figure 2. 28: Envelop Results for the Control and the Strengthening Specimens (Khan et al. 2018).

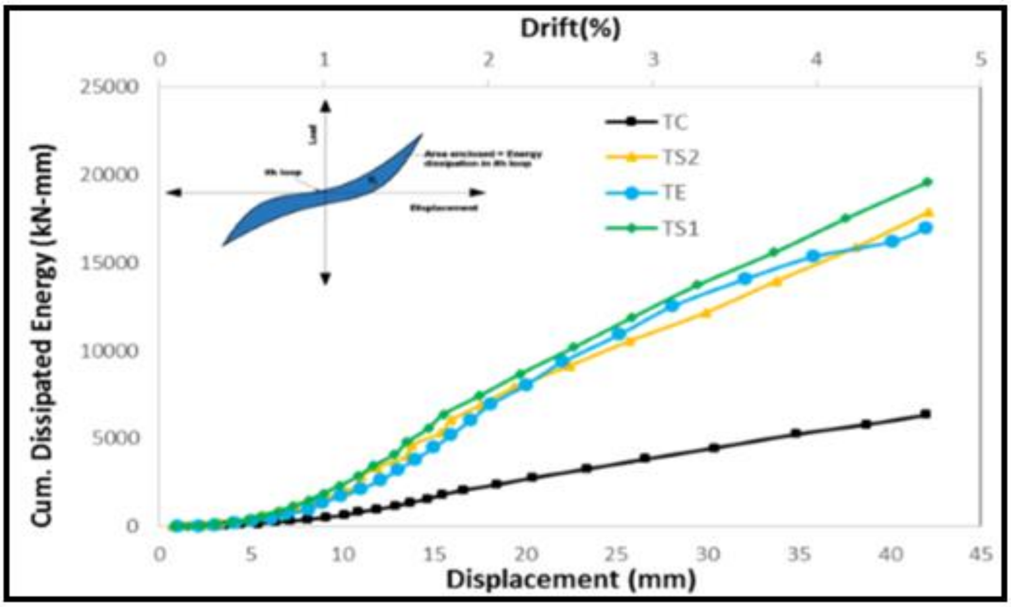

Figure 2. 29: Commutative Energy Dissipate in the Specimens RC, RS1, TS2 and TE. (Khan et al. 2018).

Table 2. 15: Improvement of Load Carrying Capacity and Deformation (Mohammed Khan et al. 2018).

Specimens	Positive Direction		Negative Direction		Strength Factor
	F_P^+(KN)	Δ_P^+(KN)	F_P^-(KN)	Δ_P^-(KN)	SF (%)
TC	48.2	18.5	-41.5	-8.6	-
TS1	105.6	12.9	-100.5	-14	2.3
TS2	103.9	13.6	-92.3	-18	2.2
TE	98.7	17	-1203	-15.2	2.44

Table 2. 16: Comparison of the Results of Different Studies on Evaluation of the Performance of Strengthened Specimens. (Khan et al. 2018).

Researchers	Joint Type	Scale	Retrofitting Material	Thickness of Jacket (mm)	Degree of Enhancement		
					Streng-th (%)	Stiffness (%)	Energy dissipate-ons (%)
Esmaeeli et al. (2015)	Interior	1:1	CFRP strengthening SHCC	25	46.7	Restored	95
Esmaeeli et al. (2015)	Interior	1:1	Prefabricated HPc	25	51.4	22.5	84
Li et al. (2013)	Interior	2:3	Ferrocement Jacket	30	16.6	34	171
Tsonos (2010)	Exterior	1:2	Shotcrete jacketing	70	115	75	120
Proposed method	Exterior	1:3	UHPFRC cast in-situ	30	125	179	210
Proposed method	Exterior	1:3	Prefabricated UHPFRC Plates	30	144	120	160

Chao et al. (2016) tested two frames, the first was control frame with concrete compressive strength 35 MPa. While the plastic zones in the second frame were casted with UHPC without stirrups. **Figures 2.30** and **2.31** show the dimensions and the reinforcement detailings for the frames, which designed as sway-special moment resisting frame according to ACI-318. The two frames tested under cyclic loadings. The key findings was that a minor damage in columns occurred when using UHPC. Thus, this reducing the need for post-earthquake repairs. In addition, UHPC frames show higher strength and greater drift capacity up to 4%. The researchers recommended to relax the confining requirements in columns when UHPC is used.

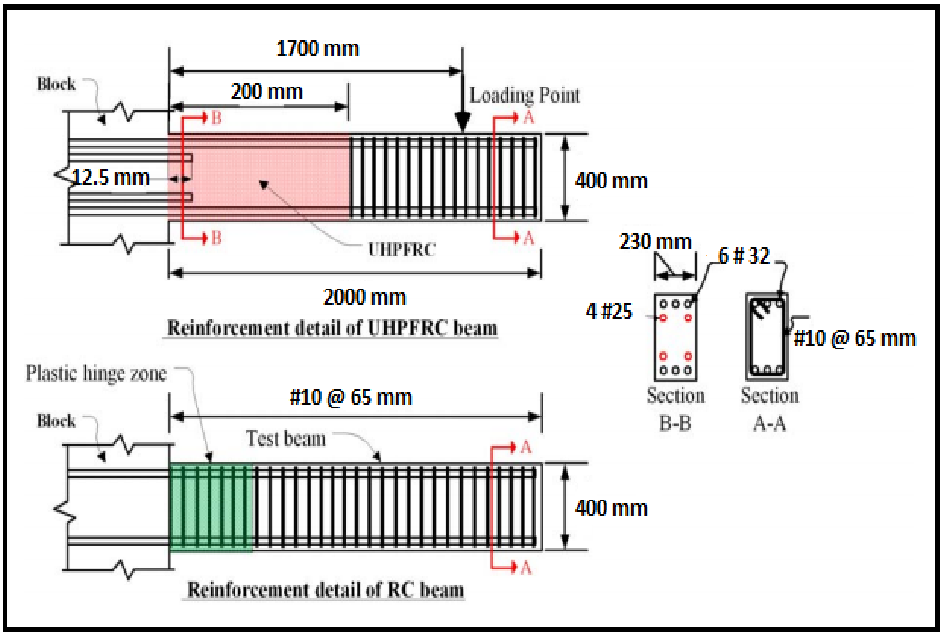

Figure 2. 30: Beam Dimensions and Reinforcements Detailings (Chao et al. 2016).

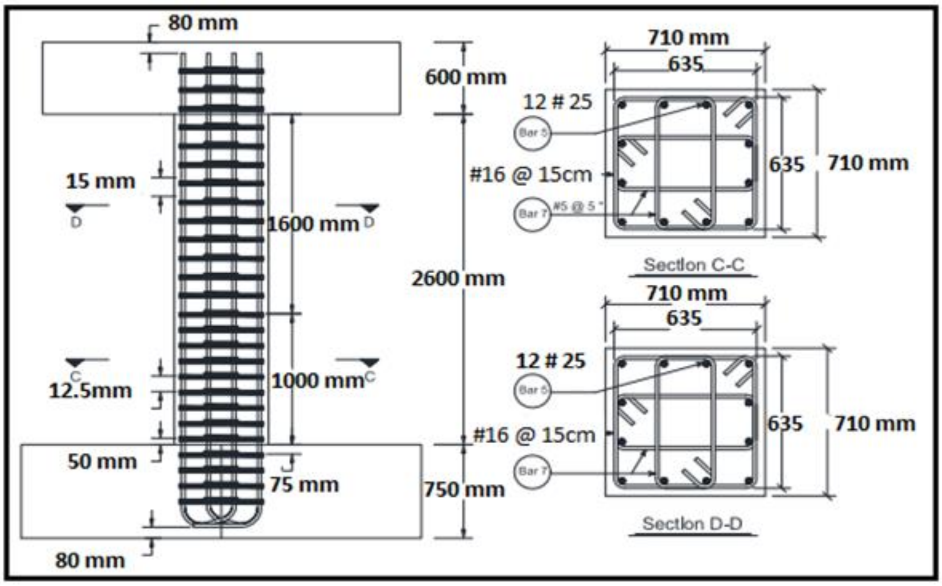

Figure 2. 31: Column Dimensions and Reinforcements Detailings (Chao et al. 2016).

While there are many researches conducted on strengthening the joints using SFRC and HSFRC, limited researches were conducted on investigation the behavior of BCJs strengthened with UHPC. However, researches used the UHPC to strengthen other frame members (beams and columns).

Alosta et al. (2017) experimentally investigated the behavior of reinforced concrete beam strengthened with UHPFRC. Three strengthening configuration were used which are the bottom side strengthening, two longitudinal sides strengthening and three sides strengthening. Similar to the joints strengthened with UHPC plates. Two attachment techniques were used which are sand blasting technique and bonding using epoxy material technique. The results show a positive enhancement on the load carrying capacity of the beams especially for the beams strengthened on three sides.

However, the ductility of the beam strengthened on the bottom side was decreased.

Safdar et al. (2016) experimentally investigated the behavior of reinforced concrete beam retrofitted with UHPFRC in the tension and compression zone. The results show that the flexure strength of the retrofitted beams were enhanced.

Hung et al. (2018) tested eight UHPC slender columns under eccentric load with different volumetric fracture of fiber. The dimensions and test setup are shown in **Figure 2.32**, while **Table 2.17** shows the different properties of the specimens. The key parameter of the study were the volumetric fracture of fiber and the amount of transverse reinforcements. Based on **Table 2.17**, the transverse reinforcements in the column satisfy the required amount for designing sway-special moment resisting frame. The results show that inclusion of steel fiber with volumetric fracture of 0.75% effectively restrained spalling and crushing of the slender UHPC column. In addition, using 1.5% volumetric fracture of fiber can compensate 70% reduction in the confinement steel with no reduction in ductility. **Figure 2.33** shows the tensile behavior of UHPC used. Based on **Figure 2.33,** the UHPC material used in this research shows less ductility comparing with the UHPC products recognized in FHWA.

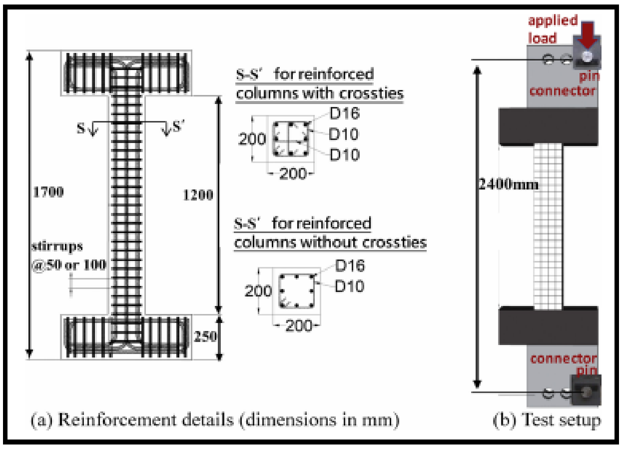

Figure 2. 32: Reinforcements Details and Test Setup (Hung et al. 2018).

Table 2. 17: Reinforcements Details for the Slender UHPC Columns (Hung et al. 2018).

Column	Steel Reinforcements				v_f (%)
	Longitudinal		Transverse		
	Rebar	ρ	Hoops	Crossties	
H5T0-F0	8-D16	4%	D10@50mm	None	0
H5T0-F150	8-D16	4%	D10@50mm	None	1.5
H5T5-F0	8-D16	4%	D10@50mm	D10@50mm	0
H5T5-F75	8-D16	4%	D10@50mm	D10@50mm	0.75
H10T0-F0	8-D16	4%	D10@100mm	None	0
H10T0-F150	8-D16	4%	D10@100mm	None	1.5
H10T510F0	8-D16	4%	D10@100mm	D10@100mm	0
H10T10-F150	8-D16	4%	D10@100mm	D10@100mm	1.50

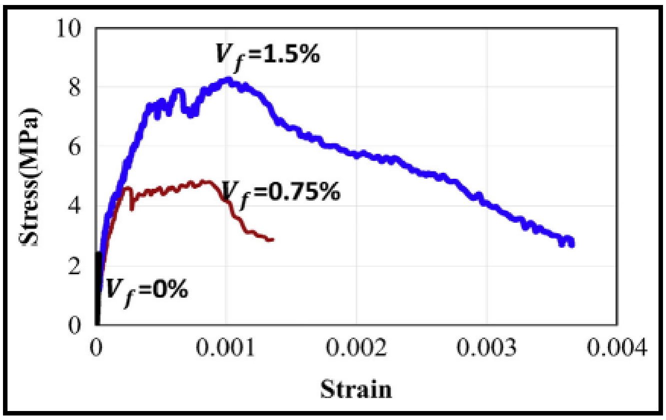

Figure 2. 33: Tensile Stress-Strain Curves of UHPC (Hung et al. 2018).

Racky (2004) conducted comparisons between NC, HSC and UHPC. The materials were examined regarding to their cost-effectiveness and sustainability. The study conducted using a design column. The columns have the same load carrying capacity and ductility. The results show that the use of UHPC generates lower cyclic-life costs. In addition, using UHPC provides higher floor surface area.

Finally, this section presents experimental studies for investigation the behavior of joints and other sub-structures strengthened with UHPC and other steel fiber reinforced materials. The next section presents the numerical approach for investigation the behavior of joints and sub-structures with UHPC in addition to experimentally studies validated using numerical approach.

2.6 Numerical Investigations of Structure Strengthened with UHPC Using F.E Programs.

Finite element modeling offer attractive field of research for investigating the behaviors of elements, sub-structures and structures; since it provide quick results with low cost. In addition, the experimental-numerical validation approach become common practice in research. Many researchers use F.E programs to validate their experimental results and/or performed numerical studies on the behavior of sub-structures strengthened with UHPC.

Chen and Graybeal (2012) modeled the structural behavior of the second generations of pi-girders strengthened by UHPC. The results showed that concrete damage plasticity CDP model was reliable in tracing the observed structural response.

Khan et al. (2018) simulated the experimentally tested exterior beam-column joints jacketed by 30 mm UHPC plates. Concrete damage plasticity CDP model provided in ABAQUS was used. The study showed that CDP can be used to predict the behavior of such joints. However, no parametric study conducted.

Alkhatib (2015) in his thesis simulated an experimental test on strengthened joints using fiber reinforced materials including UHPC. The results showed that the CDP in ABAQUS using the defaults value in ABAQUS provided good match with the experimental data. However, no parametric study conducted.

Alosta et al. (2017) numerically studied the behavior of RC beams strengthened with two sided epoxied UHPC panels. The model validated using previous experimental work. The model used to study the behavior of the strengthened beam with different UHPC panels thicknesses. The results show a positive relation between the thickness of panel and the ductility of the strengthened beam.

Abuodeh and Abed (2019) using ABAQUS to model the behavior of UHPC beam reinforced with high strength steel (HSS). After that, the model was used to investigate the effect of varying the beam depth and the reinforcing ratio on the moment-deflection response. The results show that the depth of the beam is the main parameter contributing in the FEM accuracy.

Zhu et al. (2019) used ABAQUS to investigate the behavior of damage slabs strengthened with UHPC. The model was validated using experimental test data. The FEM results show a good agreement with the experimental results. The model then used to investigate the strengthening effect and optimize the strengthening parameters.

Shirai et al. (2020) used FEM approach to investigate the behavior of RC beam strengthened with UHPC. The results used to develop a model can predict the flexural capacity. The prediction results show good match with experimental test.

2.7 Summary.

Based on the literature survey the following points summarize the main collected information:

- The joints behave as the stress concentrations points in the structure; due to the high principal shear and axial stress. The effects of these stresses lead to the formation of diagonal cracks in the joints or concrete crushing. This makes the joint vulnerable and critical region that can control the overall behavior of the frame.

- Traditionally, the sway-special design requirements are used in seismic design. Although the sway-special design requirements show some effectiveness, they are complex and difficult to implement. The required closely spaced transverse reinforcements and the assemblage of many types of longitudinal reinforcements cause difficulties in implementations. Therefore, they not laid out as in design plan as mentioned by Gencoglu and Eren (2002). Thus, researchers try to improve joints behavior using hybrid fiber reinforced material include SFRC, HSFRC and UHPFRC.
- The UHPFRC shows preferences in terms of compressive and tensile behavior in addition to high durability comparing with the other fiber reinforced material.
- While UHPC material has the higher cost comparing with HSC and NC, it has the lower cyclic-life costs as investigated by Racky (2004).
- There are many types of UHPC products with different tensile behavior. A unified definition proposed by FHWA state that UHPC material must have a multi-crack zone in its tensile behavior. Based on this definition, six UHPC classes (products) were approved (recognized as UA through UF).

- The results obtained by Hung et al. (2018), the use of 1.5% volumetric fracture of fibers can compensate 70% of the required transverse reinforcements with no losing in ductility, can improved using UHPC material with better tensile performance and higher volumetric fracture of fiber such as the products approved by FHWA.
- The UHPC class B with 2% volumetric fracture of fibers shows preferences in term of tensile behavior comparing with the other classes with same amount of fibers.
- Three techniques were used to strengthening the joint using UHPC which are using UHPC in the joint intersection, UHPC plate attached using epoxied material or sand-blasting concrete surface and in-situ cast UHPC jacket using moulds, and using UHPC in the joint intersection and the zone of expected plastic hinges in beam and columns. Although all these studies investigated enhancements on the behavior of the joint strengthened using UHPC, these investigations do not followed with parametric studies to generalize the results. In addition, the geometry of the specimens were not cover the lower limit of column to beam moment capacity (CBM) ratio. Furthermore, the UHCP material used in the study do not approved by FHWA.
- Extensive numerical researches were conducted on investigation the behavior of RC structures strengthened with UHPC. These

researches assure the ability of concrete damage plasticity (CDP) model provided in ABAQUS to captured the quasi-static behavior of RC and UHPC.

Based on the previous points, limited studies are conducted on strengthening the joints with UHCP with no evidence about the behavior of joint strengthened with UHPC at lower CBM ratio. In addition, there are no studies on the behavior of the UHCP products approved by the FHWA. Furthermore, the sway-special moment resisting design requirements do not considered in many studies. Therefore, this research will use the UHPC class B as recognized by FHWA with 2% volumetric fracture of fibers to improve ductility behavior of the sway-special exterior BCJs. The study will conducted numerically, the CDP model provided in ABAQUS will be used to build a 3-D non-linear model of exterior BCJ. The experimental tests conducted by Alkhatib (2015) will be used to validate the model. After that, a matrix of the main parameters affecting the joints behavior will be used to compare the behavior of the joints strengthened with UHPC in the intersection zone and the sway-special (SP) designed joints. The beams and columns will design according to the ACI-318 code regarding to the SMRF requirements.

The next chapter presents the modeling procedure, which include both the geometry and the material.

CHAPTER THREE:

3. MODELING.

3.1 Overview.

As mentioned in Chapter One, the main goals of this study are to numerically improve ductility behavior of sway-special exterior BCJ using UHPC. F.E structural investigation is widely used since it offers an attractive alternative to experiments with low cost and quick results. This chapter clarifies the steps of modeling such joints using commercial finite element compute program (ABAQUS). ABAQUS user's manual (2011) is used to gather the information related to modeling procedures.

3.2 Modeling Procedure.

3.2.1 ABAQUS Definition and Analysis Type

ABAQUS is a commercial engineering software package for finite element analysis. Typically complete ABAQUS environment CAE consists of four cores: ABAQUS standard (implicit), ABAQUS explicit, ABAQUS computational fluid dynamics CFD and ABAQUS electromagnetics. In this study, ABAQUS implicit is used to analyze the models since it needs less efforts in modeling.

3.2.2 Geometry of the Model.

The model geometry is developed using a set of parts including beam, columns, joint and loading plates, in addition to reinforcements. The beam, column, joint and loading plate are modeled as 3-D solid elements while the reinforcements (longitudinal, transverse) are modeled as truss elements.

3.2.3 Element Type.

An Eight-noded linear brick element (C3D8R) is used to model the solid elements including beam, columns and loading plate. While a 2-node linear 3-D truss element is used to model the reinforcement (longitudinal and transverse) (T3D2).

3.2.4 Loading plates

Three loading plates are applied to avoid the excessive stresses in the two columns ends and the tip of the beam for monotonic loading, while additional loading plate in the opposite tip of beam for cyclic loading. In addition, additional transverse reinforcements are used in the tip beam and column zones.

3.2.5 Boundary Conditions.

Half of the columns are modeled. Hence, the boundary conditions at the mid section are assumed pins. Thus, the bottom surface was pinned at the line nodes at the center, while the top surface where released to move at Y-direction.

3.2.6 Loading Steps and Increments Size.

Three steps are used which are initial step to introduce the boundary conditions, axial loading step to simulate the normal stresses in the column and push-over step to applied a monotonic displacement. Moreover, the number and size of increments are specified for each step. ABAQUS divides the load to increments and calculate the response at each increments. If a small number of increments is specified, the ABAQUS may miss key events in the response like the point of yielding which may lead to inaccurate load-deformation curves. Hence, large number of increments are specified (10000)with very small increments size (up to E-35).

3.2.7 Applying the Axial load.

The axial load is applied to the top surface of the column as uniform pressure in the global coordinates. Thus, the loads are applied as nodes load. For instant, the corner and the side nodes have quarter and half the loads of the middles nodes.

3.2.8 Surfaces and Reinforcements constrains.

The connections between the surface are idealized and assumed fully tied, while the reinforcements are assumed to be imbedded in the host material (concrete and/ or UHPC). This means that no slippage occurs between the reinforcements bars and the concrete. Thus, the development lengths are assumed to be satisfied.

Finally, Figure 3.1 shows the boundary condition and the loadings plates used in modeling.

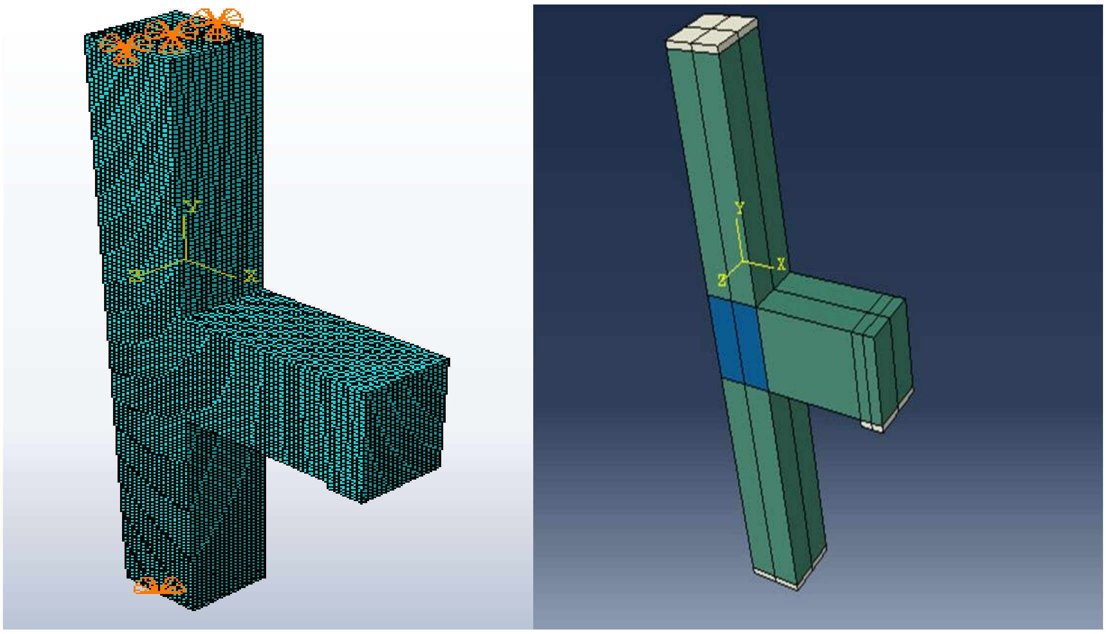

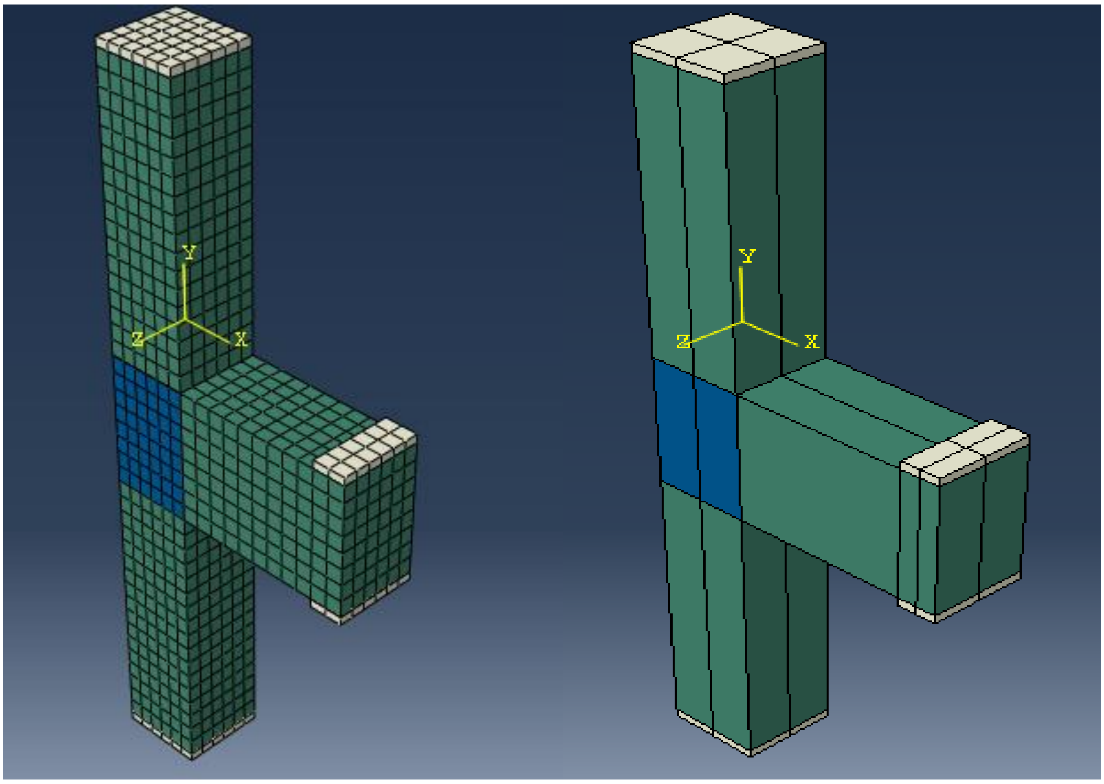

Figure 3. 1: The Boundary condition (B.C) Used in Modeling.

3.3 Materials Modeling.

Concrete and UHPC are heterogeneous materials. In other words, it is not easy to describe their behaviors without knowing their components. Also crushing and cracking affect the strength and the stiffness of the material at different stage of loadings. However, there are many proposed models to capture the behavior of such brittle materials in ABAQUS. These models mainly include concrete damage plasticity CDP model and concrete smeared cracks CSC model. CDP model can be used under cyclic and monotonic loadings while the CSC is suitable to use under monotonic loading only. Moreover, the CDP models incorporate a set of damage parameters that can trace the progress of crack patterns. While, CSC does not have this capability. Hence, CDP is used to capture the behavior of concrete and UHPC.

Briefly, to define the CDP model for concrete and UHPC, a set of input data are needed in addition to the stress-inelastic strain curve and the damage-inelastic strain curve.

Table 3.1 summarizes the parameters that use in defining CDP with defaults values assumed by ABAQUS. These values are common used by researchers include (**Alkhatib 2015** and **Alosta and Khan 2018**). While the modules of Elasticity and Poissons ratio are captured from the literature.

Table 3. 1: Parameters Defaults Values for CDP Model in ABAQUS.

Parameter symbol	ϵ	φ	σ_{b0}/σ_{c0}	K_c	ω_t	ω_c
NC	0.1	$36°$	1.16	0.67	0	1
UHPC	0.1	$36°$	1.16	0.67	0	1

Where:

$(\sigma_{b0}/\sigma_{c0})$ Or (f_{b0}/f_{c0}): The ratio of the biaxial stresses to the uniaxial stresses, ABAQUS default uses the value of 1.16 consistent with the value obtained experimentally by **Kupfer (1969),** this value is user defined.

K_c: A parameter to define the shape of the plane of failure in the three parameters **Willam** and **Warnke (1975)** yield surface, $K_c$is defined as the ratio of the second stress invariant on the tensile meridian to that on the compressive meridian which is recommended to use a value of 0.67 by ABAQUS.

ϵ: Eccentricity parameters, it is define the rate at which the $\bar{p}$ - $\bar{q}$ plane line approach the asymptote line, ABAQUS defaults use a value of 0.1, as the eccentricity go to zero the $\bar{p}$ - $\bar{q}$ become straight line consistence with the conventional **Drucker-Prager** model.

φ: It is the dilation angle measured in the $\bar{p}$ - $\bar{q}$ plane at high confinement pressure. ABAQUS default use 36° which is consistent with the recommended of φ by **Kmiecik and Kaminski (2011).**

ω_c and ω_t: Recovery Parameters. under cyclic load when load change from tension to compression and vice versa, the model assumes a recovery for compression capacity upon the closure of the tensile cracks. On the other hand, the tensile capacity is not recovered after the compressive crushing of the material, these assumptions were included in ABAQUS through the two recovery parameters ω_c and ω_t.

The stress-strain model proposed by **Saenz (1964)** is used to describe the uniaxial compression behavior for the ordinary concrete in compression. **Figure 3.2** shows the compression stress-inelastic strain curve for concrete with compressive strength 28 MPa. In addition, While **Figures 3.3** shows the tension stress-inelastic strain curve which constructed using the modified **Nayal and Rasheed (2006)** model.

For UHPC, the experimental tests conducted by **FHWA** for the UHPC class B with 2% fiber content are used to describe the uniaxial stress strain behavior for both compression and tension. **Figures 3.4** shows the UHPC compression stress-inelastic strain curves. While **Figures 3.5** shows the tensile stress-inelastic strain curve.

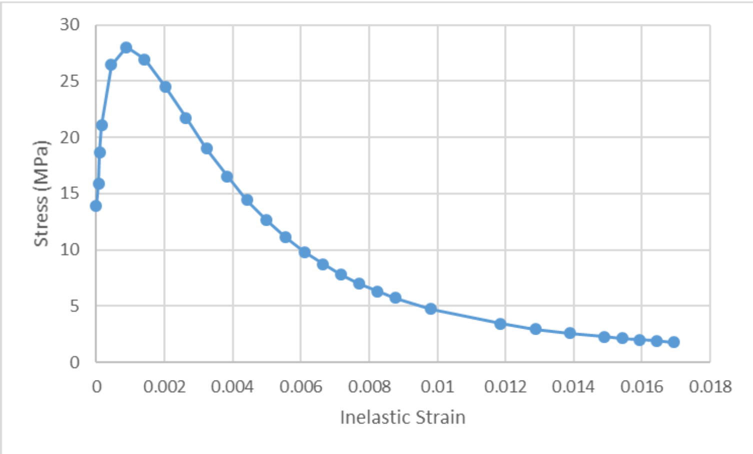

Figure 3. 2: Concrete 28 MPa Compression Stress-Inelastic Strain Curve Conducted Using Saenz model (1964).

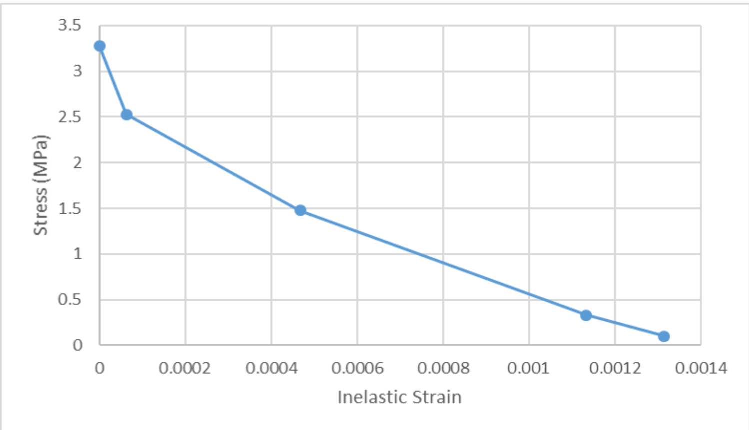

Figure 3. 3: Tensile Stress-Inelastic Strain Curve for Concrete 28 MPa Conducted Using Modified Nayal and Rasheed model (2006).

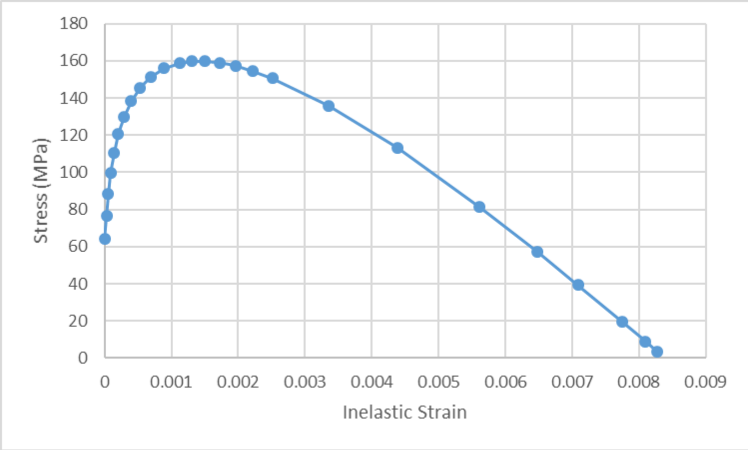

Figure 3. 4: UHPC Class B Compression Stress-Inelastic Strain Curve.

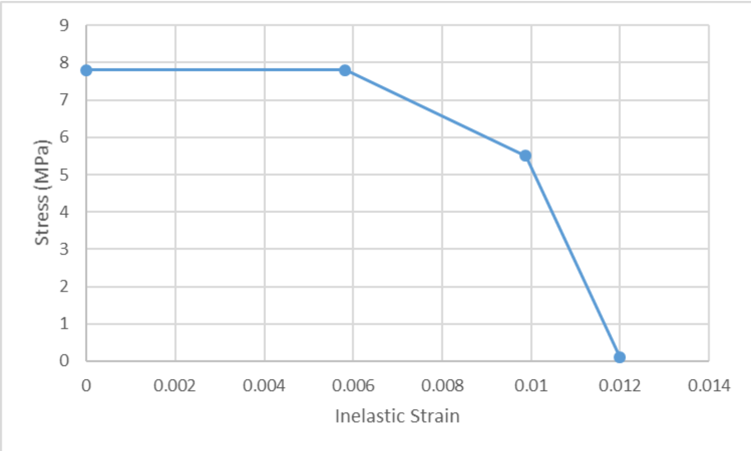

Figure 3. 5: UHPC Class B Tension Stress-Inelastic Strain Curve.

The tension damage d_t and compression damage d_c are used to characterize the degradation in strength and stiffness in the softening behavior of the material. Hence, defining the damage parameters is important. However, there are many models to evaluate the damage including **Luccioni et al. (1996)** model, **Jankowiak** and **Łodygowski (2013)** model and **Burlion et al. (2000**) model. **Birtel and Mark** (2006) proposed a new model to evaluate the damage parameters for modeling the shear failure. The evaluation of the damage parameters was linked to the crossponding plastic strain which is assumed to be proportional to the inelastic strain with constant factor b_t for tension and b_c for compression. **Birtel and Mark (2006)** suggested that a value of 0.7 for b_c and 0.1 for b_t are fitting well with the experimental results. However, the proposed value for b_t can yield in negative or decreasing value of plastic strain. Hence, a value of 0.7 is often used to evaluate the tension damage (**Nasrin et al. 2017, Al-Osta et al. 2018 and Khan et al. 2018**). **Figures 3.6.a** and **3.6.b** show the effect of varying b_t on the damage parameter for concrete and UHPC, respectively. **Equations 3.1** and **3.2** present the uniaxial damage evaluation for Birtel and Mark (2006) tension and compression damages, respectively. This model is used to evaluate the damage parameters for concrete and UHPC.

$$d_t = 1 - \frac{\sigma_t E_c^{-1}}{\tilde{\varepsilon}_t^{pl}\left(\frac{1}{b_t} - 1\right) + \sigma_t E_c^{-1}} \qquad [3.1]$$

$$d_c = 1 - \frac{\sigma_c E_c^{-1}}{\tilde{\varepsilon}_c^{pl}\left(\frac{1}{b_c} - 1\right) + \sigma_c E_c^{-1}} \qquad [3.2]$$

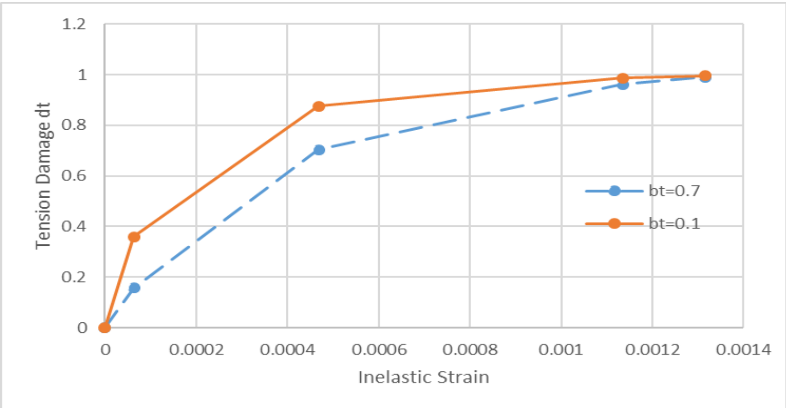

(a)

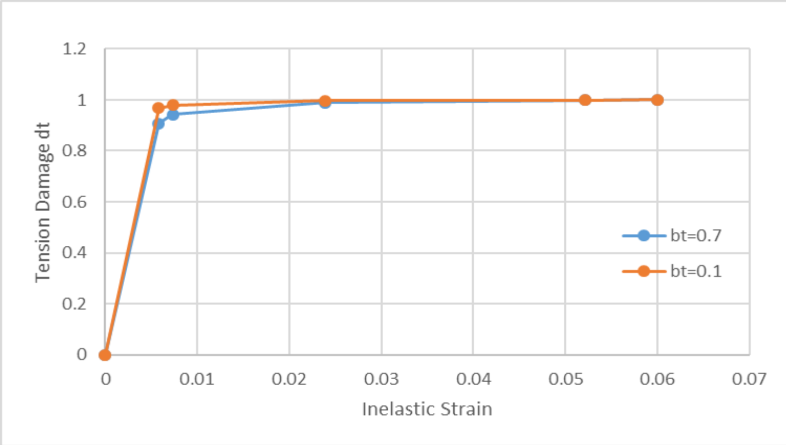

(b)

Figure 3. 6: Effect of variation b_t in the tension damage parameter d_t for: (a) Concrete and (b) UHPC.

Figures 3.7 and **3.8** show the damage-inelastic strain curves for concrete under tension and compression, respectively. While **Figures 3.9** and **3.10** show the damage-inelastic strain curves for UHPC.

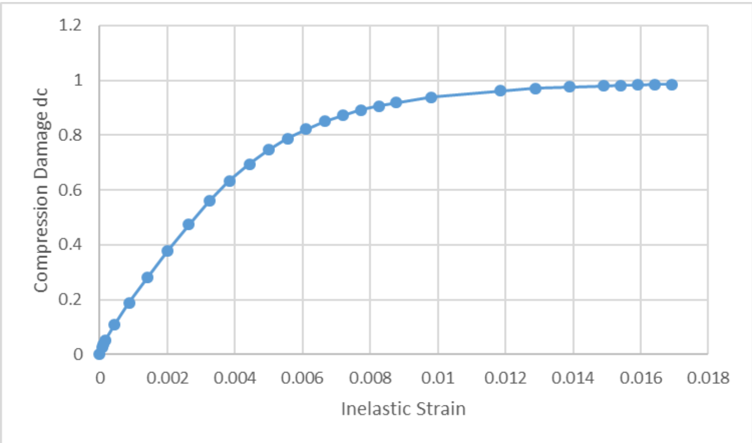

Figure 3. 7: Compression Damage-Inelastic Strain for Concrete 28 MPa.

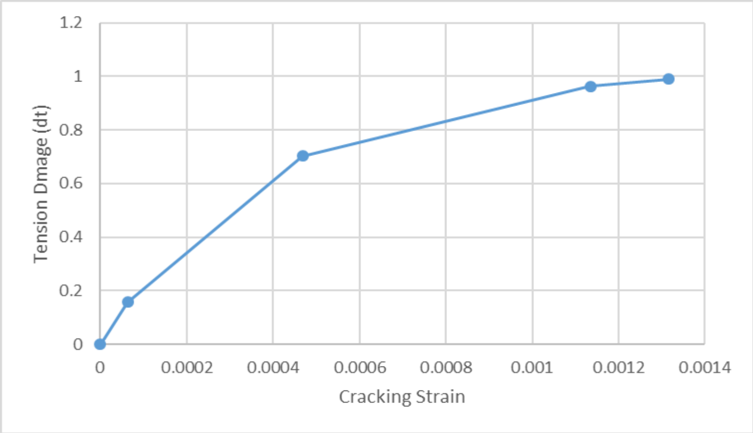

Figure 3. 8: Tension Damage-Inelastic Strain Curve for Concrete 28 MPa.

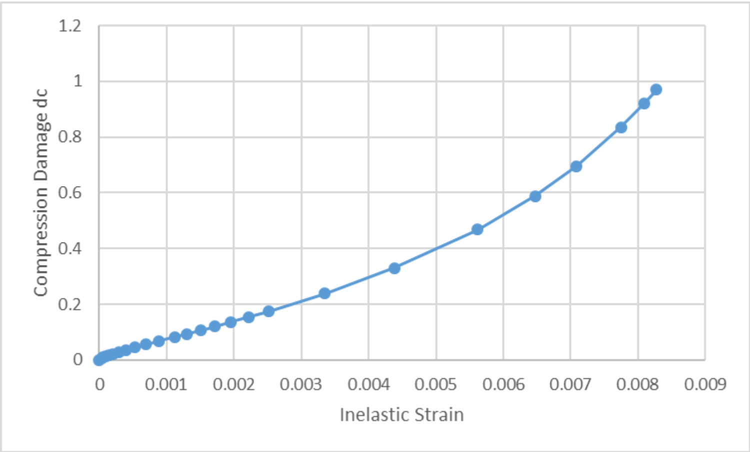

Figure 3. 9: UHPC Class B Compression Damage-Inelastic Strain Curve.

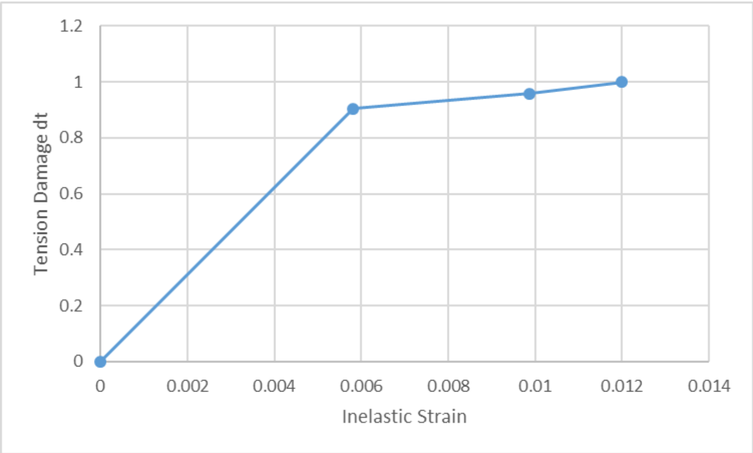

Figure 3. 10: UHPC Class B Tension Damage-Inelastic Strain Curve.

Finally, an elastic-perfectly plastic model for steel grade 60 (420 MPa) is used for simplicity as shown in **Figure 3.11**. The fracture strain of the steel was captured from local laps and it was taken as 0.0018.

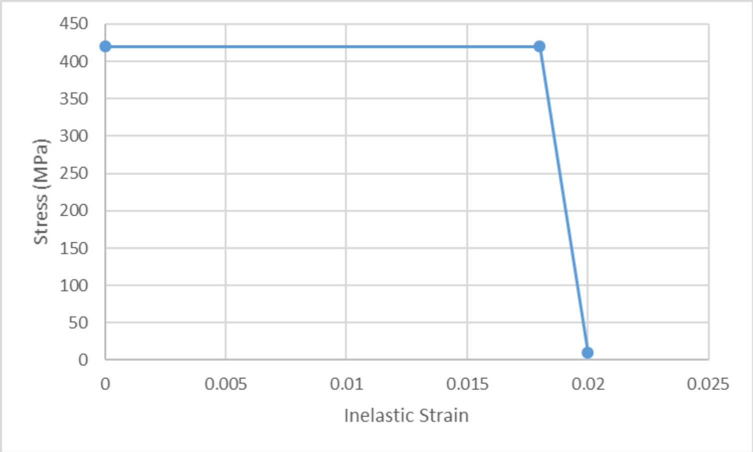

Figure 3. 11: Stress-Inelastic Strain Curve for Grade 60 Steel.

CHAPTER FOUR

4. MODEL VALIDATION.

4.1 Overview.

A Beam-column joint model is developed and verified by use of experimental results of Alkhatib (2015) that was introduced in Chapter Two. Two representative specimens were selected to develop and validate the model, namely UHPC-18MM-BCJ and NC-18MM-BCJ. Sensitivity study is conducted to obtain the suitable mesh size of the model as shown in the following section.

4.2 Sensitivity Study.

In order to get an optimized mesh size that balances solution time effort and the results precision, a sensitivity study using a mesh size of 20 through 50 was performed. Material properties are assumed as reported in **Alkhatib (2015)** thesis. **Figure 4.1** shows a comparison in results for all mesh size tried, it is clear that the resulting curves stabilize at mesh size 25 mm which is considered in this work.

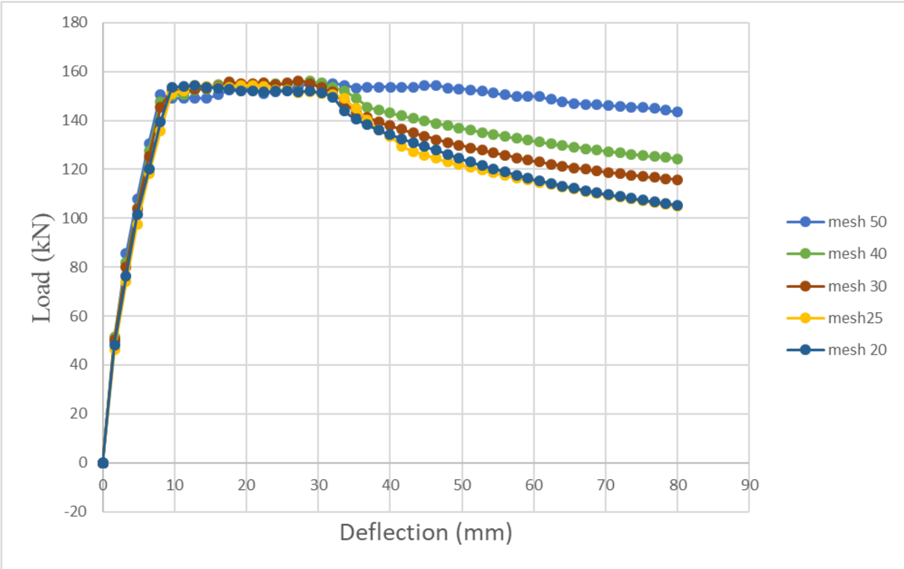

Figure 4. 1: Effect of mesh size.

4.3 Experiments by Alkhatib (2015).

The specimens have identical reinforcement details and dimensions as illustrated in **Figures 2.21** and **2.22**. The compressive behavior of NSC and UHPC used are shown in **Figure 4.2** and **4.3**, respectively. While **Figure 4.4** shows the tensile stress-strain behavior for UHPC and NC.

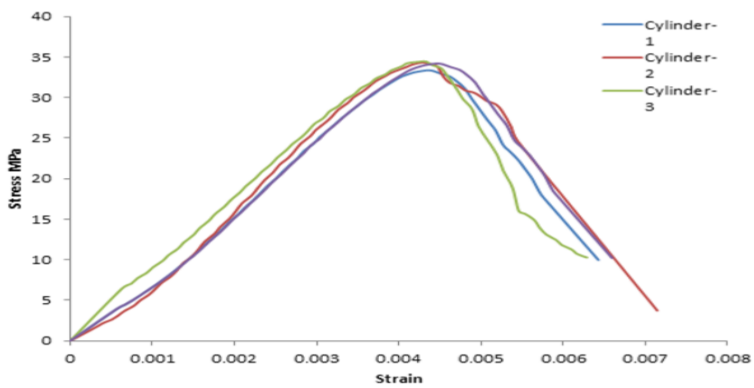

Figure 4. 2: Experimental Compressive Stress-Strain Curve for Normal Concrete. (Alkhatib 2015).

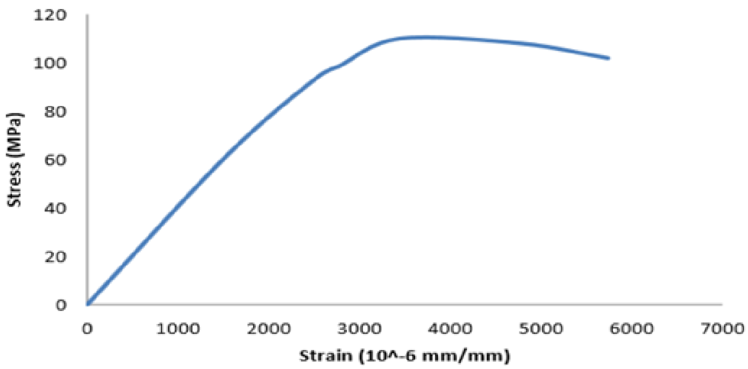

Figure 4. 3: Experimental Compressive Stress-Strain Curve for UHPC. (Alkhatib 2015).

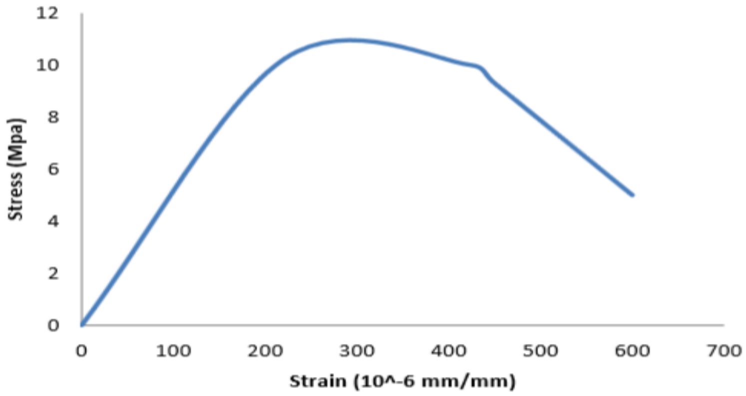

a) Expermental Tensile Stress-Strain Curve for UHPC. (Alkhatib 2015).

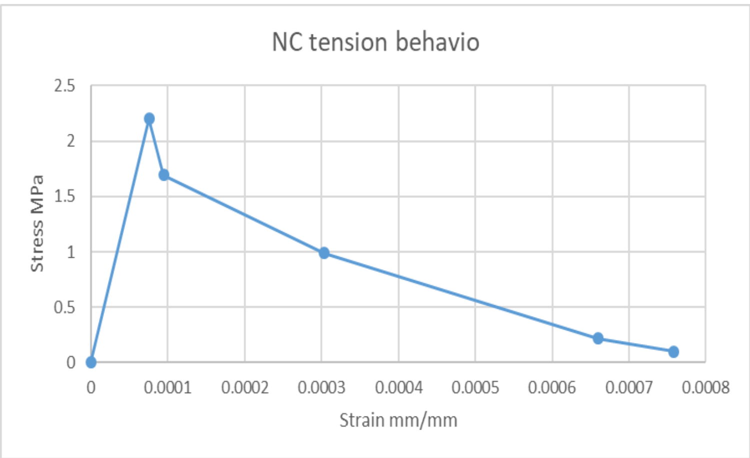

b) Tensile behavior for NC Using Nayal and Rasheed (2006) Model.

Figure 4. 4: Tensile Stress-Strain Behavior for (a) UHPC and (b) Normal Concrete. (Alkhatib 2015).

The reinforcements (longitudinal and transverse) properties used in the experimental is shown in **Table 4.1**. The tensile strength test for the longitudinal bars was conducted as shown in **Figure 4.5**. **Figure 4.6** shows the stress-plastic strain used in ABAQUS modeling for all bars, all the steel bars have modulus of elasticity (E_s) 200 GPa and poisson's ratio ($v = 0.3$). A bi-linear stress-strain model is used to describe the hardening behavior in the transverse reinforcements with slope hardening of 0.01 E_s as proposed by **Elmezaini and Ashour (2015)**.

Table 4. 1: Properties of Reinforcement Bars Used in Alkhatib (2015) tests.

Bar diameter (mm)	Cross section area (mm^2)	Yield strength (MPa)	Ultimate strength (MPa)
8	50.24	420	620
18	254	610	670

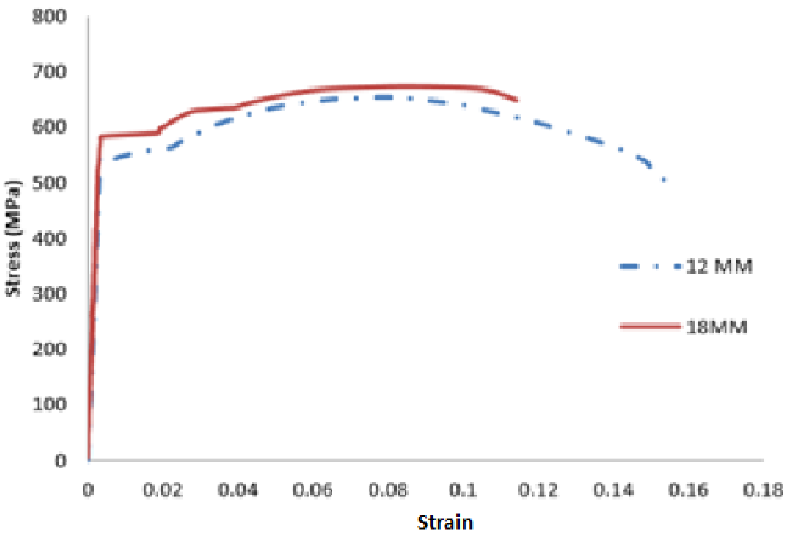

Figure 4. 5: Tensile Stress-Strain Behavior for Longitudinal Bars. (Alkhatib 2015).

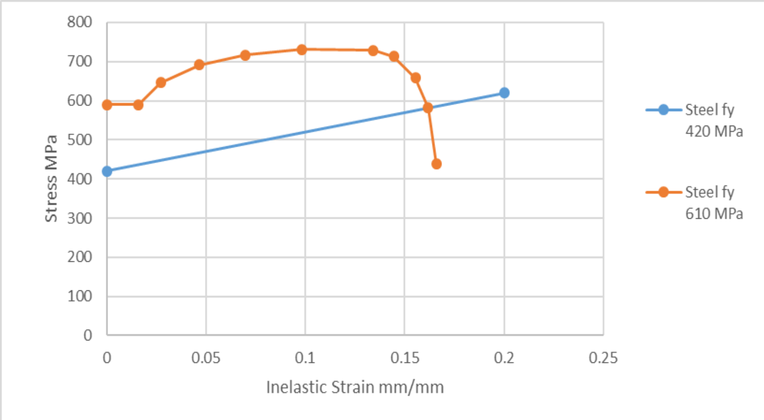

Figure 4. 6: Tensile Stress-Plastic Strain Curves Used in ABAQUS Modeling. (Alkhatib 2015).

Briefly, to define the CDP model for NC and UHPC in tension and compression, the stress-inelastic strain and damage-inelastic strain are needed. **Figures 4.7** and **4.8** show the stress and damage values against inelastic strain in tension and compression for NC and UHPC respectively. **Table 4.2** summarized the main parameters used in defining the CDP model for both concrete and UHPC, these parameters include reported material properties: modulus of elasticity and poisson's ratio, and others captured from literature include: dilation angle ψ, K_c, f_{b0}/f_{c0} and the eccentricity.

Table 4. 2: Parameters Used to Define CDP Model for Material Used by Alkhatib (2015).

Material	Modulus of Elasticity E(MPa)	Poisson's Ratio	Dilation Angle ψ	K_c	σ_{b0}/σ_{c0}
NC Concrete	29000	0.2	360	0.67	1.16
UHPC	40000	0.2	360	0.67	1.16

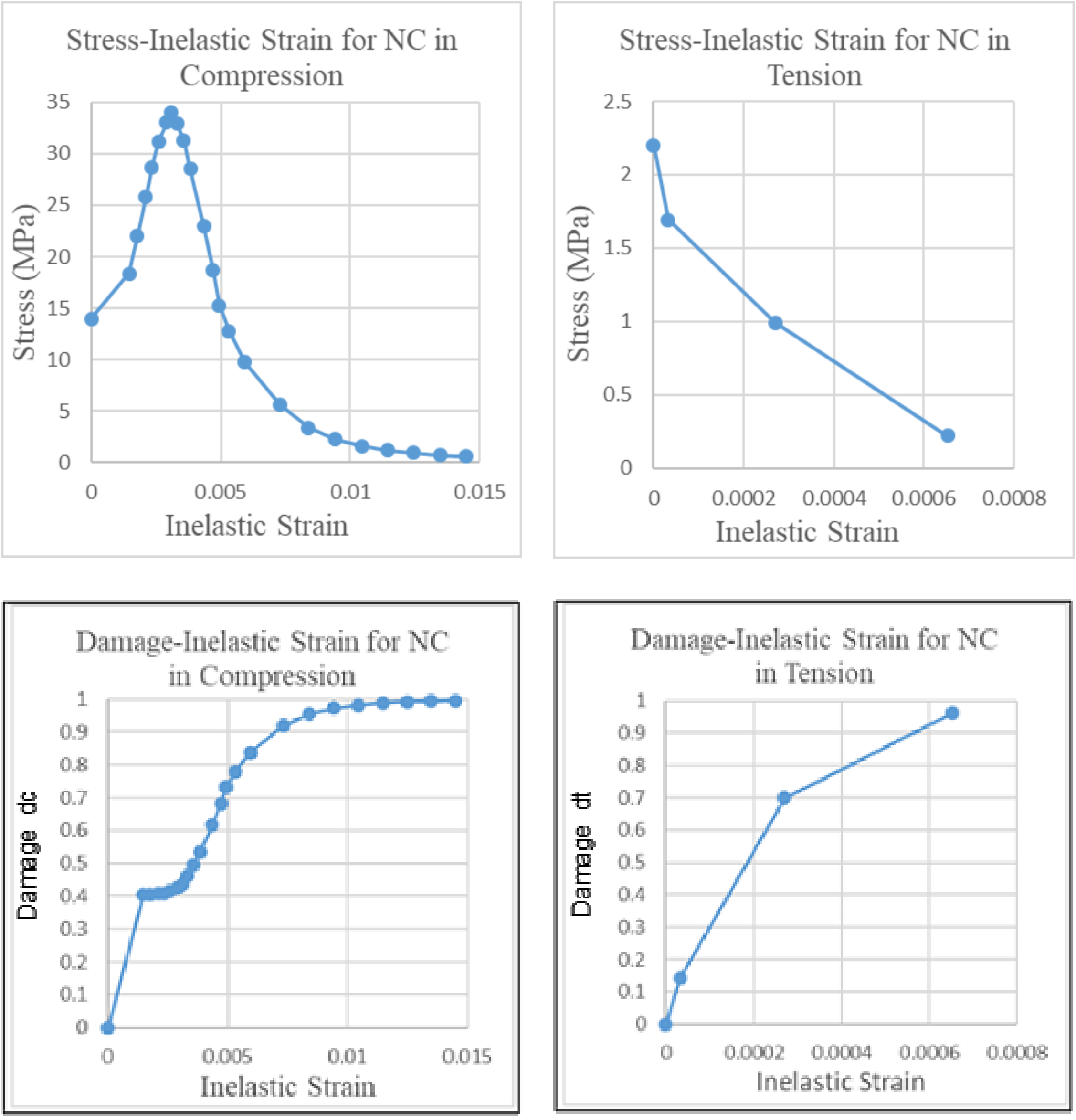

Figure 4. 7: Curves for Define NC in ABAQUS for Specimens Tested by Alkhatib (2015).

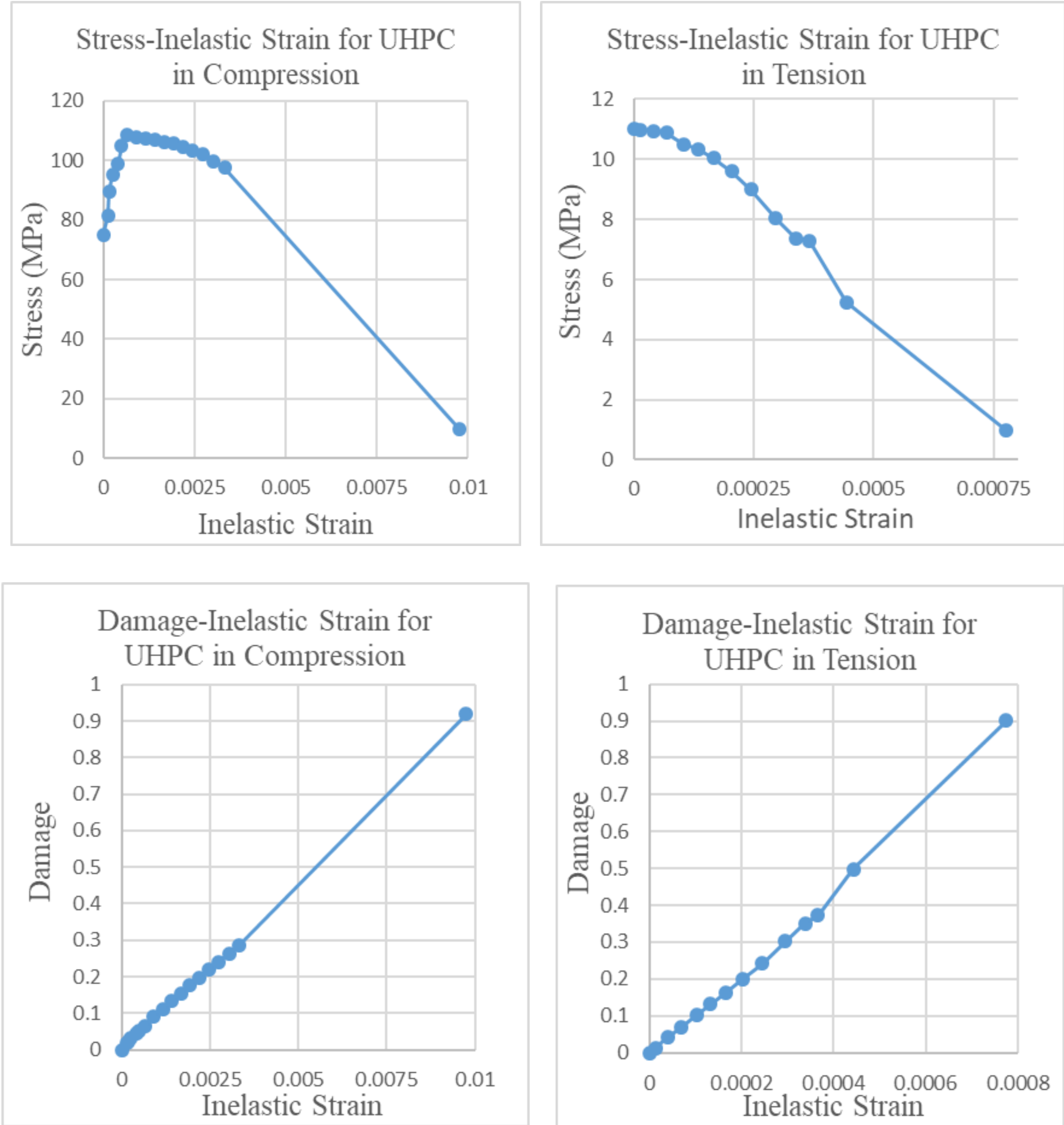

Figure 4. 8: Curves for Define UHPC in ABAQUS for Specimens Tested by Alkhatib (2015).

The specimens were subjected to constant axial load of 150 (kN). After that, the response is traced under monotonic loading (displacement control). The boundary conditions is assumed to resist rotations based on the test conditions shown in **Figure 2.23**. **Figure 4.9** shows the boundary conditions introduced at column ends.

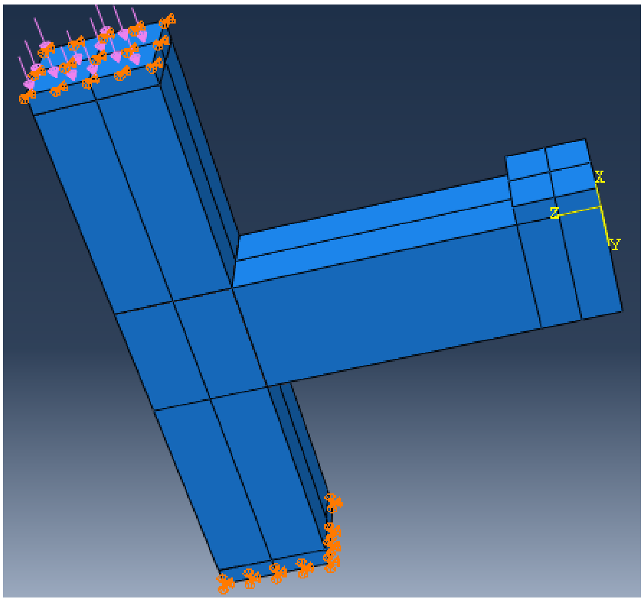

Figure 4. 9: ABAQUS Simulation for Specimens UHPC1-18MM and NC-18MM Alkhatib (2015).

Finally, a comparison between the F.E and experimental results for specimens NC-BCJ-18mm and UHPC-BCJ-18MM are shown in **Figures 4.10** and **4.11**, respectively.

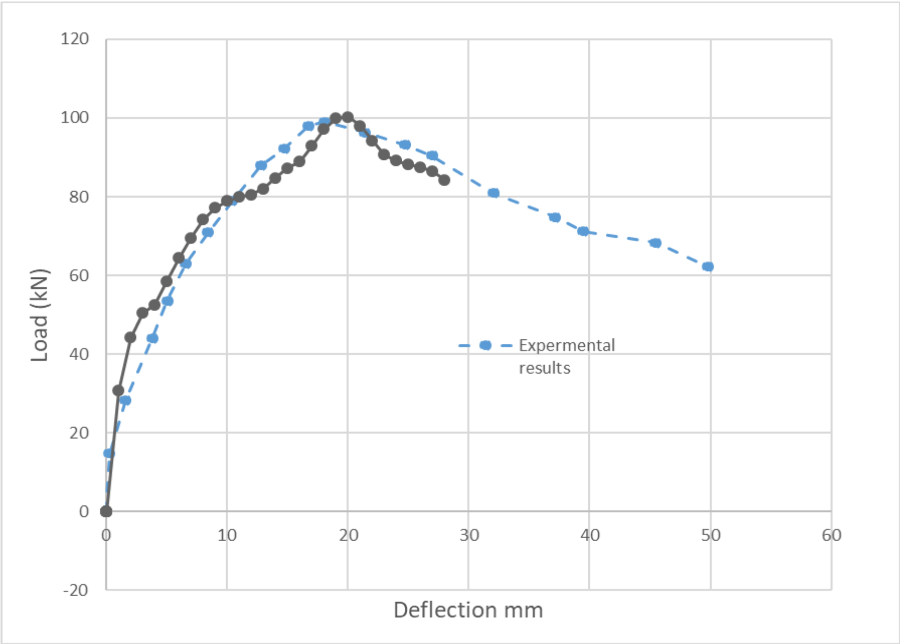

Figure 4. 10: Comparison between F.E and Experimental Results for Specimens NC-18MM tested by Alkhatib (2015).

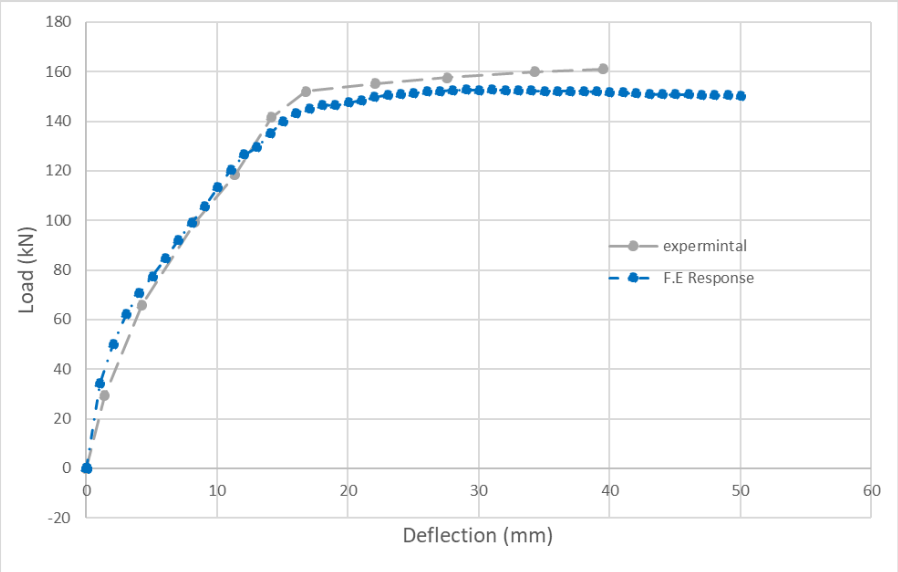

Figure 4. 11: Comparison between F.E and Experimental Results for Specimen UHPC-18MM Tested by Anas Alkhatib (2015).

The comparisons show that the model almost captured the overall behavior of the experiments. This approach of validation were widely used by many researchers as presented in the literature review. This model will be used to investigate the main features that affect ductility behavior of BCJ. The main factors will be discussed and tabulated next section.

4.4 Parametric Study.

4.4.1 General.

In order to study the behavior of the exterior beam column joints strengthened with UHPC. The key factors affecting the joints behaviors are first gathered from the literature and the concepts of structural mechanics. These factors are divided into three branches which are factors affecting the shear capacity of the joints, factors affecting the development length of the reinforcements bars and others affecting the column to beam moment capacity (CBM) ratios. However, the sway special design requires avoiding brittle failures using considerable amount of transverse reinforcements and providing sufficient development length. Thus, the factors which characterize the CBM ratio are considered. These factors include beam to column depth ratio (BCDR), the longitudinal reinforcements in columns (ρ_c) and the axial load ratio (ALR) in columns. However, other factors include the longitudinal reinforcements in the beams (assumed 0.5% and 1% for compression and tension, respectively), beam moment to shear (M/V) ratio (kept at one) and the arrangements of stirrups in column were not considered due to time limitations. Furthermore, **Table 4.3** presents the constant dimensions in the BCJ.

Table 4. 3: Constant Dimensions in the System.

Dimension	Value (m)
Floor Clear Elevation.	3.4
Width of the Column	0.5
Depth of the Column	0.5
Width of the Beam	0.5

Finally, the next section shows the range of parameters considered and the parametric matrix conducted based on these parameters.

4.4.2 Range of Parameters.

In this research, a total of 40 simulations are made to investigate the ductility of using UHPC in BCJ and check the ability of UHPC to improve the ductility behavior of sway-special exterior BCJs without using the sway special transverse reinforcements detailings.

As presented in the previous sections, three key parameters affecting the CBM ratio are considered. Each simulation is given a representative name consist of four syllable's. These syllable's are shown in **Table 4.4**. These syllable's present the type of the joint, the BCDR, (ρ_c) and ALR. For instant, the simulations (UB2-BCDR 1.6-L1-ALR 0.25) means that material UB2 is used in strengthening the joints with BCDR equal 1.6, ρ_c equal 1% and ALR equal 0.25. Another simulation is SP-BCDR 1.4-L1-ALR 0.50, this name means a control sway-special detailings joint with BCDR 1.4, ρ_c 1%, ALR 0.5. Finally, **Table 4.5** shows the variable properties for all models conducted in this study.

Table 4. 4: The Value of the Key Factors Affected the Joints Behavior in the Study.

Parameter	Value	Denoted as
Joint Type	$\grave{f}_c = 28$ MPa Sway Special Detailings	SP
	UHPC Class B with 2% Fiber Contents.	UB2
Beam to Column Depth Ratio (BCDR), the value represents the beam depth (mm) since the column depth is constant at 500 mm.	300	BCDR 0.6
	500	BCDR 1.0
	600	BCDR 1.2
	700	BCDR 1.4
	800	BCDR 1.6
Longitudinal reinforcement ratio in the column (ρ_c)	1%	L1
	2%	L2
Axial Load Ratio (ALR). The compressive strength for the concrete is 28 MPa. Thus, the value presents the normal stresses in the column	0.25	ALR 0.25
	0.50	ALR 0.50

Table 4. 5: Variable Properties for all Model

Model ID	Joint Type	BCDR	ρ_c	ALR
SP-BCDR 0.6-L1-ALR 0.25	SP	0.6	1%	0.25
SP-BCDR 0.6-L1-ALR 05	SP	0.6	1%	0.5
SP-BCDR 0.6-L2-ALR 0.25	SP	0.6	2%	0.25
SP-BCDR 0.6-L2-ALR 0.5	SP	0.6	2%	0.5
UB2-BCDR 0.6-L1-ALR 0.25	UB2	0.6	1%	0.25
UB2-BCDR 0.6-L1-ALR 05	UB2	0.6	1%	0.5
UB2-BCDR 0.6-L2-ALR 0.25	UB2	0.6	2%	0.25
UB2-BCDR 0.6-L2-ALR 0.5	UB2	0.6	2%	0.5
SP-BCDR 1-L1-ALR 0.25	SP	1	1%	0.25
SP-BCDR 1-L1-ALR 05	SP	1	1%	0.5
SP-BCDR 1-L2-ALR 0.25	SP	1	2%	0.25
SP-BCDR 1-L2-ALR 0.5	SP	1	2%	0.5
UB2-BCDR 1-L1-ALR 0.25	UB2	1	1%	0.25
UB2-BCDR 1-L1-ALR 05	UB2	1	1%	0.5
UB2-BCDR 1-L2-ALR 0.25	UB2	1	2%	0.25
UB2-BCDR 1-L2-ALR 0.5	UB2	1	2%	0.5
SP-BCDR 1.2-L1-ALR 0.25	SP	1.2	1%	0.25
SP-BCDR 1.2-L1-ALR 05	SP	1.2	1%	0.5
SP-BCDR 1.2-L2-ALR 0.25	SP	1.2	2%	0.25
SP-BCDR 1.2-L2-ALR 0.5	SP	1.2	2%	0.5
UB2-BCDR 1.2-L1-ALR 0.25	UB2	1.2	1%	0.25
UB2-BCDR 1.2-L1-ALR 05	UB2	1.2	1%	0.5
UB2-BCDR 1.2-L2-ALR 0.25	UB2	1.2	2%	0.25
UB2-BCDR 1.2-L2-ALR 0.5	UB2	1.2	2%	0.5
SP-BCDR 1.4-L1-ALR 0.25	SP	1.4	1%	0.25
SP-BCDR 1.4-L1-ALR 05	SP	1.4	1%	0.5
SP-BCDR 1.4-L2-ALR 0.25	SP	1.4	2%	0.25
SP-BCDR 1.4-L2-ALR 0.5	SP	1.4	2%	0.5
UB2-BCDR 1.4-L1-ALR 0.25	UB2	1.4	1%	0.25
UB2-BCDR 1.4-L1-ALR 05	UB2	1.4	1%	0.5
UB2-BCDR 1.4-L2-ALR 0.25	UB2	1.4	2%	0.25
UB2-BCDR 1.4-L2-ALR 0.5	UB2	1.4	2%	0.5
SP-BCDR 1.6-L1-ALR 0.25	SP	1.6	1%	0.25
SP-BCDR 1.6-L1-ALR 05	SP	1.6	1%	0.5
SP-BCDR 1.6-L2-ALR 0.25	SP	1.6	2%	0.25
SP-BCDR 1.6-L2-ALR 0.5	SP	1.6	2%	0.5
UB2-BCDR 1.6-L1-ALR 0.25	UB2	1.6	1%	0.25
UB2-BCDR 1.6-L1-ALR 05	UB2	1.6	1%	0.5
UB2-BCDR 1.6-L2-ALR 0.25	UB2	1.6	2%	0.25
UB2-BCDR 1.6-L2-ALR 0.5	UB2	1.6	2%	0.5

CHAPTER FIVE

5. RESULTS AND DISCUSSION.

5.1 Overview.

This chapter represents the main results of the simulations from ABAQUS. The results include the load-deflection curves for all simulations. In addition, comparisons that show the effects of parameters are conducted, these curves are used later to evaluate the displacement ductility of the joints for each models.

5.2 General Behavior of Beam Column Joints.

Figure 5.1 shows the general behavior for typical beam column joints. As shown, the behavior of the joint is initially linear elastic up to the first tension cracks on the tension zone close to the beam-column interface which could be noticed by a simple drop in load due to the loses of the tension capacity of concrete. Then, the tension forces are resisted by the tensile reinforcement where the beam behavior continues elastically until the tensile steel yielded. After this stage, brittle shear failure or ductile flexure failure could happen depending on reinforcement details and joint capacity as mentioned by **Abu Tahnat et al. (2018).**

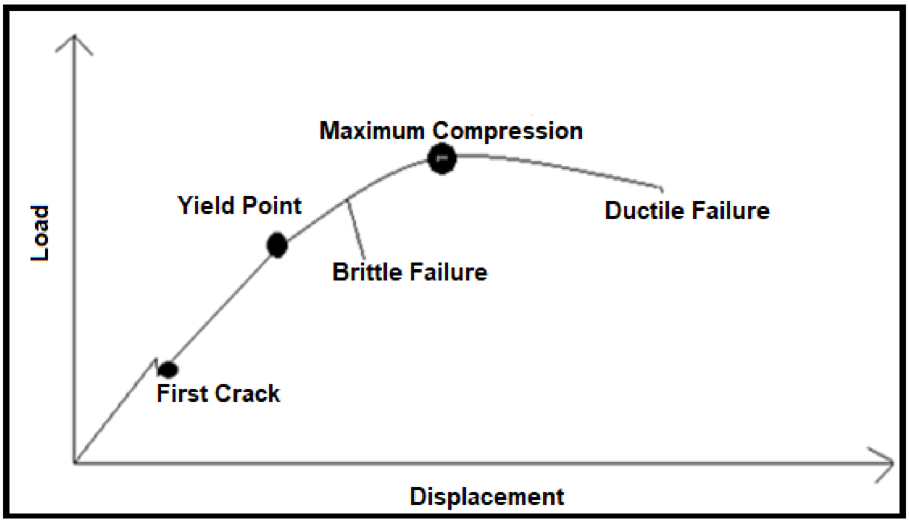

Figure 5. 1: Typical Load-Deflection Curve for Beam-Column Joints (Abu Tahnat et al. 2018).

5.3 Failure Criteria.

Referring to section 2.3 in this thesis, there are many approaches to define the ductility. The method proposed by Cohn and Bartlett (1982) is adopted and explained here. The displacement ductility of the joint is the ratio between the ultimate deflection and the yield deflection. The ultimate deflection is defined as a deflection crossponding to a 15% reduction of the peak load in the post peak value unless a cutting in the reinforcement bars occurs, which crossponds to a strain equals 0.18, while the yield deflection is defined as the deflection at instance of yielding of the tensile reinforcement in the beam. This criterion will be used for all models regardless of the mode of failure.

5.4 Results and Discussion.

A total of 40 simulations are conducted for exterior beam-columns joints. These models include different parameters which are the type of the joint (SP or UHPC), the longitudinal reinforcement in the column (1% and 2%) and ALR in the column (0.25 and 0.5). In this section, the effect of each parameter on the behavior of joints are presented. In addition, the ductility crossponding to each load-deflection curve is estimated. After that, the data are used to make comparisons between sway-special detailing joints and the joints strengthened with UHPC to evaluate the ability of UHPC in improving ductility behavior of the joints in SMRF with completely dispensing of the transverse reinforcements in the joint intersection. During the comparisons, the effects of each parameter in the behavior at different levels are discussed.

5.4.1 Effect of the Detailings and the Material of the joint on the Behavior of the Joints.

This section is conducted to check the dependency of the reinforcement detailings and the material of the joint on the Behavior of the beam-column joints. A comparison between the behavior of three BCJs is performed. The beams and the columns are identical in dimensions and reinforcement detailings, while the joint detailings in the first joints is designed according to the ordinary moment resisting frame (OMRF), the second specimen is designed according to the special moment resisting frame (SMRF), and

UHPC is used in the joints intersection of the last specimen. The behavior of these specimens is shown in **Figure 5.2.**

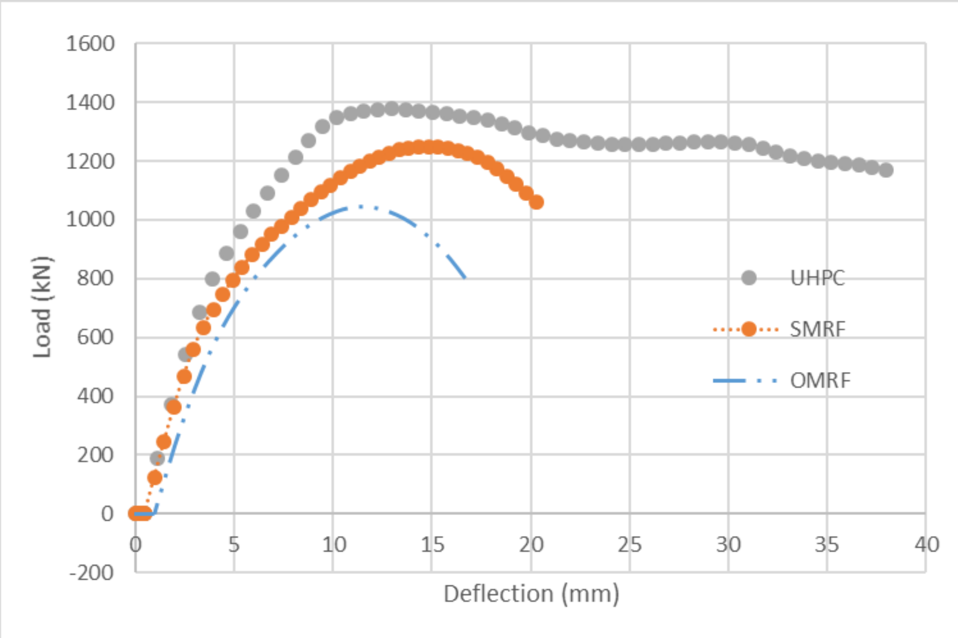

Figure 5. 2: Effect of the Detailings and the Material of the joint on the Behavior of the Simulation (BCDR1.6-L2-ALR0.25).

As shown in Figure 5.2, the UHPC shows effectiveness in strengthening the joints more than the SMRF detailings. Although flexure failure is occurred in the SMRF joint, it is failed at low level of ductility, while a brittle failure is occurred when the transverse reinforcements is not provided in the OMRF joint. The tensile and the compressive damages for the three specimens are shown in **Figure 5.3.**

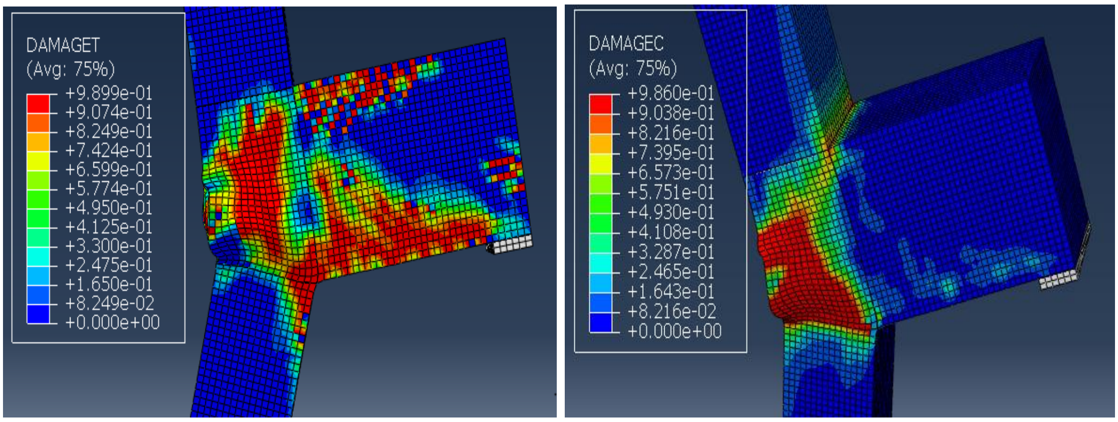

a) Tensile and Compressive Damages in OMRF Joint.

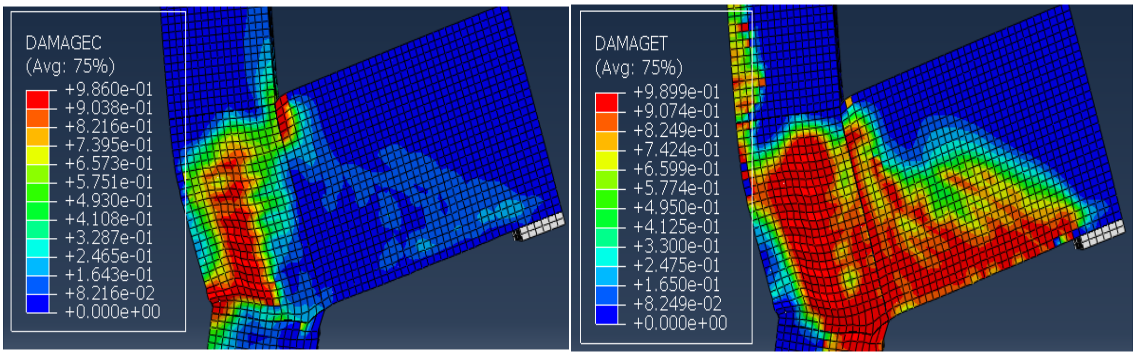

b) Tensile and Compressive Damages in SMRF Joint.

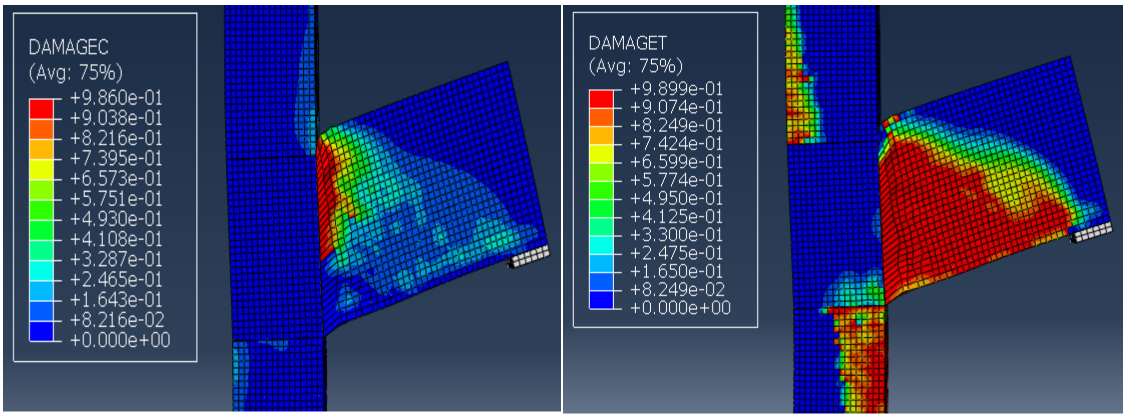

c) Tensile and Compressive Damages in UHPC Joint.

Figure 5. 3: Tensile and Compressive Damages in the Joints.

5.4.2 Effect of Varying ALR on the Behavior of the Joints.

Generally, increasing the ALR decreases the ductility of the reinforced concrete joint and enhances its behavior through minimizing the crack openings as investigated by **Alosta et al. (2018)**. Behind a certain limit, the joint will suffer compression failure due to exceed the ultimate compressive capacity of the column. However, the behavior of sway-special detailings joint is different since the confinement effect compensates the losing in capacity of the BCJ and consequently reduces the load releasing rate.

Table 5.1 shows the effect of varying ALR on the behavior of the sway-special detailings joints. While **Table 5.2** shows the effects on UHPC joints.

Table 5. 1: Effect of Varying ALR in the Ductility of SP Joints.

Parameter		SP		
BCDR	ALR	Ultimate Deflection	Yield Deflection	Ductility
ρ_c 1%.				
0.6	0.25	56.9	5.8	9.8
	0.5	60.4	5.8	10.4
1	0.25	43.3	7.0	6.2
	0.5	52.7	7.1	7.4
1.2	0.25	48.7	7.6	6.4
	0.5	50.6	7.6	6.6
1.4	0.25	42.0	8.9	4.7
	0.5	28.3	9.5	3.0
1.6	0.25	25.5	13.2	JF
	0.5	24.6	15.4	1.6
ρ_c 2%.				
0.6	0.25	56.0	5.6	10.0
	0.5	55.3	5.8	9.6
1	0.25	46.6	6.5	7.1
	0.5	46.7	6.5	7.1

1.2	0.25	43.6	7.4	5.9
	0.5	51.3	7.4	6.9
1.4	0.25	41.6	8.4	4.9
	0.5	37.4	8.3	4.5
1.6	0.25	20.3	17.5	1.2
	0.5	21.2	11.9	1.8

Table 5. 2: Effect of Varying ALR in the Ductility of UHPC

Parameter		UB2		
BCDR	ALR	Ultimate Deflection	Yield Deflection	Ductility
ρ_c 1%.				
0.6	0.25	60.5	5.8	10.3
	0.5	58.0	5.7	10.2
1	0.25	45.4	5.4	8.4
	0.5	40.8	5.4	7.5
1.2	0.25	40.6	6.1	6.7
	0.5	39.3	6.1	6.5
1.4	0.25	31.5	7.9	4.0
	0.5	29.9	8.0	3.8
1.6	0.25	30.7	11.0	2.8
	0.5	25.5	9.8	2.6

Table 5.2 (Continue): Effect of Varying ALR in the Ductility of UHPC

Parameter		UB2		
BCDR	ALR	Ultimate Deflection	Yield Deflection	Ductility
ρ_c 2%.				
0.6	0.25	56.1	6.0	9.4
	0.5	57.0	6.1	9.3
1	0.25	37.1	5.8	6.4
	0.5	38.3	5.6	6.8
1.2	0.25	39.4	7.3	5.4
	0.5	39.5	7.3	5.4
1.4	0.25	40.5	6.7	6.0
	0.5	36.5	7.0	5.2
1.6	0.25	38.0	8.5	4.5
	0.5	37.7	8.4	4.5

Based on **Tables 5.1** and **5.2**, the ductility of the joint can be significantly affected with increasing the ALR. However, the ductility can be increased or decreased because of the kink in the stiffness-strain curve, which caused a sudden change on the stiffness of the concrete in column and joints, which in turn lead to a sudden increase in the yield and ultimate deflections. However, the effect of ALR is more important at high column to beam depth ratio (BCDR). **Figures 5.4** and **5.5** show the effect of ALR on the behavior of simulations BCDR1.6-L1 and BCDR1.6-L2, respectively.

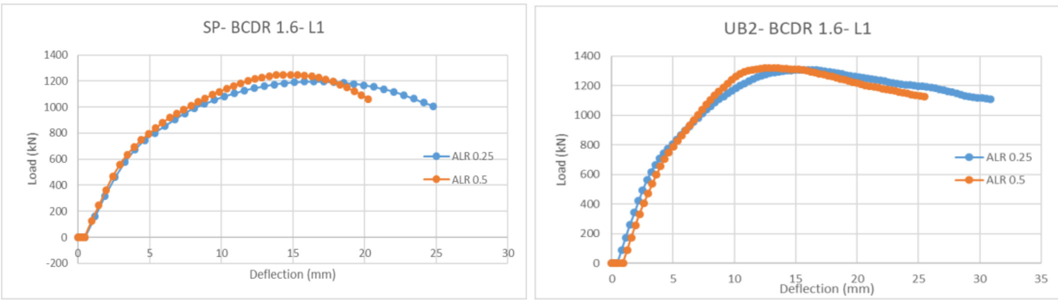

Figure 5. 4: Effect of ALR on the Behavior of Simulations BCDR1.6-L1.

As shown in **Figure 5.4,** the ALR increased the moment capacity of columns. Thus, the load carrying capacity is increased. Although the capacity is increased, the ductility is decreased consistent with the decreased in curvature in columns and joint.

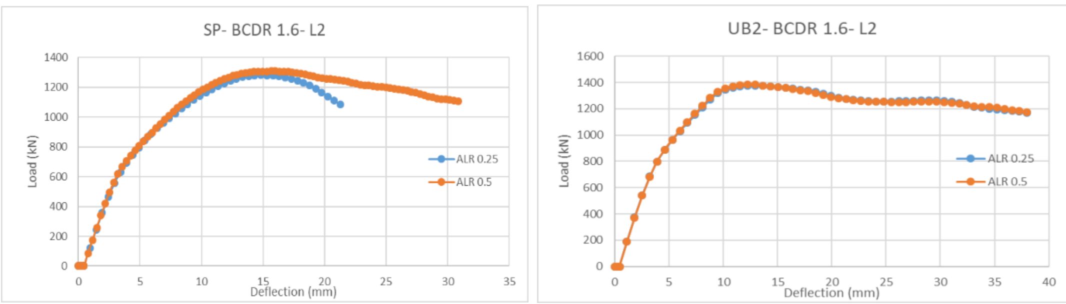

Figure 5. 5: Effect of ALR on the Behavior of Simulations BCDR1.6-L2.

As shown in **Figure 5.5**, the load carrying capacity is increased since the capacity of the column is enhanced with the increases in column longitudinal reinforcements. Thus, the ALR caused more compressive damage to the joint which yield to spall the cover. However, the core of the joint have higher capacity. Thus, the ductility is increased. on the other hand, the UHPC joint have high compression capacity. Thus, no change on the behavior occurred.

5.4.3 Effect of Varying Column Longitudinal Reinforcement Ratio (ρ_c) on Joints Behaviors.

In general, increasing column longitudinal reinforcement ratio increases the capacity and the stiffness of the column, which mean a lower ultimate deflection. However, this increases in stiffness opposed with the decrease in the axial stresses in the columns and joints. Further, when severe damage in column occurs, the longitudinal reinforcement can control the overall behavior of the system and shift it from column failure to beam flexure failure in case of avoiding joints failure as in UHPC. **Tables 5.3** and **5.4** tabulated the effect of increasing ρ_c on the ductility of SP and UHPC joints, respectively.

Table 5. 3: Effect of Varying ρ_c in the Ductility of SP Joints with 0.25 ALR.

Parameter		SP		
BCDR	ρ_c	Ultimate Deflection	Yield Deflection	Ductility
ALR 0.25				
0.6	1%	56.9	5.8	9.8
	2%	56.0	5.6	10.0
1	1%	43.3	7.0	6.2
	2%	46.6	6.5	7.1
1.2	1%	48.7	7.6	6.4
	2%	43.6	7.4	5.9
1.4	1%	42.0	8.9	4.7
	2%	41.6	8.4	4.9
1.6	1%	25.5	13.2	1.9
	2%	20.3	17.5	1.2
ALR 0.5				
0.6	1%	60.4	5.8	10.4
	2%	55.3	5.8	9.6
1	1%	52.7	7.1	7.4
	2%	46.7	5.9	7.9
1.2	1%	50.6	7.6	6.6
	2%	51.3	7.4	6.9
1.4	1%	28.3	9.5	3.0
	2%	37.4	8.3	4.5
1.6	1%	24.6	15.4	1.6
	2%	21.2	11.9	1.8

Table 5. 4: Effect of Varying ρ_c in the Ductility of UHPC Joints with 0.25 ALR.

Parameter		UB2		
BCDR	ρ_c	Ultimate Deflection	Yield Deflection	Ductility
ALR 0.25				
0.6	1%	60.5	5.8	10.3
	2%	56.1	6.0	9.3
1	1%	45.4	5.4	8.4
	2%	37.1	5.8	6.4
1.2	1%	40.6	6.1	6.7
	2%	39.4	7.3	5.4
1.4	1%	31.5	7.9	4.0
	2%	40.5	6.7	6.0
1.6	1%	30.7	11.0	2.8
	2%	38.0	8.5	4.5

Table 5.4(Continue): Effect of Varying ρ_c in the Ductility of UHPC Joints with 0.25 ALR.

Parameter		UB2		
BCDR	ρ_c	Ultimate Deflection	Yield Deflection	Ductility
ALR 0.5				
0.6	1%	58.0	5.7	10.2
	2%	57.0	6.8	8.4
1	1%	40.8	5.4	7.5
	2%	38.3	5.6	6.8
1.2	1%	39.3	6.1	6.5
	2%	39.5	6.0	6.6
1.4	1%	29.9	8.0	3.8
	2%	36.5	7.0	5.2
1.6	1%	25.5	9.8	2.6
	2%	37.7	8.4	4.5

Based on **Tables 5.3** and **5.4,** the ductility is decreased with inceasing the longitudinal reinforcements in column up to BCDR 1.4. However, the ductility of the models with BCDR 1.6 is increased. **Figure 5.6** shows the effect of increasing ρ_c in the behavior of SP and UHPC joints with BCDR 1.6.

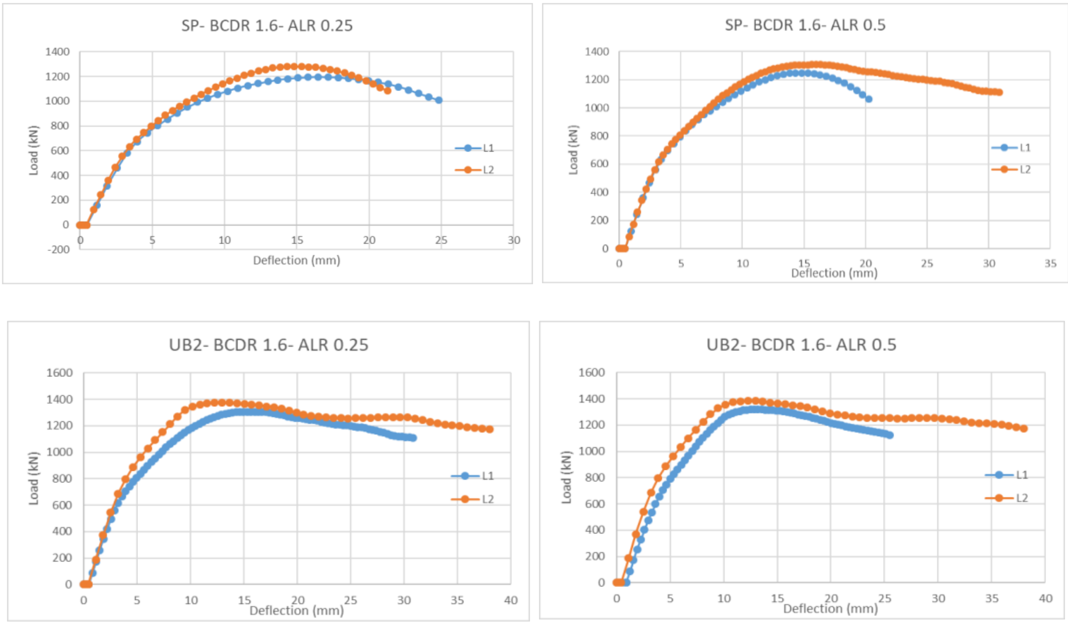

Figure 5. 6: Effect of Increasing ρ_c in the Behavior of UHPC Joints with 0.5 ALR.

As shown in **Figure 5.6,** the models with higher ρ_c have higher load carrying capacity. Thus, the increases in column capacity reduce the damage and enhance the overall behavior of the system. However, the ultimate deflection is decreased for the simulation SP-ALR0.25. This because the joint becomes more critical than the column at high deflection.

5.4.4 Effect of Varying Beam to Column Depth Ratio (BCDR) on Joints Behaviors.

In general, increasing the depth of the beam means increasing the moment capacity of the beam and the transforming stresses to the joint and column. In addition, increasing the capacity of the beam means more damage to the joints, which yields in lower ductility of the system. However, this is true up to the yielding of concrete in column (the yielding of concrete is an ABAQUS expression that refer to the end of the linear-elastic stage). Beyond this stage, the concrete begins damaging and losing the stiffness, which leads to increase the ultimate deformations. This will continue until reach the ultimate tri-axial compressive strength of concrete. After that, a severe damage with excessive deformations in concrete occurs that leads to deteriorate the ductility of the system. Hence, the ALR and $\rho_c$in column have a great effect in shifting the behavior of the system since they affect the stresses in concrete. This trend obviously appears in UHPC joints. However, the behavior of the joints is complex due to the different type of stresses affected it. Finally, the effect of varying BCDR in the behavior of the SP joints and UHPC joints is shown in **Figures 5.7** and **5.8**, respectively.

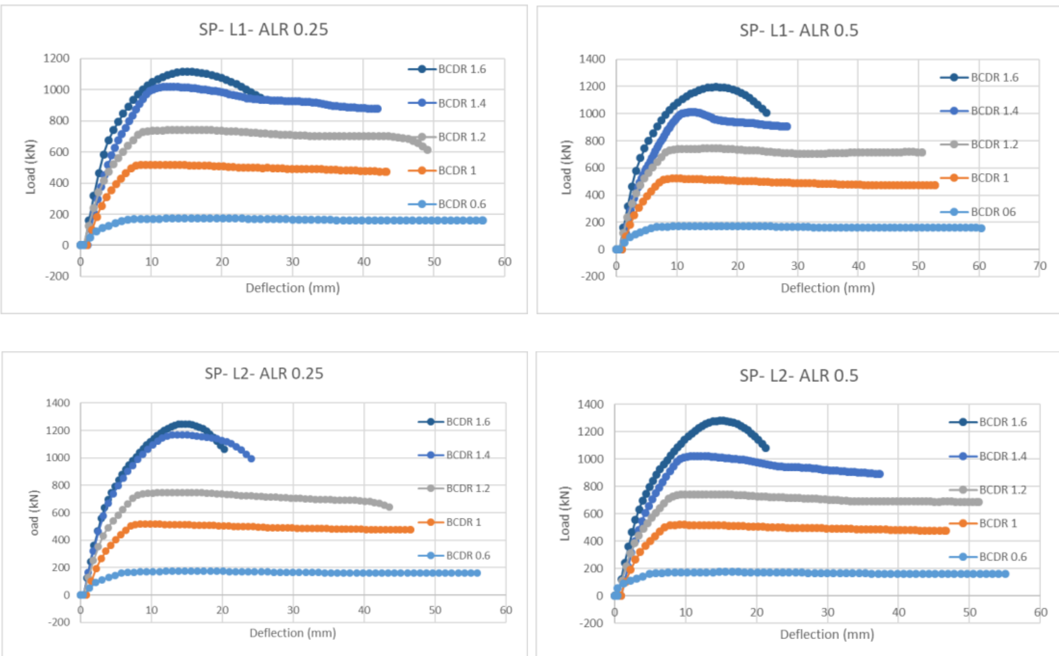

Figure 5. 7: Effect of Varying BCDR in the Behavior of SP Joints.

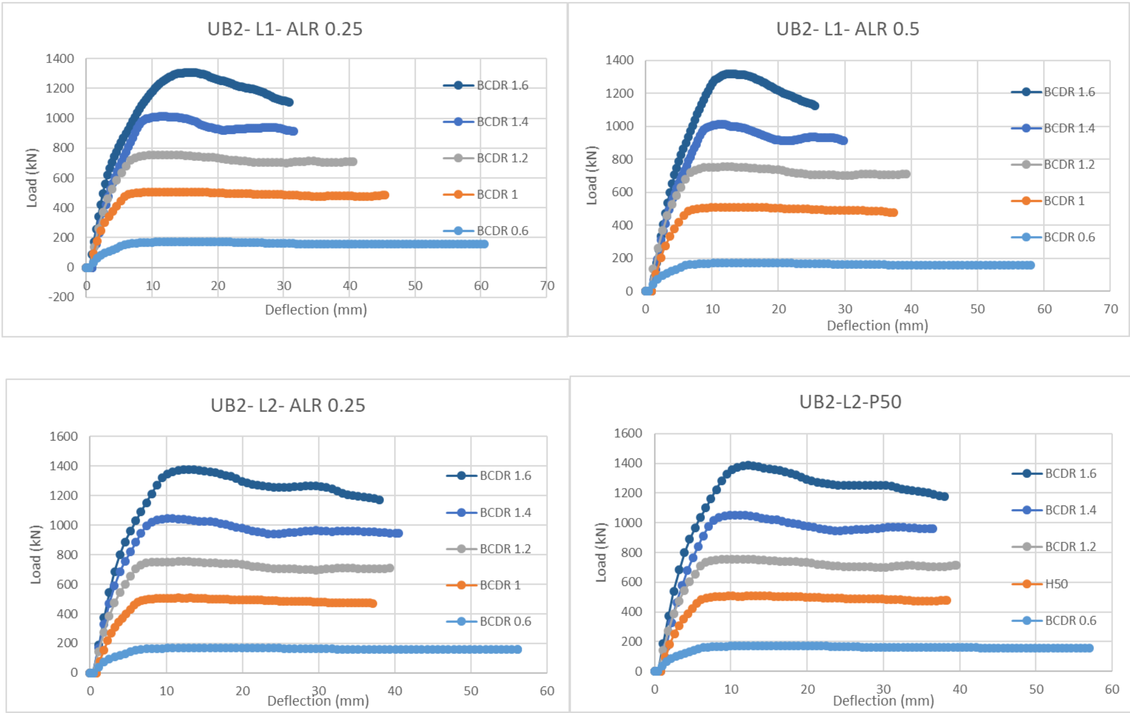

Figure 5. 8: Effect of Varying BCDR in the Behavior of UHPC Joints.

As shown in **Figure 5.7,** increasing the BCDR decreases the ultimate deflection up to BCDR 1 for SP-L1-ALR 0.25. This indicates that the yielding capacity is between the capacity of the beams depth 500 mm and 600 mm (BCDR 1 and 1.2). After that, the ultimate deflection of the joints with beam depth H60 increased, which indicate that the capacity of the beam is less than both the joint and beam capacity. After that, the ultimate deflection for BCDR 1.4 and 1.6 decreased which indicates a severe damage in joint and columns. This trend also appears for the groups of joints strengthened with UHPC. Moreover, the capacity of the SP joints with BCDR 1.6 are show lower capacity comparing with UHPC joints. This indicates that the sway-special joints are fail or about to fail. However, the ALR and the longitudinal reinforcement paly a main rule in controlling the behavior of the joint since they affect the joints and columns capacities. **Tables 5.5** and **5.6** show the effect of varying BCDR in the behavior of SP and UHPC joints, respectively.

Table 5. 5: Effect of Varying BCDR in the Ductility of SP Joints with ρ_c 1% and ALR 0.25.

Group	BCDR	Ultimate Deflection	Yield Deflection	Ductility
L1-ALR0.25	0.6	56.9	5.8	9.8
	1	43.3	7.0	6.2
	1.2	48.7	7.6	6.4
	1.4	42.0	8.9	4.7
	1.6	25.5	13.2	1.9
L1-ALR0.5	0.6	60.4	5.8	10.4
	1	52.7	7.1	7.4
	1.2	50.6	7.6	6.6
	1.4	28.3	9.5	3.0
	1.6	24.6	15.4	1.6
L2-ALR0.25	0.6	56.0	5.6	10.0
	1	46.6	6.5	7.1
	1.2	43.6	7.4	5.9
	1.4	41.6	8.4	4.9
	1.6	20.3	17.5	1.2
L2-ALR0.5	0.6	55.3	5.8	9.6
	1	46.7	5.9	7.9
	1.2	51.3	7.4	6.9
	1.4	37.4	8.3	4.5
	1.6	21.2	11.9	1.8

Table 5. 6: Effect of Varying BCDR in the Ductility of SP Joints with ρ_c 1% and ALR 0.25.

Group	BCDR	Ultimate Deflection	Yield Deflection	Ductility
L1-ALR0.25	0.6	60.5	5.8	10.3
	1	45.4	5.4	8.4
	1.2	40.6	6.1	6.7
	1.4	31.5	7.9	4.0
	1.6	30.7	11.0	2.8
L1-ALR0.5	0.6	58.0	5.7	10.2
	1	40.8	5.4	7.5
	1.2	39.3	6.1	6.5
	1.4	29.9	8.0	3.8
	1.6	25.5	9.8	2.6
L2-ALR0.25	0.6	56.1	6.0	9.3
	1	37.1	5.8	6.4
	1.2	39.4	7.3	5.4
	1.4	40.5	6.7	6.0
	1.6	38.0	8.5	4.5
L2-ALR0.5	0.6	57.0	6.8	8.4
	1	38.3	5.6	6.8
	1.2	39.5	6.0	6.6
	1.4	36.5	7.0	5.2
	1.6	37.7	8.4	4.5

5.4.5 Effect of Using UHPC on the Behavior of the Joints.

In general, UHPC is very stiff and ductile comparing with ordinary concrete. Thus, it shows effectiveness in strengthening the joints and save capacity until flexure ductile failure in beam occurs. Although the UHPC joints show less deformation comparing with sway-special joints, they show enhancement in term of ductility. This enhancement because the yield deflection in UHPC joints is often less than that for the sway-special detailings joints. In addition, the UHPC joints show less compression and tension damages at joint zone as shown in **Figure 5.2**. These results emphases the effectiveness of using UHPC. **Table 5.7** shows the behavior of SP joints against UHPC joints.

Table 5. 7: Effect of Using UHPC in the Ductility of the Joints with 0.25 ALR.

ID	Parameters		SP			UHPC		
	BCDR	ρ_C	Ultimate Deflection	Yield Deflection	Ductility	Ultimate Deflection	Yield Deflection	Ductility
ALR0.25	0.6	1%	56.9	5.8	9.8	60.5	5.8	10.3
		2%	56.0	5.6	10.0	56.1	6.0	9.3
	1	1%	43.3	7.0	6.2	45.4	5.4	8.4
		2%	46.6	6.5	7.1	37.1	5.8	6.4
	1.2	1%	48.7	7.6	6.4	40.6	6.1	6.7
		2%	43.6	7.4	5.9	39.4	7.3	5.4
	1.4	1%	42.0	8.9	4.7	31.5	7.9	4.0
		2%	41.6	8.4	4.9	40.5	6.7	6.0
	1.6	1%	25.5	13.2	1.9	30.7	11.0	2.8
		2%	20.3	17.5	1.2	38.0	8.5	4.5
ALR0.5	0.6	1%	60.4	5.8	10.4	58.0	5.7	10.2
		2%	55.3	5.8	9.6	57.0	6.8	8.4
	1	1%	52.7	7.1	7.4	40.8	5.4	7.5
		2%	46.7	5.9	7.9	38.3	5.6	6.8
	1.2	1%	50.6	7.6	6.6	39.3	6.1	6.5
		2%	51.3	7.4	6.9	39.5	6.0	6.6
	1.4	1%	28.3	9.5	3.0	29.9	8.0	3.8
		2%	37.4	8.3	4.5	36.5	7.0	5.2
	1.6	1%	24.6	15.4	1.6	25.5	9.8	2.6
		2%	21.2	11.9	1.8	37.7	8.4	4.5

Based on **Table 5.7,** UHPC shows effectiveness in confining the joints. However, the effect of using UHPC on the ductility is negligible at low BCDR as shown in **Figure 5.9,** while it shows advantages comparing with sway-special joints at high BCDR. As shown in **Figure 5.10, t**he joints strengthened with UHPC show higher load carrying capacity comparing with sway-special detailing joints. In addition, the ductility is significantly increased. This indicates that UHPC success in strength the joint and shift the failure from the joint to the beam.

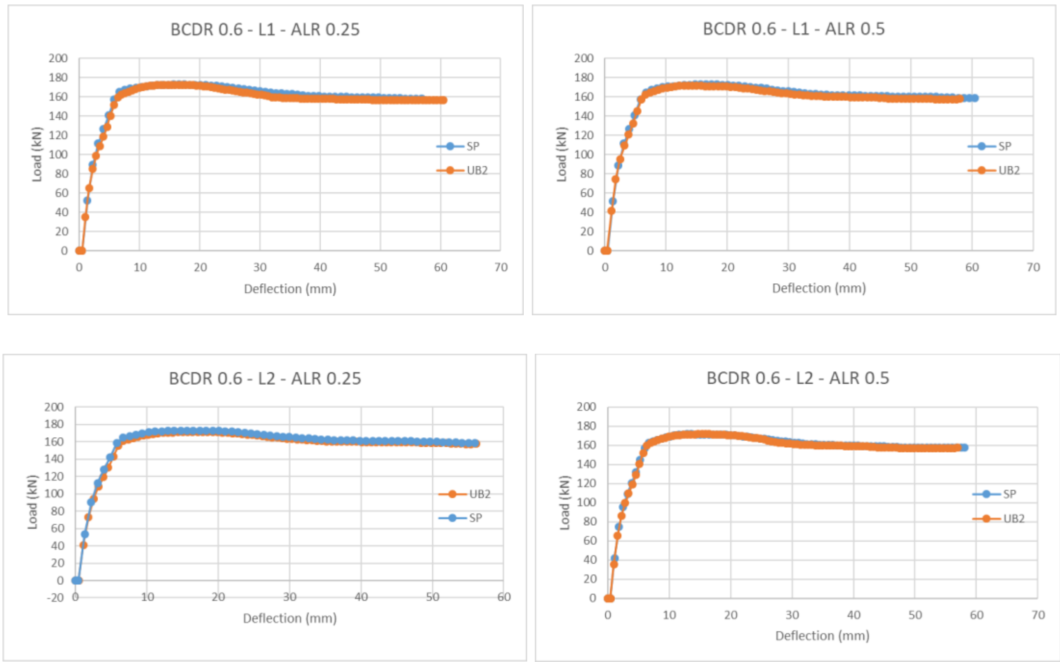

Figure 5. 9: Effect of Using UHPC in the Behavior of the Joints at BCDR 0.6.

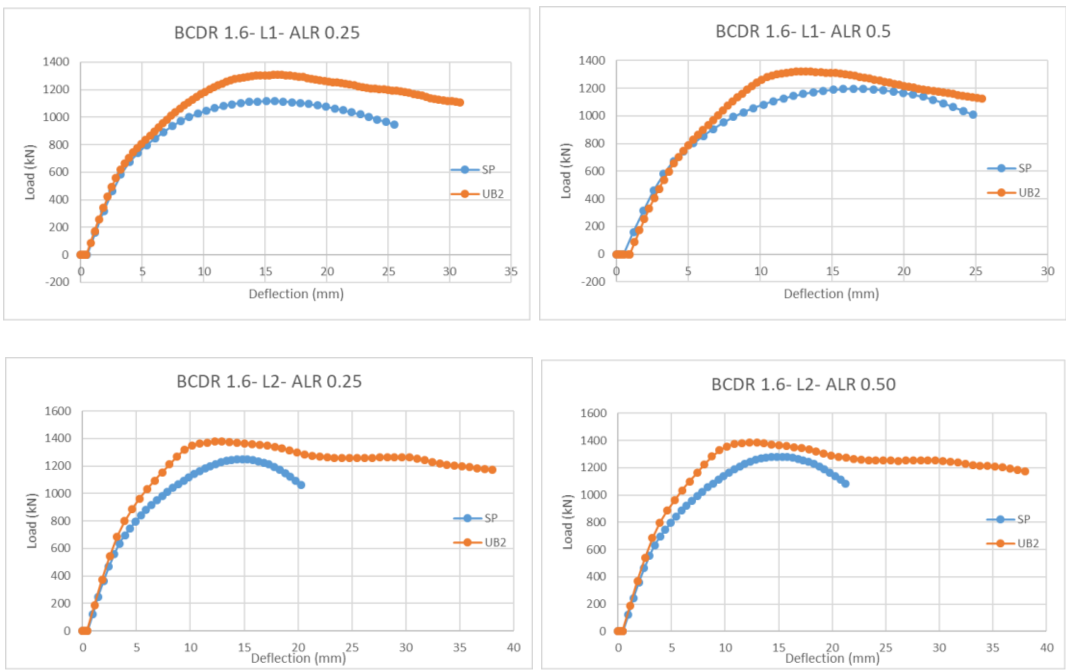

Figure 5. 10: Effect of Using UHPC in the Behavior of the Joints at BCDR 1.6.

5.4.6 Comparison between UHPC and SP Joints under Cyclic Load.

This section is conducted to compare the behavior of UHPC joints and sway-special detailings joints under cyclic load. The model BCDR1.6-L2-ALR0.25 is used. Table 5.8 tabulated the cyclic load pattern which applied to the tip of beam.

Table 5. 8: Cyclic Load Pattern.

Cyclic No	Drift Ratio	Push	Pull
	%	mm	Mm
1	.5	5	-5
2	1.5	15	-15
3	3	30	-30
4	5	50	-

Figure 5.11 shows the load-deflection curves for SP and UHPC joints.

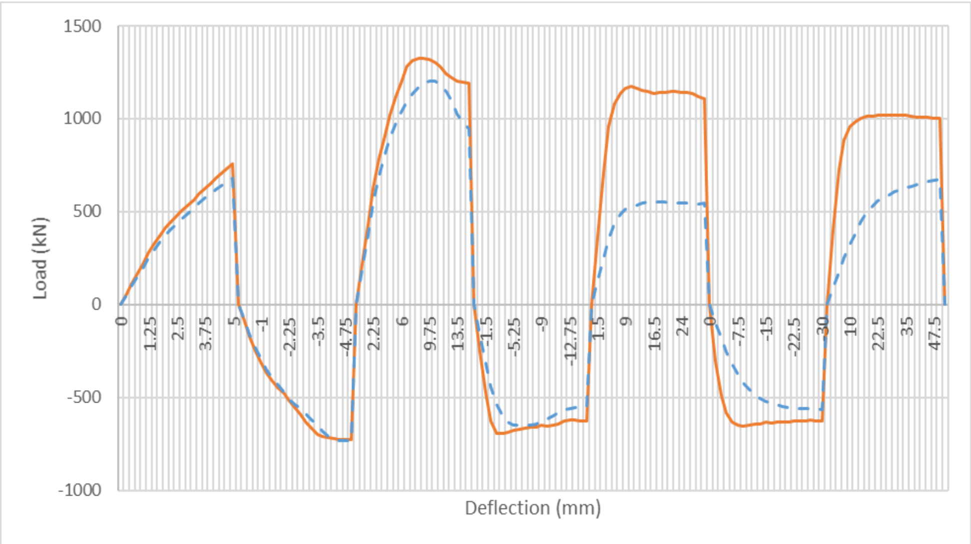

Figure 5. 11: Load-Deflection Curves for UHPC and SP Joint under Cyclic Load (BCDR1.6-L2-ALR0.25).

As mentioned before in Chapter three, two loading plates are provided on the two tips of the beam. Each loading plate is used to apply the displacement in the normal direction of the tip beam surface. Thus, no tension occurred on the concrete. After that, the displacement is slowly released. However, the reaction forces in the loading plate are not appear in the releasing stage. Thus, the loads in Figure 11 present the loads needed to pull and push the beam tip from the origin. **Figure 5.12** shows the compression and tension damages in the sway-special detailings joint and the joint strengthened with UHPC

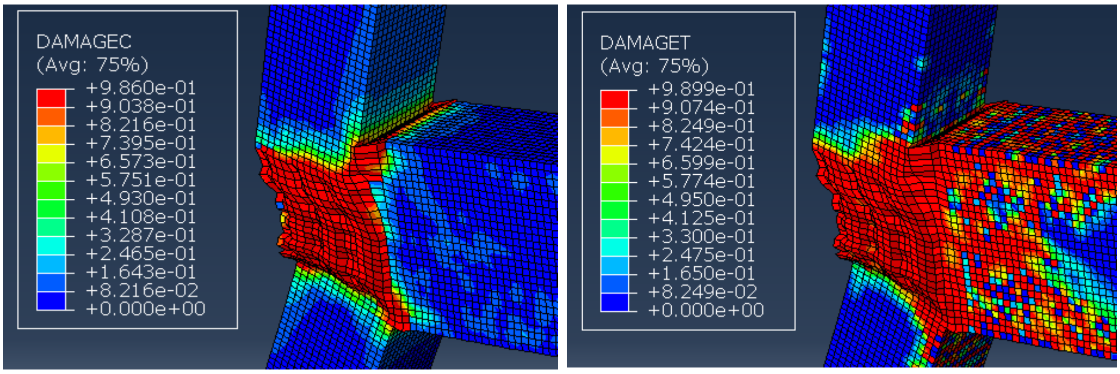

a) SP Joint.

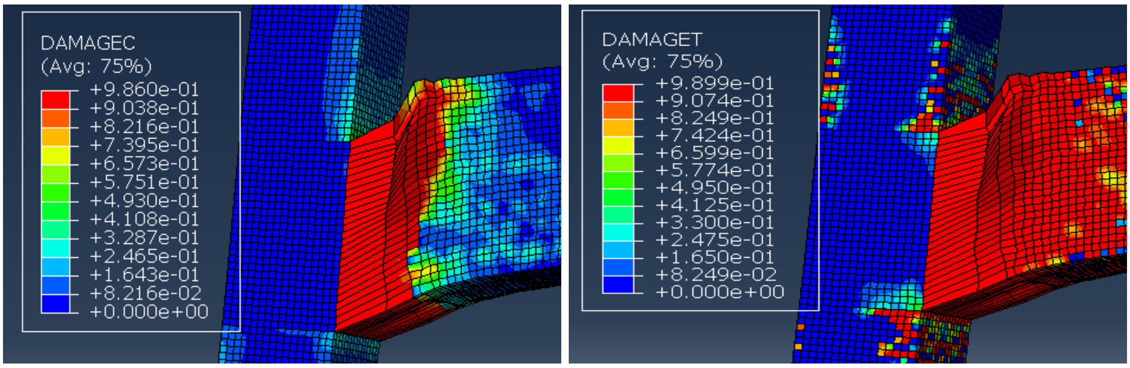

b) UHPC joint.

Figure 5. 12: Tensile and Compressive Damage in Simulation BCDR1.6-l2-ALR0.25 for: a) SP Joint and B) UHPC Joint.

Clearly, UHPC shows more effectiveness in strengthening the joint comparing with sway-special detailings at the lower column to beam moment capacity ratio.

5.5 Failure modes.

In general, the SMRF design requirements count on an over strength factor on beam of 1.25, reduction factor on flexure strength of 0.9 and a magnification factor on the load of 1.4. Thus, they assure a flexure failure in beam. In addition, the provided amount of transverse reinforcement assure a ductile failure on joints and column. However, although a flexure failure in beam is dominant in the simulations, the status of columns and joints at yield and ultimate points yielded in different behaviors that affected the ductility. In this section, the behaviors of models group (SP-L1-ALR 0.25) are traced. **Figure 5.13** Shows the F.E response for these Simulations group with marking the yield and ultimate point as 1 and 2, respectively.

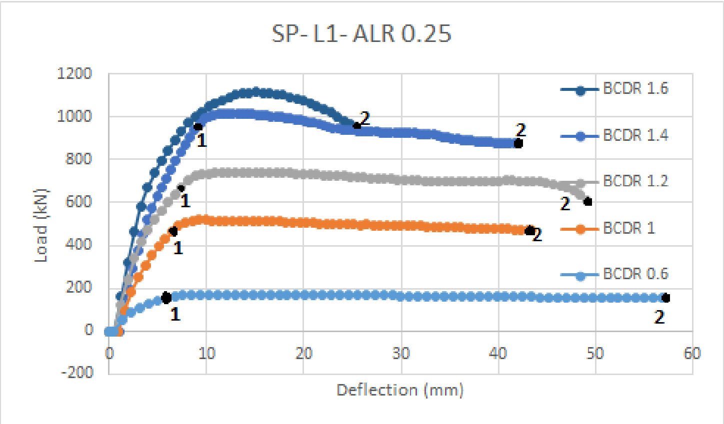

Figure 5. 13: F.E Response for Simulations Group SP-L1-ALR 0.25.

For BCDR 0.6 the mode of failure represent a crushing of concrete fiber in the top compression zone of beam after the yielding of tensile steel in beam and no damage in column and joints occurs until the ultimate point reached. **Figure 5.14** represents the response of the joints.

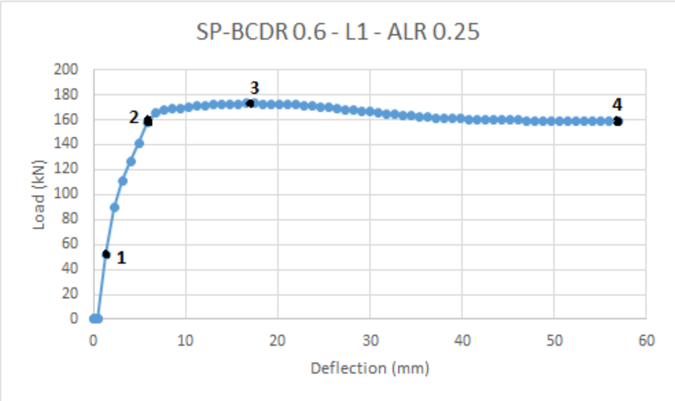

Figure 5. 14: Response of (SP-BCDR 0.6-L1-ALR 0.25) with Stages of Failures.

The points in the **Figure 5.14** mark the sequence of behavior as follows:

Point one: represents the tensile cracking in the beam. **Figure 5.15** shows the stress in the tension zone in beam at cracking.

Point Two: represents the yielding of the tensile reinforcement in the beam. **Figure 5.16** shows a 3D views of the stresses captured from ABAQUS which represent the yielding of the tensile reinforcement on beam.

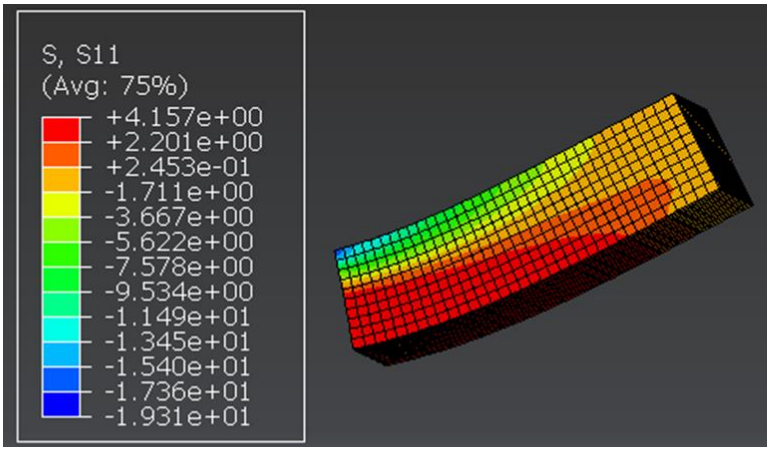

Figure 5. 15: Cracking of the Tensile Fiber in Beam (SP-BCDR 0.6-L1-ALR 0.25).

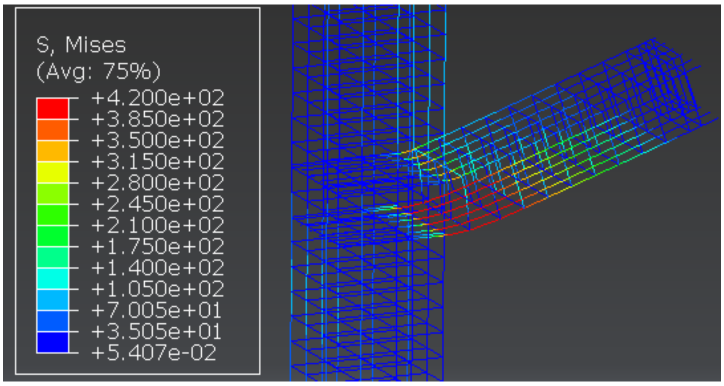

Figure 5. 16: Yielding of Tensile Reinforcement in the Beam (SP-BCDR 0.6-L1-ALR 0.25).

Point Three: represents the peak capacity of the beam. This happens when the stresses are around the maximum tri-axial compression stresses. **Figure 5.17** shows the stress-strain curve for a point in the compression zone while **Figure 5.18** shows the strain at the peak load.

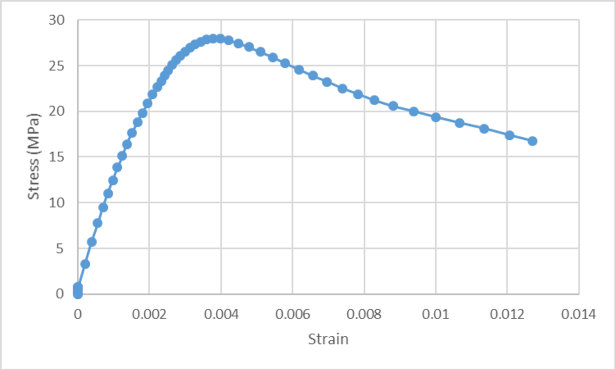

Figure 5. 17: Tri-axial Stress-Strain Curve for Point on the compression Zone of the Beam (SP-BCDR 0.6-L1-ALR 0.25).

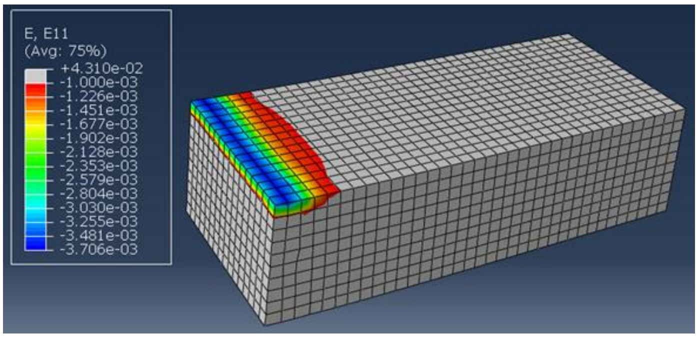

Figure 5. 18: Strain Crossponding to the Peak Load at the Compression Fiber in the Beam (SP-BCDR 0.6-L1-ALR 0.25).

As shown in **Figures 5.17** and **5.18**, the peak load is behind the peak compressive strength in the beam. This because the less strained elements in joints corners reach their peak compressive strength in the principle S11. However, the restrained elements parallel to the core is not reach their peak capacity yet and it would be higher. Hence, the connected area between beam and column is reduced. However, the difference in load capacity of the beam at its peak compressive strength is very little (1kN). This indicates that the behaviors under higher beam depths would be different. **Figures 5.19** and **5.20** show the stress-strain curve for corner joint element and the strain at that elements at peak load capacity, respectively.

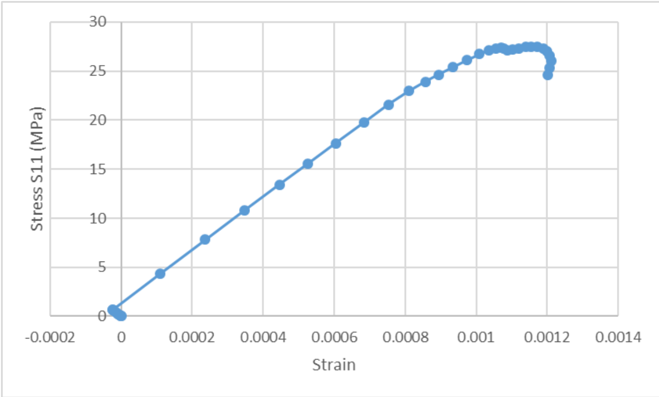

Figure 5. 19: Stress-Strain Curve for element in Joints Corner (SP-BCDR 0.6-L1-ALR 0.25).

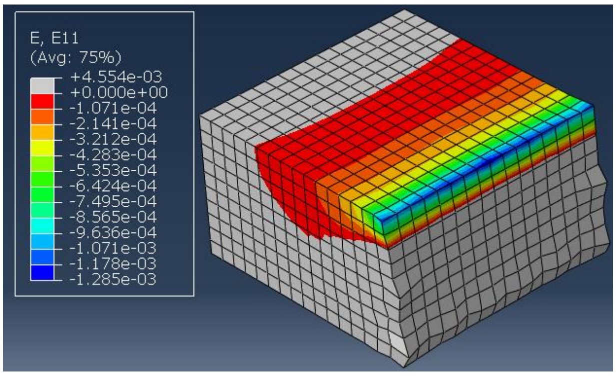

Figure 5. 20: Strain in the Joints at Peak Load (SP-BCDR 0.6-L1-ALR 0.25).

Point Four: represents the point when the steel bars rapture. This happens when the plastic strain reaches the ultimate value which is equal 0.18. **Figure 5.21** shows the plastic strain at the ultimate point. In addition, **Figure 5.22** shows the compressive and the tensile damage in the system, respectively. It is clear that the column and the joints are not affected.

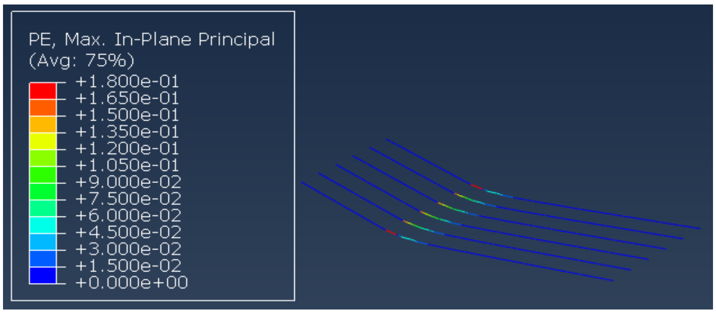

Figure 5. 21: Plastic Strain at Ultimate Point (SP-BCDR 0.6-L1-ALR 0.25).

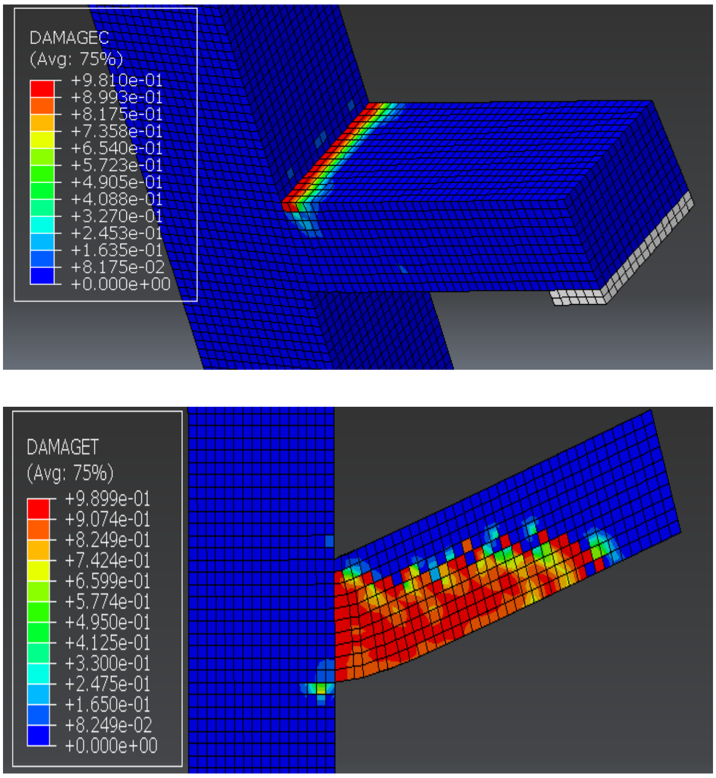

Figure 5. 22: Compressive and Tensile Damage in the System at Ultimate Point (SP-BCDR 0.6-L1-ALR 0.25).

Similar trend is shown for BCDR 1, **Figure 5.23** shows the F.E response for this joints. The failure mode is ductile flexural failure in beam.

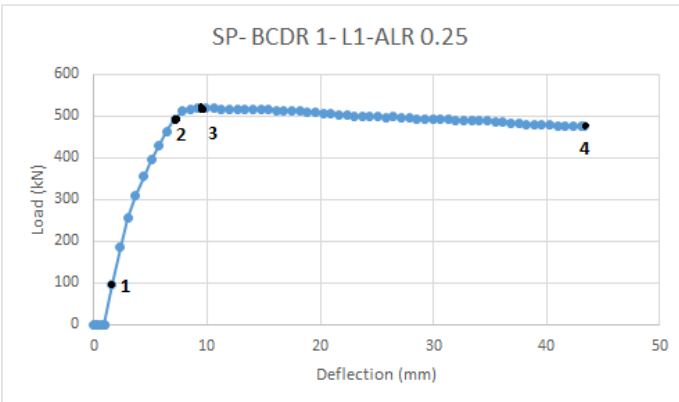

Figure 5. 23: Response of (SP-BCDR 1-L1-ALR 0.25).with Stages of Failures.

Hence, point one presents the tensile cracking on the beam, a 3D view for the stress in the beam at instant of cracking is shown in **Figure 5.24,** while

Figure 5.25 shows the instant of yielding the tensile reinforcement in the beam which presents point two.

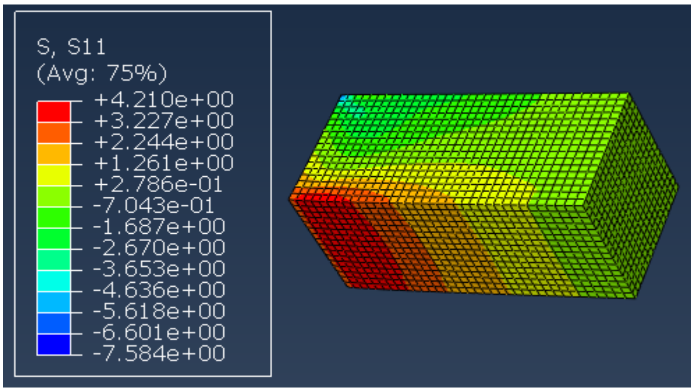

Figure 5. 24: Cracking of the Tensile Fiber on Beam (SP-BCDR 1-L1-ALR 0.25).

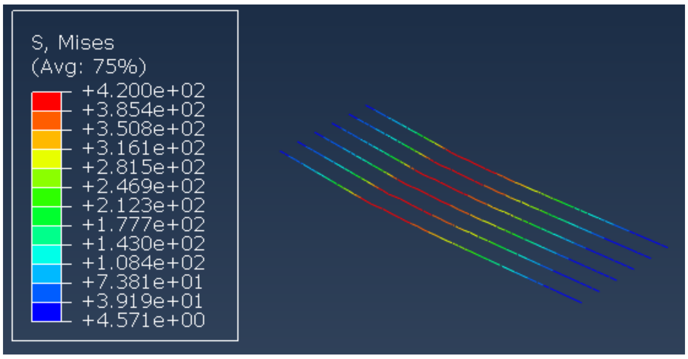

Figure 5. 25: Yielding of Tensile Reinforcement in the Beam (SP-BCDR 1-L1-ALR 0.25).

Point three presents the ultimate capacity of the beam, the stress-strain curve for a point in the compression zone and the strain at peak load are shown in **Figures 5.26** and **5.27**, respectively. Similarly to model (SP-BCDR 1-L1-ALR 0.25).the peak load capacity is behind the maximum compressive strength due to reach the peak compressive strength of the joints corners. **Figures 5.28** and **5.29** show the stress-strain curve at joint corners and the strain at peak load in the joint, respectively.

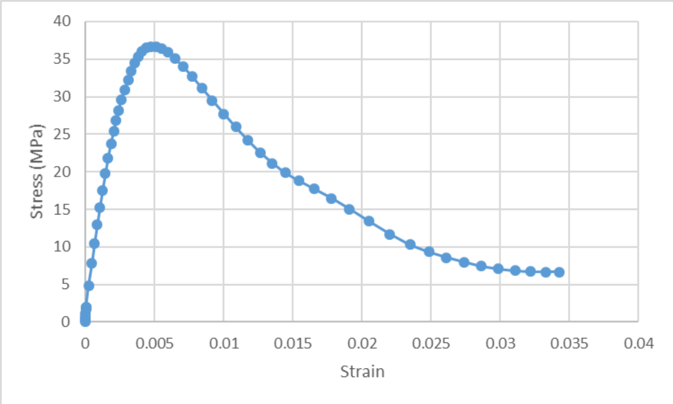

Figure 5. 26: Tri-axial Stress-Strain Curve for Point on the compression Zone of the Beam (SP-BCDR 1-L1-ALR 0.25).

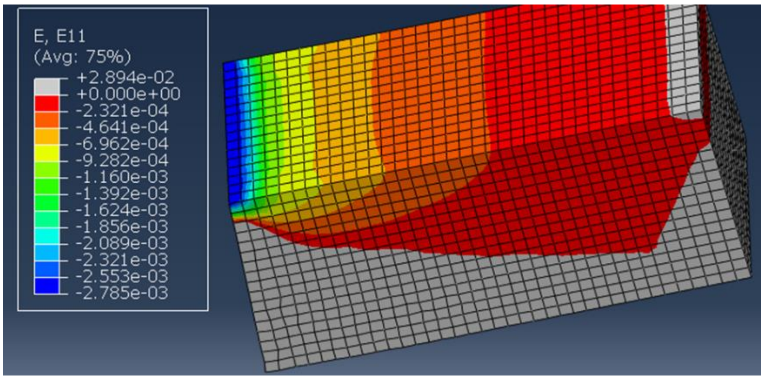

Figure 5. 27: Strain Crossponding to the Peak Load at the Compression Fiber in the Beam (SP-BCDR 1-L1-ALR 0.25).

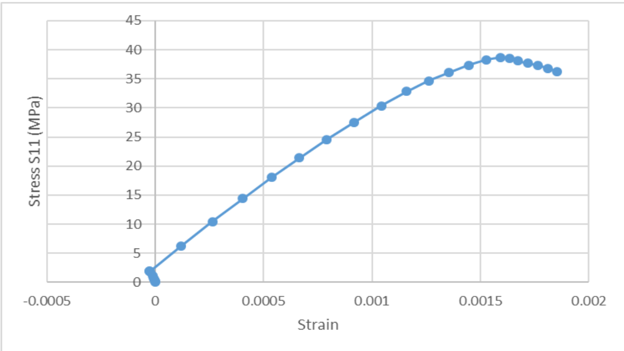

Figure 5. 28: Stress-Strain Curve for element in Joints Corner (SP-BCDR 1-L1-ALR 0.25).

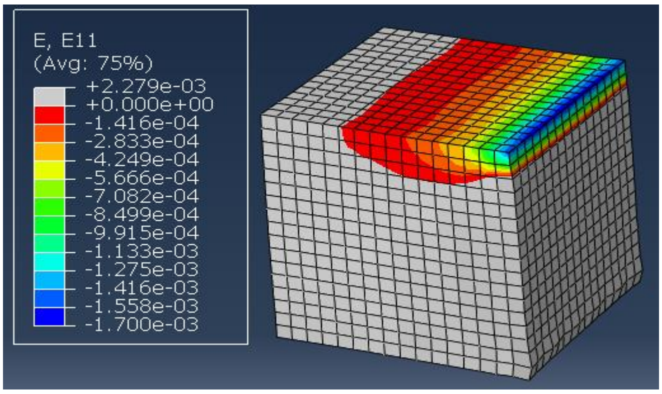

Figure 5. 29: Strain in the Joints at Peak Load (SP-BCDR 1-L1-ALR 0.25).

Finally, point four present the ultimate point when the steel is cutting at plastic strain value of 0.18. **Figure 5.30** shows the plastic strain in the tensile reinforcement of beam at the ultimate point, while **Figures 5.31** shows the compressive and the tensile damage in the system. It is clear that the column do not receive damage in compression, which indicates that the concrete is still in the elastic range without losing in stiffness. On the other hand, the joints is entered the inelastic range with limited cracks (not extended). Hence, the joints does not reach it is full capacity. Hence, increasing the beam depth explains the increasing of yield deflection and the decreasing in the ultimate deflection.

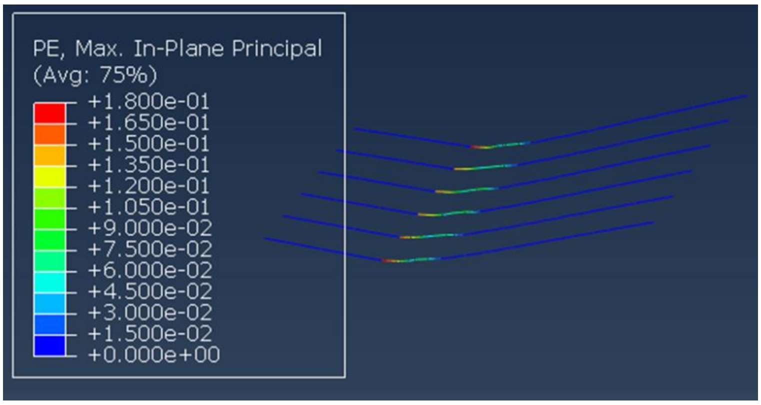

Figure 5. 30: Plastic Strain at Ultimate Point (SP-BCDR 1-L1-ALR 0.25).

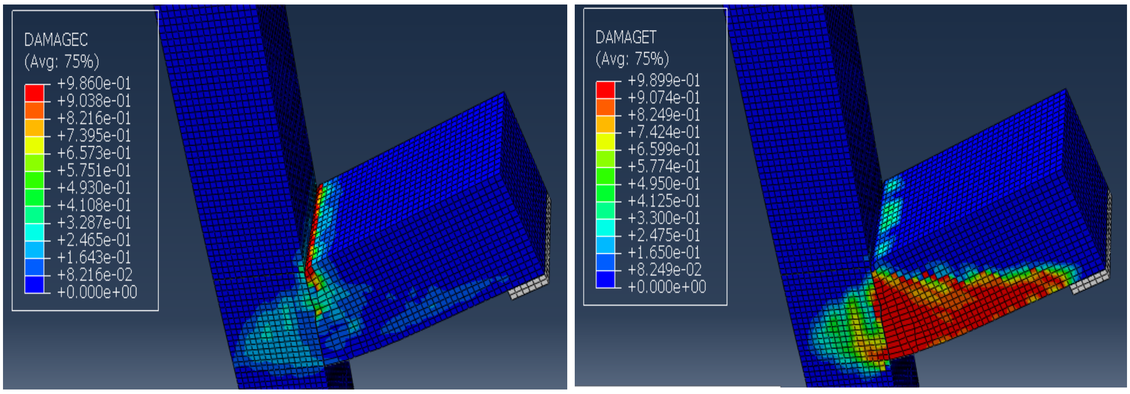

Figure 5. 31: Compressive and Tensile Damages in the System at Ultimate Point (SP-BCDR 1-L1-ALR 0.25).

For model (SP-BCDR 1.2-L1-ALR 0.25), the cracking strength is the same for the previous two model. **Figure 5.32** shows the F.E response for the model with points (1-3) which marking the sequence of failure for the model.

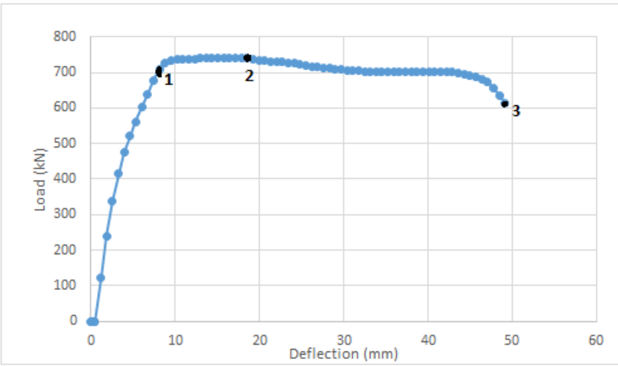

Figure 5. 32: Response of (SP-BCDR 1.2-L1-ALR 0.25) with Stages of Failures.

Point one represents the yielding of beam tensile reinforcements. **Figure 5.33** shows the compressive and the tensile damage in the system. The damage in the column and the joints indicate that the increments in yield deflection is because of the increments in beam depth and the losing in stiffness due to the damage. However, at higher beam depth a higher damage in joints and columns will occurred and consequently more losing in stiffness and higher yield deflection.

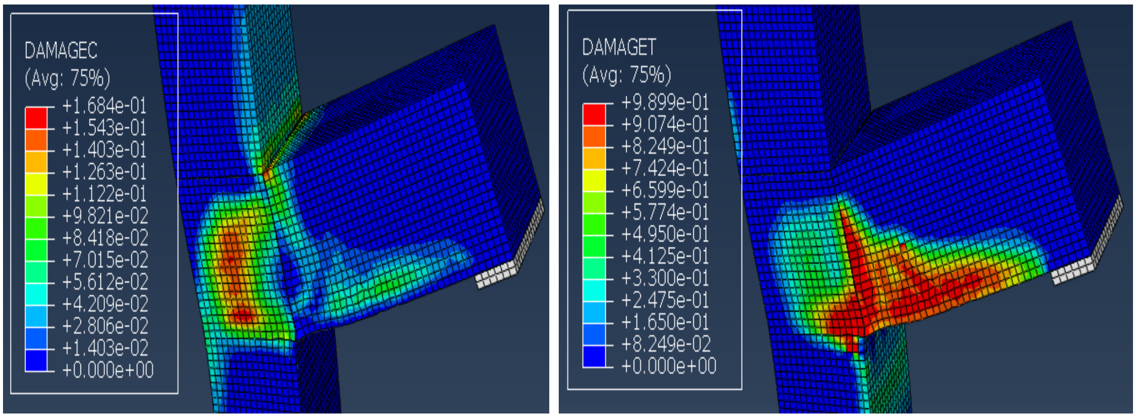

Figure 5. 33: Compressive and Tensile Damages in the System at yield point (SP-BCDR 1.2-L1-ALR 0.25).

Point two presents the peak load capacity of the system, **Figures 5.34** and **5.35** show the stress-strain curve for a point in the compression zone of the beam and the strain at peak load capacity point.

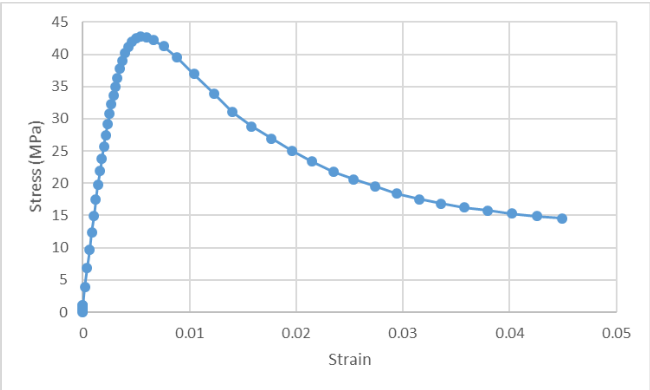

Figure 5. 34: Tri-axial Stress-Strain Curve for Point on the compression Zone of the Beam (SP-BCDR 1.2-L1-ALR 0.25).

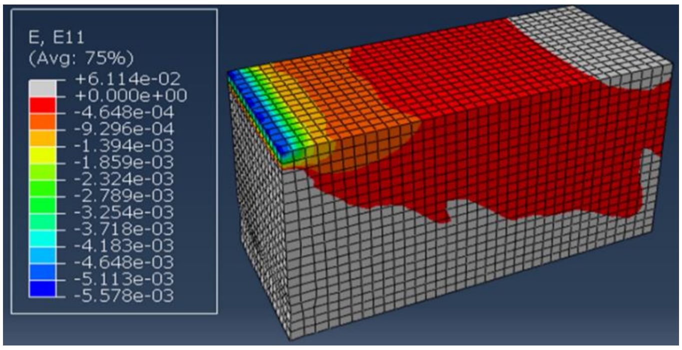

Figure 5. 35: Strain Crossponding to the Peak Load at the Compression Fiber in the Beam ((SP-BCDR 1.2-L1-ALR 0.25).

As shown in **Figures 5.34** and **5.35,** the peak load capacity is around the peak tri-axial stress capacity of the material. However, the joints corner is already reached its compressive strength. **Figure 5.36** shows the stresses in beam at point crossponding to the peak stress capacity of the joints corner. Hence, increasing the stresses in concrete and the strain in the compression steel are got over the reduction on beam sides effectiveness. However, beyond the peak capacity, the decreases on stress capacity of the corners lead to decrease the effectiveness of beam width and decrease the load capacity. However, the joints at this point is received high tensile damage as shown in **Figure 5.37,** which indicates a formations of non extended shear cracks. Hence, at higher rotations the joints will be fail.

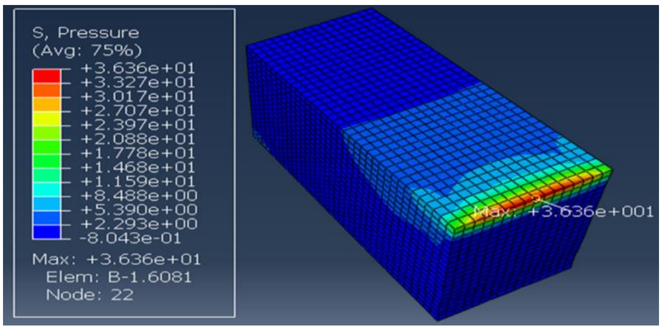

Figure 5. 36: Tri-Axial Stress in the Beam Crossponding to Peak Stress Capacity of the joints (SP-BCDR 1.2-L1-ALR 0.25).

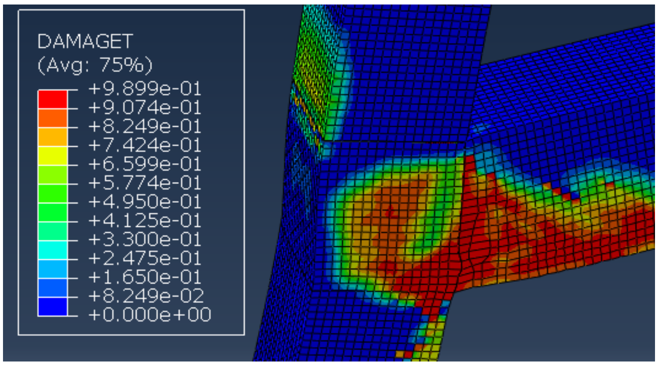

Figure 5. 37: Tensile Damage in the System at Peak Point (SP-BCDR 1.2-L1-ALR 0.25).

Point three presents the ultimate points when the Load go 15% reduction in the post peak portions. The reduction in load capacity indicates a severe reduction in stresses capacity of concrete due to the high damage. However, the compression steel is yielded as shown in **Figure 5.38**. Hence, this reduction in compression force can not be compensated. **Figure 5.39** shows the yielding in the transverse reinforcement of the beam. beyond this point, the effective depth of the beam decrease and the elements with ultimate rotations is indirectly eliminated. The stressed is transferred to the next elements and the stresses in the beam redistributed. However, the rotations in beam still increased which caused high damage to the joints. **Figure 5.40** shows the compressive and the tensile damages in the system. As shown, the joint is failed with shear due to the high rotations. However, the flexural failure on beam at this point is already happened. In addition, the high compression damage in joints indicates the spalling in joints cover. while the columns enter the inelastic range which indicates a losing in stiffness and higher ultimate deflection. However, a higher damage in the column edge connected to the beam compression zone occurred. **Figure 5.41** shows the damage in the columns.

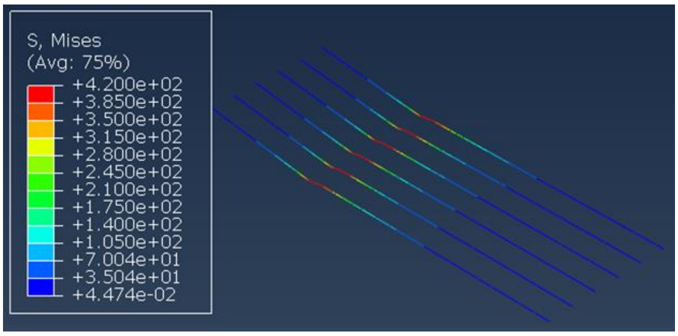

Figure 5. 38: Yielding of Beam Compression Steel (SP-BCDR 1.2-L1-ALR 0.25).

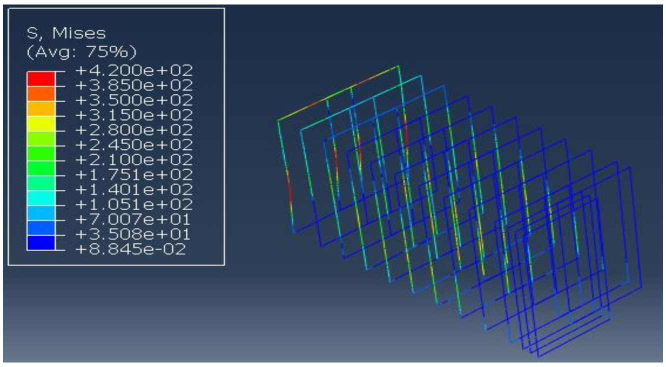

Figure 5. 39: Yielding of Beam Transverse Reinforcements (SP-BCDR 1.2-L1-ALR 0.25).

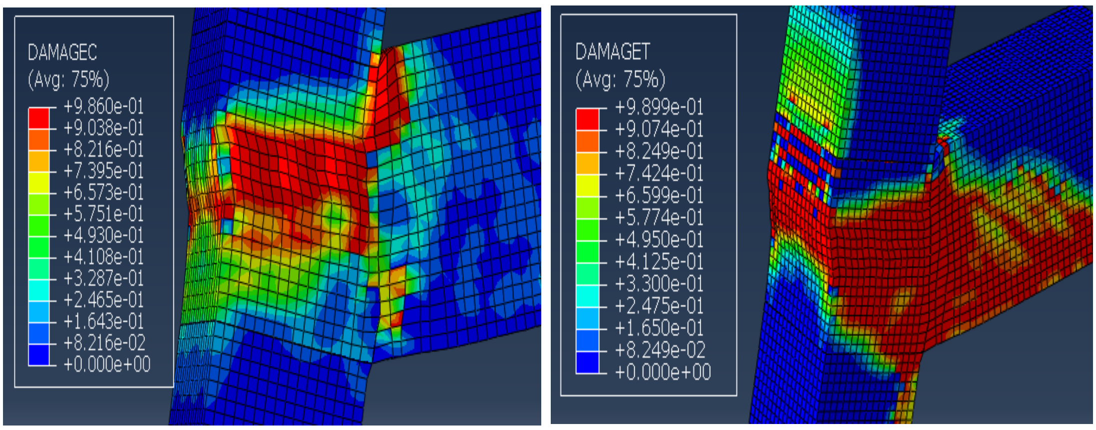

Figure 5. 40: Compressive and Tensile Damages in the System at Ultimate Point (SP-BCDR 1.2-L1-ALR 0.25).

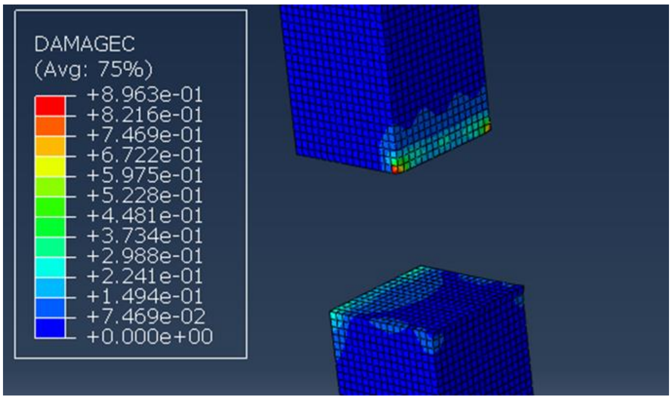

Figure 5. 41: Compressive Damage in the Columns at Ultimate Point (SP-H60-L1-P25).

The F.E response for the model (SP-BCDR 1.4-L1-ALR 0.25) is shown in **Figure 5.42**, the points (1-3) mark the sequence of failure for the model. However, the cracking stress do not marked since it is same as the other models.

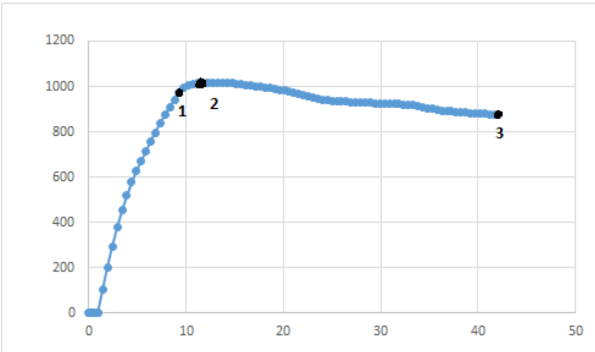

Figure 5. 42: Response of (SP-BCDR 1.4-L1-ALR 0.25) with Stages of Failures.

Point one presents the yielding of the beam tensile reinforcements. **Figure 5.52** shows the compressive and the tensile damages in the system. The damage in the columns and joint indicate a losing in stiffness. Hence, the increases in depth and the losing in stiffness cause the increases on yield deflection. However, the damage in columns is high comparing with damage in the beam. hence, the columns may fails at higher rotations. In tension, the damage in the joints indicates a formations of non-extended shear cracks. However, it also may fail at higher rotations.

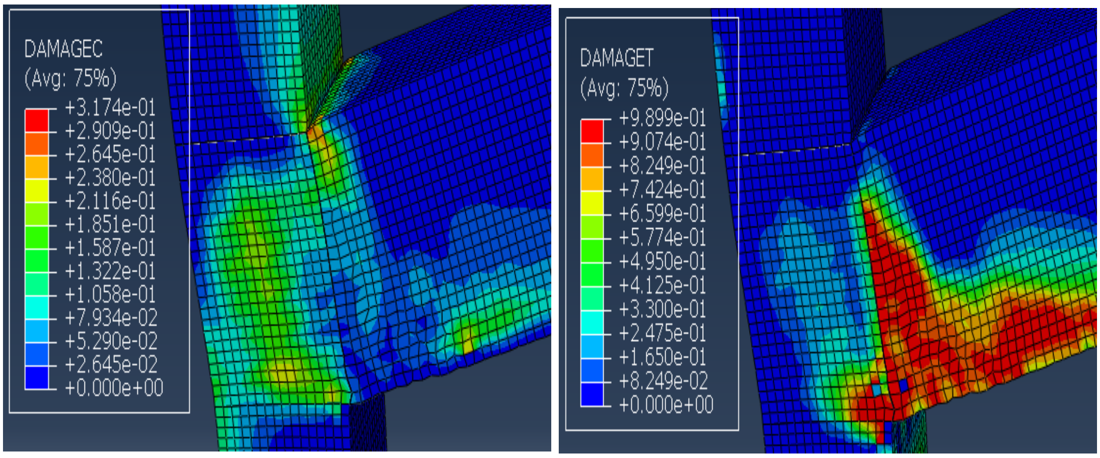

Figure 5. 43: Compressive and Tensile Damages in the System at yield point (SP-BCDR 1.4-L1-ALR 0.25).

Point two presents the peak load capacity. Similar to model (SP-BCDR 1.2-L1-ALR 0.25) at this point, the joints corner are reached their peak compressive strength. **Figures 5.44** and **5.45** show the tri-axial stress-strain curve for a point in the compression zone of the beam and the strain in the beam at the peak load point, respectively.

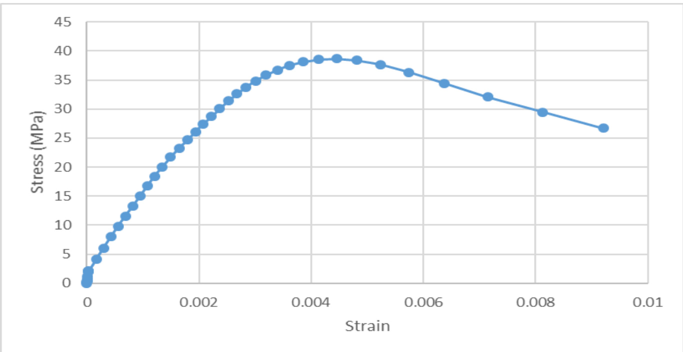

Figure 5. 44: Tri-Axial Stress-Strain Curve for Point in the Compression Zone of the Beam ((SP-BCDR 1.4-L1-ALR 0.25)

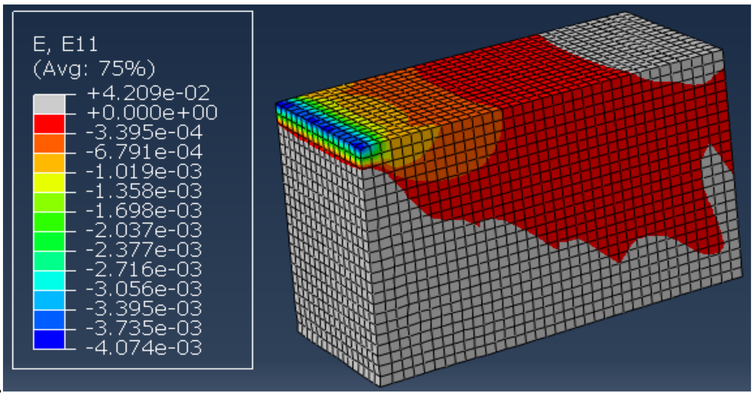

Figure 5. 45: Strain Crossponding to the Peak Load at the Compression Fiber in the Beam ((SP-BCDR 1.4-L1-ALR 0.25)

Point three presents the ultimate point when the steel is cutting. However, the reduction in load is not reach the ultimate point, which is 15% reduction of the load in the post peak portion. **Figure 5.46** shows the compressive and the tensile damage in the system. However, the cracks orientations become different at this depth. The high depths of the beam and joint explains this different. The compressions cracks in beams which extended to the middle of the beam are shown in **Figure 5.47**. Hence, the needs of skin reinforcements at this depth is important. **Figure 5.48** shows the stresses in beams stirrups.

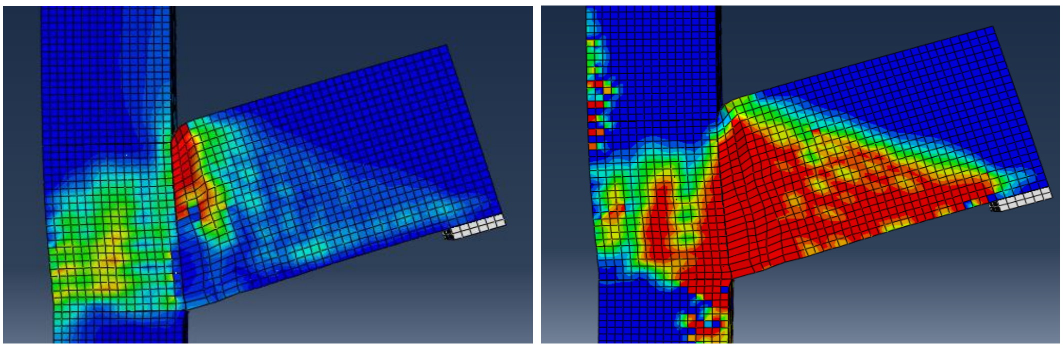

Figure 5. 46: Compressive and Tensile Damages in the System at Ultimate Point (SP-BCDR 1.4-L1-ALR 0.25)

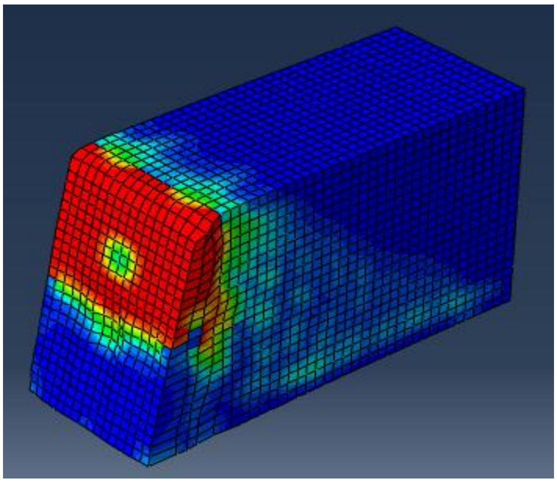

Figure 5. 47: Compressive Damage in the Beam at Ultimate Point (SP-BCDR 1.4-L1-ALR 0.25).

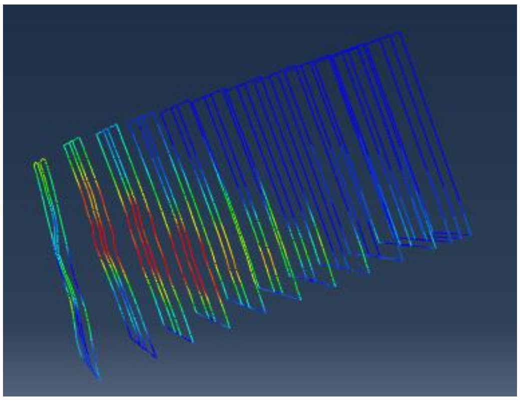

Figure 5. 48: Stress in Stirrups of the beam (SP-BCDR 1.4-L1-ALR 0.25).

For the model (SP-BCDR 1.6-L1-ALR 0.25) the (F.E) response is shown in **Figure 5.49**. The points (1-4) marks the stages of failures.

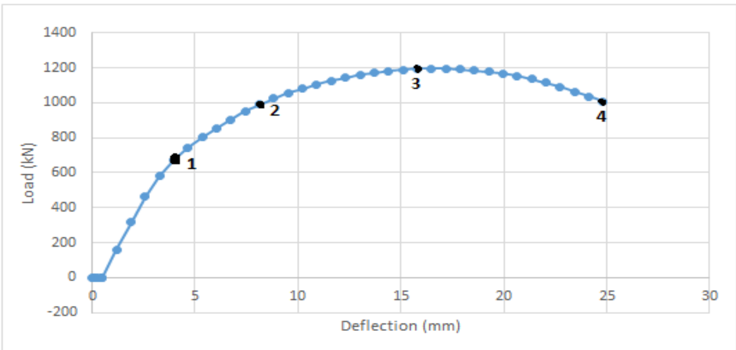

Figure 5. 49: Response of (SP-BCDR 1.6-L1-ALR 0.25) with Stages of Failures.

The failure occurs in the joints due to exceed the ultimate moment capacity of the joints. Point one represents the tensile cracking of concrete in the joints as shown in **Figure 5.50,** while point two presents the yielding of columns reinforcements at the compressions zone in the joints as shown in **Figure 5.51.** Point three presents the peak moments capacity of the joints. While point four presents the ultimate point when the load goes 15% reduction in the post peak portions due to the sever compression damage in the joints. **Figure 5.52** shows the instants of concrete crushing in the joint.

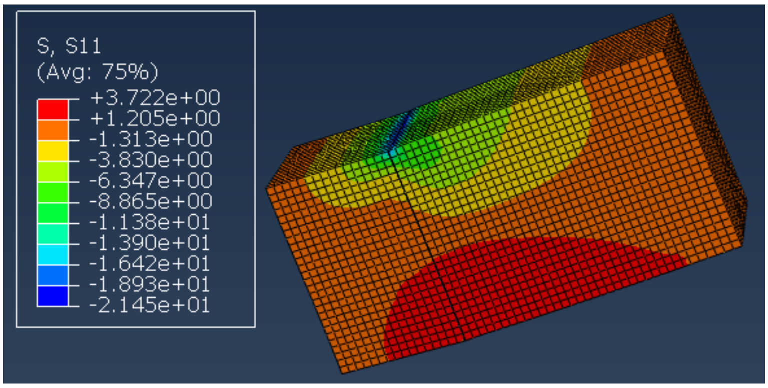

Figure 5. 50: Cracking of the Tensile Fiber on Beam and joint (SP-BCDR 1.6-L1-ALR 0.25).

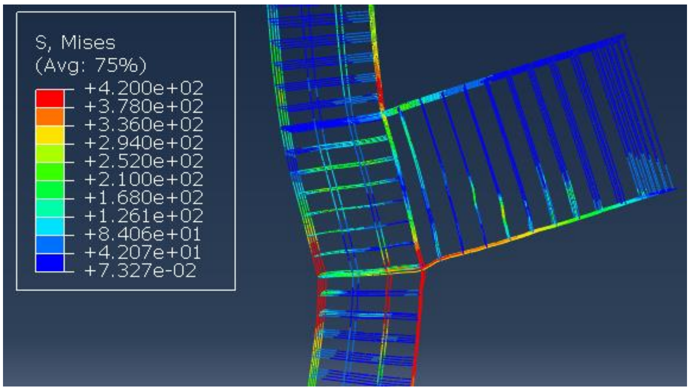

Figure 5. 51: Yielding of columns Steel (SP-BCDR 1.6-L1-ALR 0.25).

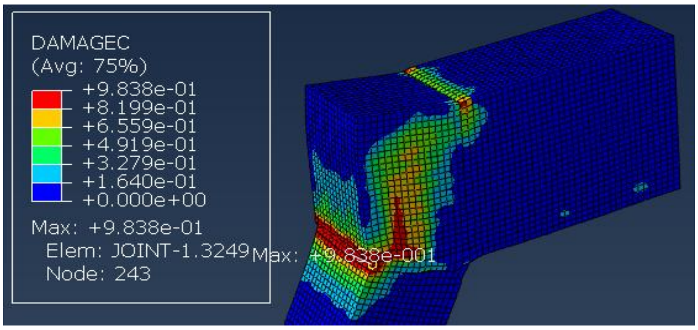

Figure 5. 52: Compression Damage in the Joints at Instant of Concrete Crushing (SP-BCDR 1.6-L1-ALR 0.25).

Finally, one can tracing the stresses in the models to analyze the capacity of the models. For the model (UB2-BCDR 1-L1-ALR 0.5), **Figures 5.53** and **5.54** show the compression block, pressure and the strain, respectively. While **Figure 5.55** shows the stresses in the beam reinforcement's in the plastic hinge zone.

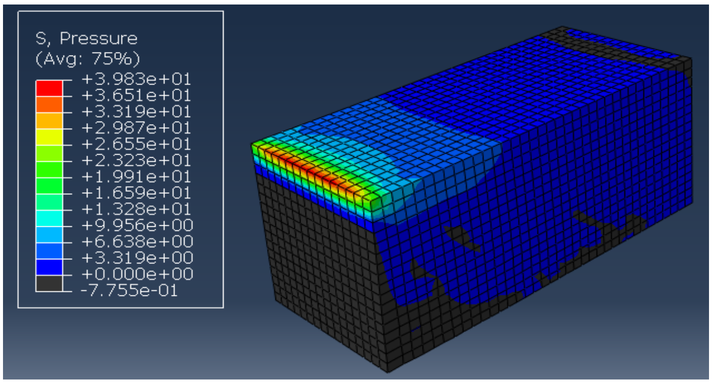

Figure 5. 53: Compressive block at peak load capacity (UB2-BCDR 1-L1-ALR 0.5).

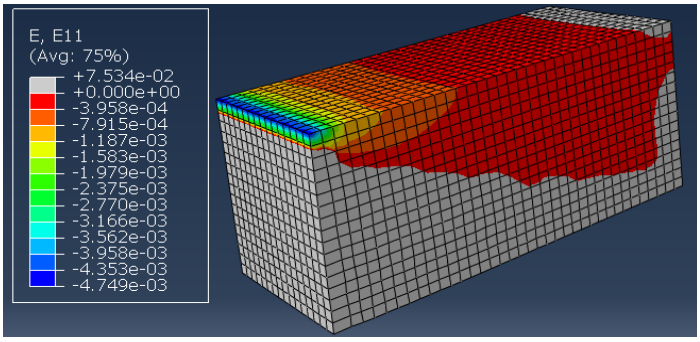

Figure 5. 54: Strains at the Critical Section of the Beam (UB2-BCDR 1-L1-ALR 0.5).

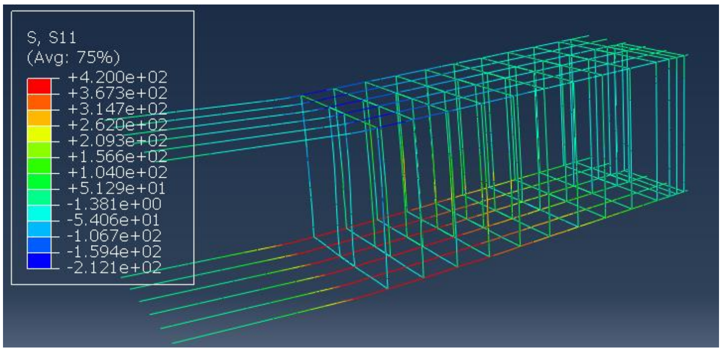

Figure 5. 55: Stress in the Beam reinforcements (UB2-BCDR 1-L1-ALR 0.5).

Based on **Figure 5.53** through **5.55**, the depth of the neutral axis is 46.4 mm and the stresses in the top and bottom reinforcements are 212 and 420 MPa, respectively. Hence, one can use the principle of mechanics to calculate the moment capacity at the critical section which is 464 kN.m which is computable with the analytical results which is 448 kN.m. However, the obtained value from ABAQUS is 512 kN.m. Thus, the additional capacity is due to the complex behavior between the stirrups and the longitudinal reinforcements.

Finally, based on the analyzing shown in this section. High cracks is developed when the beam depth equal 700 or higher. The next section presents the effect of skin reinforcements in the behaviors of the beams with depth equal or higher than 700 mm (BCDR 1.4).

5.6 Effect of Skin Reinforcements on the Behavior of the Deep Beam.

This section is conducted to study the effect of skin reinforcements on the behavior of joints. Two bars (Ø12) are added in the middle of the beam for simulation groups SP-BCDR 1.4, UB2- BCDR 1.4 and UB2-H BCDR 1.6 based on the analytical results from ABAQUS. **Figures 5.56** through **5.58** show the effect of adding skin reinforcements in the behaviors of the joints, while **Tables 5.9** tabulates the effect of adding skin reinforcements in the ductility of the joints.

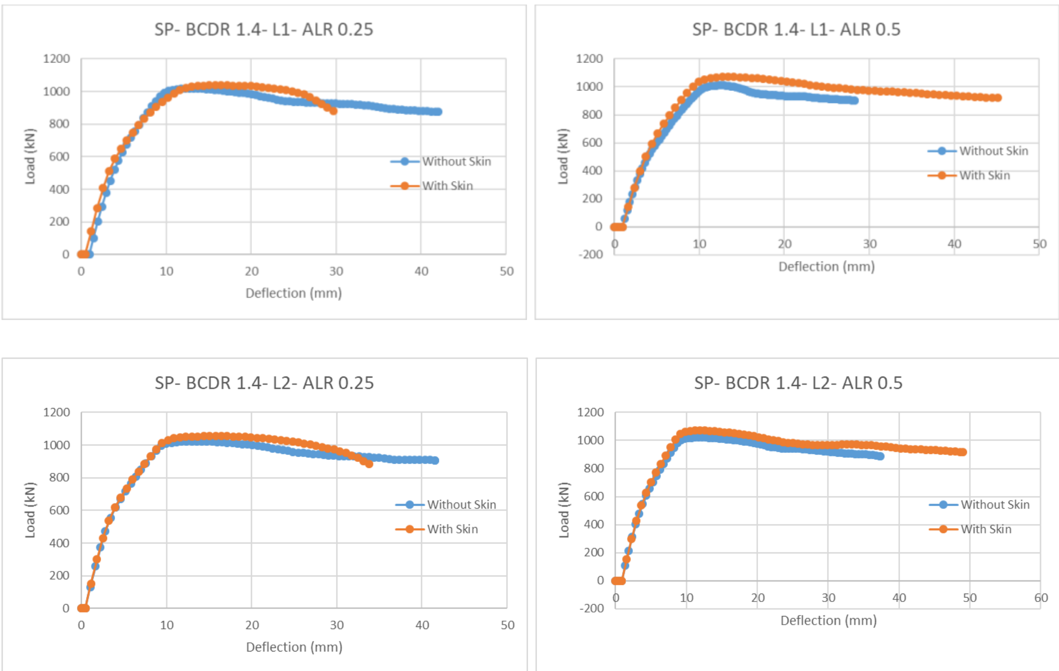

Figure 5. 56: Effect of Skin Reinforcement in the Behaviors of Joints Group (SP-BCDR 1.4).

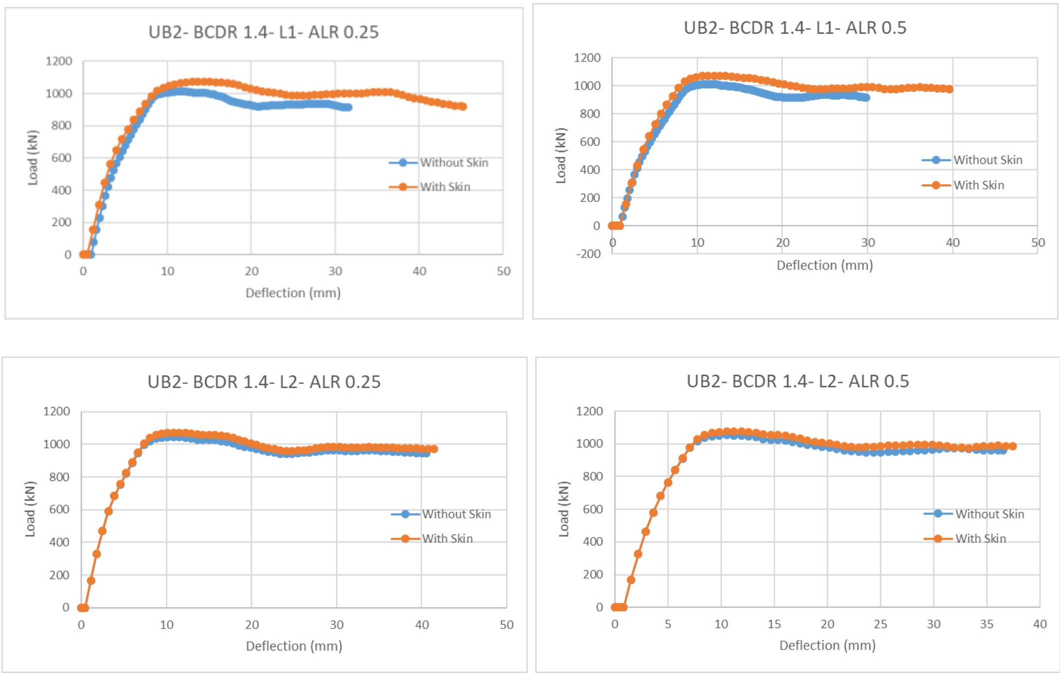

Figure 5. 57: Effect of Skin Reinforcement in the Behaviors of Joints Group (UP-BCDR 1.4).

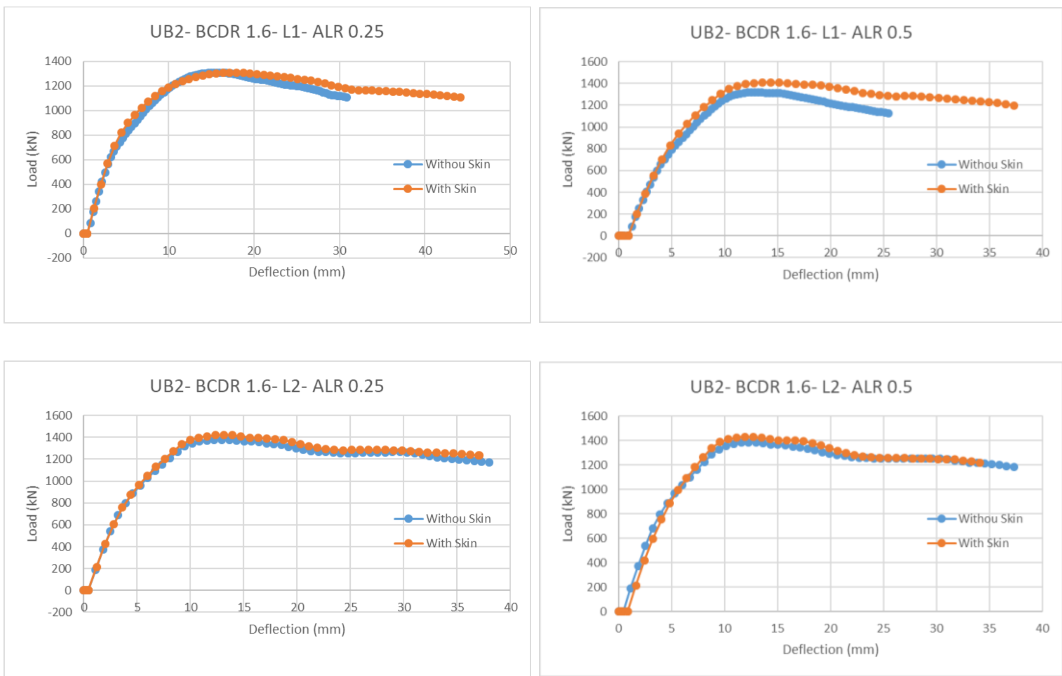

Figure 5. 58: Effect of Skin Reinforcement in the Behaviors of Joints Group (UP-BCDR 1.6).

Table 5. 9: Effect of Skin Reinforcement in the Ductility of Joints Group (SP- BCDR 1.4).

BCDR	Skin Reinforcements	Ultimate Deflection	Yield Deflection	Ductility
SP- BCDR 1.4-L1-ALR 0.25	Without	42.02	8.88	4.73
	with	29.65	7.18	4.13
SP- BCDR 1.4-L1-ALR 0.5	Without	28.26	9.50	2.97
	with	45.14	8.81	5.13
SP- BCDR 1.4-L2-ALR 0.25	Without	41.56	8.43	4.93
	with	33.83	6.79	4.98
SP- BCDR 1.4-L2-ALR 0.5	Without	37.37	8.30	4.50
	with	48.98	7.97	6.15
UB2- BCDR 1.4-L1-ALR 0.25	Without	31.55	7.85	4.02
	with	45.21	5.85	7.73
UB2- BCDR 1.4-L1-ALR 0.5	Without	29.85	7.96	3.75
	with	39.62	6.48	6.11
UB2- BCDR 1.4-L2-ALR 0.25	Without	40.54	6.73	6.02
	with	41.45	5.55	7.47
UB2- BCDR 1.4-L2-ALR 0.5	Without	36.51	7.01	5.21
	with	37.2	6.8	5.47
UB2- BCDR 1.6-L1-ALR 0.25	Without	30.71	10.97	2.80
	with	43.81	5.96	7.35
UB2- BCDR 1.6-L1-ALR 0.5	Without	25.46	9.79	2.60
	with	37.29	7.44	5.01
UB2- BCDR 1.6-L2-ALR 0.25	Without	38.00	8.46	4.49
	with	37.11	6.39	5.81
UB2- BCDR 1.6-L2-ALR 0.5	Without	37.74	8.39	4.50
	with	34.10	6.88	4.96

Based on **Table 5.9**, using skin reinforcements have a great effect in increasing the ductility of the beams with depth higher than 700 mm through minimizing the cracks in the beam. **Figure 5.59** shows the compressive cracks in beam before and after the use of skin reinforcements for the model (SP- BCDR 1.4-L1-ALR .25).

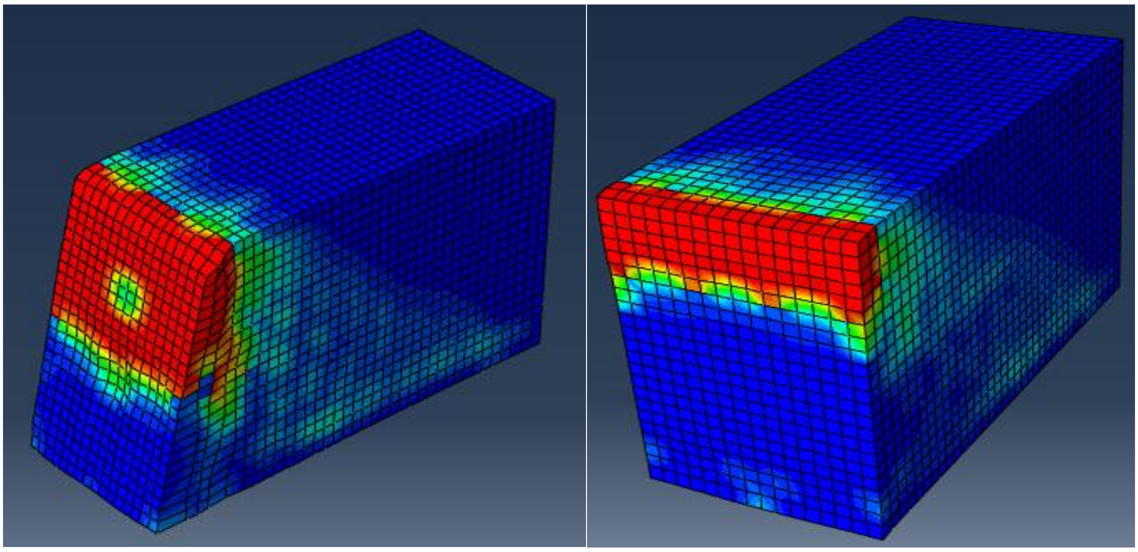

Figure 5. 59: Compression Cracks in the Beam: Left) without Skin Reinforcements and Right) After with Skin Reinforcement (SP- BCDR 1.4-L1-ALR .25).

5.8 Summary.

Based in the comparisons shown in this chapters, it is clear that the UHPC shows effectiveness in confining the sway special frame joints with complete dispensing of joints stirrups. In addition, the results show the importance of skin reinforcements in minimizing the compression cracks in the deep beams with depth equal or higher than 700 mm. Furthermore, the UHPC joints show superior in behaviors at column to beam moment capacity (CBM) ratio lower than 1.2. Thus, the next chapter is studying the behaviors of UHPC joints at CBM ratio violating the lower limit of ACI code. Finally, Table 5.10 summarizes the results of all models in this chapter.

Table 5. 10: The Results for all Models

Model ID	P_y (KN)	P_p (KN)	P_u (KN)	Δ_y (mm)	Δ_p (mm)	Δ_u (mm)	DI	MOF
SP-BCDR 0.6-L1-ALR 0.25	158	173	158	5.8	16.5	56.9	9.8	BF
SP-BCDR 0.6-L1-ALR 05	157	173	159	5.8	16.5	60.4	10.4	BF
SP-BCDR 0.6-L2-ALR 0.25	159	173	159	5.6	17.4	56.0	10.0	BF
SP-BCDR 0.6-L2-ALR 0.5	165	173	159	5.8	16.5	55.3	9.6	BF
UB2-BCDR 0.6-L1-ALR 0.25	152	173	157	5.8	13.5	60.5	10.3	BF
UB2-BCDR 0.6-L1-ALR 05	157	171	158	5.7	17.1	58.0	10.2	BF
UB2-BCDR 0.6-L2-ALR 0.25	156	172	158	6.0	17.1	56.1	9.3	BF
UB2-BCDR 0.6-L2-ALR 0.5	152	172	158	5.8	15.3	57.0	8.4	BF
SP-BCDR 1-L1-ALR 0.25	493	516	474	7.0	13.4	43.3	6.2	BF
SP-BCDR 1-L1-ALR 05	512	524	474	7.1	9.9	52.7	7.4	BF
SP-BCDR 1-L2-ALR 0.25	505	518	477	6.5	9.2	46.6	7.1	BF
SP-BCDR 1-L2-ALR 0.5	501	519	475	6.5	9.2	46.7	7.1	BF
UB2-BCDR 1-L1-ALR 0.25	478	506	485	5.4	13.5	45.4	8.4	BF
UB2-BCDR 1-L1-ALR 05	488	510	478	5.8	14.0	37.4	6.4	BF
UB2-BCDR 1-L2-ALR 0.25	458	508	472	5.8	13.1	37.1	6.4	BF
UB2-BCDR 1-L2-ALR 0.5	459	507	476	5.6	13.2	38.3	6.8	BF
SP-BCDR 1.2-L1-ALR 0.25	676	741	636	7.6	16.5	48.7	6.4	BF*
SP-BCDR 1.2-L1-ALR 05	713	744	715	7.6	15.8	50.6	6.6	BF
SP-BCDR 1.2-L2-ALR 0.25	729	747	640	7.4	13.7	43.6	5.9	BF*
SP-BCDR 1.2-L2-ALR 0.5	709	741	685	7.4	10.6	51.3	6.9	BF
UB2-BCDR 1.2-L1-ALR 0.25	718	755	709	6.1	13.7	40.6	6.7	BF
UB2-BCDR 1.2-L1-ALR 05	718	754	710	6.1	12.3	39.3	6.5	BF

UB2-BCDR 1.2-L2-ALR 0.25	732	753	710	7.3	11.5	39.4	5.4	BF
UB2-BCDR 1.2-L2-ALR 0.5	734	755	714	6.0	9.5	39.5	6.6	BF
SP-BCDR 1.4-L1-ALR 0.25	971	1018	876	9.3	7.1	33.8	4.8	BF
SP-BCDR 1.4-L1-ALR 05	951	1011	903	9.7	8.6	40.3	4.7	BF
SP-BCDR 1.4-L2-ALR 0.25	968	1022	907	8.8	8.1	32.1	4.0	BF
SP-BCDR 1.4-L2-ALR 0.5	983	1021	889	8.7	7.9	46.3	5.9	BF
UB2-BCDR 1.4-L1-ALR 0.25	959	1013	916	8.1	7.1	41.6	5.9	BF
UB2-BCDR 1.4-L1-ALR 05	944	1011	913	8.2	7.1	30.6	4.3	BF
UB2-BCDR 1.4-L2-ALR 0.25	996	1044	944	7.4	6.0	40.8	6.8	BF
UB2-BCDR 1.4-L2-ALR 0.5	978	1054	959	7.1	6.4	38.0	5.9	BF
SP-BCDR 1.6-L1-ALR 0.25	936	1116	946	7.4	8.9	42.0	4.7	JF
SP-BCDR 1.6-L1-ALR 05	992	1196	1007	8.1	9.5	28.3	3.0	BF*
SP-BCDR 1.6-L2-ALR 0.25	1215	1248	1062	12.3	8.4	41.6	4.9	BF*
SP-BCDR 1.6-L2-ALR 0.5	1243	1280	1083	12.3	8.3	37.4	4.5	BF*
UB2-BCDR 1.6-L1-ALR 0.25	1037	1307	1108	7.7	7.9	31.5	4.0	BF*
UB2-BCDR 1.6-L1-ALR 05	1263	1320	1125	10.1	8.0	29.9	3.8	BF
UB2-BCDR 1.6-L2-ALR 0.25	1270	1377	1172	8.8	6.7	40.5	6.0	11
UB2-BCDR 1.6-L2-ALR 0.5	1284	1386	1176	8.8	7.0	36.5	5.2	BF
SP-BCDR 1.4-L1-ALR 0.25-S	835	1037	878	7.18	15.8	29.7	4.1	BF*
SP-BCDR 1.4-L1-ALR 05-S	1003	1071	921	8.81	13.4	45.1	5.1	BF
SP-BCDR 1.4-L2-ALR 0.25-S	838	1055	903	6.79	16.4	33.8	5.0	BF*
SP-BCDR 1.4-L2-ALR 0.5-S	1006	1072	917	7.97	11.3	49.0	6.2	BF

Table 5.10 (Continue): The Results for all Models

Model ID	P_y (KN)	P_p (KN)	P_u (KN)	Δ_y $(mm$	Δ_p $(mm$	Δ_u $(mm$	D	MOF*
UB2-BCDR1.4-L1-ALR0.25-S	835	1074	920	5.85	13.7	45.2	7.7	BF
UB2-BCDR 1.4-L1-ALR 0.5-S	867	1071	976	6.48	12.0	39.6	6.1	BF
UB2-BCDR1.4-L2-ALR0.25-S	890	1071	971	5.55	10.9	41.5	7.5	BF
UB2-BCDR 1.4-L2-ALR 0.5-S	1073	1076	985	9.8	11.2	37.4	7.7	BF
UB2-BCDR1.6-L1-ALR0.25-S	965	1309	1113	5.96	17.2	43.8	7.4	CF
SP-BCDR 1.4-L2-ALR 0.5-S	1006	1072	917	7.97	11.3	49.0	6.2	BF
UB2-BCDR1.4-L1-ALR0.25-S	835	1074	920	5.85	13.7	45.2	7.7	BF
UB2-BCDR 1.4-L1-ALR 0.5-S	867	1071	976	6.48	12.0	39.6	6.1	BF

Where BF, BF*, CF and JF refer to beam flexure failure due to steel rapture, flexure failure due to reach 15% load reduction, column failure and joint failure, respectively.

CHAPTER SIX

6. UHPC JOINTS WITH CBM RATIO VIOLATING THE LOWER LIMIT OF ACI.

6.1 Overview.

As shown in the previous chapter, the UHPC joints are able to hold with some violations in CBM ratio. This chapter is made to establish a new lower limit of CBM ratio that can be used when UHPC is used in the joint. Although the ACI code do not consider the confinement effect in the moment capacity of the column, one can explain this neglecting because the possibility of concrete crushing in the joints. However, this is not the same for UHPC joints which have high tension and compression capacity. In this chapter, a confined moment-axial capacity interaction diagrams for the column are needed. Thus, the constitutive stress-strain models for the confined concrete are presented. After that, the behaviors for a set of model violating the lower limit of ACI are presented. Finally, the effect of stress hardening (SH) of steel reinforcements in the CBM ratio has been discussed. The value of this chapter is establishing a new lower limit for the column reinforcement configurations used in this thesis based on the confined capacity of the columns. This investigation can be later used to generalize the results for other types of joints with different column dimensions and reinforcement configurations.

6.2 Constitutive stress-strain model for concrete confined laterally.

Many constitutive models for concrete confined with rectangular hoops or spirals are proposed. **Table 6.1** summarizes some of these models.

Table 6. 1: Comparison between Concrete Confined Models. (Ali and Javad 2016).

Model name	Comment
Kent and Park (1979)	They used small scale specimens. The model assumes that the confinement increase the ductility and have no effect in the strength. **Figure 6.1**.
Sheikh and Uzumeri (1982)	The model considers the effective confined area using large scale specimens. However, it retains in unsafe stresses at high axial loads. **Figure 6.2**.
Scott et al. (1982)	The modified Kent and park model. It considers both the strength and ductility. **Figure 6.3.**
Mander et al. (1988)	The model considers the effective lateral confinement pressure, longitudinal reinforcement and loading rates. Also, it can be used for any type of sections with average compressive strength of 30 MPa.
Fafitis and Shah (1985)	The model used empirical approach to construct stress-strain curve.
Cusson and Paultre (1995).	The model is used for high strength concrete. It uses the actual stress in the transverse reinforcement instead of yield strength.
Saatcioglu and Razvi (1992)	The model was conducted based on the argument that transverse reinforcement generate lateral confinement with stress increments to resist lateral expansion. The model were improved to cover wide range of compressive strength (30-130 MPa).

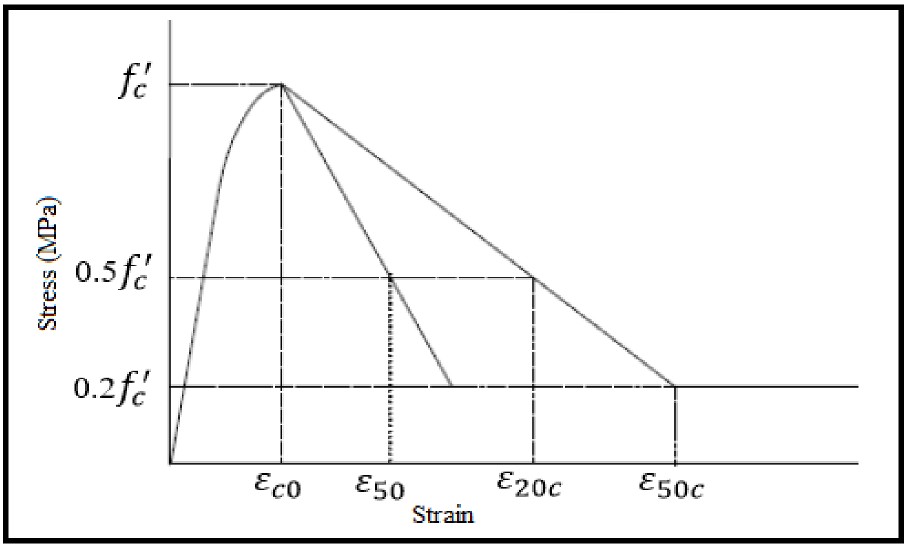

Figure 6. 1: Stress-Strain Curve for Confined Concrete. (Kent and Park 1971).

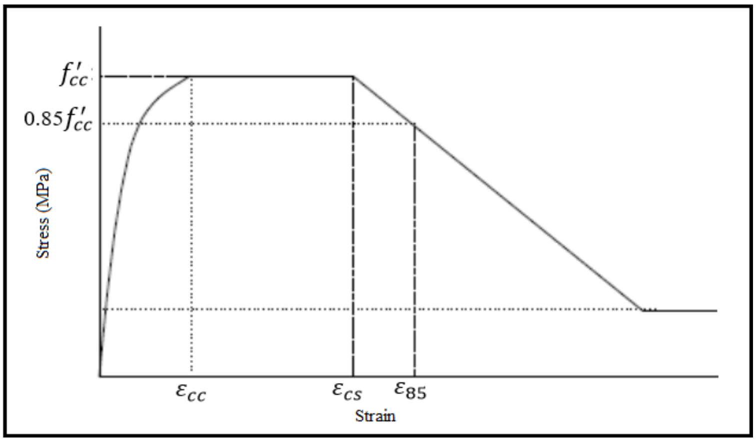

Figure 6. 2: Stress-Strain Curve for Confined Concrete. (Sheikh and Uzumeri 1982).

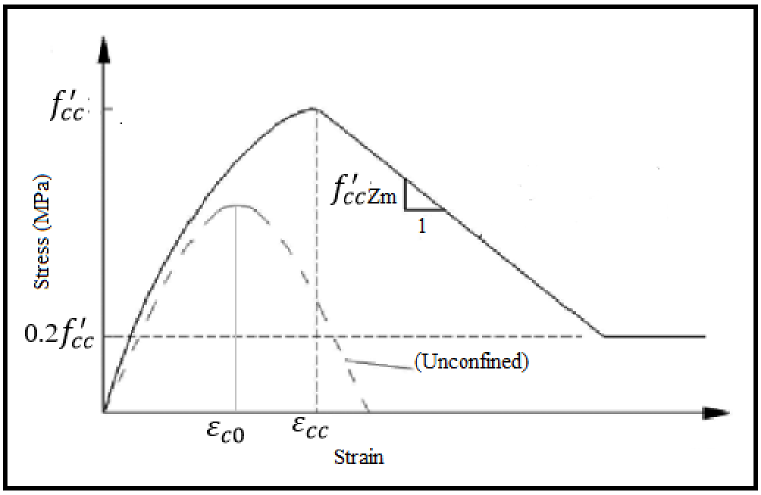

Figure 6. 3: Stress-Strain Curve for Confined Concrete. (Scott et al. 1982).

Ali and Javad (2016) conducted a comparison between these models. The study showed that the models proposed by **Mander et al. (1988) and Saatcioglu and Razvi (1992)** are considered most suitable in predicting strength and ductility for normal strength concrete; since they consider wide range of variables with many loading rates.

Figure 6.4 represents the model proposed by **Mander et al. (1988),** the model assumed that the confinement capacity of the hoops will be stored in the effectively confined concrete core. **Figure 6.5 and 6.6** show the arching action and the ineffective confined area for circular and rectangular hoops, respectively. The model consider the longitudinal and the transverse reinforcements including circular hoops, spirals and rectangular stirrups with or without crossties.

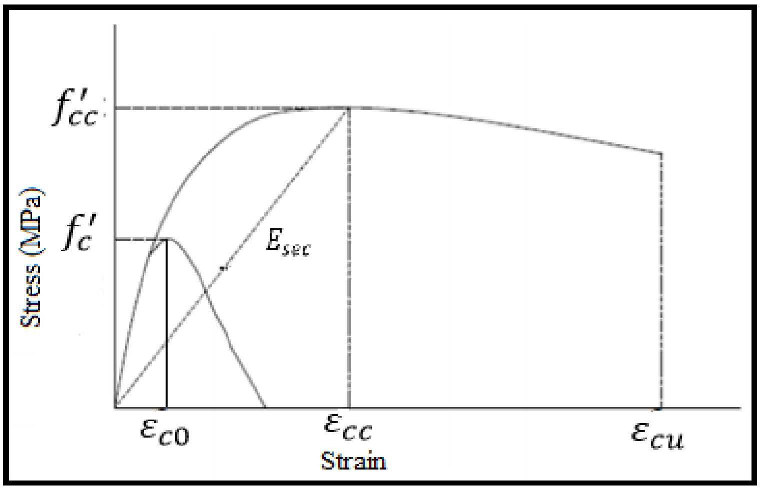

Figure 6. 4: Stress-Strain Curve for Confined Concrete. (Mander et al. 1988).

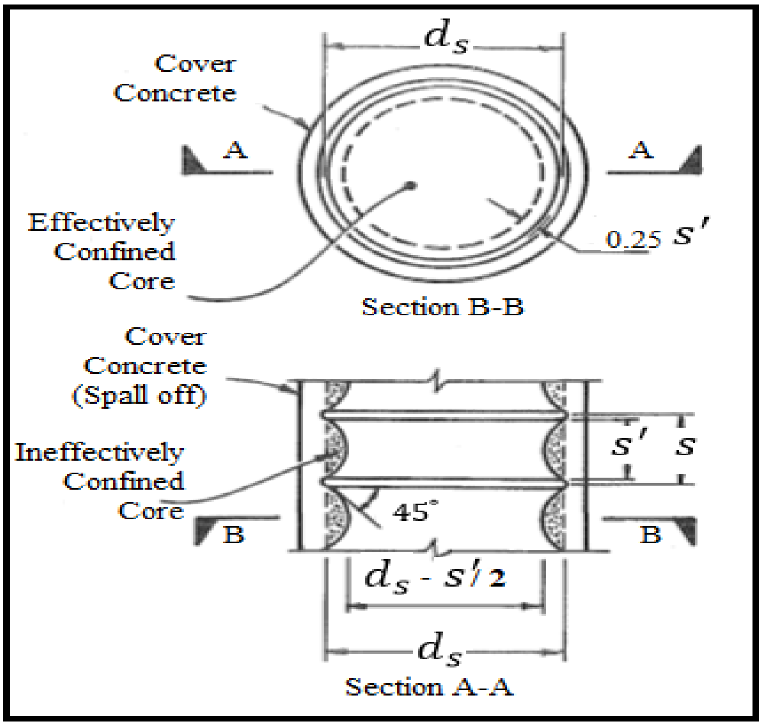

Figure 6. 5: Arching Action and Effective Confined Area with Circular Transverse Reinforcement. (Mander et al. 1988).

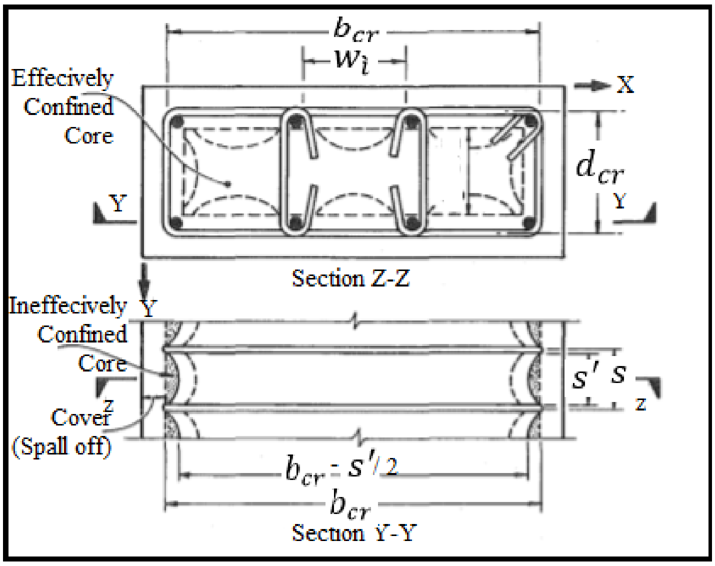

Figure 6. 6: Arching Action and Effective Confined Area with Rectangular Transverse Reinforcement. (Mander et al. 1988).

Similar to **Mander et al. (1988)** model, **Saatcioglu and Razvi (1992)** model assumed the effective confinement pressure will be restored in the effective concrete core. However, **Mander et al. (1988)** model assumed the confinement pressure will be kept until hoops fracturing. On the other hand, **Saatcioglu and Razvi (1992)** model assumes that the maximum confinement pressure will be at maximum transverse strain crossponding to peak confined compressive strength. Behind the peak stresses in the concrete, the material begins softening until failure. Thus, **Saatcioglu and Razvi (1992)** model is proposed to be more appropriate to use in this study. **Figure 6.7** represents **Saatcioglu and Razvi (1992)** model.

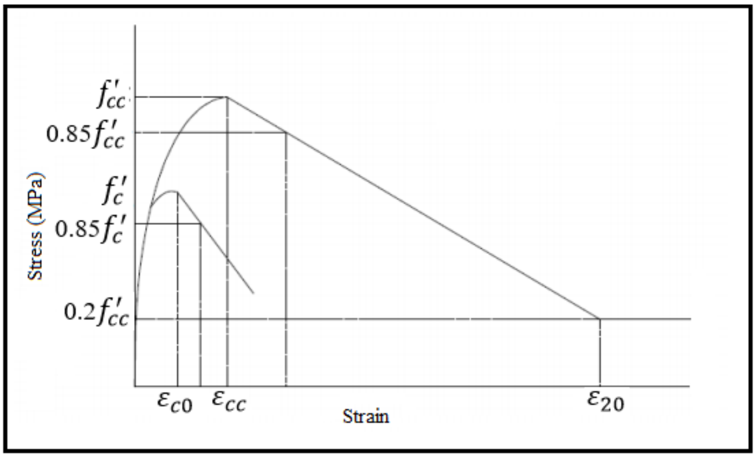

Figure 6. 7: Stress-Strain Curve for Confined Concrete. (Saatcioglu and Razvi 1992).

$$\sigma_{cc} = \grave{f}_{cc}\left[2\left(\frac{\varepsilon_c}{\varepsilon_1}\right) - \left(\frac{\varepsilon_c}{\varepsilon_1}\right)^2\right]^{(1/(1+2K)} \quad [6.1]$$

With:

$$\grave{f}_{cc} = \grave{f}_c + k_{1sr} f_{le} \quad [6.2]$$

$$k_{1sr} = 6.7(f_{le})^{-0.17} \quad [6.3]$$

$$f_{le} = \begin{cases} k_{2sv} f_l, square\ and\ circular\ \ sections \\ \frac{f_{lex}+f_{ley}}{b_{cx}+b_{cy}},\ rectangular\ sections \end{cases} \quad [6.4]$$

$$f_l = \begin{cases} \frac{2A_{sp}f_{yt}}{d_c s}, spiral \\ \frac{\sum A_v f_{yt}}{s\ b_c}, square\ section \end{cases} \quad [6.5]$$

$$k_{2sr} = \begin{cases} 1,\ spiral\ and\ closly\ spaced\ lateral \\ \quad reinforcement\ square\ sections \\ 0.26\sqrt{\left(\frac{b_c}{s}\right)\left(\frac{b_c}{s_1}\right)\left(\frac{1}{f_l}\right)}, \leq 1,\ square\ section\ without \\ \quad closly\ spaced\ hoops \end{cases} \quad [6.6]$$

$$f_{lex} = \frac{\sum A_{vx} f_{yt}}{s\ b_{cx}} \quad [6.7]$$

$$f_{ley} = \frac{\sum A_{vy} f_{yt}}{s\ b_{cy}} \quad [6.8]$$

$$\varepsilon_{cc} = \varepsilon_{c0}(1+5K) \quad [6.9]$$

$$K = \frac{k_{1sr} f_{le}}{\grave{f}_{c0}} \quad [6.10]$$

$$\varepsilon_{85} = 260\rho\varepsilon_1 + \varepsilon_{085} \quad [6.11]$$

$$\varepsilon_{20} = 5\varepsilon_{cc} \quad [6.12]$$

σ_{cc}: Confined concrete compressive strength crossponding to the traced confined concrete longitudinal strain ε.

$\grave{f}_{cc}$: Peak confined concrete compressive strength cross ponding to strain ε_1.

$0.85\grave{f}_{cc}$: 15% reduction of peak confined concrete compressive strength in descending post peak portion cross ponding to strain ε_{85}.

$0.2\grave{f}_{cc}$: 80% reduction of peak confined concrete compressive strength in descending post peak portion cross ponding to strain ε_{20}.

K: Saatcioglu and Razvi effective confinement ratio.

$\grave{f}_{c0}$: Peak unconfined concrete compressive strength crossponding to peak unconfined longitudinal strain ε_{01}, a value of 0.002 is recommended.

$0.85\grave{f}_{c0}$: 15% reduction of peak unconfined concrete compressive strength in descending post peak portion cross ponding to strain ε_{085}.a value of 0.0038 is recommended.

k_{1sr}: Effectiveness confinement ratio of effectiveness pressure restored in the concrete.

f_{le}: Effective confinement pressure.

f_{lex}: Effective confinement pressure in the x direction for rectangular sections.

f_{lex}: Effective confinement pressure in the y direction for rectangular sections.

f_l: Hoops confinement pressure.

k_{2sr}: Effective confinement pressure in the hoops.

A_v: Area of hoops cross section.

A_{vx}: Area of hoops cross section in the x direction.

A_{vy}: Area of hoops cross section in the y direction.

d_c: Center to center diameter of the core for spiral reinforcement.

b_c: Center to center core width for square sections.

b_{cx}: Center to center core width for rectangular sections in x direction.

b_{cy}: Center to center core width for rectangular sections in y direction.

s_1: Spacing between longitudinal reinforcement in rectangular section.

s: Spacing between ties.

Finally, the next section presents the methodology of evaluation the confined moment capacity of the core of the column based on **(Saatcioglu and Razvi 1992)** model**.**

6.3 Methodology of Evaluating the Moment Capacity of the Confined Core of the Column.

In general, the confinement effect has a positive influences in increasing the concrete compressive strength f_c' and the ultimate strain of the confined concrete ε_u. In other word, higher compression and moment capacities for the confined core. However, the confinement effect is significantly affected with the amount and the arrangement of the transverse reinforcement. Hence, the reinforcements detailings must be specified to construct the confined stress-strain curve of the confined concrete. The column dimensions (500mm×500mm) and the reinforcements detailings ($3\emptyset 10$ @ $100mm$) are shown in **Figure 6.8**.

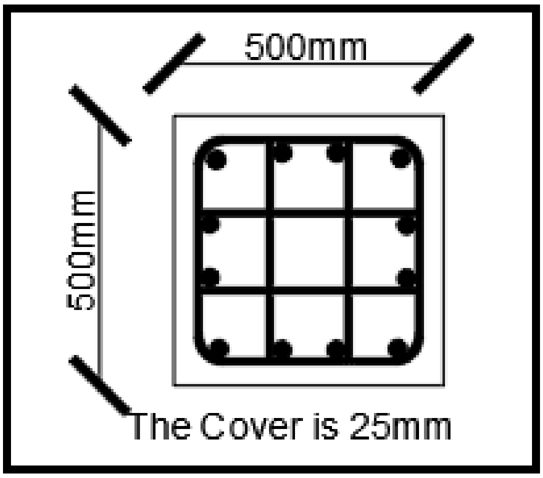

Figure 6. 8: Transverse Reinforcement Arrangement in Column.

Referring to **Saatciogle and Razvi (1992)** model which presented in the previous section, the stress-strain curve for confined concrete in the core of the column used in this study. is shown in **Figure 6.9**.

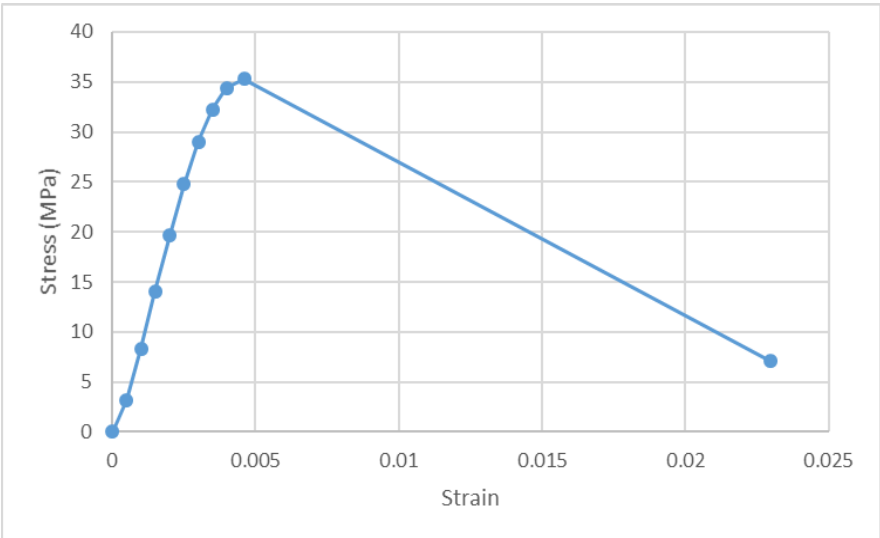

Figure 6. 9: Stress-Strain Curve for Confined Concrete Using Saatciogle and Razvi model.

Using the stress-strain curve shown in **Figure 6.9**, Whitney block parameters can be determined. The centroid of Whitney block $(\frac{a}{2})$ must be consistent with the stress-strain curve centroid. In addition, the area under the rectangular block must have the same area under the stress-strain curve. The curve is divided into two areas in which the first area is from the origin to the peak stress f'_{cc}, the peak stress is crossponding to strain 0.0046, while the second area is from the peak stress to the ultimate stress at $0.85f'_{cc}$. The ultimate stress point is crossponding to strain of 0.00943. Thereafter, the following procedure can be used to calculate the parameters of Whitney block.

Equation 6.13 which obtained from excel is described the ascending portion of the curve. The integration of this equation represents the first area while the second area can be determined using **Equation 6.14**.

$$\sigma_c = -5 \times 10^8 \varepsilon_c{}^3 + 2 \times 10^6 \varepsilon_c{}^2 + 7153\varepsilon_c - 0.3732 \qquad [6.13]$$

Then:

Area one= $\int_0^{0.0046} -5 \times 10^8 \varepsilon_c{}^3 + 2 \times 10^6 \varepsilon_c{}^2 + 7153\varepsilon_c - 0.3732 = 0.0829$

And the centroid $= \frac{\int_0^{0.0046} (-5\times10^8 \varepsilon_c{}^3 + 2\times10^6 \varepsilon_c{}^2 + 7153\varepsilon_c - 0.3732) * \varepsilon_c}{\int_0^{0.0046} -5\times10^8 \varepsilon_c{}^3 + 2\times10^6 \varepsilon_c{}^2 + 7153\varepsilon_c - 0.3732} = 0.00297$

$$\text{The second area} = \frac{1.85 f'_{cc}}{2} \times (\varepsilon_u - \varepsilon_0) = 0.1564 \qquad [6.14]$$

And the centroid of the second area= 0.00674

Thus

The total area =0.2393 and the centroid of the stress-strain curve using the weighted average = 0.00533=> $\frac{a}{2}$ = 0.00943-0.00533=0.0041

Then $a = 0.0082 \rightarrow k_2 = \frac{0.0082}{\varepsilon_u} = 0.87$

And $k_1 k_3 = \frac{Area\ under\ stress\ strain\ curve}{a * f'_{cc}} = 0.834$

After that, the main points of moment-axial capacity interaction diagram for the confined core of the column used in this study can be constructed.

Figure 6.10 shows the moment-axial capacity interaction diagrams for confined concrete core with confined compressive strength f'_{cc} 35 MPa.

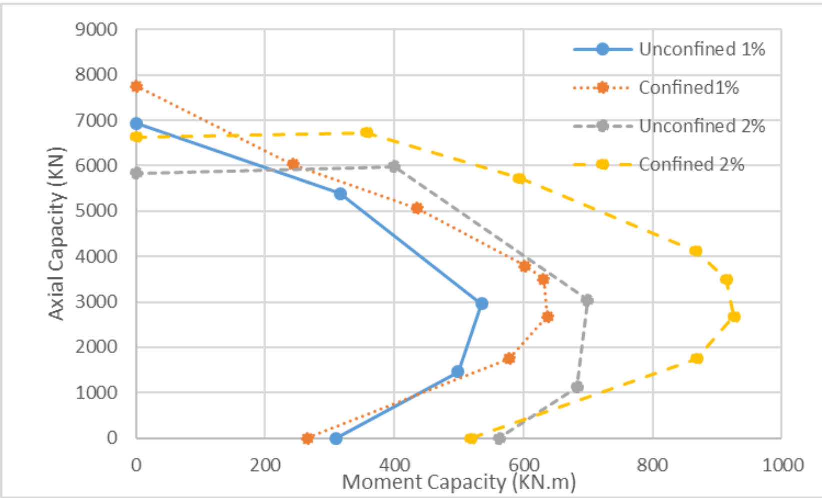

Figure 6. 10: Moment Capacity-Axial Capacity Interaction Diagrams for the confined core of the Column.

Based on the interaction diagrams shown in **Figure 6.10**, one can specify the maximum beam capacity which would be twice the moment capacity of the column for exterior joints. Thus, one can use the same approach to calculate the moment capacity of the beams confined with stirrups since the compression zone of the beam is restrained in the zone near the neutral axis as **Park and Paulay (1975).** In addition, the compression zone is restrained in the normal direction of the connected surface with UHPC joints. However, there is no significant difference in the beam moment capacity comparing with the ACI code equations. Thus, **Table 6.2** tabulates the ultimate moments capacity of the beams with depth of 300 through 1000 mm (H70) according to ACI-318.

Table 6. 2: Ultimate Moment Capacities for Beams.

Beam Depth (mm)	Ultimate Moment Capacity (kN)
300	148
500	448
600	660
700	914
800	1209
900	1544
1000	1922

Based on **Figure 6.10** and **Table 6.2**, the next section presents the behaviors of set of model with violating the lower limit of ACI code.

6.4 Behaviors for Models with CBM ratio Violating the lower limit of ACI.

In this section, the CBM ratio for a set of model with CBM ratio violating the lower limit of ACI code are revaluated based on confined moment capacity of columns core. **Table 6.3** shows the models and the crossponding CBM ratio according to ACI code and the confined model. While **Table 6.4** shows the allowable confined to ACI beam capacity ratio.

Based on the results of Chapter Five in this thesis, skin reinforcement are added for beam with depth higher than 700mm

Table 6. 3: The CBM Ratio for a Set of Model According to the ACI Code and the Confined Model.

Model ID	ACI M_{ub} (kN)	ACI M_{uc} (kN)	Confined M_{uc} (kN)	ACI CBM ratio	Confined CBM ratio	**Expected Column Failure
UB2-BCDR 1.4-L1-ALR 0.25	860	477	578	*1.11	1.34	Y/N
UB2-BCDR 1.4-L1-ALR 0.5	860	558	631	1.30	1.47	N/N
UB2-BCDR 1.4-L2-ALR 0.25	860	649	868	1.51	2.02	N/N
UB2-BCDR 1.4-L2-ALR 0.5	860	752	914	1.75	2.13	N/N
UB2-BCDR 1.6-L1-ALR 0.25	1134	477	578	*0.84	1.02	Y/N
UB2-BCDR 1.6-L1-ALR 0.5	1134	558	631	*0.98	1.11	Y/N
UB2-BCDR 1.6-L2-ALR 0.25	1134	649	868	*1.14	1.53	Y/N
UB2-BCDR 1.6-L2-ALR 0.5	1134	752	914	1.33	1.61	N/N

Table 6.3 (Continue): The CBM Ratio for a Set of Model According to the ACI Code and the Confined Model.

Model ID	ACI M_{ub} (kN)	ACI M_{uc} (kN)	Confined M_{uc} (kN)	ACI CBM ratio	Confined CBM ratio	Expected Column Failure
UB2-BCDR 1.8-L1-ALR 0.25	1463	477	578	*0.65	*0.79	Y/Y
UB2-BCDR 1.8-L1-ALR 0.5	1463	558	631	*0.76	*0.86	Y/Y
UB2-BCDR 1.8-L2-ALR 0.25	1463	649	868	*0.89	1.19	Y/N
UB2-BCDR 1.8-L2-ALR 0.5	1463	752	914	*1.03	1.25	Y/N
UB2-BCDR 2-L1-ALR 0.25	1796	752	914	*0.84	1.02	Y/N

*Violating the lower limit of CBM ratio.

**According to ACI (left) and the Confined model (right).

Y: The failure expected to be in column.

N: The failure not expected to be in column.

Table 6. 4: Confined to ACI Beam Capacity Ratio.

ρ_c	ALR	$(Confined/ACI)$ Beam Capacity Ratio
1%	0.25	1.45
1%	0.5	1.36
2%	0.25	1.60
2%	0.5	1.46

As shown in **Table 6.4**, the confined model allows a violations in CBM ratio comparing with the unconfined CBM ratio. However, the models UB2-BCDR 1.6-L1-ALR 0.25 and the models of group UB2-H80 were shown earlier in Chapter Five in this thesis. Thus, the behavior of model groups UB2-H90 and UB2-H100-L2-P50 are shown in **Figures 6.11. Table 6.5** shows the ductility of these models with the mode of failure.

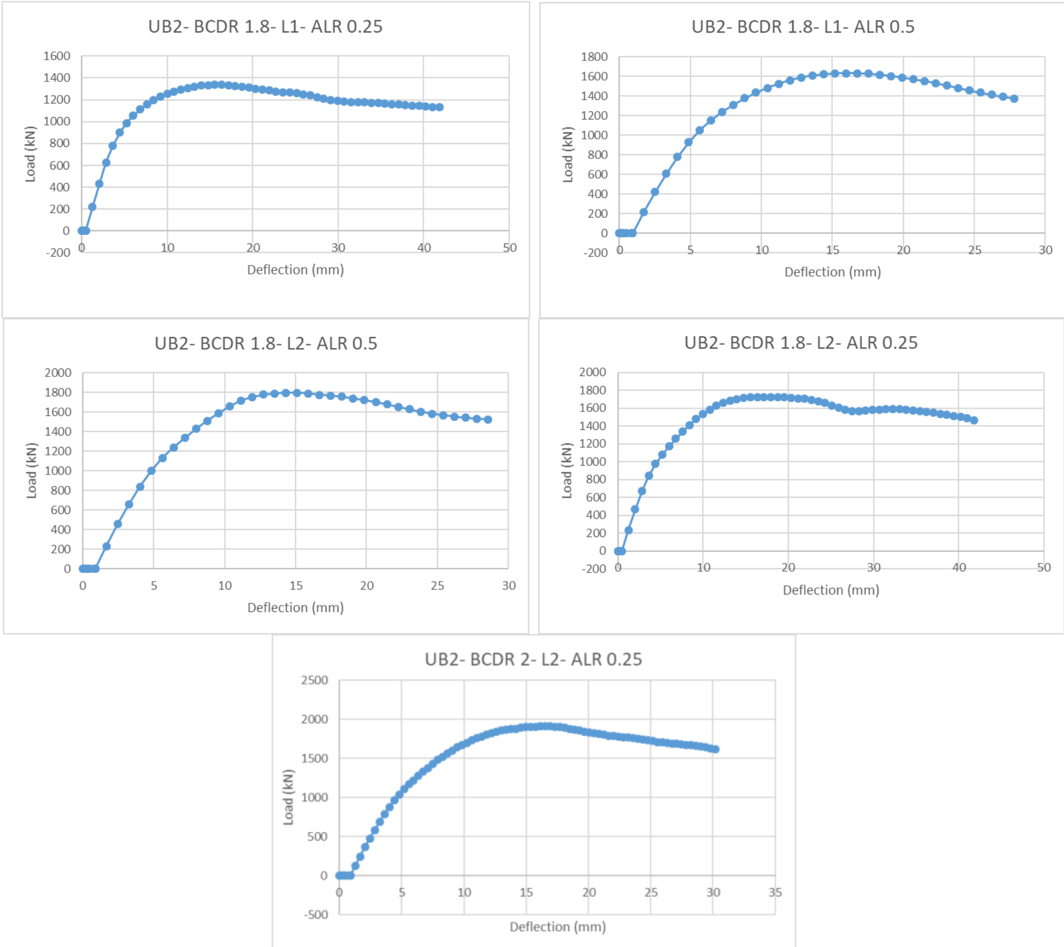

Figure 6. 11: Behaviors of the Models with CBM Ratio Violating the Lower Limit of ACI.

Table 6. 5: Ductility and Mode of Failures for Models with CBM Ratio Violating the Lower Limit of ACI

Model ID	Ultimate Deflection	Yield Deflection	Ductility	Mode of Failure
UB2-BCDR 1.8-L1-ALR 0.25	41.2	Not Yielded	-	Flexural in Column
UB2-BCDR 1.8-L1-ALR 0.5	27.1	8.19	3.30	Flexural in Column
UB2-BCDR 1.8-L2-ALR 0.25	41.4	11.21	3.69	Flexural in Beam
UB2-BCDR 1.8-L2-ALR 0.5	28.56	10.4	2.75	Flexural in Beam
UB2-BCDR 2-L1-ALR 0.25	45.78	29.4	1.56	Flexural in Beam

As shown in **Figure 6.11** and **Table 6.5,** the failures are ductile even with columns failures because of high stirrups ratio in columns. **Figure 6.12** shows the location of failures for the models specified in **Table 6.3**. These results, assure the possibility of use the confined model in predicting the capacity of columns. However, for model UB2-H80-L1-P25 the mode of failure is different with adding the skin reinforcements. **Figure 6.13** shows the failures locations for these models.

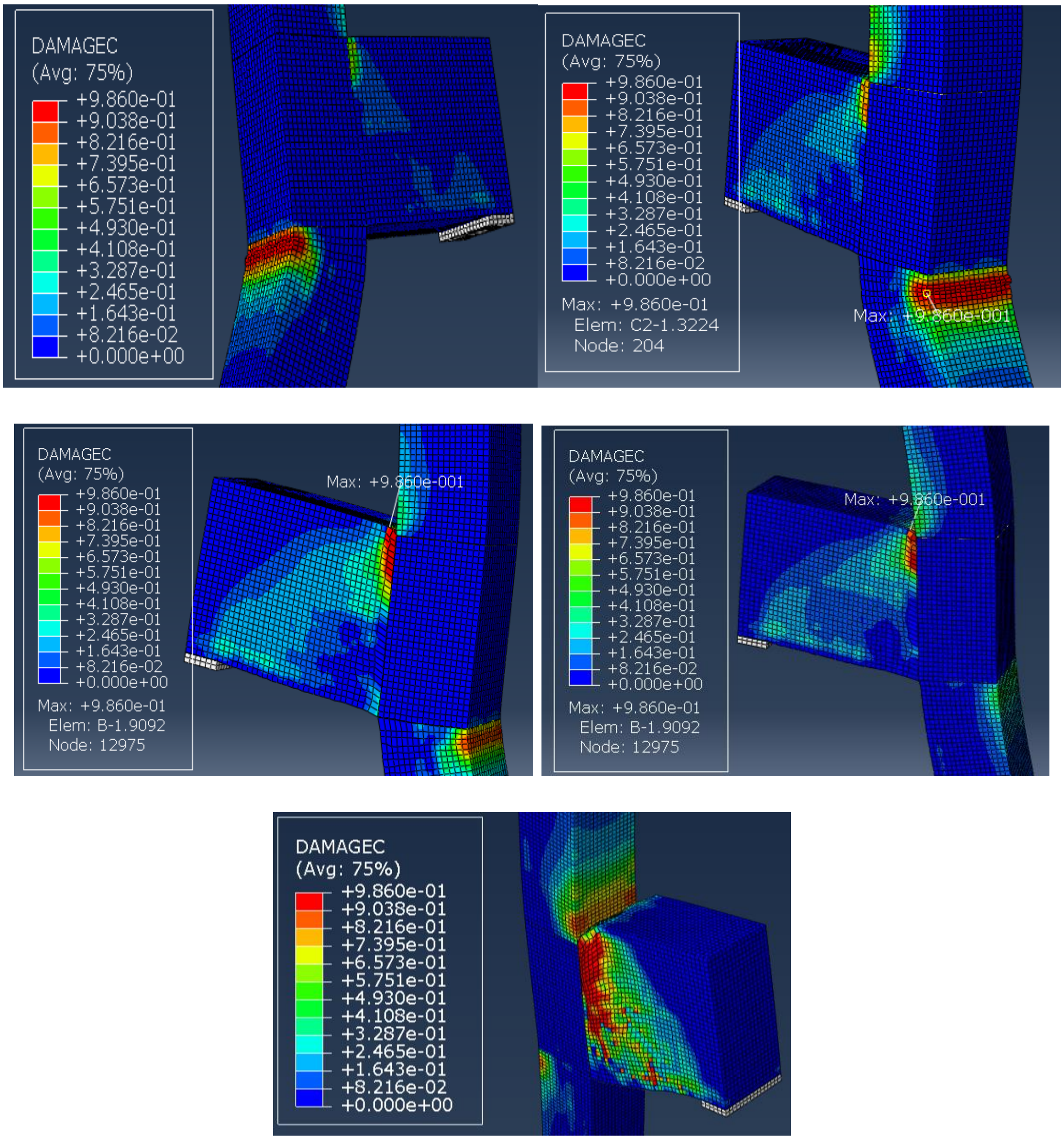

Figure 6. 12: Locations of Failures for the Models.

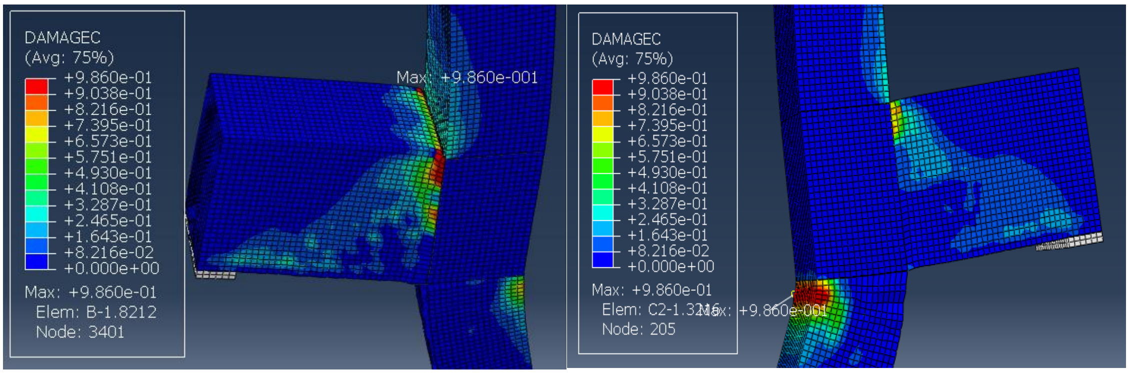

Figure 6. 13: Locations of Failures for Models (UB2-BCDR 1.6-L1-ALR 0.25) with and without Skin Reinforcements.

As shown in **Figure 6.13**, the addendum skin reinforcements have a significant effect in moving the failures from beam to column; since it mean higher moments capacity and higher rotations transfer to the columns.

Finally, the established new lower limit of CBM ratio does not count on the possibility of higher beam moment capacity due to SH in the steel reinforcements. Hence, the next section discusses its effect in the CBM ratio.

6.5 Effect of SH in the Steel Reinforcements in the CBM ratio.

This section is made to investigate the effects of stress hardening (SH) of the steel reinforcements in the CBM. For design purposes, the ACI-318 code recommended to count on $1.25f_y$. Thus, it can be significantly affected the moment capacity of the beam. Hence, **Figure 6.14** shows the stress- strain curve for steel grade 60 as tested by **Samaaneh et al. (2016)**. This curve is used to investigate the effect of SH in the beam moment capacity of the beams. **Figure 6.15** shows the effect of SH in the behaviors of model (UB2-CBDR 1.6-L2-ALR 0.5).

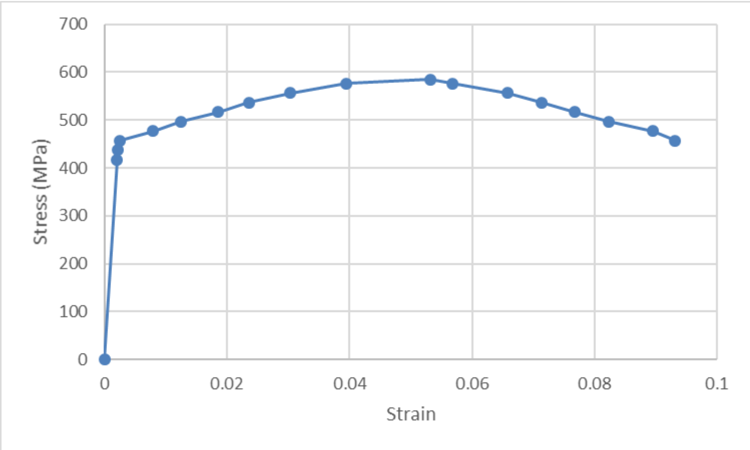

Figure 6. 14: Stress-Strain Curve for Steel Grade 60 (Samaaneh et al. 2016).

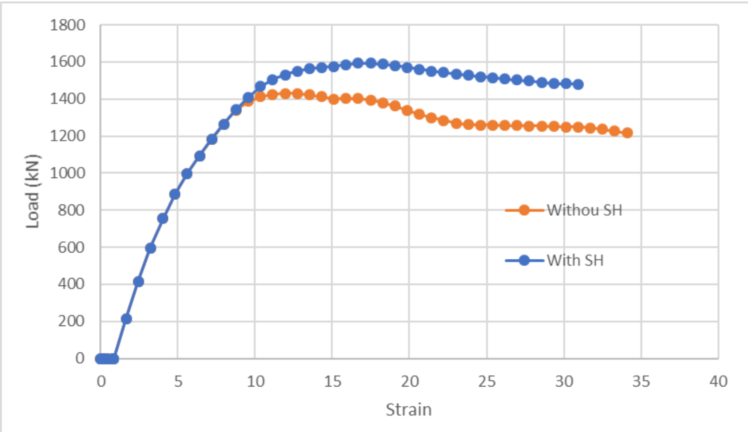

Figure 6. 15: Effect of SH in the Steel Reinforcements in the Behaviors of (UB2-CBDR 1.6-L2-ALR 0.5).

Based on **Figure 6.15**, the strain hardening in the steel reinforcements affects the ductility and the capacity of the joint. The load carrying capacity of the BCJ increased 11%, which is logical since the stresses in the reinforcements is increased. In addition, the ductility of the BCJ decreased and this is logical; because increasing the capacity of the tensile reinforcements means less deformations. However, the yield strength and the stiffness do not affected since the yield strength do not change in both model.

Finally, the confined to ACI beam moment capacity ratios specified in **Table 6.4** are changed. **Table 6.6** presents the lower CBM ratio established at different ALR and steel reinforcements ratio in column.

Table 6. 6: Allowable Confined to ACI Beam Moment Capacity Ratios Considering the Effect of SH of Steel Reinforcements.

ρ_c	ALR	$(Confined/ACI)$ Moment Capacity Ratio	Confined BCM ratio	BCM ratio considering the SH
1%	0.25	1.45	0.83	0.92
1%	0.5	1.36	0.88	0.98
2%	0.25	1.60	0.75	0.83
2%	0.5	1.46	0.82	0.91

However, the UHPC can has higher tension and compression strengths comparing with the demand strengths. Thus, the next chapter presents an analytical model to optimize the strength capacity and the volumetric fracture of fiber of UHPC.

CHAPTER SEVEN

7. ANALYTICAL MODEL.

7.1 Overview.

This chapter presents the principal stresses affecting the joints. After that, analytical model based on principal stresses derived by **Alosta and Khan (2018)** for normal strength exterior BCJs are presented and then reused to calculate the demand tension and compression capacity of UHPC. Finally, the model is validated numerically using ABAQUS. The value of this Chapter is to establish a lower tension and compression capacity of the UHPC that can used to avoid joints failures as function of beam capacity.

7.2 Analytical Model Development (Alosta and Khan 2017).

The joint is adjoining the beams and columns. It transfers the moments, shear force and axial load from member to the others providing a safe path to transfer the loads. The assemblage of many stress types causing the complex behavior of joints. **Figure 7.1** shows the moments and forces in the joints.

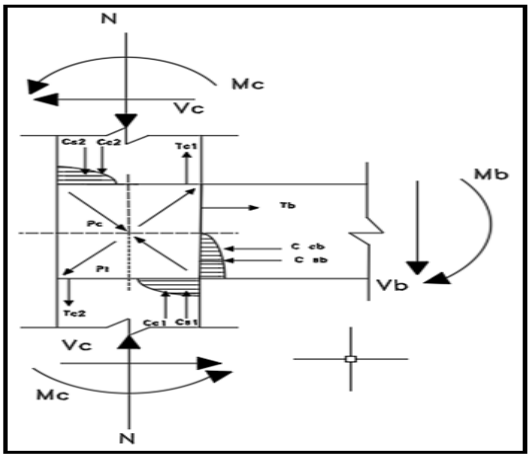

Figure 7. 1: Moments and Forces in the Exterior Beam-Column Joints.

The shear force from the beam (V_b) and axial load from the column (N) can converted to principal joint stresses σ_1 and σ_2 as present in **Equations 7.1** and **7.2**.

$$\sigma_1 = \frac{\sigma_x+\sigma_y}{2} + \sqrt{(\frac{\sigma_x+\sigma_y}{2})^2 + \tau_{xy}^2} \qquad [7.1]$$

$$\sigma_2 = \frac{\sigma_x+\sigma_y}{2} - \sqrt{(\frac{\sigma_x+\sigma_y}{2})^2 + \tau_{xy}^2} \qquad [7.2]$$

With σ_y=σ_N and assuming σ_x=0 the principle stresses can be expressed as in **Equation 7.3**.

$$\sigma_{1,2} = \frac{\sigma_N}{2} \pm \sqrt{(\frac{\sigma_N}{2})^2 + \tau_{xy}^2} \qquad [7.3]$$

Then:

$$\tau_{jh} = \sigma_1\sqrt{1 - \frac{\sigma_N}{\sigma_1}} \qquad [7.4]$$

Where:

τ_{jh}: is the shear stress of the joints.

While the demand shear force of the joints can be evaluated using the following procedure.

$$T_S - V_{Co} = V_{jh} \quad [7.5]$$

$$\frac{M_j}{j} - \frac{M_j}{L_C} = V_{jh} \quad [7.6]$$

Where:

T_S: Tension force provided by the reinforcement (N).

V_{Co}: Shear force in the column (N).

M_j: Moment in the joint. (N/mm).

L_C: Length of the column.

j: Distance between the tension and compression force couple in the joint. Its equal $\left(\frac{7}{8}\right)d$as proposed by **Li and Sanada (2017).**

Then:

$$\tau_{jh} = \frac{V_{jh}}{b_j \times h_j} = \frac{\frac{M_j}{j} - \frac{M_j}{L_C}}{b_j \times h_j} \quad [7.7]$$

Where:

b_j: is the width of the joint.

h_j: is the depth of the joint.

With equating **7.4** and **7.7,** the moment capacity of the joints is function of the principle stresses $\sigma_1$and the normal stresses σ_N as in **Equation 7.8.**

$$M_j = \frac{b_j \times h_j \times \sigma_1 \sqrt{1 - \frac{\sigma_N}{\sigma_1}}}{\left(\frac{1}{j} - \frac{1}{L_C}\right)} \quad [7.8]$$

Using the concrete compressive strength f_c' and tensile strength f_t, one can define the failure surface of concrete using Mohr-Coulomb principle. **Figure 7.2** shows Mohr-Coulomb failure surface for concrete.

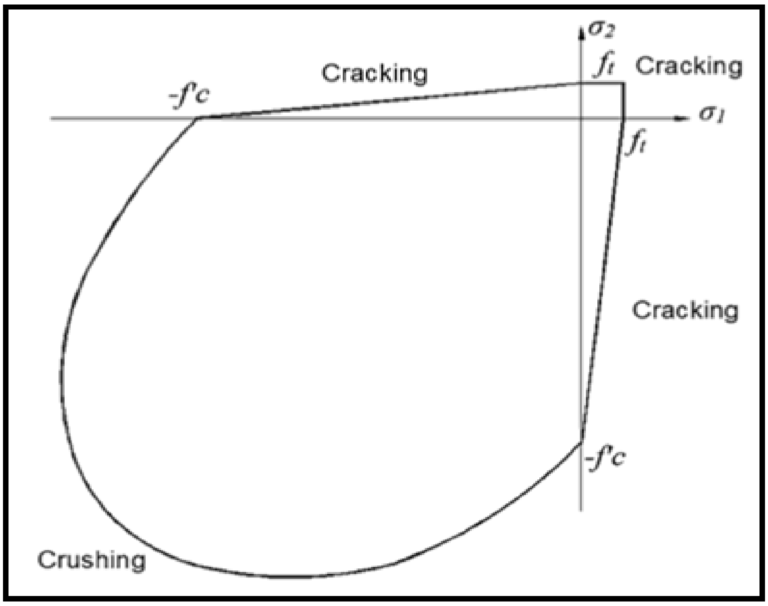

Figure 7. 2: Failure Surface for Concrete.

The equation locus in the fourth quadrant. Hence, it can be expressed as in **Equation 7.9**.

$$\frac{\sigma_1}{f_t} - \frac{\sigma_2}{f_c'} = 1 \qquad [7.9]$$

Along any stress path

$$\sigma_2 = c\sigma_1 \qquad [7.10]$$

Where the range of $1/c$ is [-1.0].

By substituting **Equation 7.6** in **7.5**

$$\sigma_1 = \frac{f_t f_c'}{f_c' - c f_t} \qquad [7.11]$$

$$\sigma_2 = \frac{c f_t f_c'}{f_c' - c f_t} \qquad [7.12]$$

By solving **Equation 6.7** with **Equation 6.4** with simultaneously varying $1/c$ [-1.0] and the normal stress σ_N [0,- f_c'], the shear stress capacity can be obtained for various value of σ_N. These values can be used to evaluate the adequacy of the joints strength. **Alosta and Khan (2018)** used this approach to conduct an interaction diagram between joint shear stress capacity τ_v and the normal stress σ_N for various strength of concrete as shown in **Figure 7.3**. However, the FEM is trend to be higher than the proposed mechanical model as shown in **Figure 7.4**.

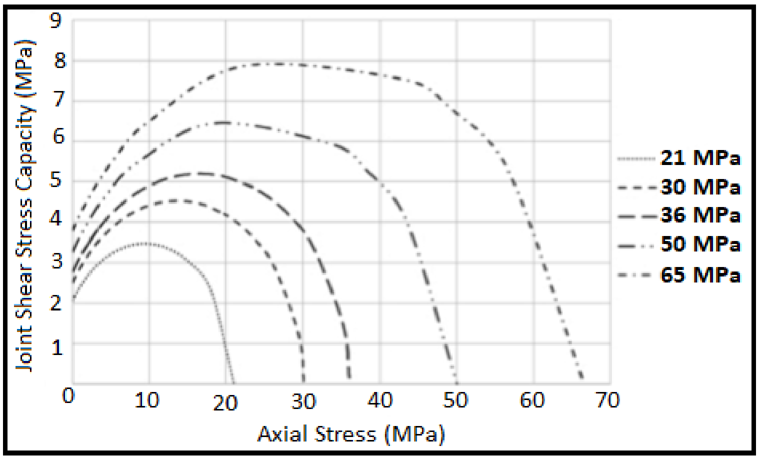

Figure 7. 3: Shear Stress Capacity-Normal Stress Interaction Diagram. (Alost and Khan 2018).

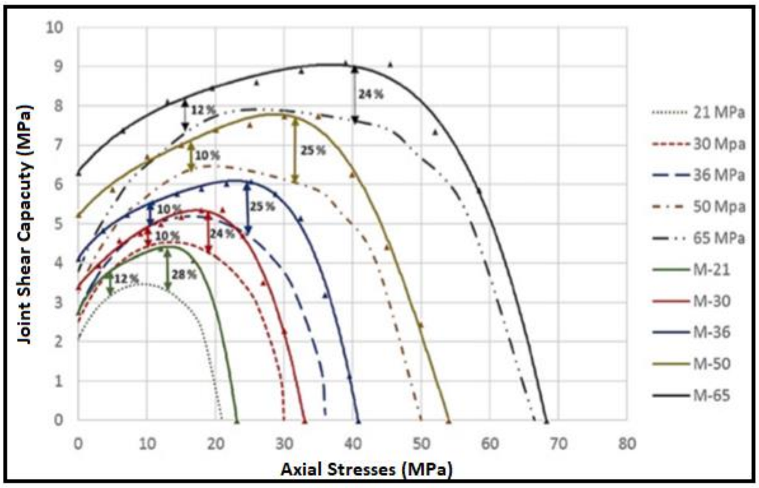

Figure 7. 4: Comparison between the FEM and the Mechanical model Results. (Alost and Khan 2018).

However, using the same approach for UHPC with well defining tension and compression capacity, one can regenerate the interaction diagram. **Figure 7.5** shows the shear stress-axial load capacity interaction diagram for UHPC class B with tension capacity of 5 through 7.5 MPa.

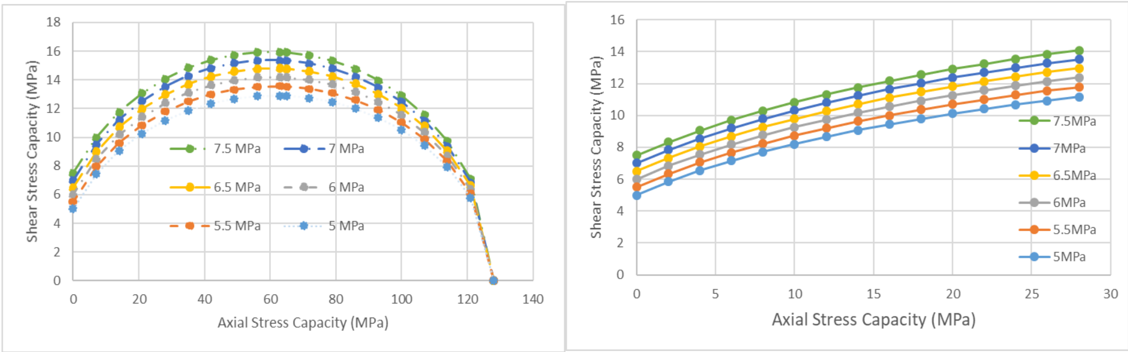

Figure 7. 5: Shear-Axial Stress Interaction Diagram for UHPC Class B with Different Tensile Strength.

Each tension capacity presents a volumetric fracture of fiber. Hence, one can control the amount of fibers using the equation proposed by **Jiuru et al. (2011)** which predict the shear stresses resisted by the steel fibers, the expression is shown in **Equation 7.12**

$$V_{fib} = 2\frac{L_f}{d_f}V_f \qquad [6.12]$$

Where:

L_f: Length of the steel fibers.

d_f: Diameter of the steel fibers.

V_f: Volumetric fracture of fiber.

However, the amount of steel fiber can affected both the capacity and the post cracking behaviors of UHPC. Thus, one shall be careful when reducing the amount of fibers. For instance, if the amount of fibers is not enough to allow the UHPC matrix to form a multi-cracking zone. The tensile capacity will begin softening after the cracking. In similar scenarios, the ductility of UHPC comparing with NC is losing. **Figure 7.6** shows the difference between the UHPC and the sway-special detailings joints. However, these curves do not consider the effect of axial loading and the stress transformed from the beam.

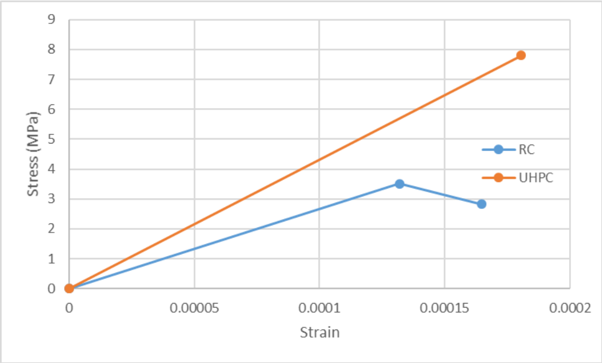

Figure 7. 6: Difference in Tensile Stress-Strain between Reinforced Concrete and UHPC at Cracking Stage.

As shown in **Figure 7.6,** the capacity of the concrete is losing after the cracking. However, this losing in capacity is compensated with stirrups. On the other hand, the UHPC with proper amount of fibers can hold it capacity after cracking.

In addition, the equivalent transverse shear stress V_S that the UHPC recovered can be calculated as in **Equation 7.12**. Consequently, the amount of transverse reinforcement recovered can be obtained. **Figures 7.7** and **7.8** show the shear stress capacity-normal stress interaction diagram for UHPC material and the recovered stress-normal stress interaction diagram. These curves are conducted assuming concrete strength 28 MPa and UHPC class B in FHWA with 2% fiber content.

$$V_S = V_{J,UHPC} - V_{J,C} \qquad [6.12]$$

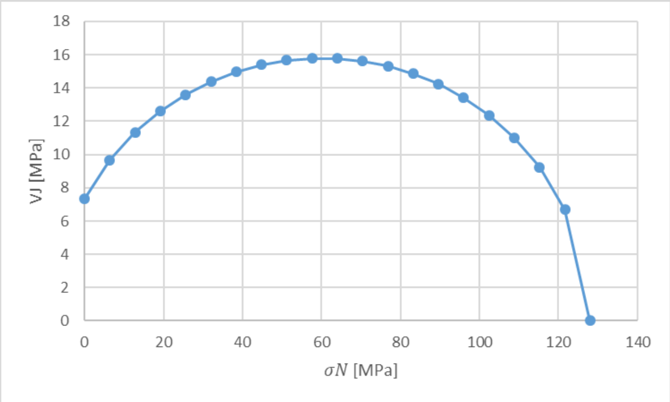

Figure 7. 7: Shear Stress Capacity-Normal Stress Interaction Diagram for UHPC Class B with 2% Fiber Content.

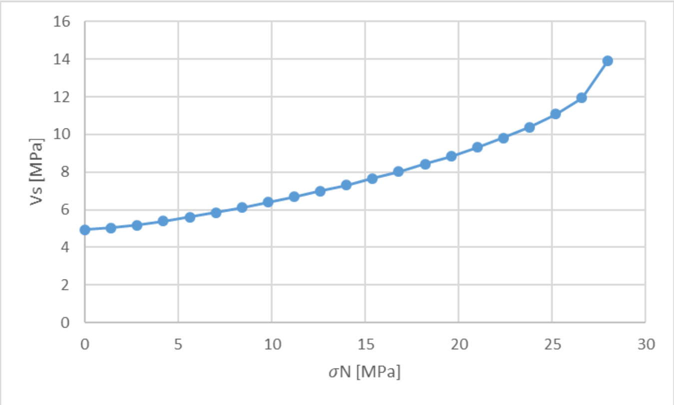

Figure 7. 8: Transverse Reinforcement Stresses Recovered-Normal Stress Interaction Diagram for UHPC Class B with 2% Fiber Content.

Vice versa, by knowing the demanding shear stress capacity of the joints, one can calculate the demand principle stresses in the joints using **Equation 7.3**. After that, the principle stresses is checked using the basic principle of Coulomb –Mohr. The next section shows the effect of decreasing the tension capacity of UHPC in the behaviors of UHPC joints. In addition, UHPC with minimum compressive and tensile strength are used to investigate the behaviors of UHPC.

7.3 Effect of Varying the Tensile Capacity of UHPC in the Behavior of the joints.

In general, increasing the tensile capacity of UHPC increases the stiffness of the joints and consequently reduce the ductility. However, this behavior occurred when the material is not cracked. Beyond the cracking stage, the behavior of the material with lower tensile capacity is deteriorated which lead to reduce the capacity and the ductility of the joint. **Figures 7.9** and **7.10** show the effect of varying the tensile capacity of UHPC for the models group UB2-BCDR 1.6-L1. The tension capacity of UHPC is reduced to 7 MPa and 5.5 MPa for ALR 0.25 and 0.5, respectively. These values are selected based on the analytical model and the shear capacity shown in Figures 7.4 with some violations based in the results of **Alosta and Khan (2018)** that the capacity can be 25% higher than the estimated.

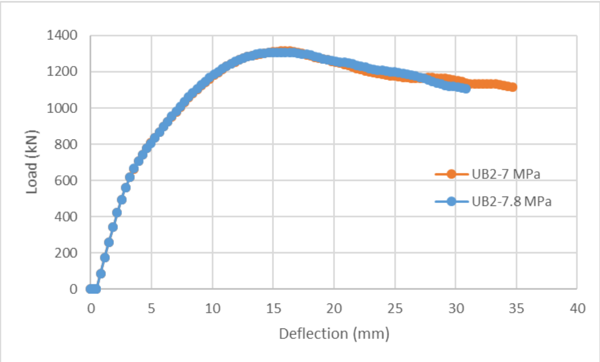

Figure 7. 9: Effect of Reducing the Tensile Capacity of UHPC in the Behavior of the Joint (UB2-BCDR 1.6-L1-ALR 0.25).

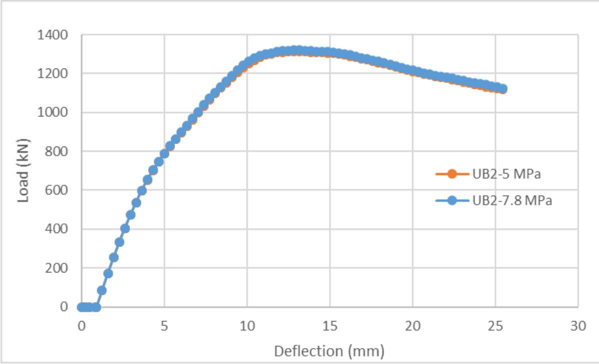

Figure 7. 10: Effect of Reducing the Tensile Capacity of UHPC in the Behavior of the Joint (UB2-BCDR 1.6-L1-ALR 0.25).

As shown in the **Figures 7.9** and **7.10**, using UHPC enhances the capacity of the joints event with some violations. The effect of decreasing the UHPC tension capacity can enhance the ductility since the ultimate deflection is increased. However, this is true for sway special frame where the beams are ductile and transfer high rotations to the joints after reaching its peak capacity. However, the effect of tension capacity of UHPC can be negligible when the demand shear capacity is less than the cracking strength of UHPC and the beam can not transfer high rotations. (i.e. there is no damage occurs in the stiffness). **Figure 7.11** shows the tensile and compressive damages in the joints.

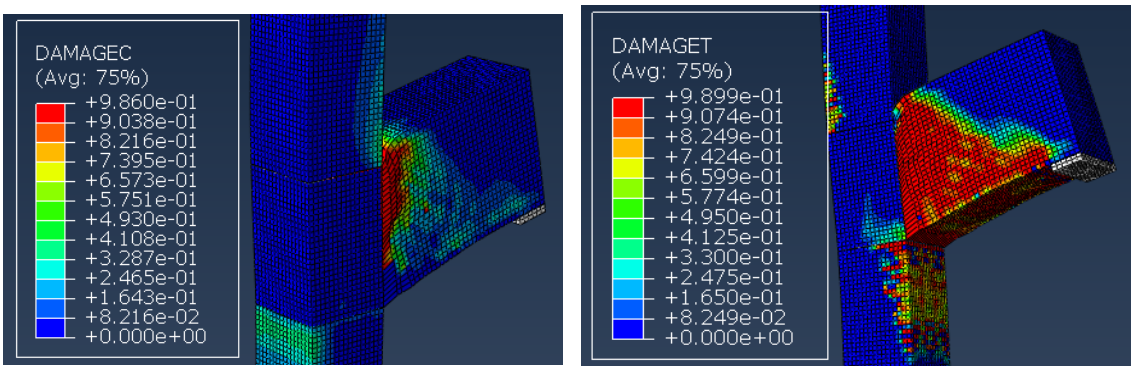

Figure 7. 11: Compressive and Tensile Damages in Models Group (UB2-BCDR 1.6-L1) with Reduced Tension Capacity of UHPC.

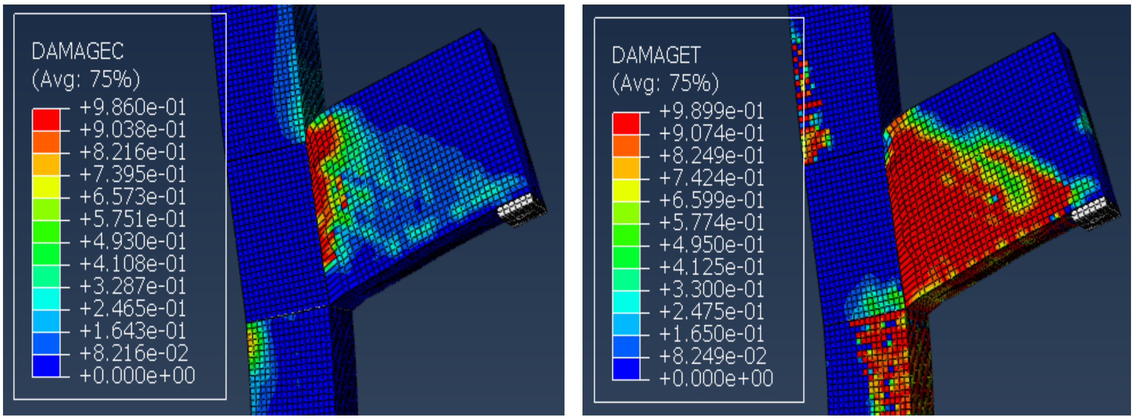

Figure 7.11 (Continued): Compressive and Tensile Damages in Models Group (UB2-BCDR 1.6-L1) with Reduced Tension Capacity of UHPC.

As shown in **Figure 7.11**, the hardening behavior of UHPC in tension avoids the cracks to extended even when it cracked. Thus, the UHPC have high fracture energy comparing with NC. However, the UHPC have high compressive strength. Hence, at low demand compressive strength the joints will be undamaged. **Figure 7.12** shows the behavior of the simulation (BCDR 1.6-L2-ALR 0.5) using UHPC class C with compressive strength 64 MPa and 2% volumetric fracture of fiber (5.8 MPa tensile strength). While **Figure 7.13** shows the behavior of the same model using UHPC class D with compressive strength 134 MPa and 1% volumetric facture of fiber (2.95 MPa tensile strength). Finally, **Figures 7.14** and **7.15** show the tensile and the compressive damage in the model using UC2 and UD1, respectively.

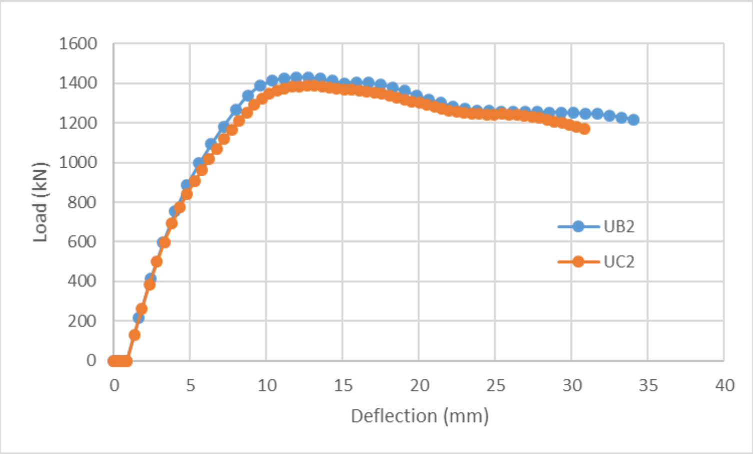

Figure 7. 12: Effect of Using UC2 in the Behavior of (UB2-BCDR 1.6-L2-ALR 0.5).

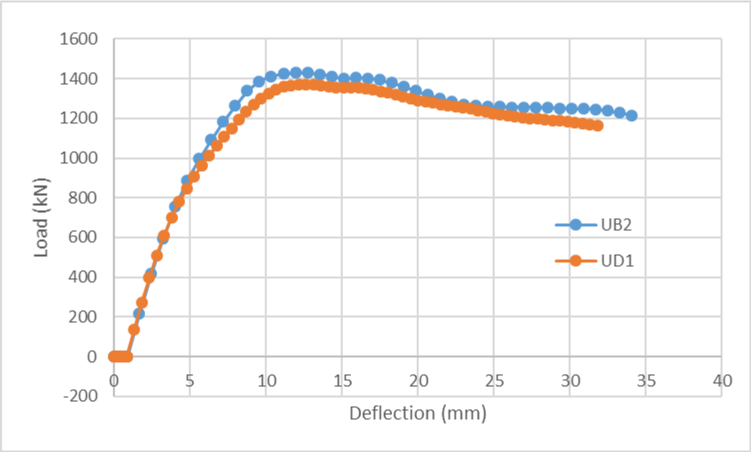

Figure 7. 13: Effect of Using UD1 in the Behavior of the simulation (BCDR 1.6-L2-ALR 0.5).

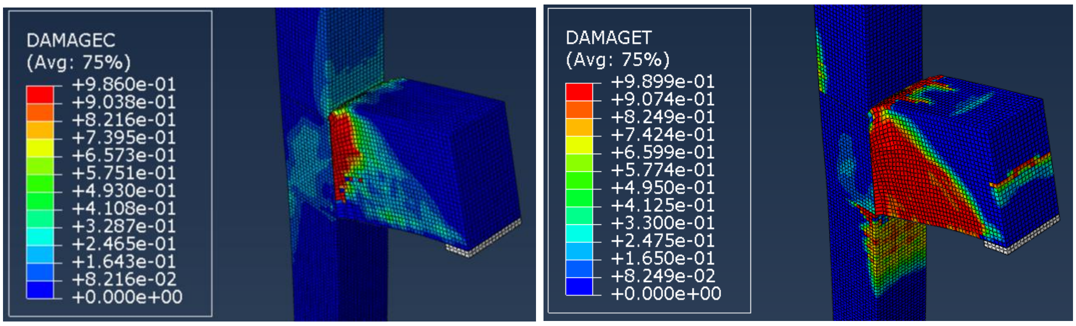

Figure 7. 14: Compressive and Tensile Damages in (UC2-BCDR 1.6-L2-ALR 0.5).

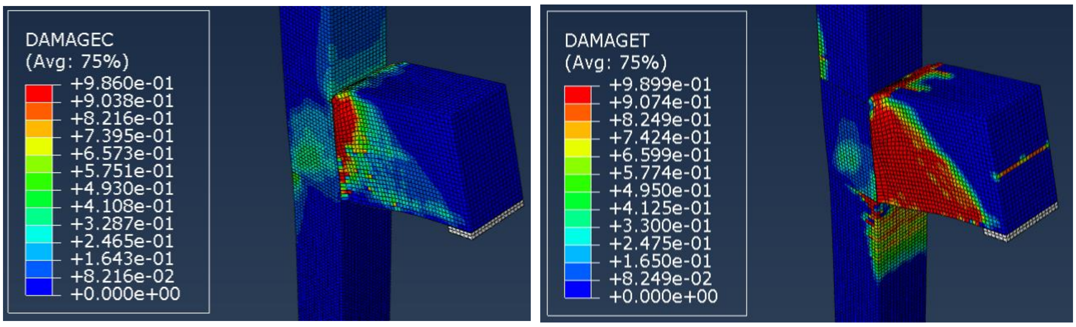

Figure 7. 15: Compressive and Tensile Damages in (UD1-BCDR 1.6-L2-ALR 0.5).

Based on **Figures 7.14** and **7.15**, the two materials (UC2 and UD1) show effectiveness in term of strength with negligible change in ductility comparing with UB2. Further, one can indicates that the hardening behavior in tension of UHPC plays main rule in avoiding the extended of cracks.

CHAPTER EIGHT

8. CONCLUSIONS AND FUTURE WORKS.

8.1 Summary.

In this research, UHPC is used to improve ductility behavior of sway-special exterior beam-column joint. The Finite Element (F.E) commercially program ABAQUS are used to create a three-dimensional (3-D) non linear models of exterior BCJs. The models are validated using published experimental tests by Alkhatib (2015). The results assure the effectiveness of using UHPC in joints strengthening without any transverse reinforcements. Furthermore, the study is extended to study the behaviors of UHPC joints with lower CBM ratio. Finally, an analytical model based principle stresses is used to optimize the tension and compression capacity demand of UHPC used in the joints. The following section shows the key findings of this research.

8.2 Key Conclusions.

Based on the information presented in this research. The following are the key findings:

- UHPC can be used in strengthening the exterior joints of the sway-special moment resisting frame with dispensing the complete amount of transverse reinforcements and covering the lower CBM ratio limit.

- Based on the results in chapter six, Saatcioglu and Razvi (1992) model is suitable in predicting the confined moment capacity of the columns.
- The lower limit of column to beam moment capacity ratio specified by the ACI code is conservative in case of sway-special detailings columns without considering the enhancement on the moment-axial capacity due to the confinement effect.
- A confined to unconfined (according to ACI code) moment capacity ratio is established. This ratio is not unique since it depends on the core to section dimensions ratio, ALR and the reinforcements configurations. In this study, the ratio is ranged between 1.02 and 1.24.
- The analytical model proposed by Alosta and Khan (2017) and presented in chapter seven can be used to evaluate the shear capacity of UHPC joints. Thus, the costs of UHPC can be optimized through true assessments of the demand tension and compression capacity. In addition, the tension capacity is related to the properties and the volumetric fracture of fiber using the expression proposed by Jiuru et al. (2011).
- The strain hardening behaviors of UHPC in tension avoid cracks extensions even when violating the cracking strength. Thus, the UHPC is most likely to fail in compression using considerable tensile capacity of UHPC.

- Based on the results in Chapter Seven, decreasing the tensile capacity of the UHPC to a certain limit can increased the ductility by increasing the ultimate deflection.
- The skin reinforcement has a significant effect in minimizing the cracks in beams with depth equal or higher than 700 mm. Hence, without the use of skin reinforcements, the system fails at low level of ductility due to high damage resulting from skin cracks.

8.3 Future Works.

While this research is assure the ability of using UHPC in strengthening the sway-special exterior BCJs with complete dispensing of the transverse reinforcements at CBM ratio violates the lower limit of ACI code. Further research are required to generalize the results. The followings are the key recommendations for further researches in this area:

- This research is deals with the exterior BCJ. However, there are other types of joints in the structures (interior joints, edge joints and roof joints). Each types of the joints can go different behaviors. Thus, extended researches are needed in investigated the behaviors of such joints.
- While this research considered the key factors affecting the CBM ratio, it is recommended to study another factors include the effect of the lateral beams and the effect of M/V ratio.

- The established new lower CBM ratio is crossponding to the dimensions and the detailings of the column used in this study. Extended research is needed to generalized the CBM ratio with different column dimensions and reinforcements detailings.
- While the established CBM ratio in Table 6.26 is limited with the maximum confined capacity of the column. Extended researches are needed in the behaviors of the joints with using UHPC in joint and column. Thus, a lower CBM ratio can be achieved.
- While the analytical model is based on the principle stresses in the joints. It is suitable to predict the demand compressive strength of UHPC. However, it is not consider the effect of tension hardening in the capacity of the joints. A new analytical model based fracture energy of the materials can be more appropriate to predict the capacity of the joints.

References

- ABAQUS version 6.13). [Computer software]. Assault Systems. Waltham. MA 2013.
- Abuodeh, O., & Abed, F. (2019, April). '***A Finite Element Model of a UHPC Beam Reinforced with HSS Bars.*** **In 2019 8th International Conference on Modeling Simulation and Applied Optimization (ICMSAO)** (pp. 1-5). IEEE.
- ACI (2011). ***Building Code Requirements for Structural Concrete.*** Committee report 318-11, American Concrete Institute, Detroit, Michigan, 509 pages.
- ACI-ASCE (1985). ***Recommendations for Design of Beam-Column Joints in Monolithic Reinforced Concrete Structures***. Committee report 352R-85. American Concrete Institute, **ACI Journal**, Vol. 82, No. 3, pp. 266-284.
- Ali, A. & Javad, M. (2016). ***Assessment of Methods for Development of Confinement Model of Low Strength Reinforced Concrete Columns: A Review*. Journal of Engineering Research and Application.** Vol. 6, Issue 10, pp. 62-65.
- Alkhatib, A.M. (2015). ***Study of high strength reinforced concrete exterior beam-column joints under cyclic loading.*** **KING FAHED UNIVERSITY OF PETRULIUM & MINIRALS.** 178 pages.
- Al-Osta, M. A., Al-Khatib, A. M., Baluch, M. H., Azad, A. K., & Rahman, M. K. (2017). ***Performance of hybrid beam-column joint***

***cast with high strength concrete*. Earthquake and Structures.** https://doi.org/10.12989/eas.2017.12.6.603

- Al-Osta, M. A., Isa, M. N., Baluch, M. H., & Rahman, M. K. (2017). ***Flexural behavior of reinforced concrete beams strengthened with ultra-high performance fiber reinforced concrete*. Construction and Building Materials,** 134, 279-296.
- Al-Osta, M. A., Khan, U., Baluch, M. H., & Rahman, M. K. (2018). ***Effects of Variation of axial load on seismic performance of shear deficient RC exterior BCJs*. International Journal of Concrete Structures and Materials,** 12(1), 46.
- Al-Osta, M. A., Rahman, M. K., Isa, M. N., & Baluch, M. H. ***Flexural Response of RC Beams Strengthened using UHPFRC Panels Epoxied to the Sides.***
- Ashour, M. J., & Elmezaini, N. (2015). ***Nonlinear Analysis of Concrete Beams Strengthened with Steel Fiber-Reinforced Concrete Layer***, *2*(3).
- Azizinamini, A., Pavel, R., Hatfield, E., and Gosh, S.K. (1999). ***Behavior of lapspliced reinforcing bars embedded in high strength concrete*. ACI Structural Journal**, pp. 826–836. doi:10.14359/737.
- Bencardino, F., Rizzuti, L., Spadea, G., & Swamy, R. N. (2008). ***Stress-strain behavior of steel fiber-reinforced concrete in compression*. Journal of Materials in Civil Engineering**, 20(3), 255-263.

- Bhargava, P., Sharma, U. K., & Kaushik, S. K. (2006). ***Compressive stress-strain behavior of small scale steel fibre reinforced high strength concrete cylinders.*** **Journal of advanced concrete technology**, 4(1), 109-121.
- Birtel, V., & Mark, P. (2006, May). ***Parameterised finite element modelling of RC beam shear failure***. **In ABAQUS users' conference (pp. 95-108).**
- Burlion, N., Gatuingt, F., Pijaudier-Cabot, G., & Daudeville, L. (2000). ***Compaction and tensile damage in concrete: constitutive modelling and application to dynamics.*** **Computer methods in applied mechanics and engineering,** 183(3-4), 291-308.
- Chao, S. H., Kaka, V., & Palacios, G. (2016). ***Seismic behavior of ultra-high-performance fiber-reinforced concrete moment frame members.*** **In First international interactive symposium on UHPC–2016.**
- Chen, L., & Graybeal, B. A. (2012). ***Modeling structural performance of second-generation ultrahigh-performance concrete pi-girders.*** **Journal of Bridge Engineering**, *17*(4), 634-643.
- Cohn, M.Z., and Bartlett, M. (1982). ***Computer-simulated flexural tests of partially pre-stressed concrete sections. ASCE Journal of Structural Division***, pp. 2747–2765.
- Concretes, U. H. P. F. R. (2002). ***Documents scientifiques et techniques.*** **Association Française de Génie Civil (AFGC).**

- Cusson, D., & Paultre, P. (1995). ***Stress-strain model for confined high-strength concrete*. Journal of Structural Engineering**, 121(3), 468-477.Desayi, P., & Krishnan, S. (1964, March). Equation for the stress-strain curve of concrete. In Journal Proceedings (Vol. 61, No. 3, pp. 345-350).
- Esmaeeli, E., Barros, J. A., Sena-Cruz, J., Fasan, L., Prizzi, F. R. L., Melo, J., & Varum, H. (2015). ***Retrofitting of interior RC beam–column joints using CFRP strengthened SHCC: cast-in-place solution.*** **Composite Structures**, 122, 456-467.
- Esmaeeli, E., Barros, J. A., Sena-Cruz, J., Varum, H., & Melo, J. (2015). ***Assessment of the efficiency of prefabricated hybrid composite plates (HCPs) for retrofitting of damaged interior RC beam–column joints.*** **Composite Structures,** 119, 24-37.
- Fafitis, A., and Shah, S. P. (1985). ***Lateral Reinforcement for High Strength Concrete Columns.*** **ACI**, vol. SP-87–12, pp. 213– 233.
- Federal high way administrations. (2018). ***Properties and Behavior of UHPC-Class Materials.*** **Publication FHWA-HRT-18-036**, Pp. 1-70 and 140-147.
- Ganesan, N., Indira, P. V., & Sabeena, M. V. (2014). ***Behaviour of hybrid fibre reinforced concrete beam–column joints under reverse cyclic loads.*** **Materials & Design** (1980-2015), 54, 686-693.
- Ghobarah, A., & Said, A. (2002). ***Shear strengthening of beam-column joints.*** **Engineering Structures**, 24(7), 881-888.

- Ghobarah, A., Aziz, T. S., and Biddah, A. (1996). ***Seismic Rehabilitation of Reinforced Concrete Beam-Column Connections.*** **Journal of Earthquake Spectra**, Vol. 12, No. 4, pp. 761-780.
- Graybeal, B. A.(2007). ***Compressive Behavior of Ultra-High-Performance Fiber-Reinforced Concrete***. **ACI Materials Journal** 104 (2), Pp. 146–52.
- Hakeem, I.Y.A. (2011). ***Characterization of an ultra-high performance concrete,*** **King Fahd University of Petroleum & Minerals** (Saudi Arabia),MSc Thesis.
- Hu, H. T., & Schnobrich, W. C. (1989). ***Constitutive modeling of concrete by using non-associated plasticity.*** **Journal of Materials in Civil Engineering,** 1(4), 199-216.
- Hughes, S. E. (Ed.). (2009). ***A quick guide to Welding and Weld inspection.*** **Elsevier**.
- Hung, C. C., Hu, F. Y., & Yen, C. H. (2018). ***Behavior of slender UHPC columns under eccentric loading.*** **Engineering Structures**, 174, 701-711.
- Jiuru, T., Chaobin, H., Kaijian, Y., & Yongcheng, Y. (1992). ***Seismic behavior and shear strength of framed joint using steel-fiber reinforced concrete.*** **Journal of Structural Engineering**, 118(2), 341-358.
- Kaliluthin, A. K., Kothandaraman, S., & Aha, T. S. (2014). ***A review on behavior of reinforced concrete beam column***

***joint*.** **International Journal of Innovative Research in Science, Engineering and Technology**, 3(4), 11299-11312.

- Kent, D. C., & Park, R. (1971). ***Flexural members with confined concrete.*** **Journal of the Structural Division**.
- Khan, M. I., Al-Osta, M. A., Ahmad, S., & Rahman, M. K. (2018). ***Seismic behavior of beam-column joints strengthened with ultra-high performance fiber reinforced concrete***. **Composite Structures**, 200, 103-119.
- Kmiecik, P., & Kamiński, M. (2011). ***Modelling of reinforced concrete structures and composite structures with concrete strength degradation taken into consideration*.** ***Archives of civil and mechanical engineering,*** *11*(3), 623-636.
-
- Koksal, H.O., Turgay, T., Karcoc, c., and Aycenk, c. (2011). ***Modeling aspects concerning the axial behavior of RC columns.*** **Conference: MATERIALS CHARACTERISATION** 2011, Vol. 72. 10 pages.
- Krenchel, H. (1964). ***Fibre reinforcement; theoretical and practical investigations of the elasticity and strength of fibre-reinforced materials.***
- Kupfer, H., Hilsdorf, H. K., & Rusch, H. (1969, August). ***Behavior of concrete under biaxial stresses.*** **In Journal Proceedings** (Vol. 66, No. 8, pp. 656-666).

- Kusumawardaningsih, Y., Fehling, E., Ismail, M., & Aboubakr, A. A. M. (2015). ***Tensile strength behavior of UHPC and UHPFRC.*** **Procedia Engineering**, 125, 1081-1086.
- Lee, C. J., Lange, D. A., Lee, J. Y., & Shin, S. W. (2013). ***Effects of fiber volume fraction and water/cement ratio on toughness development of steel fiber reinforced concrete*.** **Journal of the Korea Institute of Building Construction**, 13(1), 20-28.
- Li, B., Chi, Y., Xu, L., Li, C., & Shi, Y. (2018). ***Cyclic tensile behavior of SFRC: Experimental research and analytical model.*** **Construction and Building Materials**, 190, 1236-1250.
- Li, B., Lam, E. S. S., Wu, B., & Wang, Y. Y. (2013). ***Experimental investigation on reinforced concrete interior beam–column joints rehabilitated by ferrocement jackets*.** **Engineering Structures**, 56, 897-909.
- Lowes, L. N. (1999). ***Finite element modeling of reinforced concrete beam-column bridge connections (Vol. 1).*** **University of California, Berkeley.**
- Luccioni, B., Oller, S., & Danesi, R. (1996). ***Coupled plastic-damaged model.*** ***Computer methods in applied mechanics and engineering,*** *129*(1-2), 81-89.
- Mander, J.B.(1988). ***Theoretical Stress-Strain Model for Confined Concrete.*** **Journal of Structural Engineering ASCE**, Vol. 114, Issue 8, pp. 1827–1849.

- Mehta, P. K., & Aïtcin, P. C. (1990). ***Principles underlying production of high-performance concrete. Cement,*** **concrete and aggregates**, 12(2), 70-78.
- Nasrin, S., Ibrahim, A., Al-Osta, M., & Khan, U. (2017***). Behavior of Retrofitted UHPC Beams Using Carbon Fiber Composites under Impact Loads.*** **In Structures Congress 2017** (pp. 392-402).
- Nataraja, M. C., Dhang, N., & Gupta, A. P. (1999). ***Stress–strain curves for steel-fiber reinforced concrete under compression.*** **Cement and concrete composites,** 21(5-6), 383-390.
- Nayal, R., & Rasheed, H.A. (2006). ***Tension Stiffening Model for Concrete Beams Reinforced with Steel and FRP Bars*. Journal of Materials in Civil Engineering**, pp. 831-841.
- Park, R., & Paulay, T. (1975). **Reinforced concrete structures**. John Wiley & Sons.
- Prem, P. R., Bharatkumar, B. H., & Iyer, N. R. (2012). ***Mechanical properties of ultra high performance concrete.*** **World academy of Science, Engineering and Technology,** 68, 1969-1978.
- Racky, P. (2004, September). ***Cost-effectiveness and sustainability of UHPC.*** **In Proceedings of the International Symposium on Ultra High Performance Concrete**, Kassel, Germany (pp. 797-805).

- Razvi, S. R., and Saatcioglu, M. (1989). ***Confinement of Reinforced Concrete Columns with Welded Wire Fabric.*** **ACI Structural Journal**, vol. 86, no. 5. pp. 615– 623.
- Richart, F. E., Brandtzaeg, A., and Brown, R. L. (1928). ***A study of the failure of concrete under combined compressive stresses***. Bulletin 185, **Univ. of Illinois Engineering Experimental Station**, Champaign, page 111.
- Richart, F. E., Brandtzaeg, A., and Brown, R. L. (1929). ***The failure of plain and spirally reinforced concrete in compression. Bulletin 190***, **Univ. of Illinois Engineering Experimental Station**, Champaign. Page 111.
- Roberto T. Leon. (1989). ***Interior Joints with Variable Anchorage Lengths.*** **Journal of Structural Engineering**. 15 pages.
- Saatcioglu, M., & Razvi, S. R. (1992). ***Strength and ductility of confined concrete.*** **Journal of Structural engineering**, 118(6), 1590-1607.
- Saenz, L. P. (1964). ***discussion of" Equation for the Stress-Strain Curve of Concrete" by Desayi and Krishnan***. **Journal of the American Concrete Institute**, 61, 1229-1235.
- Safdar, M., Matsumoto, T., & Kakuma, K. (2016). ***Flexural behavior of reinforced concrete beams repaired with ultra-high performance fiber reinforced concrete (UHPFRC).*** **Composite structures**, 157, 448-460.

- Sarkar, P., Agrawel, R., and Menon, D. (2007). ***Design of RC beam-column joints under seismic loading - A review.*** **Journal of Structural Engineering** (Madras) 33(6):449-457, pp. 1-3.
- Scott, B. D., Park, R., & Priestley, M. J. (1982, January). ***Stress-strain behavior of concrete confined by overlapping hoops at low and high strain rates.*** **In Journal Proceedings** (Vol. 79, No. 1, pp. 13-27).
- Shannag, M. J., Abu-Dyya, N., & Abu-Farsakh, G. (2005). ***Lateral load response of high performance fiber reinforced concrete beam–column joints.*** **Construction and Building Materials**, 19(7), 500-508.
- Sheikh, S. A., & Uzumeri, S. M. (1980). ***Strength and ductility of tied concrete columns.*** **Journal of the structural division**, 106(ASCE 15388 Proceeding).
- Shirai, K., Yin, H., & Teo, W. (2020, February). ***Flexural capacity prediction of composite RC members strengthened with UHPC based on existing design models.*** In **Structures** (Vol. 23, pp. 44-55). Elsevier.
- Sivakumar, A., & Santhanam, M. (2007). ***Mechanical properties of high strength concrete reinforced with metallic and non-metallic fibres.*** **Cement and Concrete Composites**, 29(8), 603-608.

- Sujivorakul, C. (2012). ***Model of hooked steel fibers reinforced concrete under tension.*** In High performance fiber reinforced cement composites 6 (pp. 19-26). Springer, Dordrecht.
- Systèmes, D. (2011). ***ABAQUS® UManual (version 6.11). SIMULIA, a division of Dassault Systèmes***, Providence, Rhode Island.
- Tsonos, A. D. G. (2010). ***Performance enhancement of R/C building columns and beam–column joints through shotcrete jacketing.*** **Engineering Structures**, 32(3), 726-740.
- Vandewalle, L., Nemegeer, D., Balazs, L., Barr, B., Barros, J., Bartos, P., ... & Falkner, H. (2003). RILEM TC 162-TDF: ***Test and design methods for steel fibre reinforced concrete'-sigma-epsilon-design method-Final Recommendation.*** **Materials and Structures**, 36(262), 560-567.
- Wadekar, A. P., & Pandit, R. D. (2014). ***Study of Different Types Fibres used in High Strength Fibre Reinforced Concrete***.
- Wahalathantri, B.L., Thambiratnam, B., Chan, T. and Fawzia, S. (2011). ***A Material Model for Flexural Crack Simulation in Reinforced Concrete Elements Using ABAQUS***. **Queensland University of Technology**. pp. 260-264.
- Willam, K. J., & Warnke, E. P. (1975). ***Constitutive model for the triaxial behavior of concrete. International association of bridge and structural engineers, Seminar on concrete structure subjected***

to triaxial stresses, paper III-1, Bergamo, Italy, May 1974. *IABSE Proc. 19*.

- Wuest, J., EPF, C., Brühwiler, E., & ETH, D. (2008, March). ***Model for predicting the UHPFRC tensile hardening***. **In Ultra High Performance Concrete (UHPC): Proceedings of the Second International Symposium on Ultra High Performance Concrete**, Kassel, Germany (No. 10, p. 153).
- Yoo, D., and Yoon, Y. (2015). ***Structural performance of ultra-high-performance concrete beams with different steel fibers***. **Engineering Structures** 102 (2015), pp.409–423.
- Zhu, Y., Zhang, Y., Hussein, H. H., & Chen, G. (2019). ***Numerical modeling for damaged reinforced concrete slab strengthened by ultra-high performance concrete (UHPC) layer***. **Engineering Structures,** 110031.

Websites.

- https://quake06.stanford.edu/centennial/tour/stop10.html
- https://theconstructor.org/concrete/high-strength-vs-high-performance-concrete/8617/

Appendix.

Figures A.1 through **A.23** shows the simulations detailings for BCDR 0.3 through 2 and for SP and UHPC joints.

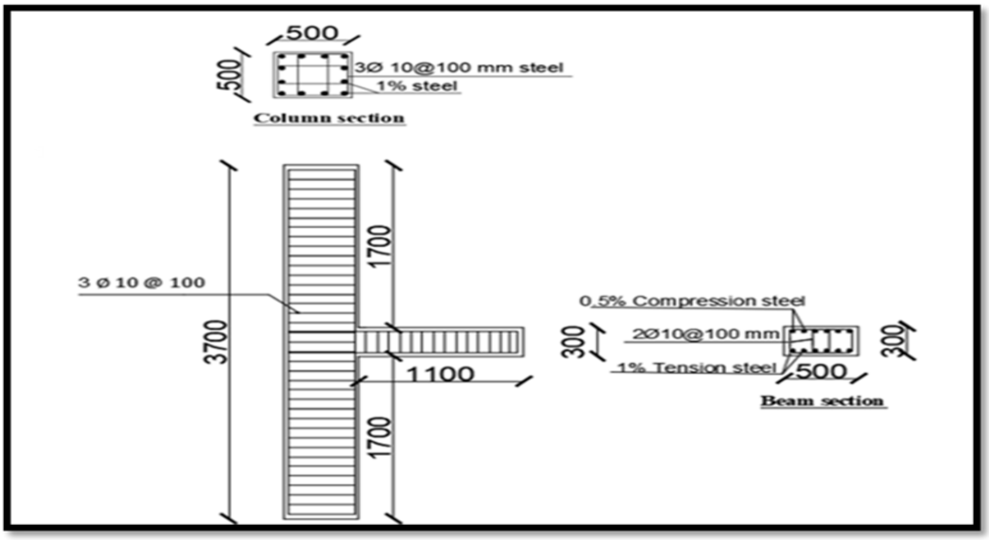

Figure A.1: SP-BCDR 0.6-L1

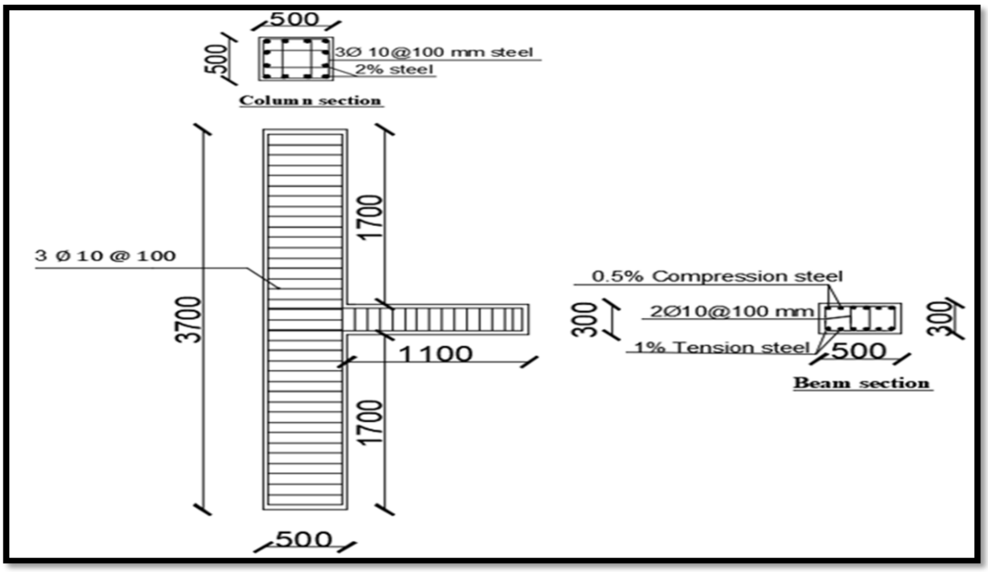

Figure A.2: SP-BCDR 0.6-L2

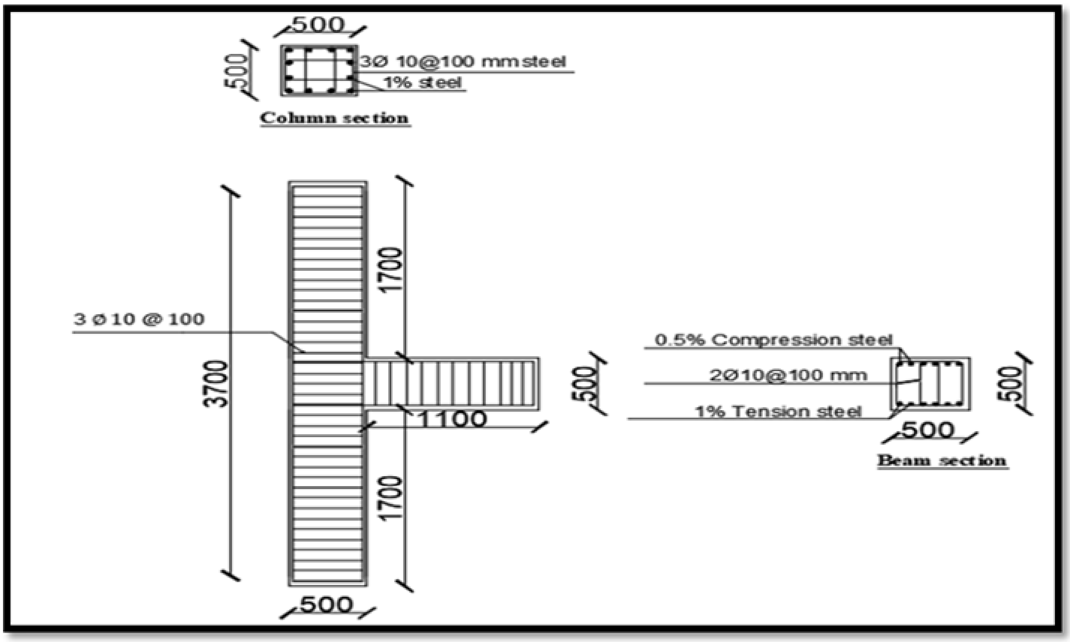

Figure A.3: SP-BCDR 1-L1

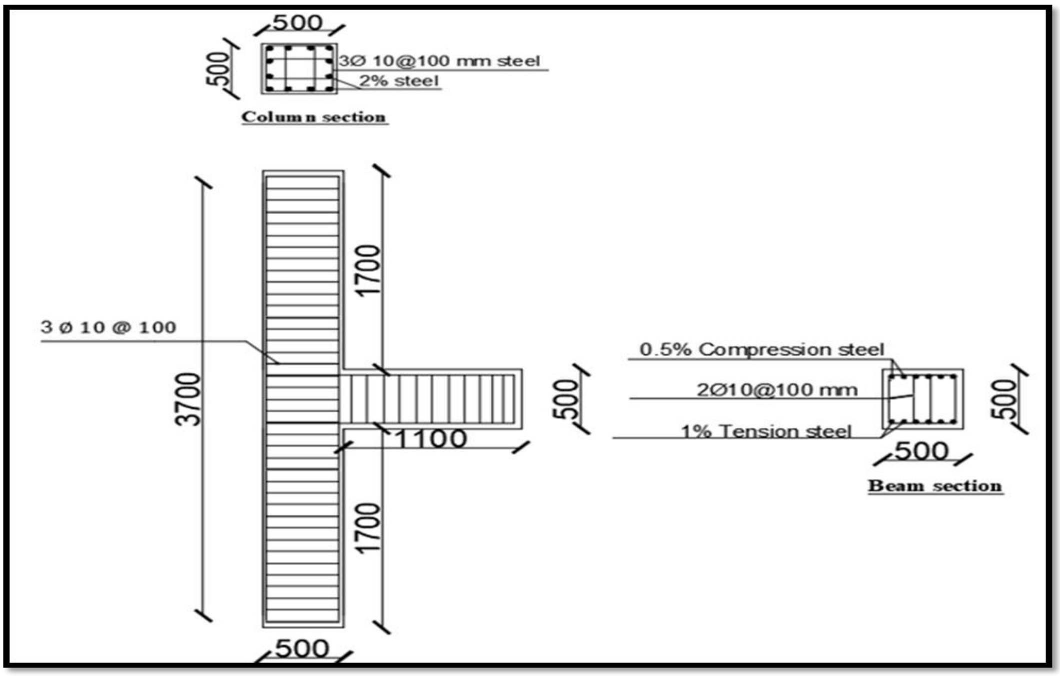

Figure A.4: SP-BCDR 1-L2

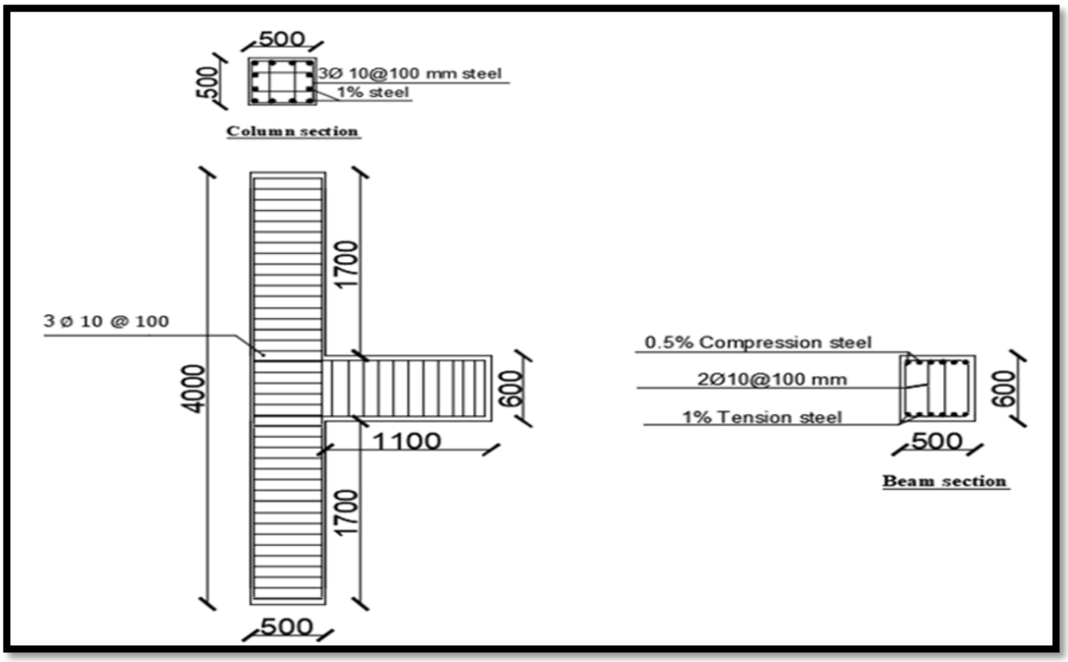

Figure A.5: SP-BCDR 1.2-L1

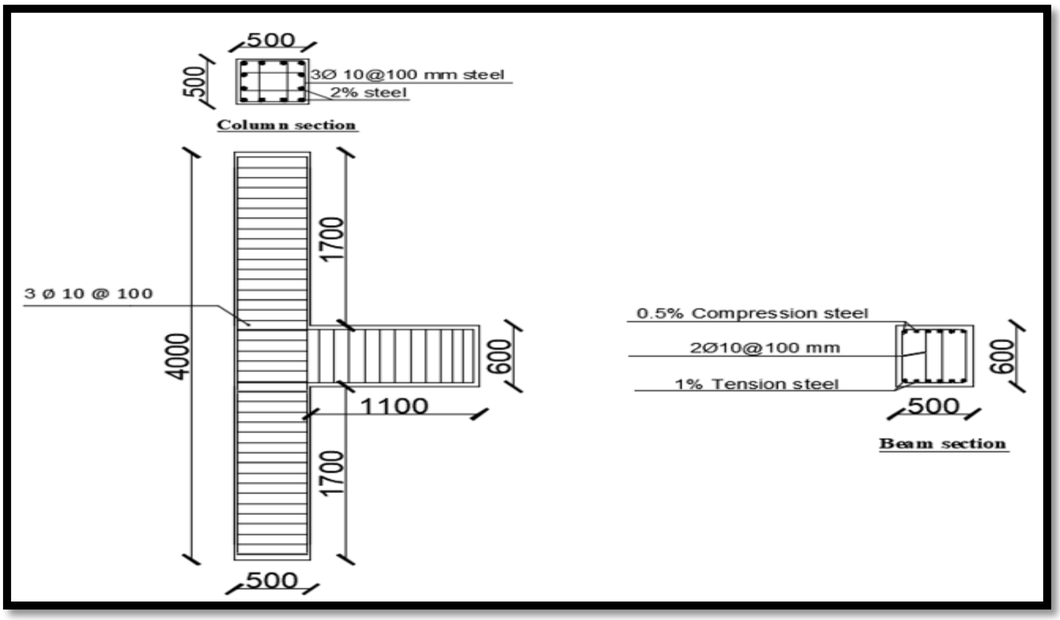

Figure A.6: SP-BCDR 1.2-L2

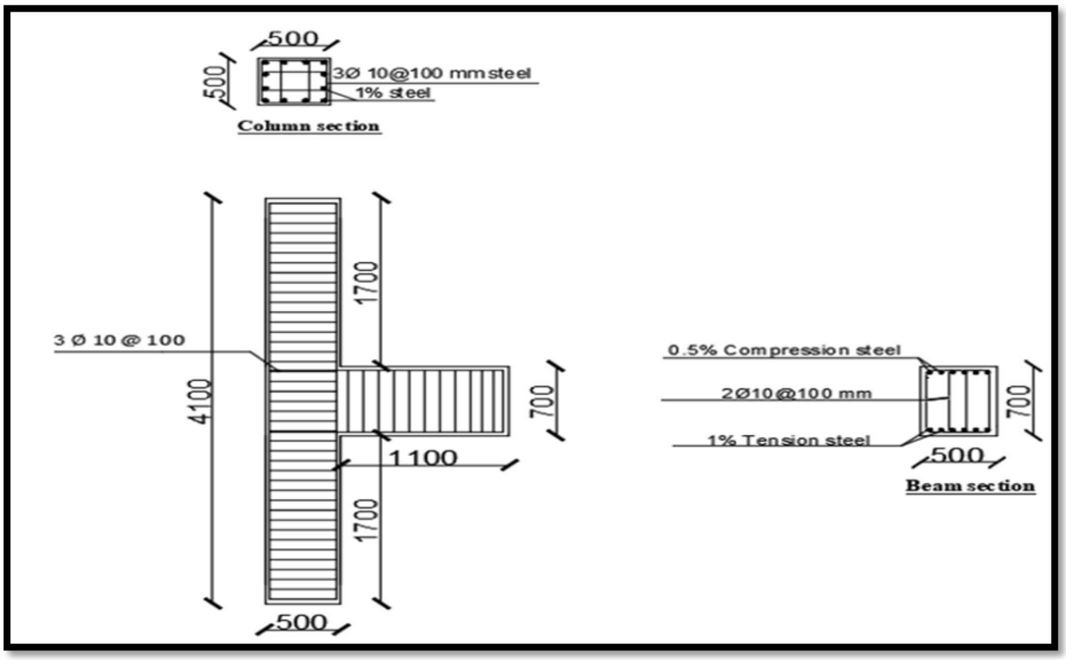

Figure A.7: SP-BCDR 1.4-L1

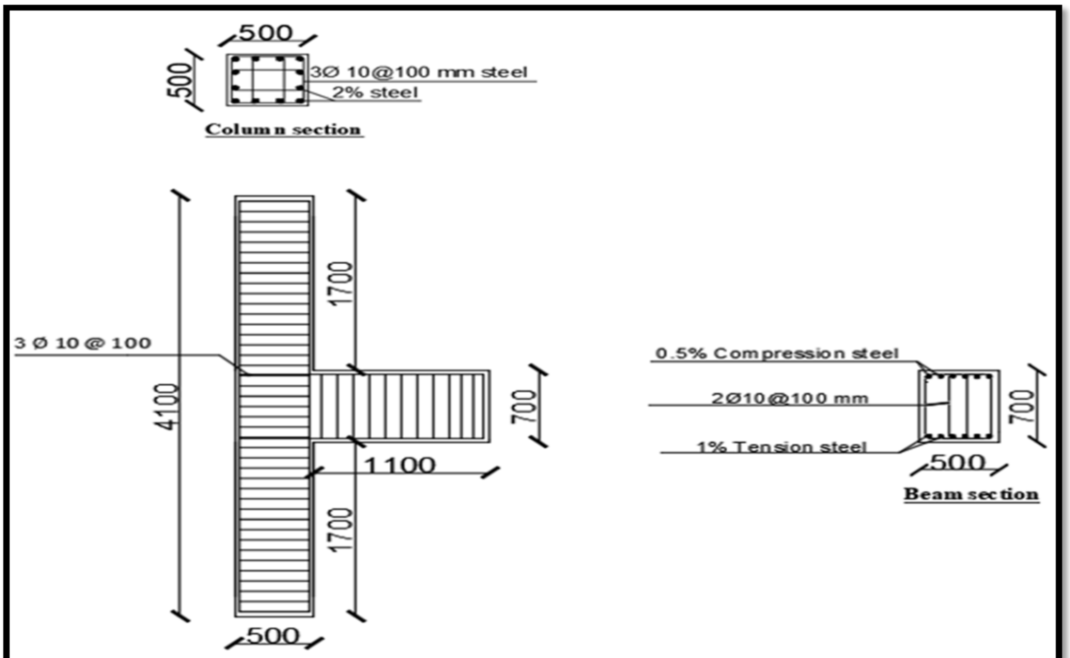

Figure A.8: SP-BCDR 1.4-L2

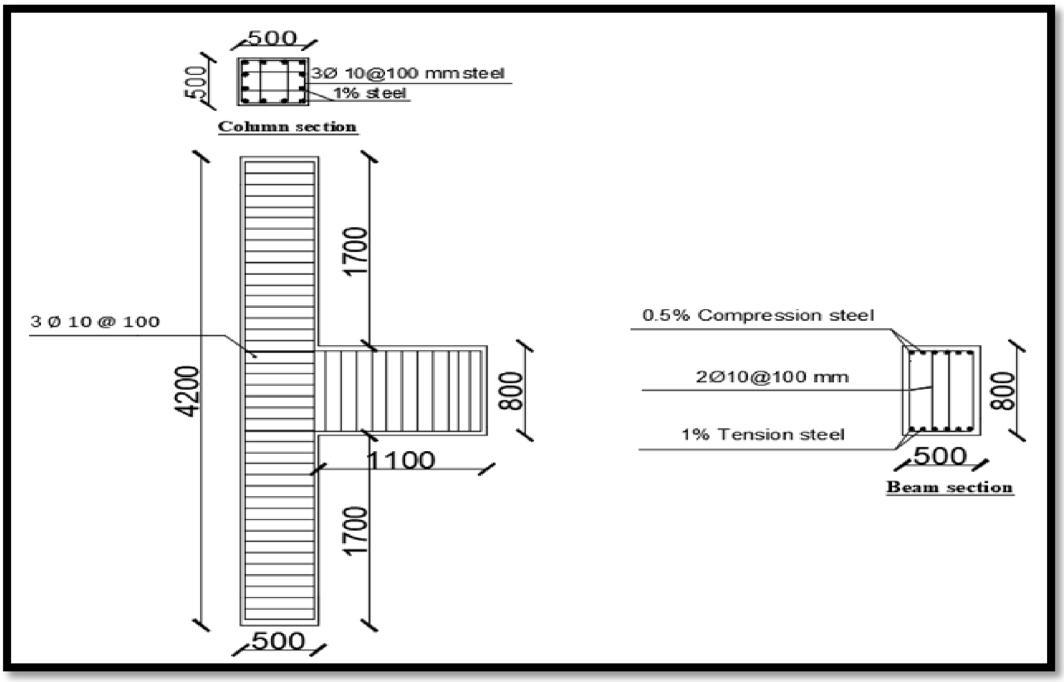

Figure A.9: SP-BCDR 1.6-L1

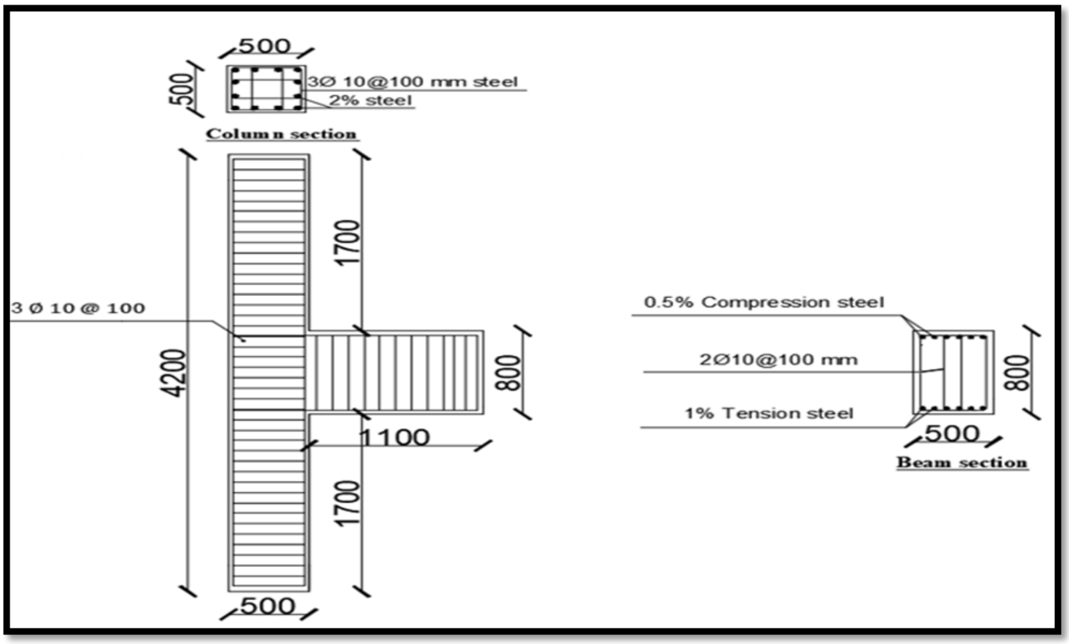

Figure A.10: SP-BCDR 1.6-L2

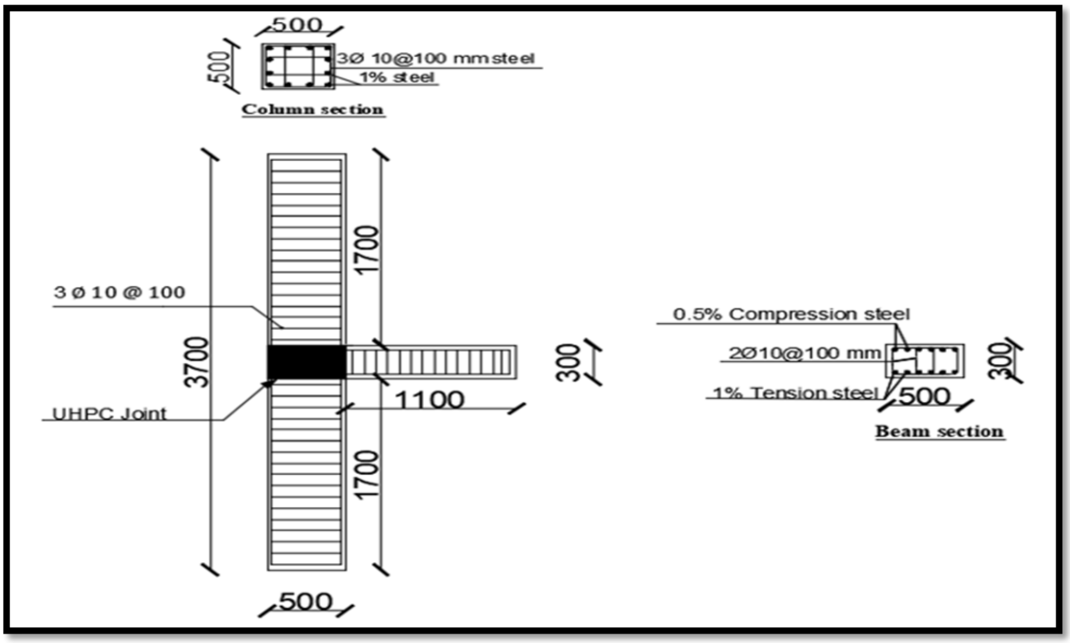

Figure A.11: UB2-BCDR 0.6-L1

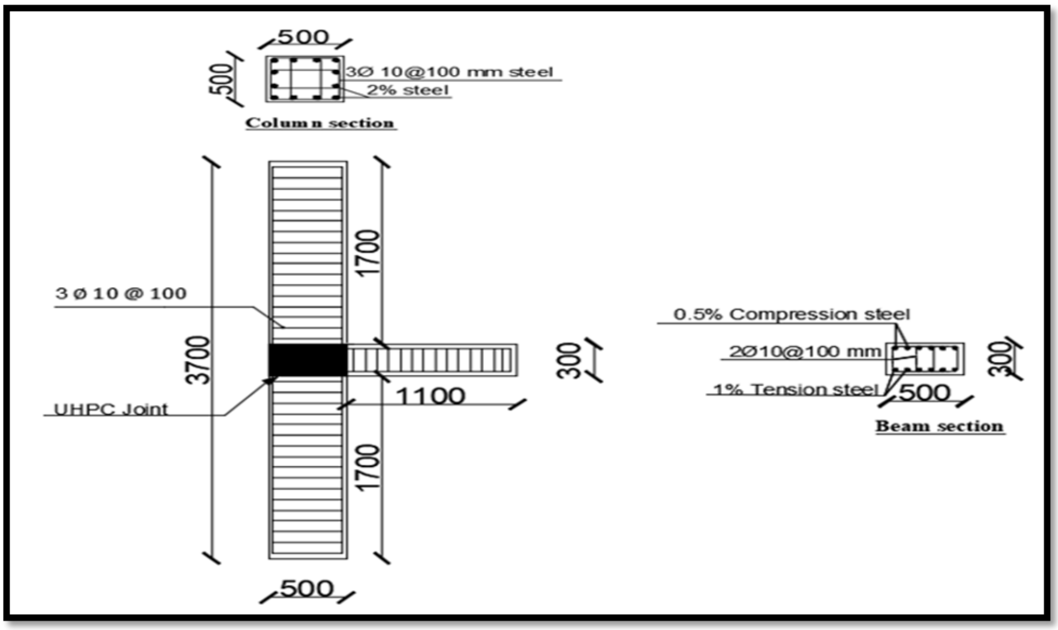

Figure A.12: UB2-BCDR 0.6-L2

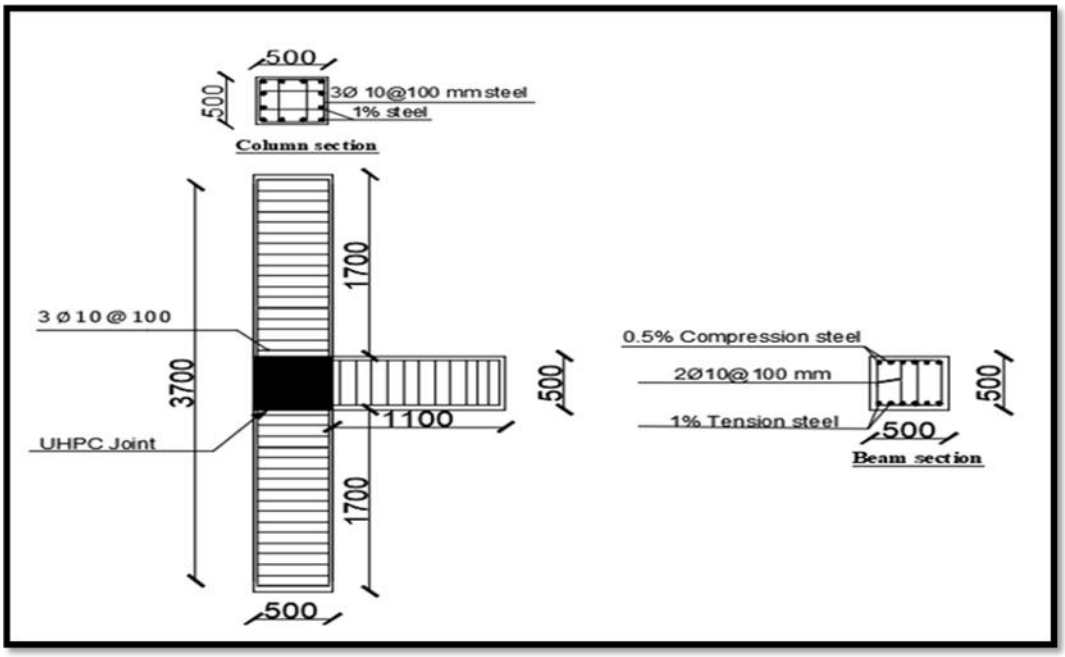

Figure A.13: UB2-BCDR 1-L1

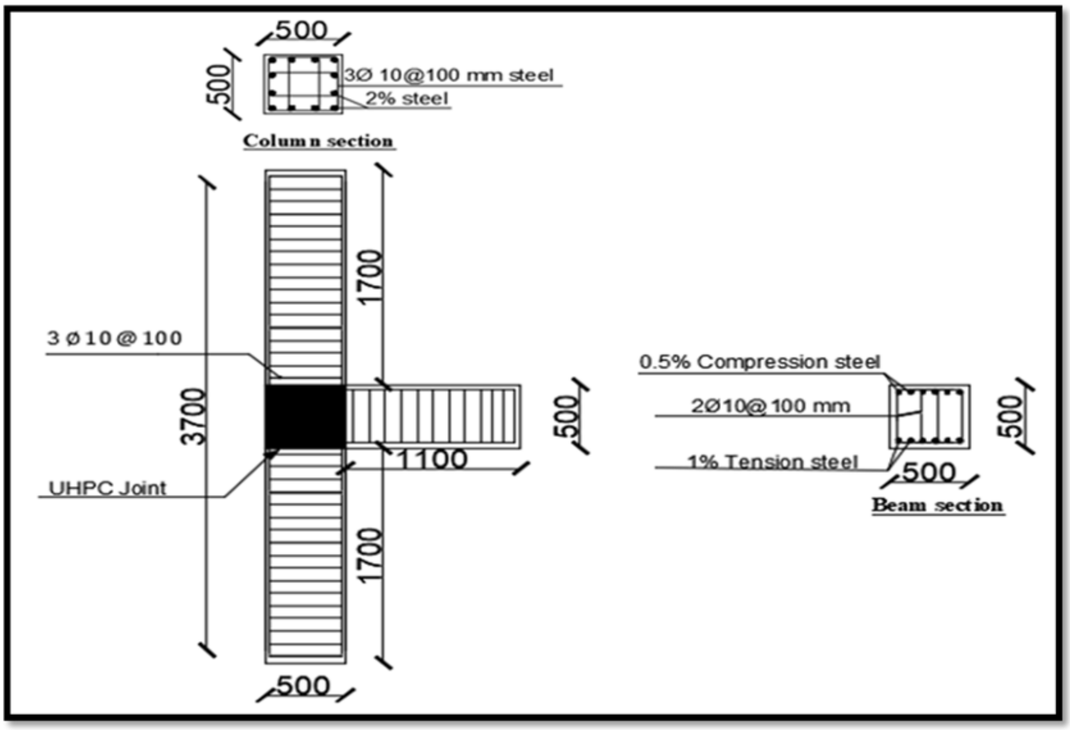

Figure A.14: UB2-BCDR 1-L2

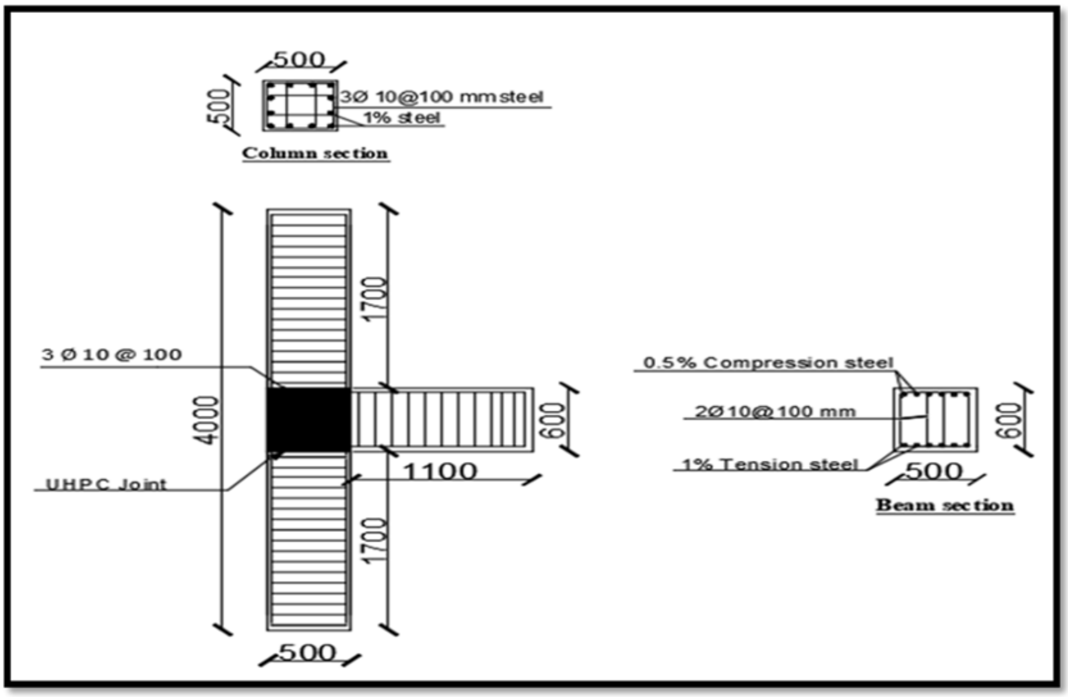

Figure A.15: UB2-BCDR 1.2-L1

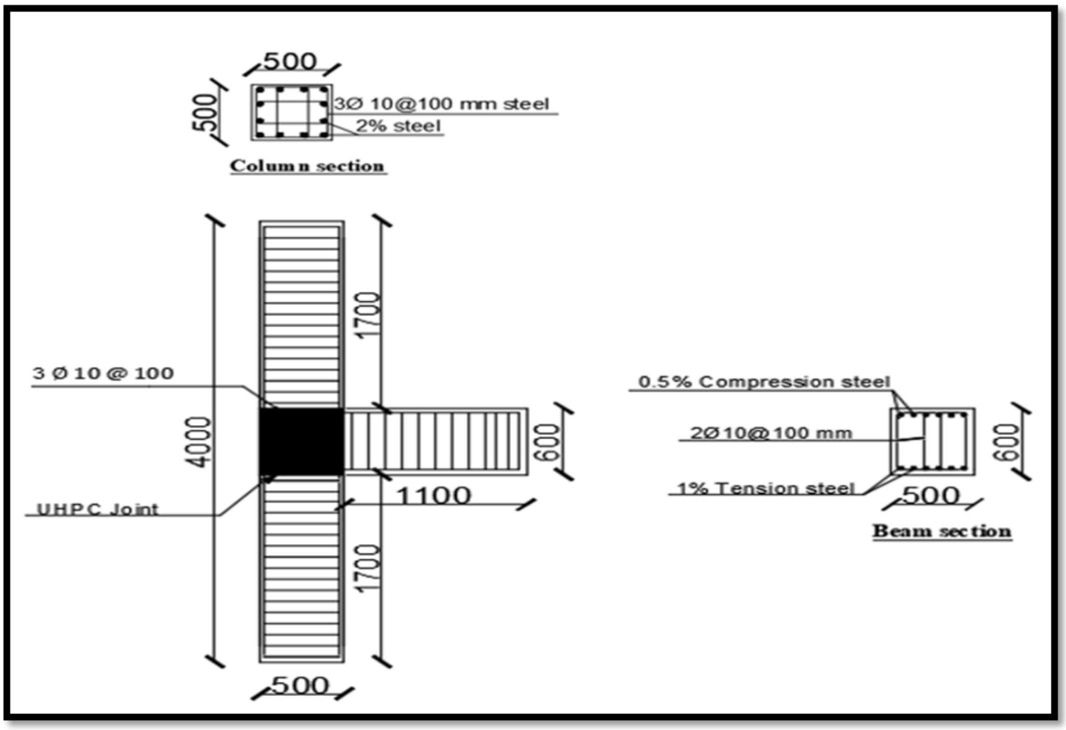

Figure A.16: UB2-BCDR 1.2-L2

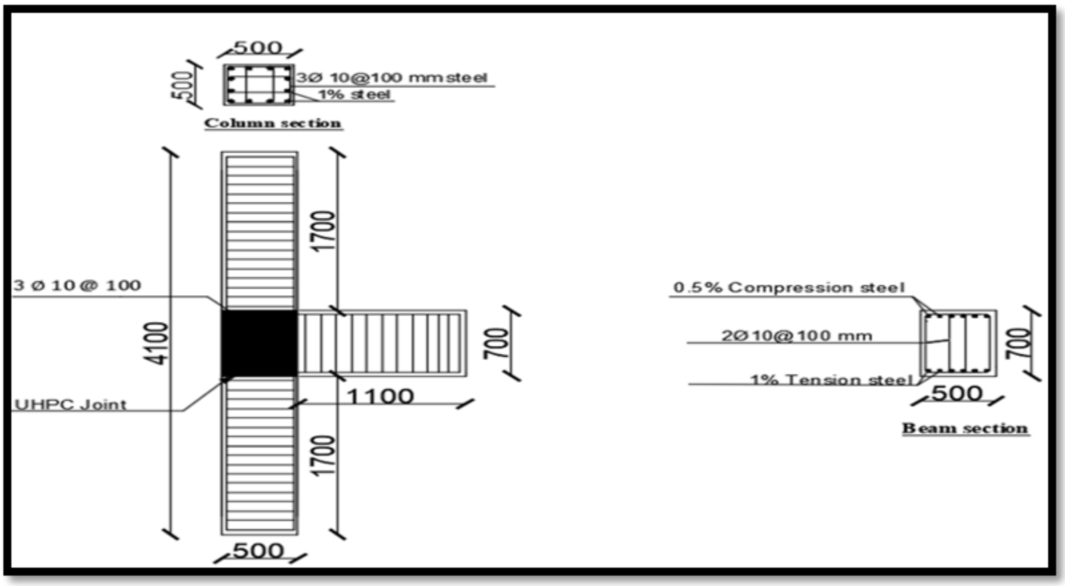

Figure A.17: UB2-BCDR 1.4-L1

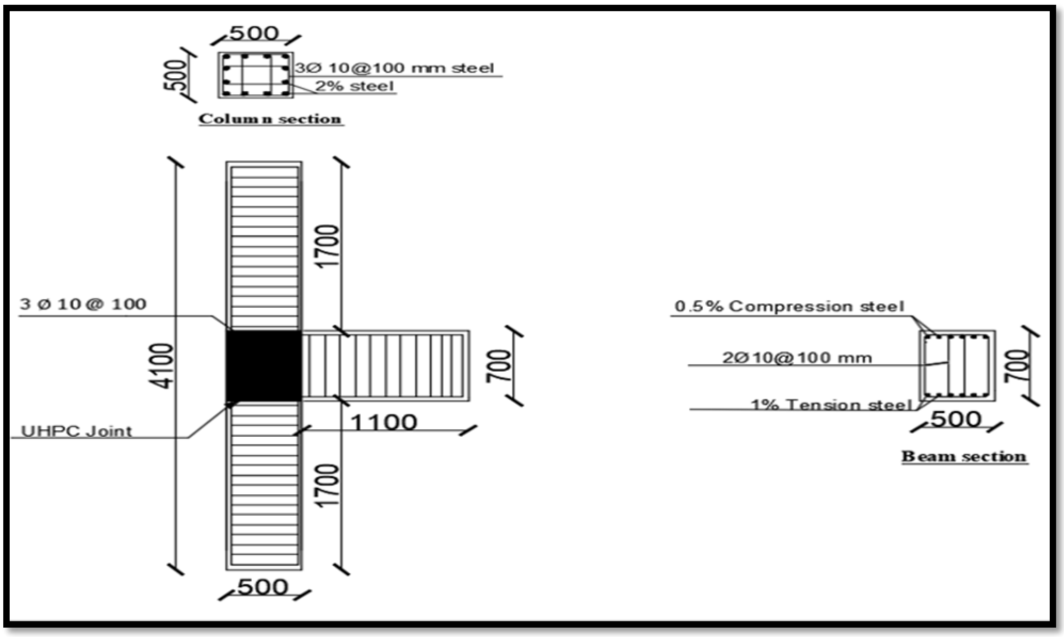

Figure A.18: UB2-BCDR 1.4-L2

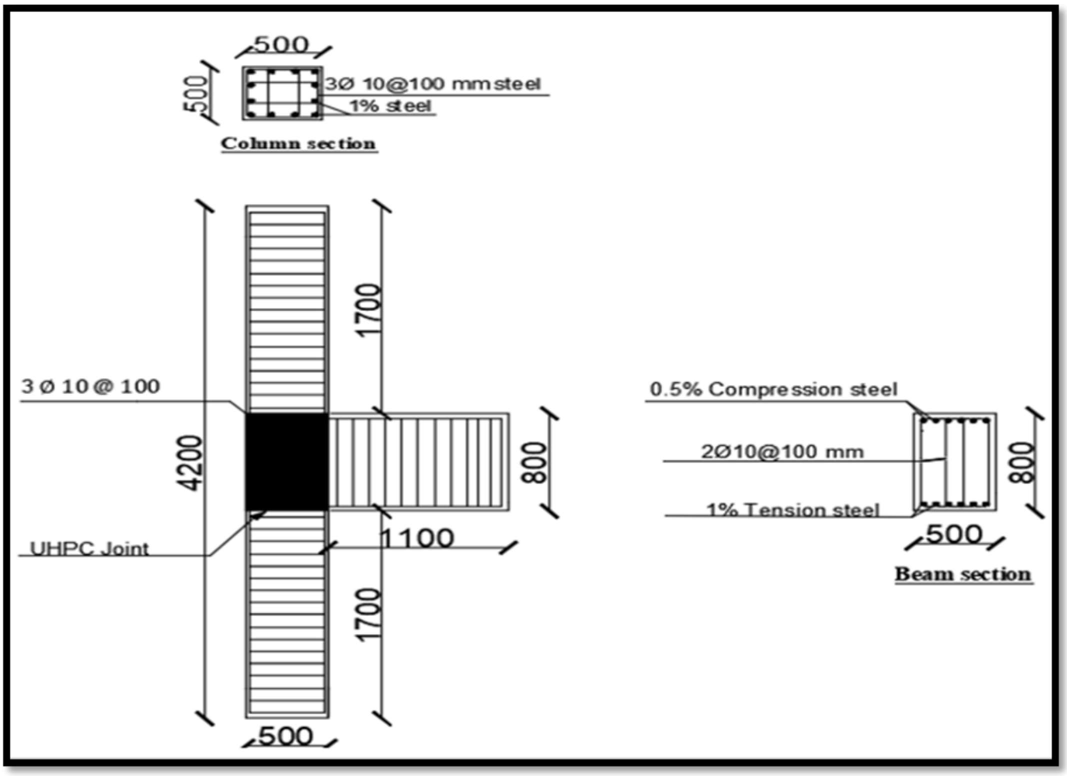

Figure A.19: UB2-BCDR 1.6-L1

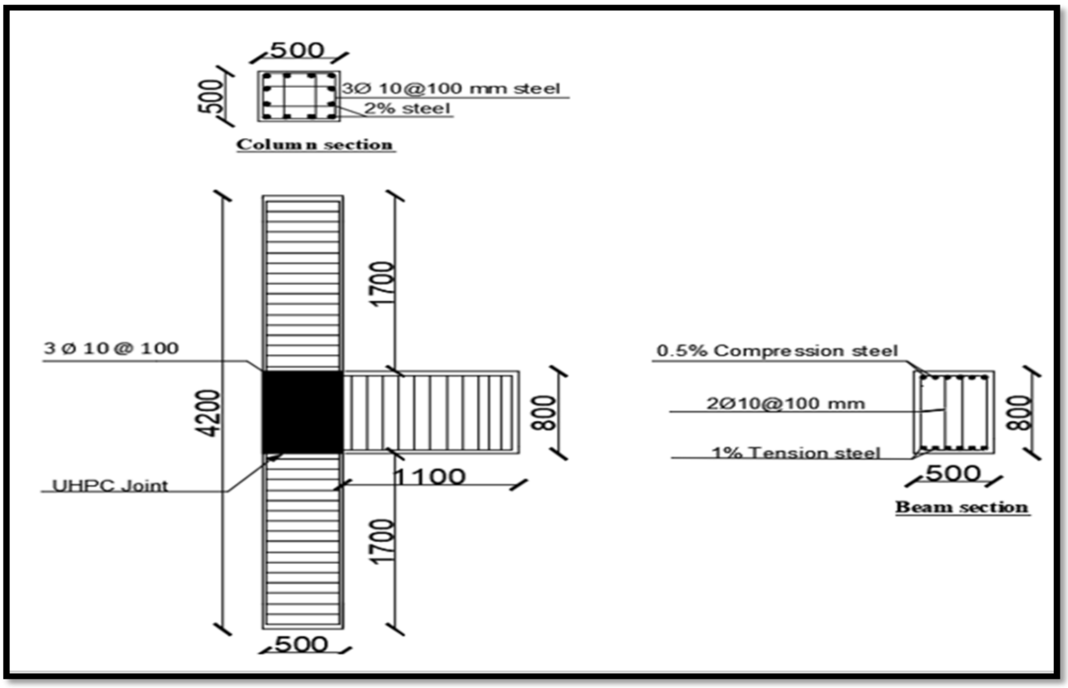

Figure A.20: UB2-BCDR 1.6-L2

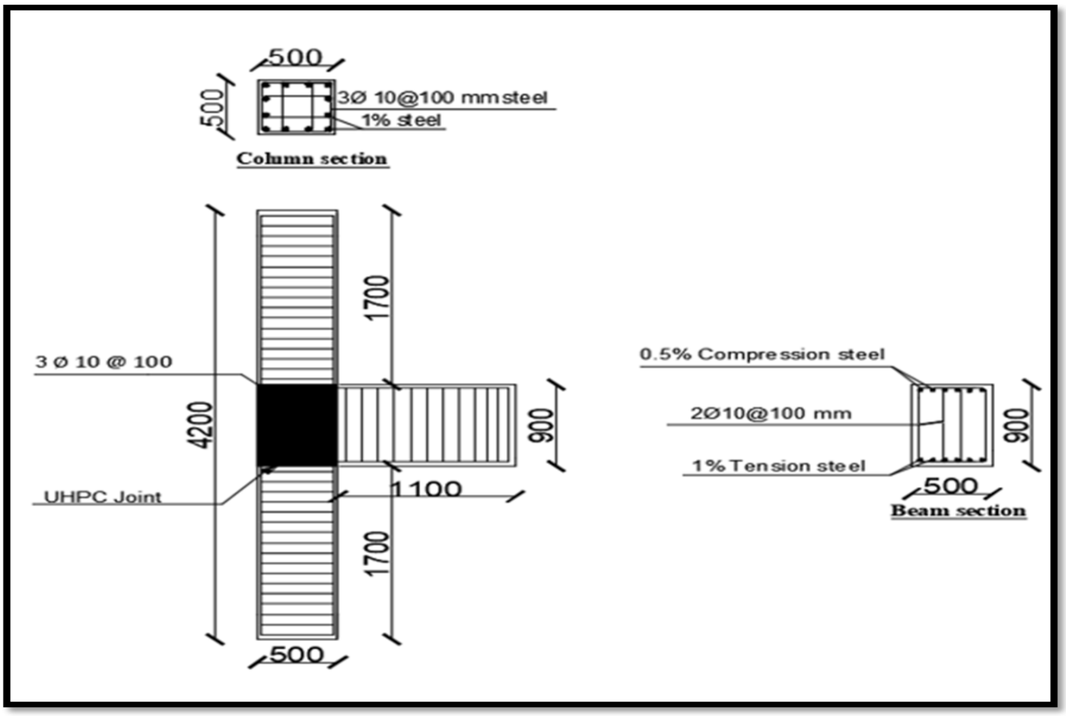

Figure A.21: UB2-BCDR 18-L1

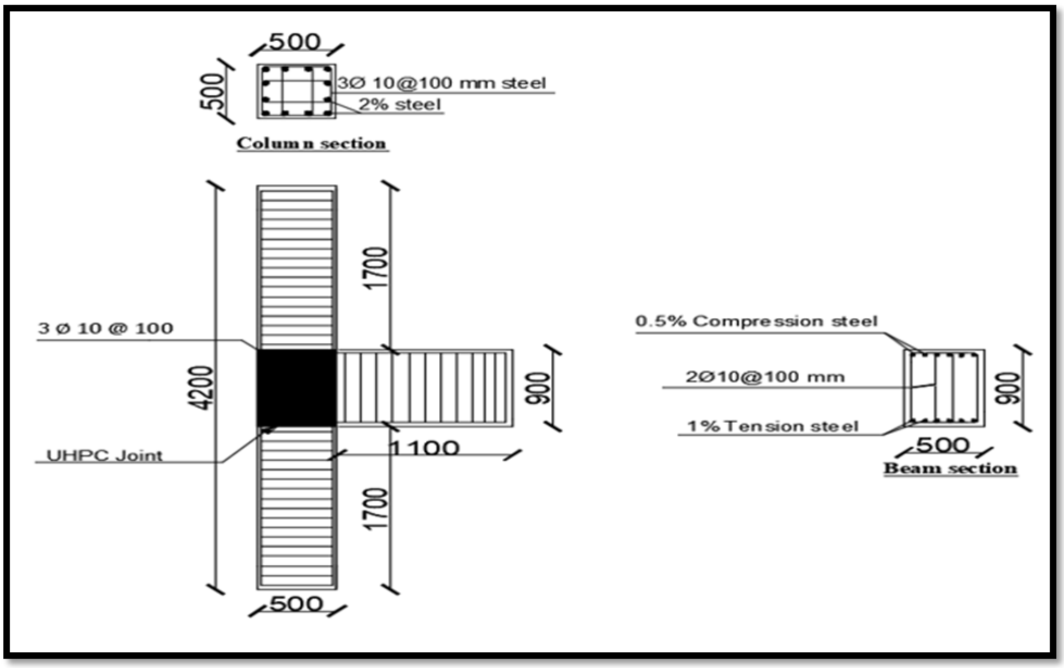

Figure A.22: UB2-BCDR 18-L2

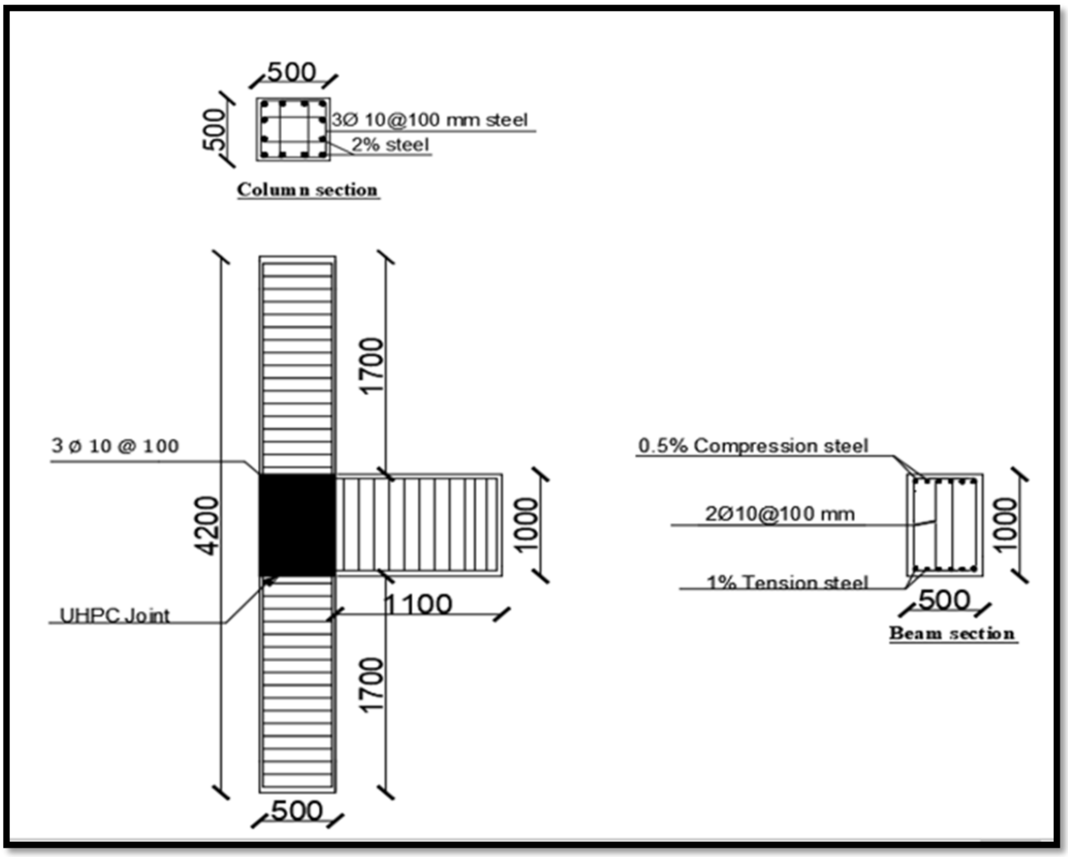

Figure A.23: UB2-BCDR 18-L2

جامعة النجاح الوطنية

كلية الدّراسات العليا

تطوير أداء ممطولي للعقد الخرسانية الخارجية ذات التمايل الخاص باستخدام مادة الخرسانة فائقة الأداء.

اعداد

فايز رائد فايز أبو سفاقة

إشراف

د. محمد سماعنة

د. منذر دويكات

قدمت هذه الأطروحة استكمالا لمتطلبات الحصول على درجة الماجستير في هندسة الإنشاءات بكلية الدراسات العليا في جامعة النجاح الوطنية، نابلس-فلسطين.

2020

تطوير أداء ممطولي للعقد الخرسانية الخارجية ذات التمايل الخاص باستخدام الخرسانة فائقة الأداء.

اعداد

فايز رائد فايز أبو سفاقة

إشراف

د. محمد سماعنة

د. منذر دويكات

الملخص

إن المفاصل الخرسانية هي أكثر العناصر الحرجة في المنشأ. لذلك فإن كودات التصميم ومن ضمنها الكود الأمريكي للخرسانة يوفر متطلبات حازمة لتصميم العقد الخرسانية في المنشآت ذات التمايل الخاص لمنع انهيارها مع درجة ممطولية منطقية تحت تأثير الأحمال الزلزالية. على كل حال, إن تجمع العديد من أنواع الستليح الطولي والعرضي يسبب مشاكلا في التنفيذ. هذا البحث يهدف إلى تطوير أداء ممطولي للعقد الخرسانية الخارجية في المنشأت ذات التمايل الخاص مع استغناء كامل عن التسليح العرضي وذلك باستخدام مادة الخرسانة فائقة الأداء (UHPC).

تم استخدام الخرسانة فائقة الأداء من صنف ب وتحتوي على ما نسبته حجميا 2% من الألياف الفولاذية كما تم اعتمادها من مؤسسة الطرق الفدرالية (FHWA). تم عمل البحث بالتحليل العددي باستخدام برنامح العناصر المحدودة أبكس (ABAQUS). تم استخدام هذا البرنامج لبناء نموذج محاكاة ثلاثي الأبعاد لعقدة خرسانية خارجية و التحقق من نتائج النموذج باستخدام بيانات اختبارية منشورة. بعد ذلك, تم عمل مصفوفة نماذج باستخدام المتغيرات الرئيسية المؤثرة على تصرف العقد الخرسانية. هذه المتغيرات تتصمن النسبة بين العمق الكلي لمقطع الجاسئ بالنسبة للعمق الكلي لمقطع العمود (من 0.6 إلى 1.6 مع 0.1 زيادة), نسبة الحمل الرأسي (0.25 و 0.5) ونسبة التسليح الطولي في العمود (1% و 2%). تم استخدام نتائج المحاكاة لمصفوفة النماذج للمقارنة بين

تصرف العقد الخرسانية ذات التفاصيل للتمايل الخاص مع العقد الخرسانية المقواة باستخدام الخرسانة فائقة الأداء في مدى القوة, الممطولية و نوع الأنهيار الحاصل. إن النتائج قد أكدت إمكانية استخدام الخرسانة فائقة الأداء في تقوية العقد الخرسانية في المنشآت ذات التمايل الخاص بدون فقد في القوة والممطولية.

زيادة على ذلك, إن العقد الخرسانية المقواة بالخرسانة فائقة الأداء أظهرت تفضيلا في الأداء على الحد النسبي الأدنى بين عزم العمود وعزم الجاسئ مع بعض الانتهاكات في هذه النسبة. لفحص مدى هذه الانتهاكات, تم تقييم عزم العمود باستخدام النموذج الذي اقترحه ساتسيوجلو ورازفي (Saatcioglu and Razvi 1992) للخرسانه المحصورة. بعد ذلك, تم حساب النسبة بين عزم العمود المحصور إلى عزم العمود غير المحصور (حسب الكود الأمريكي ACI). لقد وجد أن هذه النسبة تتراوح بين 1.02 و1.20 وذلك يعتمد على نسبة الحمل الرأسي ونسبة التسليح الطولي في العمود. هذه النسب مرتبطة بأبعاد وتفاصيل التسليح للعمود المستخدمة في هذا البحث. ختاما, تم استخدام النموذج التحليل الذي اقترحه الأسطا وخان (Alosta and Khan 2017) لتقييم سعة العقد الخرسانية الخارجية الخالية من التسليح العرضي لقوى القص في تقييم سعة العقد الخرسانية المدعمة بالخرسانة فائقة الأداء وربطها بنسبة الألياف الفولاذية المثلى لاستخدامها بالمادة.

بشكل مختصر, هذا البحث يشير إلى إمكانية استخدام الخرسانة فائقة الأداء في تقوية العقد الخرسانية الخارجية ذات التمايل الخاص على الحد النسبي الأدنى لعزم العمود المحصور إلى عزم الجاسئ مع استخدام النسبة الحجمية المثلى للألياف الفولاذية حسب قوة القص المطلوبة.